INEEL/EXT-2002-1613

31 December 2002

Fundamental thermal fluid physics of high temperature flows in advanced reactor systems

NUCLEAR ENERGY RESEARCH INITIATIVE PROGRAM
INTEROFFICE WORK ORDER (IWO) MSF99-0254
FINAL REPORT FOR PERIOD 1 AUGUST 1999 TO 31 DECEMBER 2002

D. M. McEligot, K. G. Condie, T. D. Foust, G. E. McCreery, R. J. Pink and D. E. Stacey

A. Shenoy, G. Baccaglini (General Atomics)
R. H. Pletcher (Iowa State U.)
J. M. Wallace and P. Vukoslavcevic (U. Maryland)

J. D. Jackson (U. Manchester, UK)
T. Kunugi (Kyoto U., Japan)
S.-i. Satake (Tokyo U. Science, Japan)

INEEL/EXT-2002-1613

Fundamental thermal fluid physics of high temperature flows in advanced reactor systems

NUCLEAR ENERGY RESEARCH INITIATIVE (NERI) PROGRAM
INTEROFFICE WORK ORDER (IWO) MSF99-0254
FINAL TECHNICAL REPORT FOR
1 AUGUST 1999 TO 31 DECEMBER 2002

D. M. McEligot, K. G. Condie, T. D. Foust, G. E. McCreery,
R. J. Pink and D. E. Stacey, INEEL

A. Shenoy and G. Baccaglini, General Atomics
R. H. Pletcher, Iowa State U.
J. M. Wallace and P. Vukoslavcevic, U. Maryland

J. D. Jackson, U. Manchester, UK
T. Kunugi, Kyoto U., Japan
S.-i. Satake, Tokyo U. Science, Japan

31 December 2002

Idaho National Engineering and Environmental Laboratory
Idaho Falls, Idaho 83415

Prepared for
U. S. Department of Energy
Office of Nuclear Energy
Under DoE Idaho Operations Office
Contract DE-AC07-99ID13727

Fundamental thermal fluid physics of high temperature flows in advanced reactor systems

D. M. McEligot (INEEL), G. Baccaglini (General Atomics), K. G. Condie (INEEL), T. D. Foust (INEEL), J. D. Jackson (U. Manchester), T. Kunugi (Kyoto U.), G. E. McCreery (INEEL), R. J. Pink (INEEL), R. H. Pletcher (Iowa State), S.-I. Satake (Toyama U.), A. Shenoy (General Atomics), D. E. Stacey (INEEL), P. Vukoslavcevic (U. Montenegro) and J. M. Wallace (U. Maryland)

Table of contents

Fundamental thermal fluid physics of high temperature flows in advanced reactor systems

NUCLEAR ENERGY RESEARCH INITIATIVE (NERI) PROGRAM
INTEROFFICE WORK ORDER (IWO) MSF99-0254
FINAL TECHNICAL REPORT

31 December 2002

Lead = Idaho National Engineering and Environmental Laboratory (INEEL)

Collaborators General Atomics Company, Dr. A. S. Shenoy and Dr. G. Baccaglini
Iowa State University, Prof. R. H. Pletcher
University of Maryland, Profs. J. M. Wallace and P. Vukoslavcevic

International collaborators (unfunded)
Prof. J. D. Jackson, Univ. Manchester, UK
Prof. T. Kunugi, Kyoto University, Japan
Prof. S.-i. Satake, Tokyo University of Science, Japan
Drs. V. Blet, D. Tenchine and J.-P. Moro, Commissariat a l'Energie Atomique (CEA), Grenoble, France

Technical report for the period 1 August 1999 to 31 December 2002

Field of Research and Development: Thermal fluid physics: engineering science, computational science and transport processes

Scope of Work Element/Area: Fundamental science and technology plus high efficiency reactors, low output reactors and passive nuclear plant safety systems

Executive summary

The **objective** of this laboratory/university/industry collaboration of coupled computational and experimental studies addresses fundamental science and engineering to develop supporting knowledge required for reliable approaches to new and advanced reactor designs for improved performance, efficiency, reliability, enhanced safety and reduced costs and waste and for small reactors for remote power and hydrogen generation. It *provides basic thermal fluid science knowledge* to develop increased understanding for the behavior of fluid systems at high temperatures, application and improvement of modern computation and modeling methods and incorporation of enhanced safety features. The project promotes, maintains and extends the nuclear science and engineering base to meet future technical challenges in design and operation of high efficiency reactors, low output reactors and nuclear plant safety; it brings recognized thermal fluid mechanics authorities, Profs. Pletcher, Vukoslavcevic and Wallace and their students, into the nuclear science and engineering research community.

This basic thermal fluids research applies first principles approaches (Direct Numerical Simulation and Large Eddy Simulation) coupled with experimentation (heat transfer and fluid mechanics measurements). Turbulence is one of the most important unresolved problems in engineering and science, particularly for the complex geometries occurring in advanced reactor systems and their passive safety systems. *Prof. Pletcher* extended LES to generic idealizations of such

geometries; *Profs. Satake and Kunugi* supported these studies with DNS. *Profs. Wallace and Vukoslavcevic* developed miniaturized multi-sensor probes to measure turbulence components in high temperature flows. *INEEL* conducted experiments to obtain fundamental turbulence and velocity data for generic idealizations of the complex geometries of advanced reactor systems. *Prof. Jackson* conducted measurements of the effects of buoyancy forces on flow in circular tubes, channels and annuli. *Drs. Shenoy and Baccaglini at General Atomics* provided thermal-hydraulic data needs for Modular Helium Reactors and reviewed the computational techniques and supporting results to determine their applicability to gas-cooled reactor operation.

The unique INEEL Matched-Index-of-Refraction flow system, the World's largest such facility, was applied for the first time to obtain fundamental data on flows through complex geometries important in the design and safety analyses for advanced reactors. Successful completion of the *study provides the following new fundamental and engineering knowledge*, which was not available in the literature:

- o Time-resolved data plus flow visualization of turbulent and laminarizing phenomena in accelerated flow around obstructions (spacer ribs) in annuli.
- o Application of DNS and LES for the first time to complex turbulent flows occurring in advanced reactors
- o Fundamental data of internal turbulence distributions for assessment and guidance of computational thermal fluid dyunamics (CTFD) codes proposed for design and safety analyses for advanced gas-cooled reactors

Task A: Heat transfer and fluid flow in advanced reactors, Drs. A. S. Shenoy and G. Baccaglini, General Atomics GA has identified six areas of thermal hydraulic phenomena in which the application of Computational Fluid Dynamic techniques can improve the safety of advanced gas cooled reactors. Dr. Baccaglini provided performance parameters for normal and emergency operations to support the planning of computational techniques and experiments. He and Dr. Shenoy interacted with the analysts and reviewed the collaborators's tasks to assure that the results of this project will be applicable to the improvement of reactor safety.

Task B: Complex flow measurements, INEEL The goals of the INEEL experimental portion of the study are to provide fundamental measurements to answer the scientific needs identified in the proposal and to guide code development and assess code capabilities for treating generic forced convection problems in advanced reactors. Flow through idealized, complex reactor geometries was examined without complicating thermal phenomena; laser Doppler anemometry was employed with INEEL's unique Matched-Index-of-Refraction (MIR) flow facility to determine the velocity and turbulence fields. The innovation of the INEEL MIR system is its large size compared to earlier systems; it provides means for measurements for the portion of the study dwelling on forced convection in complex reactor geometries.

INEEL conferred with General Atomics staff to identify generic features of complex advanced reactor geometries and to determine parameter ranges of interest. Required capabilities of predictive techniques and features of experiments to assess these capabilities were tabulated. Conceptual experimental models were developed for laser Doppler velocimeter measurements in the large INEEL MIR flow system to examine flow in complex core geometries (ribbed annular cooling channels and control rod configurations) and in the transition from cooling channels to formation of jets issuing into a plenum. Two experimental models have been used. These experiments addressed two thermal/hydraulic phenomena selected by GA: (1) normal operation at full or partial loads and (2) loss of forced reactor core cooling.

The first experimental model was a ribbed annulus forming an annular jet exhausting into the larger surrounding test section of the MIR flow system. The initial MIR experiments were aimed at obtaining benchmark data to test the capabilities of CFD codes to handle ribbed annular geometries

without the complications of turbulent transport (i.e., laminar flow requiring no turbulence modeling, although localized turbulence may exist within eddies shed from the spacer ribs). Streamwise-periodic flow was observed away from the ends of the model. Preliminary flow visualization measurements were obtained by injecting small air bubbles into the oil flow in the annulus. These observations, recorded in photographs, outlined the eddy which forms behind the spacer rib due to separation and recirculation.

LDV data for two velocity components were obtained at $Re_{D,h} = 4\dot{m}/(\Pi(D_o+D_i)\mu) \approx 1120$ as radial, axial and circumferential profiles of U, V, u' and v' as well as spectral analyses. These conditions correspond to some stages during a pressurized cooldown (LOFA) event. The measured radial profile of the streamwise velocity component away from the ribs has been compared to the analytical solution for laminar flow in an axisymmetric annulus (i.e., without ribs). With a radius ratio of about 0.82, the analytic solution is close to that of a parallel plate duct which would have $U/V_b = 1.5$ at the centerplane. Between ribs (circumferentially) the flow must accelerate due to the blockage of the ribs. The shape of the measured profile agrees with the analytic prediction for a bulk velocity about twelve per cent higher than the value which applies in the space between the ribs axially.

As expected, the LDV data showed that a slow recirculating region formed behind a rib. This region could be expected to produce a "hot spot" if the inner surface were heated. However, frequency spectra for the flow in this region demonstrated an oscillating flow characteristic of eddy shedding from a circular cylinder. Increased levels of fluctuations u' and v' were also observed. Consequently, at these flow conditions a "hot spot" would likely be ameliorated by the oscillating turbulent flow (and thermal conduction in the solid rod). Turbulence is also indicated in profiles from radial traverses obtained at positions downstream of the spacers. For example, the profiles of streamwise mean velocity show steeper gradients near the wall than for the laminar flow further away from the ribs. For (long) circular cylinders, eddy shedding at a non-dimensional frequency $St \approx 0.2$ occurs for $Re_D >$ about 50. For the long rectangular spacer, $St = wf/V_b \approx 0.15$ and $Re_w = V_b w/\nu \approx 1000$, where w is the average width of a rib in the circumferential direction.

Calculations for the conditions of the experiment were conducted using a general-purpose CFD code, Fluent. These efforts demonstrated the difficulty in applying CFD codes to this three-dimensional geometry.

The second experiment addressed flow in coolant or control rod channels and an idealized two-stage jet transition from generic coolant channels to a plenum. It is a combined experiment focusing on flow in the ribbed annulus upstream and the first stage of this geometric transition, a jet issuing from a converging flow simulating the exit from cooling channels into a collecting plenum (or impingement chamber). The circular annulus has a nominal outer diameter of about 150 mm (6 in.) and inner diameter of about 135 mm (5.4 in.). Model length is about 1.5 meters with five periodic cells formed by the spacer ribs. Four ribs are distributed radially around the circumference as for a GA control rod. These sets are spaced longitudinally with pitch p/s of about forty. The ribs have widths w/s of about two and lengths L/s of about ten.

Flow visualization experiments were conducted for flow entering, within and exiting the impingement chamber of the apparatus using air bubbles injected in the inlet piping. The flow patterns and streamlines recorded compare closely to those obtained earlier using water flow through a thin planar model of the chamber. As expected, the flow remained attached further along the convergence than in the planar model since the cross section remained constant, giving a favorable pressure gradient, rather than diverging.

Measurements for the flow in the annulus were completed with our LDV system. Two-component (axial and radial) LDV measurements were obtained in the ribbed annulus at $Re \approx 6900$, based on the hydraulic diameter between the ribs axially. Data were obtained in cells 3, 4

and 5 at axial positions halfway between spacers to test the streamwise periodicity of velocity profiles. The flow in the third cell was considered to be representative of the streamwise-periodic pattern, so most measurements were concentrated there. Data were obtained along radial and axial traverses, at locations downstream from spacer ribs and furthest removed from the spacer ribs, both horizontally and circumferentially. The circumferential variation of streamwise velocity was measured at a constant mid-annular radius at positions midway between spacer ribs in the axial direction. The accelerating flow between the ribs induced reductions in the streamwise velocity fluctuations near the wall and in the central region (radially) and increases were observed in the subsequent decelerating flow. The consequent reduction and enhancement of heat transfer parameters (respectively) would pose challenges to turbulence models typically used in commercial codes so numerical predictions for this case could be misleading.

Task C: Direct Numerical Simulation (DNS) development, Prof. T. Kunugi / Kyoto U. and Prof. S.-i. Satake / Toyama U. Profs. Satake and Kunugi are developing DNS for use in high temperature gas (or superheated vapor) flows with transport property variation. Their results assist evaluation of sub-grid-scale models used in LES and of other CFD approaches and will also help in the interpretation of hot wire measurements in these conditions.

They have successfully applied their DNS code for flow in circular tubes with strongly varying gas properties to the conditions of Run 445 from the experiments by Shehata and McEligot [IJHMT, 1998]. In that run the flow entered the heating section as a fully-developed turbulent one and, due to the strong heating (causing property variation and acceleration), was effectively laminarized within about twenty-five diameters [Satake et al., IJHFF, 2000].

DNS calculations were next initiated for Run 635, at a higher Reynolds number and lower heating rate, conditions which other investigators have found difficult to predict adequately with so-called advanced turbulence models. In addition, calculations were initiated for Run 618, at the same inlet Reynolds number as Run 635 but with a lower heating rate. Run 618 represents a turbulent flow that has reduced heat transfer parameters due to effects of property variation but no apparent laminarization; as such it is comparable to normal operating conditions for cooling channels in a GA advanced gas-cooled reactor. Runs 635 and 445 correspond to conditions expected to occur as the Reynolds number decreases during a transient LOFA. With these DNS calculations, it appears that the sub-turbulent state of Run 635 is easier to calculate than that of turbulent Run 618. Calculations for Run 635 are essentially complete but Run 618 requires more computation to converge.

Task D: Large Eddy Simulation (LES) development, Prof. R. H. Pletcher, Iowa State The main thrust of this task is to extend LES methodology to a broader class of flows with heat transfer, particularly flows characteristic of those occurring in modern nuclear reactors. Prof. Pletcher's earlier LES channel flow code treated strongly varying gas flows with buoyancy effects. He and his graduate students modified this code to apply to circular geometries, such as tubes and annuli. Several cases were addressed:

- o Horizontal turbulent channel flows with buoyancy
- o Vertical turbulent channel flows with buoyancy
- o Circular tube with buoyancy
- o Annular flow, isothermal validation case
- o Annular flow, case with inner wall heating
- o Ribbed annulus, isothermal case for comparison with INEEL experiments

Most calculations account for variation of gas properties - thermal conductivity, viscosity and density - with temperature and for buoyancy effects. The tube geometry corresponds to coolant channels in GA prismatic reactors and to an MIT concept for gas-cooled fast breeders. The annular

geometry occurs in control rod geometries in GA reactors and in the HTTR and comparable reactors.

LES results have been obtained for vertical upward flow of air in a channel heated on one side and cooled on another. Such a channel flow corresponds closely to flow in an annular passage of large radius ratio, e.g., the vertical annular flow between the core barrel and the reactor vessel wall or fuel coolant passages of the Japanese HTTR. One observes that buoyancy induces a "laminarizing" effect near the heated wall, reducing the turbulent kinetic energy, Reynolds stress and Nusselt number. However, the friction coefficient and temperature fluctuations are increased near this wall. The property variations modify the local Reynolds number ; this modification may partially explain observed structural changes. This work is the first known LES study of a vertical flow accounting for buoyancy and variations in fluid properties.

In progress are some comparisons with the mixed convection data obtained by our partners at CEA Grenoble for upward turbulent flow between vertical parallel plates at different wall temperatures [Moro, Saez and Hopfinger, 2nd EF Conf. Turb. Heat Transfer, Manchester, 1998]. This situation is comparable to LES code predictions mentioned above. Comparisons for their isothermal flow at a Reynolds number of 6775 based on the mean velocity and channel half-width have been completed and show reasonable agreement.

Additional comparisons have been made with the measurements of Shehata and McEligot for heat transfer to strongly-heated turbulent flow in a vertical pipe. Their Runs 445, 618 and 635 were considered. Comparisons have been made with the data taken at x/D = 14 and 25. Fairly good agreement has been observed between the large eddy simulations and the data. The simulations are based on a quasi-developed assumption. Step-periodic boundary conditions for temperature are used in the streamwise direction. To initiate the simulations, the experimentally-observed values of the wall temperature distributions and the local Reynolds numbers were employed. With high heating rates, property variations cause the streamwise change in temperature from inlet to outlet of the computational domain to be a function of the radial position in the pipe. The level of agreement between simulations and experiment was found to depend on how this radial variation is represented.

In the case where a series of fairly short (in terms of hydraulic diameters) ribbed spacers are used in an annulus, as in the experiments of Task B and the coolant channels for GA control rods and HTTR fuel elements, it is possible to embed a set of ribs within a quasi-developed, spatially-periodic computational region. This approach enables the simulation of the complete flow field around the ribbed region and should provide valuable detailed information about the flow including information that would be difficult to achieve experimentally. Such a procedure was implemented. Simulations were made for Reynolds numbers of 500 and 1200 based on the bulk velocity and hydraulic diameter both evaluated for the unobstructed portion of the annulus. The general flow pattern around the spacers, as seen in contours of mean streamwise centerline velocity and plots of streamlines, corresponds to the experimental observations. Measured and computed profiles of the mean streamwise velocity midway (axially and circumferentially) between the spacers showed quite good agreement.

Task E: Multi-sensor probe development, Profs. J. M. Wallace and P. Vukoslavcevic, U. Maryland Prof. James M. Wallace and Visiting Prof. Petar Vukoslavcevic (from the University of Montenegro) developed miniaturized multi-sensor probes to measure instantaneous turbulence components in high temperature flows. These probes were developed for employment by INEEL and other collaborators to measure fluctuating velocity components and temperature in high temperature gas flow through vertical pipes and channels for assessment of predictions and to understand the fundamental effects of this heating on the physics of the flow.

Two versions of test probes were designed and constructed, as well as a calibration test facility. The calibration facility for the hot-wire probes that are to be operated at high temperature has been designed to provide a variable and uniform velocity and temperature flow field in the speed range of 0.5-15 m/s and temperature range from ambient room temperature to over 600 °C. The speed and temperature profiles are uniform over most of the nozzle exit area for different speeds and the temperature range. The variation is less than one per cent in the region in which the probe, temperature and velocity sensors are tested and calibrated.

In order to determine the best probe geometrical arrangement and sensor separation, several test probes were constructed and tested. Based on experiments, the best sensor arrangements were chosen for final boundary-layer type probes. The final boundary layer probe types are similar to the test types. The main difference, because they must be positioned as close as possible to the wall, is that they also have an additional prong designed to be used as a spatial distancer. They have two hot wire sensors for velocity components and a single "cold" wire sensor for instantaneous temperature. The diameter of the sensor "volume" is about one millimeter. For calibration, two nonlinear algebraic equations have been derived. Each has seven constants to be determined. A simple numerical algorithm has been developed to solve those two equations for the case of known fluid temperature.

Two operating parameters have to be optimized for a probe of given geometrical arrangement and flow conditions: the overheat ratio of the velocity sensors and the current of the temperature sensor. The probes have been designed to be used in a wide range of flow condition (speed and temperature) and the choice of these two parameters should be in accordance with a given flow condition. The first flow to be investigated with this probe was at the University of Manchester (Task F) with a low speed (0.9 to 3 m/s) and moderate temperature (up to 200 C). Calibration coefficients were determined for these conditions and responses of the velocity component and temperature measurements were examined for ranges of velocity, temperature and angular orientation. It was found that the probe is capable of measuring simultaneous turbulent velocity fluctuations at low speeds and moderate temperatures, i.e., for cases corresponding to the experiment at the University of Manchester, with an accuracy of order of one per cent. These conditions are considered to be very complex at low speed, due to mutual sensors influence and deviation of the cooling law.

The principal application of such hot-wire probes within the scope of this NERI project is to measure turbulence very close to heated walls. Thus, it is important to be able to extend the velocity range to below 0.9 m/s, if possible. Two approaches have been tested. The first is to reduce the sensor temperature for the case where the air temperature is expected to be low, as in the COPPEC facility for free or mixed convection flows of our partners at CEA Grenoble. For air temperatures of about 100 C, the approach utilized in the research mentioned above can be extended to speeds as low as 0.4 m/s. The other approach is to reduce the diameters of the velocity sensors to about one micron. Preliminary results show that the minimum speed can be reduced to 0.4 m/s at temperatures as high as 200 C.

Task F: Mixed convection, Prof. J. D. Jackson, U. Manchester Prof. Jackson and colleagues at Manchester conducted three experiments emphasizing buoyancy effects. The first obtained data on velocity in strongly heated air flow through a vertical heated pipe under conditions of mixed convection to determine the effects of buoyancy forces combined with property variation on local mean velocity and turbulent fluctuations. A second experiment provided data on the influence of the temperature dependence of fluid properties and buoyancy on heat transfer for the case of air flowing in a passage of annular cross section with a heated core. In the third experiment local mean velocities and turbulent fluctuations were measured using LDV in water flowing in a vertical passage of annular cross section with a heated core under conditions of mixed convection. Data were also obtained in a wide vertical channel flow with heating from one side.

Prof. Jackson and his colleagues operated a circular tube test facility with a vertical, heated section providing either specified distributions of heat flux or temperature along the tube with air flow in either the upward or downward direction. The combination of flow range and tube diameter allows measurements that are either buoyancy-affected or predominantly buoyancy-free. Their local Nusselt number data for mixed convection show very clear evidence of the importance of the thermal boundary condition on mixed convection heat transfer and that severe impairment of heat transfer can occur in a variety of ways. Using a Pitot-tube/thermocouple probe and the miniature multi-sensor probe of Profs. Vukoslavcevic and Wallace (Task E), they obtained measurements of velocity and temperature profiles in the radial direction near the exit for the upward flow case under buoyancy-influenced conditions at Reynolds numbers from 6,000 to 20,000.

A comprehensive programme of experiments to study the effects of property variations and buoyancy on local heat transfer with upward and downward gas flow has been completed using the annular facility. Some main results are as follows.

- o An empirical correlation, including the thermal entry region, has been obtained for heat transfer under conditions of negligible influence of buoyancy
- o The criterion for buoyancy influences to have a significant effect on heat transfer in the annulus has been found to be that the buoyancy parameter, $Bo^* = Gr^*/(Re^{3.425}\, Pr^{0.8})$, must be greater than about 5×10^{-7}. When the Re and Gr* are such that Bo* exceeds that value, differences are evident between the results for upward and downward flow under otherwise identical conditions.
- o For descending flow (the buoyancy-opposed case) Nusselt number is greater than for ascending flow (the buoyancy-aided case). This behaviour is similar to that found with circular tubes.
- o For descending flow the effectiveness of heat transfer is always enhanced in relation to that evaluated at the same value of Reynolds number and core-to-bulk-temperature ratio using the correlation equation for forced convection. The enhancement of heat transfer in the present buoyancy-opposed experiments using an annulus is less strong than for circular tubes.
- o For values of Bo* of about 10^{-3} the upward and downward flow data come together. The flow is buoyancy dominated. Under such conditions Nusselt number is almost independent of Reynolds number and varies with Grashof number as in heat transfer by free convection.

The third of the three investigations which Prof. Jackson and his colleagues at Manchester have contributed to this NERI project was a study of the influence of buoyancy on turbulent flow and heat transfer in the case of water flowing through a vertical passage of annular cross section having a uniformly heated core and adiabatic outer casing. Measurements of velocity, turbulence and heat transfer were made under conditions of forced convection (negligible buoyancy influence) and also mixed convection (covering a range of buoyancy influence from weak to very strong) with both upward and downward flows. The results provide direct confirmation of the mechanism by which turbulence production in heated vertical passages is either reduced or increased due to the mean flow field being distorted by the influence of buoyancy, causing turbulent diffusion to be either less effective or more effective and turbulent heat transfer to be either impaired or enhanced in relation to that for conditions of forced convection. Results of computational simulations of the experiments -- using a developing flow formulation which takes account of variable properties and buoyancy influence and incorporates the low-Reynolds-number k-ε turbulence model of Launder and Sharma -- were also compared directly with measurements of velocity, turbulence and heat transfer.

Recognition and technology transfer Prof. Shin-ichi Satake, Tokyo University of Science, received the 1999 JSME Outstanding Young Scientist award from the Japan Society of Mechanical Engineers, for his study on elucidation of characteristics of heat and fluid flow and construction of a data base in a turbulent pipe flow via DNS. Prof. Richard H. Pletcher, Iowa State U., was named a Life Fellow of American Society of Mechanical Engineers and Prof. Dr. Donald M. McEligot, INEEL, was selected to be a member of the US Scientific Committee for the 12th International Heat Transfer Conference held in Grenoble in August 2002. Prof. J. Derek Jackson was appointed as an Honorary Professor at the University of Manchester and an Honorary Visiting Professor at UMIST.

The Principal Investigator, Prof. Dr. Donald M. McEligot, received from the Idaho Academy of Science its annual award as their Distinguished Scientist for 2002. Prof. James M. Wallace of the University of Maryland has been elected to be the Vice-Chairman of the Fluid Dynamics Division of the American Physical Society; the incumbent of this position automatically is promoted to Chairman in a later year. Prof. Shin-ichi Satake of Toyama University was awarded a faculty position at the Tokyo University of Science.

At the 12th International Heat Transfer Conference, Prof. Tomoaki Kunugi of Kyoto University received a 2002 International SFT Award from the Société Francaise de Thermique to recognize and encourage his achievement in heat transfer research.

The ***key results*** of the present fundamental study are the publications and presentations to the thermal fluids community. Since August 1999, the project collaborators have had twenty-two archival papers published or in press, forty-nine conference presentations and twenty invited presentations relating to this collaborative NERI project. They also have fiftypublications and presentations on other topics. The list of these scholarly accomplishments follows this Executive Summary.

Accomplishments The overall accomplishments during the project may be summarized as follows:

- o GA identified areas of concern and provided support in planning required computational techniques and experiments
- o DNS of laminarizing and "subturbulent" gas flow completed, turbulent initiated, for circular tubes
- o First LES conducted for vertical mixed convection with property variation; channel code extended to circular tubes, annuli and ribbed annuli
- o MIR experiment for flow in complex reactor geometry (ribbed annuli) designed, fabricated, tested and employed for LDV measurements
- o Three- and four-sensor miniature probes developed, tested, calibrated and operated
- o Obtained data for mixed convection with property variation and arbitrary thermal boundary conditions in tubes, channels and annuli
- o Prof. S.-i. Satake selected as Outstanding Young Engineering Scientist by JSME
- o Prof. J. M. Wallace elected for succession to Chairman of the APS Fluid Dynamics Division
- o Prof. D. M. McEligot selected as 2002 Distinguished Scientist by Idaho Academy of Science

- o 22 technical publications, 49 presentations and 20 invited talks related to project
- o Brought fluid mechanics authorities and students into nuclear science community

Concluding remarks An overview of the project includes:

- o Assembled productive international team of recognized engineering scientists in fluid mechanics and heat transfer
- o New basic experiments and analyses accomplished to address operation of advanced gas-cooled reactors at full or partial loads and loss of forced reactor core cooling
- o New students and faculty brought into nuclear science and engineering community
- o Team and resulting accomplishments have benefited from contributions of experienced scientists from Japan, UK, France and Montenegro – has supplemented DoE investment
- o New fundamental results obtained in Large Eddy Simulation, Direct Numerical Simulation and measurements for complex flow geometries and mixed convection with property variation
- o Technical papers, presentations and reports completed and other recognition received

31 December 2002

Scholarly accomplishments of collaborators of NERI project 990254,

"Fundamental thermal fluid physics of high temperature flows in advanced reactor systems"

August 1999 to date

Awards

Prof. Shin-ichi Satake, Tokyo University of Science, received the 1999 JSME Outstanding Young Scientist award from the Japan Society of Mechanical Engineers, Tokyo, 6 April 2K, for study on elucidation of characteristics of heat and fluid flow and construction of data base in a turbulent pipe flow via DNS

The Principal Investigator, Prof. Dr. Donald M. McEligot, received from the Idaho Academy of Science its annual award as their Distinguished Scientist for 2002 "for his pioneering experiments and analyses in convective thermal fluid physics and for his technical leadership in developing the World's largest Matched-Index-of-Refraction system to study complex flow phenomena." Prof. James M. Wallace of the University of Maryland has been elected to be the Vice-Chairman of the Fluid Dynamics Division of the American Physical Society; the incumbent of this position automatically is promoted to Chairman in a later year.

At the International Heat Transfer Conference in Grenoble in August, Prof. Kunugi received a 2002 International SFT Award from the Société Francaise de Thermique to recognize and encourage his achievement in heat transfer research, based on his technical paper

> Kunugi, T., N. Saito, Y. Fujita and A. Serizawa, 2002. Direct numerical simulation of pool and forced convective flow boiling phenomena. *Heat Transfer 2002* (Proc., 12th International Heat Transfer Conf.).

Publications and presentations relating to collaborative NERI project

Archival publications

Ezato, K., A. M. Shehata, T. Kunugi and D. M. McEligot, 1999. Numerical predictions of transitional features of turbulent forced gas flows in circular tubes with strong heating. *J. Heat Transfer*, 121, pp. 546-555.

Jackson, J. D., with P. An and J. Li, 1999. Study of the cooling of a uniformly heat vertical tube by an ascending flow of air and a falling water film. *Int. J. Heat Fluid Flow*, 20, pp 268-279.

Jackson, J. D., with O. Buyukalaca and S. He, 1999. Heat transfer in a pipe under conditions of transient turbulent flow. *Int. J. Heat Fluid Flow*, 20, pp 115-127.

Sherif, S. A., and R. H. Pletcher, 1999. An analytical procedure for predicting the response of constant-temperature hot-wire and film anemometers. *Measurement*, 25, pp. 193-201.

Chidambaram, N., and R. H. Pletcher, 2000. A colocated-grid fully coupled algorithm for large eddy simulation of incompressible and compressible flows. *Numerical Heat Transfer, Part B: Fundamentals,* 37, pp. 1-23.

Jackson, J. D., and S. He, 2000. A study of turbulence under conditions of transient flow in a pipe. *J. Fluid Mech.*, 408, pp. 1-38, April.

Satake, S., T. Kunugi and R. Himeno, 2000. Reynolds number effect on turbulent structures in a pipe flow via DNS. *Adv. Turbulence VIII* (Ed.: C. Dopazo), Barcelona: CIMNE, pp. 663-666.

Vincont, J.-Y., S. Simoens, M. Ayrault and J. M. Wallace, 2000. Passive scalar dispersion in a turbulent boundary layer from a line source downstream of an obstacle on the wall. *J. Fluid Mech.*, 424, pp. 127-167.

Balaras, E., U. Piomelli and J. M. Wallace, 2000. Self-similar states in turbulent mixing layers. *J. Fluid Mech.*, 446, pp. 1-24.

Satake, S.-i., T. Kunugi, A. M. Shehata and D. M. McEligot, 2000. Direct numerical simulation on laminarization of turbulent forced gas flows in circular tubes with strong heating. *Int. J. Heat Fluid Flow*, 21, pp. 526-534.

Nishimura, M., S. Fujii, A. M. Shehata, T. Kunugi and D. M. McEligot, 2000. Prediction of forced gas flows in circular tubes at high heat fluxes accompanied by laminarization. *J. Nuc. Science and Technology*, 37, pp. 581-594..

Satake, S.-i., T. Kunugi and R. Himeno, 2000. High Reynolds number computation for turbulent heat transfer in a pipe flow. *Lecture Notes in Computer Science 1940, High Performance Computing* (Eds.: M. Valero et al.), Berlin: Springer-Verlag, pp. 514--523.

Kim, W. S., C. Talbot, B. J. Chung and J. D. Jackson, 2002. Mixed convection heat transfer with variable properties to air flowing through a vertical passage of annular cross section. *Trans., Institution of Chemical Engineers Part A, Chemical Engineering Research and Design,* 80, Part A, pp. 239-245.

Wu, T.-H., Z. Xu and J. D. Jackson, 2002. Mixed convection heat transfer to water flowing through a vertical passage of annular cross section. *Trans., Institution of Chemical Engineers Part A, Chemical Engineering Research and Design*, 80, Part A, pp. 246-251.

Wang, J., J. Li and J. D. Jackson, 2002. Mixed convection heat transfer to air flowing upwards through a vertical plane passage. *Trans., Institution of Chemical Engineers Part A, Chemical Engineering Research and Design,* 80, Part A, pp. 252-260.

Jackson, J. D., T. Wu and Z. Xu, 2002. Turbulent, buoyancy-influenced flow and heat transfer in a vertical annulus. *Heat Transfer 2002* (Proc., 12th International Heat Transfer Conf., Grenoble).

Jackson, J. D., and J. Li, 2002. Influences of buoyancy and thermal boundary conditions on heat transfer with naturally-induced flow in a tube. *Heat Transfer 2002* (Proc., 12th International Heat Transfer Conf., Grenoble).

Mikielewicz, D. P., A. M. Shehata, J. D. Jackson and D. M. McEligot, 2002. Temperature, velocity and mean turbulence structure in strongly-heated internal gas flows. Comparison of numerical predictions with data. *Int. J. Heat Mass Transfer* , 45, pp. 4333-4352.

Vukoslavcevic, P., and J. M. Wallace, 2002. The simultaneous measurement of velocity and temperature in heated turbulent air flow using thermal anemometry. *Meas. Sci. Technol.* 13, pp. 1615 – 1624.

Jackson, J. D., with S.He and Z. Xu, 2002. An experimental investigation of buoyancy-opposed wall jet flow. *Int. J. Heat Fluid Flow*, in press.

Petrovic, D., P. Vukoslavcevic and J. M. Wallace, 2003. The accuracy of turbulent velocity component measurements by multi-sensor hot-wire probes: a new approach to an old problem. *Exp. Fluids*, in press.

Dailey, L. D., N. Meng and R. H. Pletcher, 2003. Large eddy simulation of constant heat flux turbulent channel flow with property variations: Quasi-developed model and mean flow results. *Journal of Heat Transfer,* in press.

Conference publications and presentations

Satake, S.-i., T. Kunugi, A. M. Shehata and D. M. McEligot, 1999. Direct numerical simulation on laminarization of turbulent forced gas flows in circular tubes with strong heating. Proc., 1st International Symp. Turbulence Shear Flow Phenomena, Santa Barbara, Cal., September, pp. 475-480.

Jackson, J. D., with S. He and Z. Xu, 1999. Velocity, turbulence and temperature fields in buoyancy-opposed wall jet flow. 1st International Symposium on Turbulence Shear Flow Phenomena, Santa Barbara, Calif., 12 – 15 September.

Jackson, J. D., J. Li and P. An, 1999. The influence of thermal boundary conditions on mixed convection heat transfer in vertical tubes. Proc., 3rd Baltic Heat Transfer Conference, Sopot, Poland, Progress in Engineering Heat Transfer, pp 197-207, 22 – 25 September.

Avancha, V. R., and R. H. Pletcher, 2000. Large eddy simulation of the turbulent flow past a backward facing step. AIAA Paper 2000-0542, 38th AIAA Aerospace Sciences Meeting, January.

Satake, S., and T. Kunugi, 2000. Reynolds number effect on turbulent heat transfer in a pipe flow with uniform heat flux via DNS. Proc., 3rd Int. Sym. Turbulence, Heat and Mass Transfer, Nagoya, Japan, April, pp. 77-84.

Jackson, J. D., J. Li, J.C. Romero-Villaneuva and L. Aznar-Meseguer, 2000. Effects of non-uniform thermal boundary conditions on heat transfer by mixed convection to air flowing upwards in a vertical tube. Proc., 3rd Int. Symp. Turbulence, Heat and Mass Transfer, Nagoya, Japan, April, pp. 711-718.

Jackson, J. D., J. Li and S. He, 2000. CFD Modelling of flow in a vertical passage with interactions between turbulent mixed convection and thermal radiation. Computational Fluid Dynamics 2000 - CFD2K, Montreal, Canada, June.

Satake, S., T. Kunugi and R. Himeno, 2000. Reynolds number effect on turbulent structures in a pipe flow via DNS. 8th European Turbulence Conference, EUROMECH, Barcelona, Spain, June 27-30.

Vincont, J.-Y., S. Simoens, M. Ayrault and J. M. Wallace, 2000. Scalar flux measurements and models of a plume emitting from a wall line source downstream of an obstacle on the wall of a

turbulent boundary layer. 8th European Turbulence Conference, EUROMECH, Barcelona, Spain, June 27-30.

Balaras, E., U. Piomelli and J. M. Wallace, 2000. Large-eddy simulations of mixing layers. 8th European Turbulence Conference, EUROMECH, Barcelona, Spain, June 27-30.

Jackson, J. D., and J. Li, 2000. Influences of buoyancy on turbulence for conditions of heat transfer by combined forced and free convection to air in a vertical tube. 8th European Turbulence Conference, EUROMECH, Barcelona, Spain, June.

Jackson, J. D., and J. Li, 2000. Influences of buoyancy and thermal boundary conditions on heat transfer with naturally-induced flow. Technical Committee Meeting on Natural Circulation Data and Methods for Innovative Nuclear Power Plant Design, Vienna, Austria, July

Jackson, J. D., with T. Wu, S. He and B. Kuester, 2000. Influences of buoyancy on heat transfer and flow stability in an annulus with downward flow. 5th International Symposium on Heat Transfer, pp. 210-216, Beijing, China, August.

Jackson, J. D., with Z. Xu and S. He, 2000. Influences of counter-current flow on a buoyancy-opposed wall jet. 5th International Symposium on Heat Transfer, pp. 229-234, Beijing, China, August.

Jackson, J. D., J. Li, O. Kohlhase and D. Kramer, 2000. Combined effects of buoyancy and thermal boundary condition on convective heat transfer to air flowing downwards in non-uniformly heated vertical tube. 5th International Symposium on Heat Transfer, pp. 196-203, Beijing, China, August.

Jackson, J. D., and J. Li, 2000. Velocity and temperature profiles in buoyancy-influenced ascending pipeflow. ANS/ENS 2000 International Winter Meeting and Embedded Topical Meetings, Washington, D.C., USA, November. *Trans., Amer. Nuclear Soc.*, 83, pp 388-389, .

Jackson, J. D., and J. Li, 2000. On the mechanisms by which heat transfer is impaired in buoyancy-aided pipeflow. 53rd Annual Meeting, American Physical Society Division of Fluid Dynamics, Washington D.C., November. *Bull., Amer. Phys. Soc.*, 45 (No. 9), p. 173.

Vukoslavcevic, P., D. Petrovic and J. M. Wallace, 2000. The influence of velocity gradients on turbulent velocity field statistical properties. 53rd Annual Meeting, American Physical Society Division of Fluid Dynamics, Washington D.C., November. *Bull., Amer. Phys. Soc.*, 45 (No. 9), p. 140.

Meng, N., and R. H. Pletcher, 2000. Large eddy simulation of rotating channel flows with and without heat transfer. Proc. ASME Heat Transfer Division-2000, Vol. 5, pp. 213-224, ASME Int. Mech. Engr. Congress, November.

Lee, J. S., and R. H. Pletcher, 2001. Large eddy simulation of a turbulent channel flow with buoyancy effects. AIAA paper 2001-0431, 39th AIAA Aerospace Sciences Meeting, January

Jackson, J.D., J. Li, C. Talbot, W.S. Kim and B.J. Chung, 2001. On the mechanism of impairment of heat transfer in buoyancy-aided turbulent pipeflow. Turbulent Heat Transfer III, Anchorage, Alaska, USA, March.

Jackson, J. D., Z. Xu, T. Wu and S. He, 2001. Computational studies of buoyancy opposed mixed convection in a vertical annulus. American Nuclear Society 2001 Student Conference, Texas A&M University, Texas, USA, April.

Jackson, J. D., J. Li, J. Wang and P. Jiang, 2001. Studies of buoyancy-influenced convective heat transfer to air flowing in a vertical plane passage. American Nuclear Society 2001 Student Conference, Texas A&M University, Texas, USA, April.

Jackson, J. D., T. Wu, Z. Xu and S. He, 2001. Influence of buoyancy on mean flow and turbulence. American Nuclear Society 2001 Student Conference, Texas A&M University, Texas, USA, April.

Jackson, J. D., Z. Xu, T. Wu and S. He, 2001. Computational simulations of buoyancy-opposed mixed convection in a vertical passage of annular cross section. 9th Annual Conference of the CFD Society of Canada, Waterloo, Ontario, Canada, 27th – 29th May.

Jackson, J. D., J. Li, C. Talbot, W. S. Kim and B. J. Chung, 2001. Studies of variable property, buoyancy-influenced heat transfer in vertical passages with relevance to high temperature gas-cooled reactors. ASME paper NHTC2001-P1558, National Heat Transfer Conf., Anaheim, June.

Lee, J. S., and R. H. Pletcher, 2001. Large eddy simulation of variable property turbulent flow in a vertical channel with buoyancy effects and heat transfer. ASME paper NHTC01-1556, 35th National Heat Transfer Conference, Anaheim, June.

Jackson, J. D., 2001. Some striking features of heat transfer with fluids at pressures and temperatures near the critical point. Int. Conf. Energy Conversion and Appl. (ICECA 2001), Wuhan, China, June.

Jackson, J. D., and S. He, 2001. Wall shear stress in accelerating pipe flows. International Conference on Energy Conversion and Application 2001, Wuhan, China, June.

Jackson, J. D., T. Wu, Z. Xu and S. He, 2001. Turbulent heat transfer under conditions of buoyancy-opposed mixed convection in an annulus. International Conference on Energy Conversion and Application 2001, Wuhan, China, June.

Wu, T.-H., Z. Xu, S. He and J. D. Jackson, 2001. Influence of buoyancy on mean flow and turbulence under conditions of mixed convection in an annulus. 2nd International Symposium on Turbulence and Shear Flow Phenomena, Stockholm, Sweden, June.

Jackson, J. D., T.-H. Wu and Z. Xu, 2001. Mixed convection heat transfer to water flowing through a vertical passage of annular cross section. 7th UK National Conference on Heat Transfer, Nottingham, UK, 11th-12th September.

Jackson, J. D., J. Li and J. Wang, 2001. Buoyancy-influenced convective heat transfer to air flowing upwards in a plane passage. 7th UK National Conference on Heat Transfer, Nottingham, UK, 11th-12th September.

Jackson, J. D., W.S. Kim, C. Talbot and B.J. Chung, 2001. Variable property, mixed convection heat transfer to air flowing in a vertical annulus. 7th UK National Conference on Heat Transfer, Nottingham, UK, 11th-12th September.

Jackson, J. D., Z. Xu and T. Wu, 2001. Effects of buoyancy on the flow in a vertical passage of annular cross section with a heated core. 9th International Conference on Laser Anemometry Advances and Application, Limerick, Ireland, 12th-14th September.

Shenoy, A. S., L. L. Parme and J. M. Bolin, 2001. Passive safety design of the GT-MHR. American Nuclear Society Winter Meeting, Reno, USA, November.

McEligot, D. M., K. G. Condie, T. D. Foust, G. E. McCreery, R. J. Pink, D. E. Stacy, A. Shenoy, G. Baccaglini, R.H. Pletcher, J.M. Wallace, J. D. Jackson, T. Kunugi, S.-i. Satake and P. Vukoslavcevic, 2001. Fundamental thermal fluid physics of flows in advanced reactor systems. American Nuclear Society Winter Meeting, Reno, USA, November. *Trans., ANS,* 85, pp. 37-38.

Jackson, J. D., Z. Xu and T. Wu, 2001. Measurements of velocity, turbulence and heat transfer in buoyancy-aided flow. APS Division of Fluid Dynamics, 54th Annual Meeting, San Diego, USA, November. *Bull., Amer. Phys. Soc.*, 46 (No. 10), p. 74.

Vukoslavcevic, P., and J. M. Wallace, 2001. A probe to simultaneously measure the velocity and temperature fields in strongly heated turbulent flows. APS Division of Fluid Dynamics, 54th Annual Meeting, San Diego, USA, November. *Bull., Amer. Phys. Soc.*, 46 (No. 10), p. 89.

Jackson, J. D., and W.S. Kim, 2002. Computational modelling of mixed convection experiments – gas cooled reactors. Universities Nuclear Technology Forum, Lancaster, UK, 10 – 12 April.

Jackson, J. D., and Z. Xu, 2002. Measurements of buoyancy-influenced turbulent flow for validating CFD codes used in nuclear reactor applications. Universities Nuclear Technology Forum, Lancaster, UK, 10 – 12 April.

Jackson, J. D., J. Li and J. Wang, 2002. The effects of buoyancy on turbulent flow and heat transfer in a vertical plane passage. Euromech 9th European Turbulence Conference, Southampton, UK, 2-5 July.

Satake, S.-i., T. Kunugi, A. M. Shehata and D. M. McEligot, 2002. DNS of forced gas flows in circular tubes at various heating rates. Presentation OFS 12, 12th International Heat Transfer Conference, Grenoble, August .

Jackson, J. D., 2002. Consideration of the heat transfer properties of supercritical pressure water in relation to its use as a coolant in advanced nuclear reactors. 13 th Pacific Basin Nuclear Conference, Shenzhen, China, 21 - 25 October.

Xu, X., J. S. Lee and R. H. Pletcher, 2002. Cartesian-based finite volume formulation for LES of mixed convection in a vertical turbulent pipe flow. Paper IMECE2002-HT-32748, ASME International Mechanical Engineering Congress, New Orleans, November.

Lee, J. S., X. Xu and R. H. Pletcher, 2002. Large eddy simulation of mixed convection in a vertical annular pipe flow. Paper IMECE2002-HT-32746, ASME International Mechanical Engineering Congress, New Orleans, November.

McCreery, G. E., T. D. Foust, D. M. McEligot, K. G. Condie and R. J. Pink, 2002. Measurements and code comparisons for advanced gas reactor coolant channels containing spacer ribs. Paper IMECE2002-33597, ASME International Mechanical Engineering Congress, New Orleans, November.

McCreery, G. E., R. J. Pink and D. M. McEligot, 2002. Flow visualization in an axisymmetric Matched-Index-of-Refraction apparatus compared with a rectangular cross-section representation. Heat Transfer Visualization session, ASME International Mechanical Engineering Congress, New Orleans, November.

Vukoslavcevic, P., and J. M. Wallace, 2002. A method to determine the time constant of a cold-wire temperature sensor. 55th Annual Meeting, American Physical Society Division of Fluid Dynamics, Dallas, November. *Bull., Amer. Phys. Soc.*, 47 (No. 10), p. 148.

Invited presentations

Kunugi, T., 1999. MARS for multiphase calculation. 8th Int. Symp. Computational Fluid Dynamics, 5-10 September, Bremen, Germany.

Jackson, J. D., J. Li and P. An, 1999. The influence of thermal boundary conditions on mixed convection heat transfer in vertical tubes. 3rd Baltic Heat Transfer Conference, Sopot, Poland, 22-25 September.

Pletcher, R. H., 2000. Large-eddy simulation of flows with heat transfer. Mechanical Engineering Seminar Series, Louisiana State University, February.

Kunugi, T., S. Satake and A. Sagara, 2000. Direct numerical simulation of turbulent free-surface high Prandtl number fluid flows in fusion reactors. 13th International Symposium on Heavy Ion Inertial Fusion, 13-17 March, San Diego.

McEligot, D. M., 2000. Strongly-heated internal gas flows. Tohoku U., Sendai, April

McEligot, D. M., 2000. Fundamental thermal fluid physics of high temperature flows in advanced reactor systems. JAERI, Oarai, April.

McEligot, D. M., J. D. Jackson, A. S. Shenoy and G. Baccaglini, 2000. Fundamental thermal fluid physics of high temperature flows in advanced reactor systems. Workshop on the Nuclear Energy Research Initiative (NERI), Amer. Nuclear Soc. Annual Meeting, San Diego, Cal., June, INEEL/CON-2000-00438.

Jackson, J. D., and J.Li, 2000. Influences of buoyancy and thermal boundary conditions on heat transfer with naturally-induced flow. Technical Committee Meeting on Natural Circulation Data and Methods for Innovative Nuclear Power Plant Design, Vienna, Austria, July.

Becker, S., K. G. Condie, C. M. Stoots and McEligot, D. M., 2000. Effect of a roughness element on development of the viscous layer for a turbulent boundary layer. Minnowbrook III Workshop on Boundary Layer Transition and Unsteady Aspects of Turbomachinery Flows, Syracuse Univ. Conf. Center, Blue Mt. Lake, N. Y., August.

Jackson, J. D., 2000. Studies of the influences of buoyancy on turbulence and heat transfer in vertical passages. 5th International Symposium on Heat Transfer, Beijing, China, August.

McEligot, D. M., 2000. Fundamental thermal fluid physics of high temperature gas flows in advanced reactors. Fachgebiet Strömungslehre und Aerodynamik, Technische Universität Darmstadt, Germany, October.

McEligot, D. M., 2000. Fundamental thermal fluid physics of high temperature gas flows in advanced nuclear reactors. Institut für Kernenergetik und Energiesysteme, Uni. Stuttgart, Germany, October.

McEligot, D. M., 2000. Development of Reynolds stresses in the viscous layer downstream of a roughness element in a transitioning boundary layer. Institut für Nichtlineare Dynamik, Georg-August-Universität Göttingen, Germany, October.

McEligot, D. M., 2000. Recent studies with the World's largest Matched-Index-of-Refraction flow system. Department of Applied Physics, Delft University of Technology, Delft, Netherlands, November.

Jackson, J. D., J. Li, C. Talbot, W.S. Kim and B.J. Chung, 2001. On the mechanism of impairment of heat transfer in buoyancy-aided turbulent pipeflow. Turbulent Heat Transfer III, Anchorage, Alaska, USA, March.

McEligot, D. M., 2001. Fundamental thermal fluid physics of high temperature flows in advanced reactor systems.
CEA, Saclay, France, May
CEA, Grenoble, France, May

McEligot, D. M., 2001. Signatures of coherent structures in the viscous layers of converging turbulent flows. Graduietenkolleg "Strömungsinstabilitäten und turbulenz," Georg-August-Universität Göttingen, Germany, May.

Jackson, J. D., 2001. Some striking features of heat transfer with fluids at pressures and temperatures near the critical point. Int. Conf. Energy Conversion and Appl. (ICECA 2001), Wuhan, China, June

Jackson, J. D., 2001. Applied research and formation in nuclear engineering within the UK University system. Panel Discussion on Applied Research and Formation in the Nuclear Field International Conference on E. Fermi and Nuclear Energy, University of Pisa, Italy, 15th -16th October.

McEligot, D. M., 2001. Development of Reynolds stresses in the viscous layer downstream of a roughness element in a transitioning boundary layer. Univ. Wyoming, 25 October.

Jackson, J. D., 2002. The Naturally Induced Cooling Experiment (NICE). European Union Concerted Action Project SCACEX (Scaling of Containment Experiments) Kick-off meeting, Becker Technologies GmBH, Eschborn, Frankfurt, Germany, 5-6 February.

McEligot, D. M., 2002. Development of the viscous layer downstream of a roughness element in a transitioning boundary layer. Boise State Univ., Boise, Idaho, 19 April.

McEligot, D. M., 2002. Recent studies with the World's largest Matched-Index-of-Refraction flow system.
Lehrstuhl für Strömungsmechanik, Uni. Erlangen, Germany, 26 August
Univ. Limerick, Limerick, Ireland, 2 September

Jackson, J. D., 2002. Influences of buoyancy on turbulent flow and convective heat transfer in vertical passages. Joint MU/RGU research meeting, Robert Gordon University, Aberdeen, Scotland, September.

Jackson, J. D., 2002. Consideration of the heat transfer properties of supercritical pressure water in relation to its use as a coolant in advanced nuclear reactors. 13th Pacific Basin Nuclear Conference, Shenzhen, China, 21 - 25 October.

Technical papers in preparation

Moro, J.-P., and P. Vukoslavcevic, 2003. A method to calibrate a hot-wire X-array for applications in very low-speed flows of variable temperature.

Jackson, J. D., with J. Wang and J.-k. Li, 2003. Influence of buoyancy on turbulent air flow in a vertical plane passage. In preparation for 3rd International Symposium on Turbulence and Shear Flow Phenomena (TSFP-3), Sendai, Japan, 25–27 June.

McCreery, G. E., R. J. Pink, K. G. Condie and D. M. McEligot, 2003. Fluid dynamics of ribbed annuli. In preparation for NuReTH-10, Seoul, October.

Jackson, J. D., J. Li and J. Wang, 2003. Studies of heat transfer having relevance to nuclear reactor containment cooling by buoyancy-driven airflow. In preparation for NuReTH-10, Seoul, October.

Kim, W. S., J. D. Jackson and S. He, 2003. Variable property buoyancy-influenced heat transfer to air flowing i a vertical passage of annular cross-section. In preparation for NuReTH-10, Seoul, October.

Other recognition

Prof. Richard H. Pletcher, Iowa State U., named Life Fellow of American Society of Mechanical Engineers, 2001.

Prof. Dr. Donald M. McEligot, INEEL, promoted to INEEL Science and Engineering Fellow, highest technical grade at INEEL, 2000.

Prof. James M. Wallace, Univ. Maryland, Chairman of the Organizing Committee for the Fluid Dynamics meeting of the American Physical Society, Washington, D. C., November 2K.

Prof. Dr. Donald M. McEligot, INEEL, was selected to be a member of the US Scientific Committee for the 12th International Heat Transfer Conference to be held in Grenoble in August 2002.

Prof. Tomoaki Kunugi, Kyoto U., Member of Organizing Committee for 2nd Japan-Korea Symposium on Nuclear Thermal Hydraulics and Safety, Fukuoka, Japan, 15-18 October 2000.

Dr. Arkal S. Shenoy, General Atomics, Assistant Technical Program Chair for Topical Meeting on Advanced Nuclear Installations Safety at American Nuclear Society meeting, San Diego, June 2K.

Prof. R. H. Pletcher, Iowa State U., Chairman, session for Symposium on Numerical Simulation of Turbulent Flow and Heat Transfer at the 1999 International Mechanical Engineering Congress and Exposition, November 1999.

Prof. R. H. Pletcher, Iowa State U., Chairman, session on LES/DNS at the 38th AIAA Aerospace Sciences Meeting, January 2K.

Prof. J. Derek Jackson, Univ. Manchester (UK), Chairman, Keynote session, 3rd Int. Symposium on Turbulence, Heat and Mass Transfer, Nagoya, April 2K.

Prof. Dr. Donald M. McEligot, INEEL, Chairman, session on mixed convection, 3rd Int. Symposium on Turbulence, Heat and Mass Transfer, Nagoya, April 2K.

Prof. Dr. Donald M. McEligot, INEEL, was elected to the Executive Committee (4 year term) of the Aerospace Nuclear Science and Technology Technical Group of the American Nuclear Society, 2001.

Prof. T. Kunugi, Kyoto U., Steering committee member
Thermal Engineering Division, JSME, April 1999 - March 2000.
Power and Energy System Division, JSME, April 2000 - March 2001.

Prof. T. Kunugi, Kyoto U., Research specialist committee member
Integrated Energy Systems for Thermonuclear Fusion, AESJ, April 1999 - March 2001.
Advanced Thermal Systems for Fusion Energy Extraction, AESJ, April 1999 - March 2001.

Prof. Dr. Donald M. McEligot, INEEL, Member, Heat Transfer Committee, Gas Turbine Division, ASME

Prof. Dr. Donald M. McEligot, INEEL, was selected to be a member of the US Scientific Committee for the 12th International Heat Transfer Conference held in Grenoble in August 2002.

Prof. Shin-ichi Satake of Toyama University was awarded a faculty position at the Tokyo University of Science, April 2002 .

Prof. J. Derek Jackson was appointed as
Honorary Professor at the University of Manchester
Guest Professor, Tsinghua Univ., Beijing, China
Guest Professor, Huazhong Univ. Science and Technology, Wuhan, China
Honorary Visiting Professor, UMIST, December 2002

Bernard, P. S., and J. M. Wallace, 2002. *Turbulent flow: Analysis, measurement and prediction.* New York: Wiley.

Other publications and presentations

McEligot, D. M., 1999. Maximum allowable heat flux for a submerged horizontal tube bundle. *Convective Flow and Pool Boiling* (Ed.: F. Mayinger and M. Lehner), Philadelphia: Taylor and Francis, pp. 413-417.

McCreery, G. E., K. G. Condie, J. C. Crepeau, R. Clarksean, Y. G. Guzennec, R. S. Brodkey and D. M. McEligot, 1999. Flow visualization and velocity measurements in a model fuel storage canister. Global '99 - International Conference on Future Energy Systems, Jackson, Wyo., August.

Kunugi, T., 1999. MARS for multiphase calculation. Proc., 8th Int. Symp. Computational Fluid Dynamics, 5-10 September, Bremen, Germany.

Becker, S., K. G. Condie, C. M. Stoots and D. M. McEligot, 1999. Reynolds stress development in the viscous layer of a transitional boundary layer. IUTAM Symposium on Laminar-Turbulent Transition, Sedona, Ariz., September.

Kunugi, T., S. Satake and Y. Ose, 1999. Direct numerical simulation of turbulent free surface flow. Proc., 1st Int. Symp. Turb. and Shear Flow Phenomena, Santa Barbara, 12-15 September, pp. 621-626.

Jackson, J. D., with X. Cheng, P. Bazin, P. Cornet, D. Hittner, J. Lopez Jimenez, A. Naviglio, F. Oriolo and H. Plank, 1999. Experimental data base for containment thermalhydraulic analysis. NURETH 9 Conference, San Francisco, 3-8 October.

Jackson, J. D., with X. Cheng, J. Lopez Jimenez, P. Bazin, A. Naviglio, F. Oriolo, H. Plank, D. Hittner and P. Cornet, 1999. Common experimental data base for the development of physical models and correlatons for thermal-hydraulic containment analysis (DABASCO). European Commission FISA 99 Conference, Luxembourg, November.

Jackson, J. D., with D. Tenchine, M. Berthoux, J.U. Knebel, P. An, A. Naviglio and G. Caruso, 1999. Thermalhydraulics of passive decay heat removal systems (POOLTHY). European Commission FISA 99 Conference, Luxembourg, November.

Jackson, J. D., and J.C. Hatchman, 1999. Measurement of the thermal resistance of paint coatings using a simple transient cooling method. *Proc., Inst. Mechanical Engineers,* 213 Part A, pp 45-56, December.

Kunugi, T., S. Satake and A. Sagara, 2000. Direct numerical simulation of turbulent free-surface high Prandtl number fluid flows in fusion reactors. Proc., 13th International Symposium on Heavy Ion Inertial Fusion, HIF2000, 13-17 March, San Diego, 2000. To appear in *Nuclear Instruments and Methods in Physics Research, Section A.*

Kunugi, T., S. Satake and Y. Ose, 2000. Direct numerical simulation of carbon-dioxide gas absorption caused by turbulent free surface flow. 3rd Int. Sym. on Turbulence, Heat and Mass Transfer, Nagoya, Japan, April, pp. 225-232. Accepted for *Int. J. Heat and Fluid Flow.*

Kunugi, T., 2000. MARS for multiphase calculation. *Computational Fluid Dynamics Journal,* 9, No.1, April, pp. - .

Jackson, J. D., P. An, A. Reinert and M. Ahmadinejad, 2000. Effects of non-condensible gas on the condensation of steam. IAEA Technical Committee Meeting on Experimental Tests and Qualification of Analytical Methods for Thermohydraulic Phenomena of Advanced Water Cooled Reactors, Villigen, Switzerland, International Atomic Energy Agency, Vienna, IAEA-TECDON-1149, pp. 53-82, May.

Jackson, J. D., C.L. Zhao, S. Doerffer, J.E. Byrne and H. Falaki, 2000. Effect of pool turbulence on direct contact condensation at a steam/water interface. IAEA Technical Committee Meeting on Experimental Tests and Qualification of Analytical Methods to Address Thermohydraulic Phenomena in Advanced Water Cooled Reactors, Villigen, Switzerland, International Atomic Energy Agency, Vienna, IAEA-TECDON-1149, pp. 13-20, May.

Kunugi T., and S. Satake, 2000. Direct numerical simulation of turbulent free-surface flow with carbon-dioxide gas absorption . Fourth Int. Symp. Gas Transfer at Water Surfaces, 5-8 June, Eden Roc Resort & Spa, Miami Beach.

McEligot, D. M., 2000. The unique INEEL Matched-Index-of-Refraction flow system for CFD validation. 2000 Scientific Conf. on Obscuration and Aerosol Research, Aberdeen Proving Ground, Md., June.

McEligot, D. M., 2000. The unique INEEL Matched-Index-of-Refraction flow system (poster). 2000 Scientific Conf. on Obscuration and Aerosol Research, Aberdeen Proving Ground, Md., June.

Yamamoto, Y., T. Kunugi and A. Serizawa, 2000. Turbulence statistics and scalar transport in an open-channel flow. 8th European Turbulence Conference, EUROMECH, Barcelona, Spain, 27-30 June. Also *Adv. Turbulence VIII* (Ed.: C. Dopazo), pp. 231-234.

Becker, S., C. M. Stoots, H. Lienhart, D. M. McEligot and F. Durst, 2000. LDA measurements of transitional flows in a large refractive-index-matched flow facility. 10th International Symp. on Applications of Laser Techniques to Fluid Mechanics, Lisbon, July.

Becker, S., K. G. Condie, C. M. Stoots and D. M. McEligot, 2000. Reynolds stress development in the viscous layer of a transitional boundary layer. *Laminar-Turbulent Transition* (Ed: H. F. Fasel and W. S. Saric). Berlin: Springer, pp. 327-332.

Jackson, J. D., with Z. Xu and S. He, 2000. Influences of counter-current flow on a buoyancy-opposed wall jet. 5th International Symposium on Heat Transfer, Beijing, China, pp 229-234, August.

Jackson, J. D., 2000. Studies of the influences of buoyancy on turbulence and heat transfer in vertical passages. 5th International Symposium on Heat Transfer, Beijing, China, pp 111-132, August.

Becker, S., K. G. Condie, C. M. Stoots and McEligot, D. M., 2000. Reynolds stress development in a transitioning boundary layer. Amer. Physical Soc. Fluid Dynamics meeting, Washington, November. *Bull., Amer. Phys. Soc.*, 45 (No. 9), p. 35.

Kunugi, T., Y. Yamamoto and S.-i. Satake, 2000. Coherent structure of wind driven turbulent free surface flow. Amer. Physical Soc. Fluid Dynamics meeting, Washington, November. *Bull., Amer. Phys. Soc.*, 45 (No. 9), pp. 79-80.

Li, N., J.-Y. Vincont and J. M. Wallace, 2000. Scalar transport in a turbulent mixing layer. Amer. Physical Soc. Fluid Dynamics meeting, Washington, November. *Bull., Amer. Phys. Soc.*, 45 (No. 9), pp. 164-165.

Jackson, J. D., with X. Cheng, J. Lopez Jimenez, P. Bazin, A. Naviglio, F. Oriolo, H. Plank, D. Hittner and P. Cornet, 2000. Common experimental data base for the development of physical models and correlatons for thermal-hydraulic containment analysis (DABASCO). EUR 19532 EN, pp. 490-499.

Jackson, J. D., with D. Tenchine, M. Berthoux, J.U. Knebel, P. An, A. Naviglio and G. Caruso, 2000. Thermalhydraulics of passive decay heat removal systems (POOLTHY). EUR 19532 EN, pp. 711-720.

Jackson, J. D., with X. Cheng, P. Bazin, P. Cornet, D. Hittner, J. Lopez Jimenez, A. Naviglio, F. Oriolo and H. Plank, 2001. Experimental data base for containment thermalhydraulic analysis. *J. Nuclear Eng. Design*, 204, pp. 267-284.

Ichimiya, K., S. Takema, S. Morimoto, T. Kunugi and N. Akino, 2001. Movement of impingement heat transfer by a single circular jet with a confined wall. *Int. J. Heat Mass Transfer*, 44, pp. 3095-3102.

Becker, S., C. M. Stoots, H. Lienhart, D. M. McEligot and F. Durst, 2001. Refractive-index-matched LDV technique for investigations of laminar-to-turbulent boundary-layer transition. 2nd International Symp. Turb. Shear Flow Phenomena, Stockholm, Sweden, June.

Avancha, R., and R. H. Pletcher, 2001. Large eddy simulation of the turbulent flow past a backward facing step with heat transfer and property variations. Second International Symposium on Turbulence and Shear Flow Phenomena, Stockholm, June.

Stoots, C. M., S. Becker, K. G. Condie, F. Durst and D. M. McEligot, 2001. A large-scale matched index of refraction flow facility for LDA studies around complex geometries. *Exp. Fluids*, 30, pp. 391-398.

Avancha, R., and R. H. Pletcher, 2001. Large eddy simulation of the turbulent flow past a backward facing step. Third AFOSR International Conference on DNS/LES, Arlington, Texas, August.

Meng, N., and R. H. Pletcher, 2001. Large eddy simulation of a rib-roughened turbulent channel flow with heat transfer and property variations. Third AFOSR International Conference on DNS/LES, Arlington, Texas, August.

Jackson, J. D., 2001. Applied research and formation in nuclear engineering within the UK University system. Panel Discussion on Applied Research and Formation in the Nuclear Field, International Conference on E. Fermi and Nuclear Energy, University of Pisa, Italy, 15 -16 October .

Simoens, S., M. Ayrault and J. M. Wallace, 2002. The velocity field in the cavity between two square two-dimensional obstacles at the wall of a turbulent boundary layer. APS Division of Fluid Dynamics, 54th Annual Meeting, San Diego, USA, November. *Bull., Amer. Phys. Soc.*, 46 (No. 10), pp. 62-63.

Ning, L., J. M. Wallace and E. Balaras, 2001. Scalar transport and vortex dynamics in a turbulent mixing layer. APS Division of Fluid Dynamics, 54th Annual Meeting, San Diego, USA, November. *Bull., Amer. Phys. Soc.*, 46 (No. 10), pp. 169-170.

Avancha, R. V. R., and R. H. Pletcher, 2002. Large eddy simulation of the turbulent flow past a backward-facing step with heat transfer and property variations. *Int. J. Heat Fluid Flow*, 23, pp. 601-614.

Becker, S., C. M. Stoots, K. G. Condie, F. Durst and D. M. McEligot, 2002. LDA-measurements of transitional flows induced by a square rib. *J. Fluids Engineering*, 124, pp. 108-117.

Jackson, J. D., and J. Wang, 2002. Experimental study of combined radiative and convective heat transfer with relevance reactor pressure vessel cooling. Universities Nuclear Technology Forum, Lancaster, UK, 10 – 12 April.

Jackson, J. D., T.J. Lu, Z. Xu and C.Y. Zhao, 2002. Measurements of effective thermal conductivity of new materials. Universities Nuclear Technology Forum, Lancaster, UK, 10 – 12 April.

Clarksean, R. L., J. C. Crepeau and D. M. McEligot, 2002. Computational modeling of the fluid flow in a representative spent nuclear fuel canister. Annual Meeting, Amer. Nuclear Soc., Hollywood, Fla., June.

Satake, S., T. Kunugi and S. Smolentsev, 2002. DNS of MHD turbulent free surface flow. *Trans. JSME B*, 68, No. 667.

Jackson, J. D., 2002. Report on Work Package 2: Turbulent convective and radiative heat transfer. 2nd Meeting of the European Union Concerted Action Project "Scaling of Containment Experiments" (SCACEX) at Rez, Prague, 3-5 July.

Lee, J. S., and R. H. Pletcher, 2002. Large eddy simulation of the effects of rotation on heat transfer in a ribbed channel. *Heat Transfer 2002* (Proc., 12th International Heat Transfer Conf., Grenoble).

McCreery, G. E., K. G. Condie, R. L. Clarksean and D. M. McEligot, 2002. Convective processes in spent nuclear fuel canisters. *Heat Transfer 2002* (Proc., Twelfth International Heat Transfer Conference, Grenoble, August), Paper IHTC-1267, pp. 663-668.

Jackson, J. D., P. An and M. Ahmadinejad, 2002. Effects of non-condensible gas on the condensation of steam. *Heat Transfer 2002* (Proc., 12th International Heat Transfer Conf., Grenoble).

Kunugi, T., N. Saito, Y. Fujita and A. Serizawa, 2002. Direct numerical simulation of pool and forced convective flow boiling phenomena. *Heat Transfer 2002* (Proc., 12th International Heat Transfer Conf., Grenoble).

Knight, K. J., C. Barringer, J. M. Berkoe, G. E. McCreery, R. J. Pink and D. M. McEligot, 2002. Physical and computational modeling for chemical and biological weapons airflow applications. Paper IMECE 2002-34451 ASME International Mechanical Engineering Congress , New Orleans, November.

Simoens, S., M. Ayrault and J. M. Wallace, 2002. Scalar transport in the cavity between two square two-dimensional obstacles at the wall of a turbulent boundary layer. 55th Annual Meeting, American Physical Society Division of Fluid Dynamics, Dallas, November. *Bull., Amer. Phys. Soc.*, 47 (No. 10), pp. 165-166.

Fundamental Thermal Fluid Physics of High Temperature Flows in Advanced Reactor Systems

D. M. McEligot (INEEL), K. G. Condie (INEEL), T. D. Foust (INEEL), J. D. Jackson (U. Manchester), T. Kunugi (Kyoto U.), G. E. McCreery (INEEL), R. J. Pink (INEEL), R. H. Pletcher (Iowa State), S.-I. Satake (Toyama U.), A. Shenoy (General Atomics), D. E. Stacey (INEEL), P. Vukoslavcevic (U. Montenegro) and J. M. Wallace (U. Maryland)

Introduction

Background The ultimate **goal** of the study is the improvement of predictive methods for safety analyses and design of advanced reactors for higher efficiency and enhanced safety and for deployable reactors for electrical power generation, process heat utilization and hydrogen generation. While key applications would be advanced gas-cooled reactors (AGCRs) using the closed Brayton cycle (CBC) for higher efficiency (such as the proposed Gas Turbine - Modular Helium Reactor (GT-MHR) of General Atomics [Neylan and Simon, 1996]), results of the proposed research should also be valuable in reactor systems with supercritical flow or superheated vapors, e.g., steam. Higher efficiency leads to lower cost/kwh and reduces life-cycle impacts of radioactive waste (by reducing waste/kwh). The outcome will also be useful for some space power and propulsion concepts and for some fusion reactor concepts as side benefits, but they are not the thrusts of the investigation. The **objective** of the project ***is to provide fundamental thermal fluid physics knowledge and measurements*** necessary for the development of the improved methods for the applications.

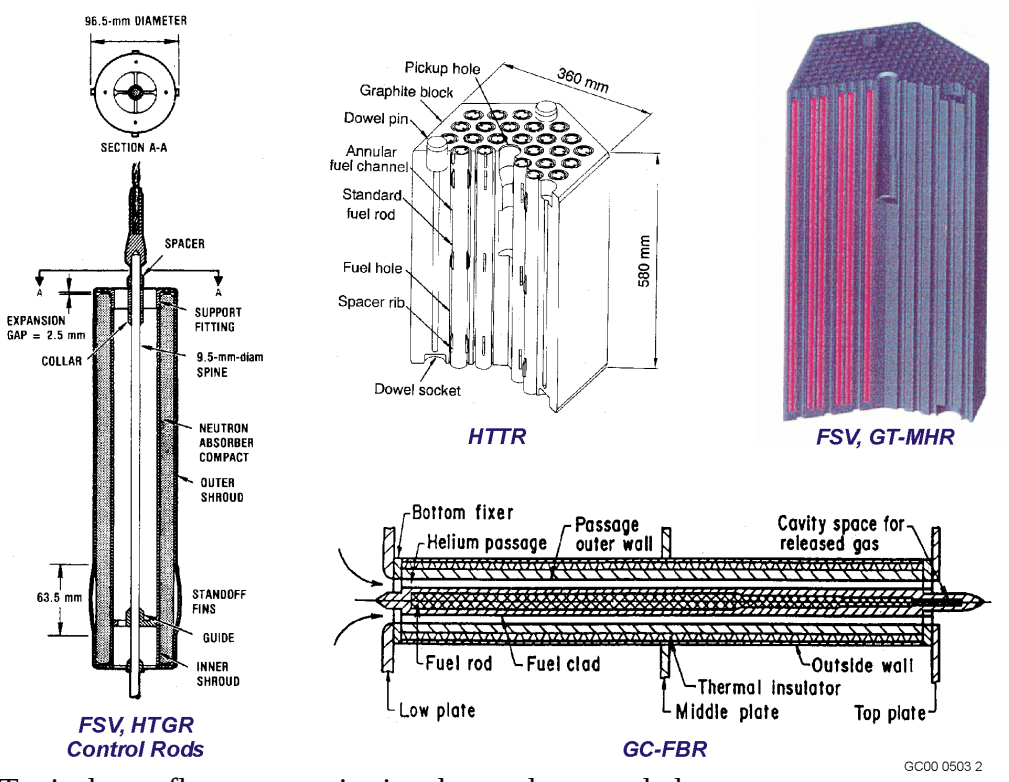

Fig. I-1. Typical core flow geometries in advanced gas-cooled reactors.

Advanced gas reactors and combined cycle concepts offer the potential of high thermal efficiency and enhanced safety [Kugeler, 1996]. Gas-cooled reactors are also ideal for use in small deployable systems; historically, one of the first GCRs was an Army reactor for this purpose, the ML-1 at NRTS (now INEEL). In addition to improving efficiency, AGCR-CBCs enhance system safety by removing steam and water components. Safety is inherently enhanced by avoidance of the steam cycle: no flashing or boiling is possible, there are no neutronic reactions with the coolant, no chemical reactions between coolant and fuel and no corrosive corrosion products. Passive safety features include a negative coefficient of reactivity, core power and power density, passive reactor cavity cooling systems and below-grade containment for protection from aircraft and terrorist actions.

General effects of strong heating of a gas **are variation of the transport properties**, reduction of density causing **acceleration** of the flow in the central core, **and** - in some cases - significant **buoyancy forces**. The ranges of temperatures and, hence, property variation that should be considered for safety analyses in some applications are as follows:

	Temperature range (K)			Property variation		
	T_{in}	$T_{wall,max}$	ρ/ρ_i	V/V_I	k/k_i	c_p/c_{pi}
GT-MHR	573	1873	0.31	3.3	2.6	1.1
HTTR	673	1873	0.36	2.8	2.3	1.1
GC-FBR	723	1323	0.55	1.8	1.6	1.06
Fusion blanket	563	973	0.08	12.5	0.17	5.1

P = 25 MPa

As a single example of consequent application problems --> general-purpose commercial Computational Thermal Fluid Dynamic (CTFD) codes do not necessarily provide accurate or conservative predictions for these conditions [McEligot, Shehata and Kunugi, 1998]. While a knowledgeable turbulence modeler could adjust a model so that the predictions agree with the data, the results would not likely be useful beyond the particular situation -- and the normal design engineer does not possess that level of expertise. Growth of the internal thermal boundary layer leads to readjustment of any previously fully-developed turbulent momentum profile. No truly fully-established conditions are reached because the temperature rises -- leading, in turn, to continuous axial and radial variation of properties such as the gas viscosity. To advance technology for gas-cooled reactors, the High Temperature Engineering Test Reactor (HTTR) is under development by the Japan Atomic Energy Research Institute; first criticality was attained on 10 November 1998 [Ogawa, 1998]. In an application such as the HTTR (or reduction of flow scenarios in other plants) another complication arises. To obtain high outlet temperatures, design gas flow rates are kept relatively low. For example, at the exit of the HTTR cooling channels, the Reynolds number is about 3500. In this range the heat transfer parameters may appear to correspond to turbulent flow or to laminar flow or to an intermediate behavior, depending on the heating rate [Bankston, 1970], with consequent differences in their magnitudes.

Some typical core flow geometries are demonstrated in Figure I-1. As just ***one example***, the HTTR is typical of the designs which can be developed in order to obtain high gas outlet temperatures. High pressure helium flows through annular cooling channels surrounding the fuel rods [Takase, 1996, 1997]. These rods are centered in the flow channel by three sets of longitudinal rib spacers per rod, as seen in Figure I-1b. Thus, the **flow geometry is** more

complex than a simple annulus (which has been studied extensively). At the low Reynolds numbers involved, the ribs introduce competing flow phenomena: their wakes can be expected to increase turbulence and mixing directly downstream; however, between the ribs the flow is accelerated, providing a countering stabilizing or laminarizing effect. Also there are stagnation regions with reduced velocities and, thereby, increased thermal resistance leading to "hot spots." ***Flow field measurements are needed to provide understanding of the local interactions between these phenomena.*** Comparable geometries and low Reynolds numbers occur in control rod channels of typical General Atomics reactors (Figure I-1a).

For design predictions, reactor thermal hydraulic (TH) codes often neglect hydrodynamic and thermal entries. For turbulent flow this approximation is probably justified for local values of heat transfer and friction coefficients after passage of about fifteen to thirty characteristic lengths. For length-averaged values to become constant, the distance required is probably about five to ten times longer, say 100 to 300 characteristic lengths. Consequently, the blockage of the longitudinal rib-shaped spacers leads them to serve as periodic exit/entry geometries, initiating redevelopment of momentum and thermal internal boundary layers.

In summary, key features of flows of gases/vapors in advanced reactor systems for high efficiency are

- property variation, due to the high temperatures necessary, and
- complex flow passages.

These are the topics addressed by the present work.

The **organization of this report** is as follows. The next section places the **needs** in perspective **from a safety viewpoint**. The following section summarizes the **state of related knowledge**, by others and by the co-investigators who are leaders in the research on these topics. From this information **engineering and scientific needs** are identified. The **present work**, addressing these needs, is presented via a summary of the tasks and details of each task. The present work is followed by brief descriptions of the **accomplishments** and **some concluding remarks.**

A coupled development of numerical predictions with experimental assessment is needed in order to provide the benefits of DNS to improve TH codes for safety analyses and design. ***Validated*** DNS predictions can be employed to assist development of Large Eddy Simulations or other CFD treatments which, in turn, can provide correlations or modules of "corrections" to be attached as optional subroutines to TH codes. While DNS and LES cannot be applied directly in reactor thermal hydraulic codes or in design parameter studies in practice because their computer run times are too long, they should become useful for performance and safety predictions for "final" designs as well as for calibrating TH codes.

The **present project** consists of coupled analytical and experimental studies addressing the complications of gas property variation, complex geometries and buoyancy effects. Drs. Arkal Shenoy and Guido Baccaglini of General Atomics provided initial guidance on the needs of the nuclear industry. Complementing each other, Professors Pletcher, Satake and Kunugi

developed LES and DNS predictive techniques from first principles. INEEL and the Universities of Maryland and Manchester collaborated on the experiments. Maximum temperatures over 400°C could be treated in the U. Manchester apparatus; there is no inherent limit to the maximum temperatures that can be reached in the DNS/LES calculations. The simulations were compared with results obtained from the experimental phases. Dr. Shenoy and coworkers reviewed the results for application to realistic designs for advanced gas-cooled reactors that use the closed Brayton cycle for higher efficiencies.

Results of the proposed work should advance understanding of the complex flows in reactor systems and components. Reducing the uncertainty factors in performance of advanced designs will enhance system safety and will allow use of reduced "hot spot factors" to permit operation at higher temperatures, providing higher thermal efficiencies and thereby reduced waste. Ultimately, reliable DNS and LES approaches will permit performance predictions for "final" designs of complex geometries and will provide information to develop codes and correlations for use in transient thermal hydraulic system safety codes. While it may be some time before final designs of AGCRs are ready, much LES and DNS development must be accomplished before they can be applied completely.

Thermal fluid considerations for safety analyses As shown in Figure I-1, proposed advanced gas-cooled power reactors in the U.S. have design differences from the Japanese HTTR research reactor mentioned above. For power generation higher flow rates are used, giving higher Reynolds number in the passages. Annular cores are employed with a central reflector region with high thermal capacitance, causing slow, gradual thermal response to disturbances. It is appropriate to consider three of several operating modes.

The design for ***full power operation*** is intended to be a steady-state condition. Flow and, therefore, Reynolds numbers in the coolant passages are large so forced convection dominates the heat transfer problem. Typical Reynolds numbers are of the order of 50,000; consequently, buoyancy forces and thermal radiation are not significant and the phenomenon of laminarization is unlikely. A concern during this mode of operation is the potential damage to metallic components from ***local hot spots*** caused by poor mixing of the high-temperature jets that enter the lower plenum from the coolant channels. The temperature, momentum and turbulence ***profiles of the gas exiting the channels serve as initial conditions for the passages forming these jets.***

The most extreme accident scenario is believed to be a ***LOFA/LOCA*** = a simultaneous Loss of Flow Accident and Loss of Coolant Accident. The compressors stop so there is no flow. The coolant leaks to atmospheric pressure so there is no significant residual coolant in the channels as opposed to the high pressure operating condition. Allowable temperatures are high, e.g., 1600°C for the central region. The main thermal problems become thermal conduction and thermal radiation. Since the Grashof number varies as ρ^2, it drops to near zero; approximate calculations show that heat transfer in the reactor by natural convection would be less than 0.1 per cent of the heat transfer rate. The important thermal questions become adequate evaluation of the thermal capacitances of the various materials in the reactor and the thermal emissivity of the exposed surfaces involved, particularly the metals used in the vessel and the reactor internals.

A scenario likely to occur more frequently is the ***LOFA alone***. Coolant is not lost so helium remains at its high pressure operating condition. Due to the high thermal capacitance of the structure, the transient problem is quasi-steady as far as the fluid physics is concerned. That is, fluid residence times in the passages are much shorter than the characteristic thermal response times of the solids forming the passage surfaces and determining the thermal boundary conditions; the convection problem can be treated as instantaneously steady. The flow varies from its initial high Reynolds number to near zero as the temperature differences are reduced, approaching thermal equilibrium. During this transient the flow sequentially passes from the high-Reynolds-number turbulent regime, though the low-Reynolds-number turbulent and laminarizing regimes, to laminar flow. For predictions, the ***most difficult and uncertain conditions are the low-Reynolds-number turbulent and laminarizing flows***, particularly with gas property variation and complex geometries. Also of concern is the mixing of the hot plumes from the core into the upper plenum during this accident scenario (comparable to the jets into the lower plenum during normal operation).

During the LOFA two cases of natural circulation become of interest: that between the hotter and cooler channels within the core and that between the vessels and cooling panels of the passive cavity cooling system. In both cases, natural circulation is induced by differences in buoyancy forces but ***within the passages themselves the flow can be considered to be predominantly forced*** from the surroundings (although this forced convection may be modified by buoyancy forces within the passages and thermal radiation across them). In the cooling channels the fluid is typically high pressure helium and in the cavity cooling system it would be air or an air-helium mixture at atmospheric pressure (the higher thermal conductivity of helium can be an advantage to passive cooling systems [McEligot and Taylor, 1996]). ***Neither geometry is necessarily a simple circular tube or simple annulus***.

The present work addresses these predominantly forced convective problems of the LOFA scenario.

Related work For summaries of studies on the **effects of property variation** on turbulent and laminar internal gas flows, the reader is referred to reviews by McEligot [1986; McEligot, Shehata and Kunugi, 1998]. While not all-inclusive and concentrating primarily on forced convection, these reviews can provide useful introductions to the subject. Reviews of mixed convection in vertical tubes are presented by Jackson and coworkers [Jackson, Cotton and Axcell, 1989; Cotton and Kerwin, 1995]. Useful reviews of the status of numerical prediction techniques for turbulent flows have been published by Nagano and Shimada [1995] and Iacovides and Launder [1995]. Nagano and Shimada relate modeling techniques to Direct Numerical Simulations (DNS) and their potential. Iacovides and Launder relate their study to applications for internal cooling passages of gas turbine blades, a complicated problem with some features of the present study; of particular interest is their conclusion that "the first essential in modeling such flow is to adopt a low-Reynolds-number model for the sublayer region." The reader is referred to these reviews for general background on computational fluid dynamics (CFD).

The **interaction between hot jets** from the cooling channels and the walls of the lower plenum (potential hot spots) **can be an impinging jet problem** which is dependent on the initial conditions of the jets (= the exit profiles from the channels). The literature on heat transfer and

flow of impinging jets is vast and growing [Martin, 1977; Downs and James, 1987; Hrycak, 1981; Webb and Ma, 1995; Ma et al, 1997]. The primary application has been for enhancement of convective heat transfer parameters [Gardon and Akfirat, 1965] so much of the literature concentrated on integral heat transfer quantities, such as local or average heat transfer coefficients (e.g., Goldstein and Behbahani [1982], Hrycak [1983], Liu and Lienhard [1993], Ma et al. [1997]). For gas turbine cooling, the jet is formed by passage through a short orifice passage so the initial velocity profile of the jet is near uniform; this uniform profile is typical of many experiments where the jet is formed from a converging nozzle and of many numerical predictions.

Cooper et al. [1993] conducted a relatively wide range of measurements of impinging jets, focusing on data to assist turbulence modeling. Results include mean and fluctuating velocities and turbulent shear stresses. They comment that, while the topic has been the subject of many experiments, none could have been said to have been designed with the needs of turbulence modeling in mind. Usually the flow conditions at the nozzle exit are insufficiently prescribed or too far above the plate to be useful. Their experiment is one of the few where the jet was formed from a long tube, somewhat like some reactor problems, e.g., Figure I-4b later. Apparently there are no data for jets with significantly non-uniform temperature profiles as in the case of the flow from annular cooling channels to the upper plenum. In contrast to the usual experiment with a uniform potential core in the initial jet, the annular case has a recirculating, turbulent region downstream from the central rod forming the annulus.

As indicated above, simulations of some **effects of strong heating** of a gas involve the low-Reynolds-number turbulent range. In fact, Kawamura [1979] demonstrated nicely that adequate predictions of some phenomena with significant property variation were obtained when their results were also good in the low temperature-difference limit as the gas properties become effectively constant (his Figure I-1). Therefore, it is appropriate that codes and their turbulence models be initially examined for fully-developed flow in a circular tube ***with*** uniform wall heat flux and the ***constant properties idealization*** to assess their capabilities to simulate low-Reynolds-number flows in the simplest case. In any event, most engineers would want both heat and momentum transfer to be handled adequately for constant properties before treating cases with property variation.

Most of the early data for gas heating with significant property variation were obtained with circular tubes of small diameters so forced convection dominated [McEligot, 1986]. With test sections typically less than thirteen mm (D < 1/2 inch) probes could not be inserted for useful profile measurements and, therefore, the experiments could only provide integral wall parameters, such as local heat transfer coefficients and friction coefficients. These data gave initial tests of turbulence models accounting for temperature-dependent transport properties, as demonstrated by McEligot and Bankston [1969], Bankston and McEligot [1970] and Kawamura [1979].

Since the 1960s, measurements with larger test sections have been conducted by Hall and Jackson and colleagues at the University of Manchester to examine effects introduced by buoyancy forces aligned with or opposing the flow [Jackson, Cotton and Axcell, 1989]. These studies have led to criteria for significant buoyancy effects in turbulent flow for circular tubes.

Most recent work on the topic of laminarization by heating has been conducted in Japan. Measurements of local heat transfer coefficients and friction factors for transitional and laminarizing flows have been obtained by Ogawa et al. [1982] and Ogawa and Kawamura [1986] with circular tubes. Local Nusselt numbers were measured for annuli by Fujii et al. [1991] and Torii et al. [1991]. The first investigator to succeed in applying an advanced turbulence model to laminarization by heating apparently was Kawamura [1979]. He concluded that a modified k-kL model gave good agreement with the experiments. Fujii et al. [1991] employed three types of turbulence models for comparisons to their measurements of strongly-heated turbulent gas flow in an annulus. Torii et al. [1991] and Torii and Yang [1997] applied modified k-ε models for predicting streamwise variation of heat transfer parameters in low-Reynolds-number turbulent and laminarizing flows in circular tubes and annuli. Torii et al. [1993] also attempted to apply the Reynolds-stress model of Launder and Shima to St{Re} data for a circular tube; they concluded that predictions were comparatively poor in the range of turbulent-to-laminar transition.

Turbulence models have generally been developed for conditions approximating the constant properties idealization. **The few "advanced" turbulence models applied for high heating rates** [Kawamura, 1979; Fujii et al., 1991; Torii et al., 1993; Torii and Yang, 1997] **were developed *without* the benefit of measured velocity, turbulence and temperature distributions in strongly-heated, dominant forced flow** for guidance or testing. Thus, it is not certain whether the agreement with wall temperature data for moderate and strong wall heat fluxes, that was obtained in some cases with such models, was fortuitous or not. ***Before they can be applied with confidence to gas-cooled systems with high heat fluxes and axially varying heat flux, turbulence models and other numerical predictive techniques must be validated by comparison of predictions with careful measurements of the internal flow, turbulence and thermal distributions for conditions with significant gas property variation.***

Annular flow is often encountered in engineering applications such as gas-cooled nuclear reactors and heat exchangers. In annular flow, the position of zero shear stress is not coincident with the position of maximum velocity. A relative decrease in the turbulent kinetic energy subjected to the strong shear on the inner wall is observed. These phenomena become more remarkable with decrease of the radius ratio. An intensive experiment was reported by Rehme [1974] for fully-developed turbulent flow in an annulus with a thin inner rod. Distributions of mean velocity and Reynolds stresses were measured in annular flows with various radius ratios. Large eddy simulations (LES) with cylindrical coordinates were performed by Schumann [1975] for an annular flow. The study employed the wall law as the wall boundary condition since only a relatively small number of radial nodes were used.

In advanced reactor design, radius ratios are typically "large," in the range r_i/r_o from about 0.8 to 0.95 and the central rod must be supported and centered radially. Consequently, the passage is interrupted by spacers rather than corresponding to the idealized smooth annulus usually studied.

Takase has obtained measurements and predictions for an annulus with the heated central rod supported by rib-shaped spacers as in the HTTR. The data consisted of convective heat transfer coefficients at locations between the ribs plus friction factors based on the pressure drop across a representative cell in the streamwise-periodic region [Takase, 1996]. These coefficients

were increased substantially compared to accepted results for smooth annuli, as one would expect. By applying a general-purpose commercial code (Fluent) with a modified-"standard" k-ε turbulence model, he obtained numerical predictions for Reynolds numbers from 3000 to 20,000 [Takase, 1997]. "Constants" in the model were adjusted "so as to obtain the predicted values with sufficient accuracy with the experimental results;" consequently agreement of average heat transfer and friction coefficients is reasonable but predictions should be considered to be qualitative. Predicted mean velocity, turbulence kinetic energy, wall temperature and heat transfer coefficient distributions are given but no data are available to assess their validity.

Typical reactor system thermal hydraulic codes do not account for radial property variation or low-Reynolds number turbulent flow properly. Conceptually, one can apply various commercial, "general-purpose" CFD codes to these situations. However, most turbulence models employed in these codes fail to give adequate heat transfer predictions for the simplest internal flows [Mikielewicz et al., 2002]. ***Direct Numerical Simulations should give reasonable predictions, particularly at low Reynolds numbers -- but only recently have these techniques been extended to gas flows with property variation [Satake et al., 2000].***

Despite the fact that there is an urgent need for better methods of predicting the thermal features of turbulent flows that are technologically important, at the present time, no workable general theory is known by which the phenomena can be accurately predicted in configurations of practical interest. Although progress is needed at all levels of turbulence modeling, the recent advances in computer technology and the outlook for continued advances in the future suggest that it may be timely to give increasing attention to research on direct numerical simulation (DNS) and large eddy simulation (LES) of turbulent flow to move these capabilities toward larger and more relevant problems. ***The majority of DNS and LES studies have been for planar channel flows under isothermal conditions. A few studies involving flows with heat transfer have been reported, but most of those have employed the passive scalar approach in which the effects of property variations were neglected. Notable exceptions are the works of the Co-investigators: LES studies of Wang and Pletcher [1996] and Dailey and Pletcher [1998] and DNS predictions of Satake et al. [2000] where significant property variations were taken into account. Simulations of flows in channels of circular or annular cross section are very sparse, especially with heat transfer.***

A coupled development of numerical predictions with experimental assessment is needed in order to provide the benefits of DNS to improve TH codes for safety analyses and design. For example, validated DNS predictions can be employed to assist development of Large Eddy Simulations [Dailey and Pletcher, 1998] or other CFD treatments which, in turn, can provide correlations or modules of "corrections" to be attached as optional subroutines to TH codes. While DNS and LES cannot be applied directly in reactor thermal hydraulic codes or in design parameter studies in practice because their computer run times are too long, they should ultimately become useful for performance and safety predictions for "final" designs as well as for calibrating TH codes.

Mikielewicz et al. [2002] conducted simulations of the predictive capabilities of a range of turbulence models for the simplest case, fully-developed flow in a circular tube with uniform wall heat flux and the **constant properties** idealization; eleven models were considered. The

Reynolds number range covered was $4000 < Re < 6 \times 10^4$ and the Prandtl number used was 0.7, for air. Several popular models could be immediately eliminated from further consideration. Some models do not even handle high-Reynolds-number flows well for heat transfer. Several k-ε models designed for use at low Reynolds number also gave poor results.

For dominant forced convection ***with significant gas property variation,*** in low Mach number flow of common gases through a circular tube, apparently the only published profile data available to guide (or test) the development of predictive turbulence models have been K. R. Perkins's and Shehata's measurements of mean temperature distributions [Perkins and McEligot, 1975] and mean velocity distributions [Shehata and McEligot, 1995, 1998] for this situation. Their careful measurements are now available to examine this problem and these serve as bases for evaluation of predictive techniques for mean quantities. Small single wire probes were introduced through the open exit in order to obtain pointwise temperature and velocity measurements. In addition to the usual difficulties of hot wire anemometry, the temperature range of his experiment introduced additional problems such as radiation corrections; these difficulties, their solutions and related supporting measurements are described in a report by Shehata and McEligot [1995]. Their experiments concentrated on three characteristic cases with gas property variation: turbulent, laminarizing and intermediate or "subturbulent" (as denoted by Perkins).

A number of **turbulence models**, developed for turbulent flows under conditions of uniform fluid properties, were applied by Mikielewicz et al. [2002] for the purposes of simulating experiments with ***strongly-heated***, ***variable property*** gas flows at low Reynolds numbers in a vertical circular tube, i.e., the conditions of Shehata and McEligot. The selection of models included a mixing length model, eddy diffusivity models, a one-equation k model and two-equation models of the k-ε type with low-Reynolds-number treatments; this selection is representative of models which have been widely used is but not all-inclusive. The wall-to-bulk temperature difference is underestimated by over forty percent in the worst case and by about thirty per cent in the case of one "low-Reynolds-number" k-ε model.

Colleagues of **Professors Kunugi** and McEligot have developed or extended additional turbulence models and have assessed them at the conditions of Shehata's experiments. The k-ε turbulence model of Abe, Kondoh and Nagano [1994], developed for forced turbulent flow between parallel plates with the constant property idealization, has been successfully extended by Ezato et al. [1999]. For thermal energy transport, the turbulent Prandtl number model of Kays and Crawford [1993] was adopted. Fujii "extended" his k-kL- $\overline{u}\overline{v}$ model from the annular case to treat flow in circular tubes. Since his model evolved from the one by Kawamura, it is expected that his results would be comparable to those of Kawamura. Nishimura utilized a Reynolds stress model (RSM) from Shima with turbulent heat flux and thermal energy fluctuation equations; the heat flux equations contain two extra terms to take account of anisotropy of turbulence and velocity turbulence-thermal energy gradient production for the pressure-temperature fluctuation gradient correlation terms [Nishimura, Fujii et al., 2000]. Each of these models provided reasonable predictions of mean velocity and temperature distributions.

Overall, simulations of the low-Reynolds-number internal flows have been made using about fifteen turbulence models. Possible effects of buoyancy forces at these conditions were considered and it was concluded that forced convection dominated the heat transfer parameters.

Numerical predictions forecast the development of turbulent transport quantities, Reynolds stress and turbulent heat flux, as well as turbulent viscosity and turbulent kinetic energy, plus mean velocity and temperature distributions, wall heat transfer parameters and pressure drops. In contrast to earlier approaches of other investigators, validation focused on comparisons to the measurements of the developing mean velocity and temperature fields. **One may conclude** that existing low-Reynolds-number turbulence models and commercial codes should be used with ***caution*** for

- low-Reynolds-number, fully-established, ***constant-property*** flow and
- strongly-heated, internal gas flows

For strongly-heated turbulent or laminarizing gas flows, five models were found to give reasonable agreement with the internal profile measurements of Shehata. However, it is not clear that extension to other conditions can be done with confidence; for example, it has already been demonstrated that one model yields incorrect trends for conditions with significant buoyancy effects [Bates et al., 1974].

For examining turbulent flows in complex geometries, **INEEL** has recently developed the world's largest Matched-Index-of-Refraction flow system and has placed it in operation. By using transparent models and optical techniques, measurements can be made that would be otherwise impossible. In addition to improved spatial and temporal resolution, perpendicular velocity components and turbulent shear stresses can be determined effectively to "y = 0" (or less). The first experiment with this facility examined the structure of the viscous layer of a boundary layer during the transition process induced by a square rib; the results included the first measurements for $\overline{uv}$ at y^+ less than about thirty in a transitional boundary layer [Becker et al., 2002]. Excellent data were obtained to $y^+ = 0.2$ or less.

As noted above, the interaction between hot jets from the cooling channels and the walls of the lower plenum (potential hot spots) is an **impinging jet problem** which is dependent on the initial conditions of the jets (= the exit profiles from the channels). Recently for the EM Science program, Keith G. Condie and Glenn E. McCreery of the INEEL staff conducted an experiment with the MIR flow system to measure the flow and turbulence characteristics of a semi-confined impinging jet [McCreery et al., 2002]. The jet is formed from a long circular tube, comparable to the cooling channels of a reactor in the sense that jet is not formed from a uniform, potential flow. Their laser Doppler velocimeter measurements provide the distributions of the mean and fluctuating velocity components.

New Particle Tracking Velocimetry (PTV) techniques were developed by Profs. Guezennec and Brodkey of Ohio State with the Glenn E. McCreery of INEEL staff as part of an EM Science grant to the University of Idaho, INEEL and OhSU in order to accomplish individual particle tracking (IPT). Current PTV methods concentrate on small fields of view (e.g., 8 x 8 x 8 cm^3 [Kasagi and Matsunaga, 1995]) and data processing is conducted off-line after recording. For IPT the field of view must track erratic particles in all three coordinate directions via real time feedback from the deduced instantaneous particle motion; in their experiment, tracking distances of the order of a meter are involved. (Additional statistics can be determined later by analyzing off-line the motion of all particles which remain in the field of view as individual particles are tracked.) The first two phases, development of a versatile PTV

system for INEEL and conversion of it to a particle tracking system with a programmable moving traverse (MPT), are essentially complete.

The **University of Maryland** group has **extensive experience** designing, fabricating, developing and using **multi-sensor hot-wire probes**. **Vukoslavcevic and Wallace** [1981] analyzed the errors created by the necessary neglect of the effects of the local turbulent velocity gradient field on measurements of the three velocity components and the streamwise vorticity components with a four-sensor "Kovasznay" probe. This study was followed by an investigation by Park and Wallace [1993] where these effects were studied for both X-array and four-sensor-array hot-wire probes using an experimental data base that included the necessary instantaneous velocity gradient information. These studies demonstrated that, if the separation between the sensors is larger than about four viscous lengths, rather large errors in the measured Reynolds shear stress and the measured streamwise vorticity are incurred.

These results led the group [Vukoslavcevic et al., 1991] to develop a nine-sensor probe in order to measure not only all the components of the velocity vector, but also all the elements of the velocity gradient tensor. With this information many variables of interest for turbulent flows - the vorticity vector, the strain rate tensor, the vorticity stretching/compression term, the full turbulent dissipation rate - are available. This probe was used for extensive measurements in a turbulent boundary layer by Balint et al. [1991]. Much of this measurement technique development has been summarized in review articles by Wallace [1986] and Wallace and Foss [1995].

The probe was improved to include twelve sensors and considerable effort was given to developing accurate and efficient data reduction and analysis algorithms for it by Marasli et al. [1993] and Vukoslavcevic and Wallace [1996]. This twelve-sensor probe has been used to measure turbulence properties in a circular cylinder wake [Nguyen (1993)], in the atmospheric surface layer [Folz, 1997] and in a two-stream mixing layer [Loucks, 1998].

Professor Pletcher's research group has developed algorithms and methodology for direct and large eddy simulations of turbulent flows with heat transfer using a compressible formulation of the Navier-Stokes equations. This approach to direct and large eddy simulations is thought to be somewhat novel in its flexibility for treating flows with significant property variations. Basically, this flexibility is achieved by employing a coupled, compressible formulation with low Mach number preconditioning [Pletcher and Chen, 1993]. With preconditioning, the numerical stiffness and slow convergence associated with traditional compressible formulations are avoided and, in fact, the convergence rate becomes virtually independent of Mach number in the low speed regime.

Large eddy simulation results with significant heat transfer using this approach were reported by Wang and Pletcher [1996] and Dailey and Pletcher [1998]. Wang and Pletcher considered a channel flow with one wall heated and the other cooled at a temperature ratio of 3. Dailey and Pletcher reported on quasi-developed flows with uniform heat flux heating and cooling with wall to bulk temperature ratios of 1.485 and 0.564, respectively. Both studies confirmed that even for flows at very low Mach numbers (0.001), significant levels of (per cent) density rms fluctuations are present. One of the most relevant findings of this study is that many of the results from the simulations for both heating and cooling tend to collapse toward the same

distribution when plotted in semi-local coordinates. The semi-local coordinates are obtained by using local properties (density and viscosity) when computing the friction velocity (wall shear stress divided by local density) and y^+.

A clear dependence on the wall to bulk temperature ratio is evident with the mean velocity profile in conventional wall coordinates for the three heat flux cases. When the data are plotted in semi-local coordinates, the spread in the curves is greatly reduced. For reference, the constant property DNS results of Kim et al. [1987] and the experimental data of Niederschulte et al. [1990] were employed. A similar effect was observed for the mean temperature profile and again the data were significantly compressed by use of semi-local coordinates. The remarkable thing is that this near similarity extends to distributions of fluctuating quantities also.

Kawamura et al.[1994] and **Satake** and Kawamura [1995], performed **LES calculations** for turbulent heat transfer in an annulus. The calculation procedure was based on Schumann's numerical method but adopted the non-slip boundary condition at the wall. Particular attention was given to the flow structures in the inner wall region. **Satake and Kasagi** [1996] carried out **DNS calculations** for fully-developed turbulent channel flow and heat transfer, with an assumption of a thin layer adjacent to the wall in which a virtual body force acts to damp spanwise velocity fluctuations as a mechanism for turbulence control. Satake and Kunugi [1998a] developed a technique for DNS of turbulent pipe flow; the Navier-Stokes equations were discretized in cylindrical coordinates without a singularity at the axis by means of a radial flux formulation based on a finite control volume description. This approach was then extended to the problem of an axisymmetric impinging jet with outflow confined between two parallel discs [Satake and Kunugi, 1998b]. Predictions show good agreement with the impinging jet measurements of Nishio et al. [1996] including distributions of the Reynolds shear stress, a difficult quantity to measure. The treatment was further extended to include solution of the energy equation for a circular tube [Satake and Kunugi, 1998c]; three thermal boundary conditions were considered: uniform heat flux, a cosine distribution and circumferentially non-uniform wall temperature. Preliminary calculations were accomplished with full gas property variation using the properties of air [Satake et al., 2000].

With the data of Perkins and of Shehata, detailed **internal mean profiles for predominantly forced flow** in a circular tube **are now available** for the following approximate conditions:

Re_{in}	q^+_{in}	Temperature	Velocity
8520	0.0010	X	
6020	0.0011	X	
6030	0.0018	X	X
6020	0.0035	X	X
6040	0.0045	X	
4260	0.0045	X	X
3760	0.0055	X	

The non-dimensional heat flux q^+_{in} is defined here as $q''_w/(Gc_pT_{in})$. From the graph of flow regime criteria by Fujii et al. [1991], one can see these measurements span a range from turbulent behavior at moderate heating rates to rapidly laminarizing flows at strong heating rates.

The hot-wire data of Shehata and McEligot [1998] for assessment of predictions with significant ***property variation*** are constrained to mean velocities and temperature. ***Turbulence***

modelers ask for measurements of the fluctuating components to guide and test their developments; for Reynolds stress models (or for calculating Lumley's anisotropy invariant map [Fischer, Jovanovic and Durst, 1998]) all normal and shear stresses are required. ***Such data are not available.*** Further, it is not yet clear whether the laminarization observed is due to viscous effects or to induced acceleration. Laser Doppler velocimetry measurements are usually impractical for these conditions: the optical access destroys the thermal boundary condition in the vicinity of the access and index-of-refraction fluctuations can bias the velocity data as can thermophoresis of the seed particles.

Observations for **annular flows** with property variation have been obtained by Fujii et al. [1991] and **by Jackson and coworkers at U. Manchester**, but only with external wall thermocouples and pressure taps; comparable data for combined effects of high temperatures and consequent buoyant forces have also been provided by Jackson and colleagues. Criteria for the importance of buoyant forces in annuli are still to be developed; in approximate analogy to natural convection in wide ducts, the governing Grashof number could be based on gap spacing in some situations or to gap width (circumference) in others.

Engineering needs include

- Development of computational techniques for predicting the response of advanced high temperature gas-cooled reactors during emergency cooling following a loss of forced cooling flow accident.
- Development of computational techniques for mixing of hot jets (streaks) from the core into the lower plenum during normal reactor operation.
- Development of computational techniques for mixing of hot plumes from the core into the upper plenum during pressurized loss of forced coolant flow.
- Unambiguous "benchmark" data to assess those techniques and to guide further development as necessary
- Application of computational techniques developed and experimental measurements to the complex geometries of advanced gas-cooled reactors.

Scientific needs include

- Determination whether viscous effects or acceleration are responsible for the reduction of heat transfer parameters and laminarization in strongly heated gas flows
- Evaluation of criteria for buoyant instabilities and mixed convection in annular geometries
- Measurements of turbulence statistics in strongly heated flows to assist simulation and modeling developments
- Examination of the effects of flow acceleration and deceleration through complex geometries as in generic cooling channels and control rod channels

Present work

Technical approach A coupled experimental and analytical attack was mounted. The ***technical objective*** is to develop fundamental knowledge needed for improved predictive techniques for use in the technology development of advanced reactor concepts and their passive safety systems. An overview of the approach is provided as Figure I-2.

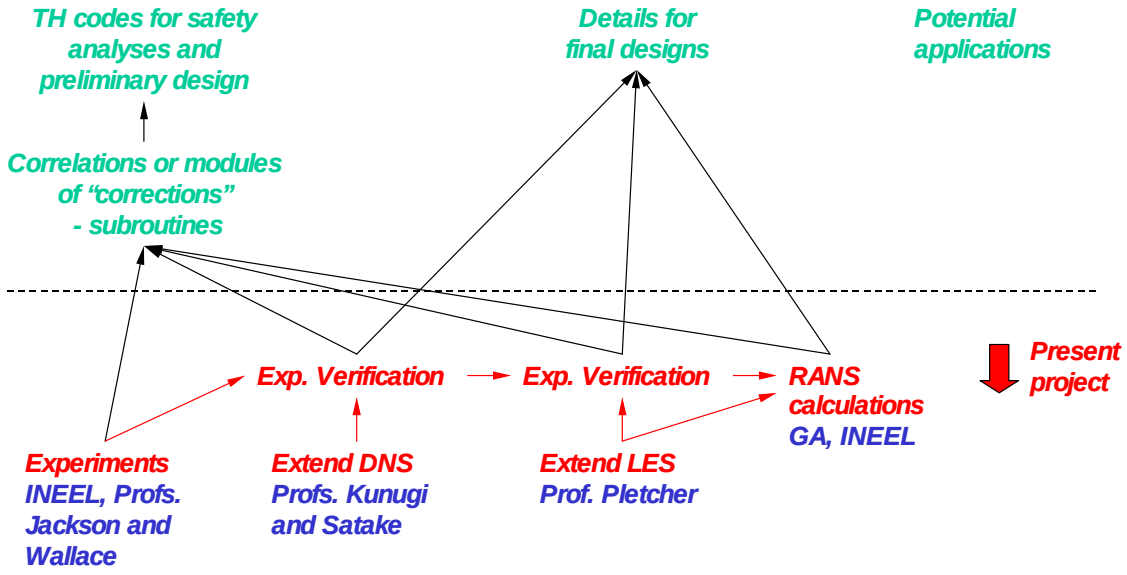

Fig. I-2. Overview of technical approach and relation to potential applications

The following **tasks** are being addressed:

A. Heat transfer / fluid flow in advanced reactors Identification of normal and emergency thermal-hydraulic performance conditions of high temperature gas-cooled reactors that need to be analyzed and development of Design Data Needs (DDN) which specify the thermal-fluid data and correlations needed for the required computational techniques. Review of application of results for normal and emergency operations of advanced gas-cooled reactors for high thermal efficiency and safe operation (Drs. A. Shenoy and G. Baccaglini, General Atomics)

B. Measurements of velocity and turbulence fields for generic idealizations of advanced reactor geometries (McEligot, Condie, McCreery and Pink, INEEL)

C. Extension of DNS to complex reactor geometries of high-temperature gas-cooled reactors (Satake, Tokyo Univ. Science; Kunugi, Kyoto U.)

D. Extension of LES to complex reactor geometries of high-temperature gas-cooled reactors (Pletcher, Iowa State)

E. Development of miniaturized turbulence probes for high temperature gas flows (Wallace and Vukoslavcevic, U. Maryland)

F. Measurements of the effects of buoyancy forces on flow in tubes and annuli (Jackson, U. Manchester)

Task A. Heat transfer/fluid flow in advanced reactors -- Dr. A. S. Shenoy, Dr. G. Baccaglini and C. Ellis, General Atomics (GA)

The Modular Helium Reactor (MHR) is an ultra-safe, meltdown-proof, helium-cooled reactor which is based on thirty years of high temperature gas-cooled reactor experience and is representative of a Generation IV advanced reactor design. The MHR takes advantage of the unique properties of helium gas as coolant, graphite as moderator and coated particles as fuels. The Gas Turbine-Modular Helium Reactor (GT-MHR) couples the helium-cooled modular reactor core with a gas turbine to produce electricity directly from the high-temperature helium coolant at efficiencies approaching fifty per cent. The GT-MHR preliminary design has been completed and its final design is now in progress.

One of the inherent safety features of gas-cooled reactors is their capability of maintaining a gas environment for cooling the core under a major loss of containment. During normal operation the thermal energy from the core is removed by forced convection and during severe accidents, in which the coolant forced flow and/or the coolant containment is lost, it is removed by conduction, radiation or natural circulation. This task has involved first the selection of key operating conditions and the thermal hydraulic phenomena related to the safe operation of advanced gas-cooled reactors under normal and accident conditions. Following this selection, this task consisted of a careful review of the experimental and analytical work done under this project and establishment of the analytical techniques and experimental data that can be applied for improving the capability of predicting the GT-MHR reactor response.

General Atomics identified six areas of thermal hydraulic phenomena in which the application of improved Computational Fluid Dynamic techniques can improve the safety of advanced gas cooled reactors.

- Normal Operation at Full or Partial Loads
  - Coolant flow distribution through reactor core channels
  - Mixing of hot jets in the reactor core lower plenum

- Loss of Forced Reactor Core Cooling
  - Mixing of hot plumes in the reactor core upper plenum
  - Distribution of coolant flow between hotter/cooler reactor core channels
  - Rejection of heat by natural convection and thermal radiation at the vessel outer surface

- Loss of Forced Reactor Core Cooling and Loss of Coolant Inventory
  - Prediction of reactor core depressurized cooldown
  - Rejection of heat by natural convection and thermal radiation at the vessel outer surface

Figure A-1 illustrates these areas. During the “kickoff” meeting in September 1999 each of these areas was presented and discussed and experiments that could be conducted by INEEL and/or the University of Manchester were identified. Details of existing geometries and performance parameters were subsequently provided to INEEL for the conceptual design of their experiment on generic complex flows in advanced reactors, with particular emphasis on the configurations of cooling channel exits into the lower plenum (hot jets).

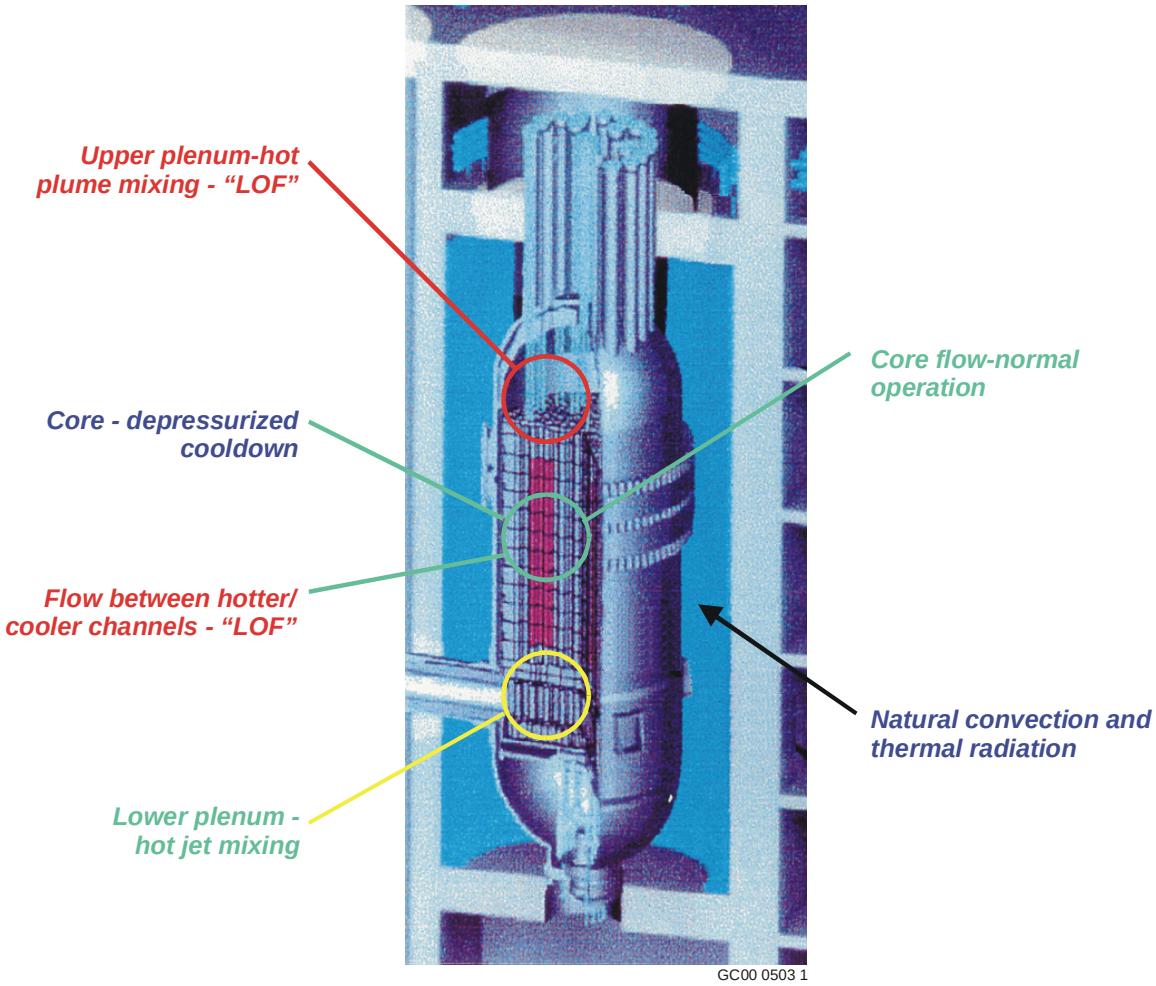

Fig. A-1. Thermal/hydraulic response phenomena of interest for safety analyses.

The high-temperature gas-cooled reactors use pressurized helium as coolant to enhance the heat transfer process. Under extreme accident conditions these reactors can lose their capabilities for forced circulation of their coolant (Loss of Forced Cooling Accident, LOFA), and/or lose the capability of containing the coolant (Loss of Coolant Accident, LOCA).

During full power operation, forced convection is the dominant heat transfer mechanism within the helium flowing from the core to the heat sink. Typical Reynolds numbers within the coolant passages in the graphite core are on the order of 50,000. Under these conditions turbulent mixing is the predominant contributor to the heat transfer process and buoyancy or thermal radiation are of lesser importance. During partial load operations (e.g., as low as fifteen per cent of the design power) the helium inventory is reduced to maintain the same volumetric flow rate at the turbine inlet. Under these conditions the typical Reynolds number within the core coolant passages may be reduced to values around 5, 000 or lower, at which point a potential transition from turbulent to laminar flow could occur. Computational techniques with supporting test data are needed to address the heat transfer from the fuel to the coolant during this transition from turbulent to laminar flow, including the possibility of an early laminarization of the flow near the walls.

Another area, which requires further development, is the prediction of the turbulent mixing of the high temperature coolant jets that enter the plenum beneath the core. Poor mixing of these jets can cause local hot spots resulting in potential damage of metallic components. Conditions of the flow through the lower plenum of the core during normal operation are in the following ranges:

Helium temperature	700 – 850°C
Helium pressure	40 – 80 atm
Flow type	Stagnant to highly turbulent

The design issue in this case is the need for predicting the amount of turbulent mixing occurring between the hotter coolant jets and the rest of the flow before these hot jets impinge on the metallic components at the exit of the core lower plenum. Due to the complexity of the flow path in the lower plenum, computational techniques with supporting test data are needed to address this turbulent mixing process.

Under the first accident scenario, LOFA, helium remains at its high pressure operating conditions within the undamaged vessel (also called a "pressurized conduction cooldown"). Conditions are:

Helium temperature	400 – 1600°C
Helium pressure	40 – 80 atm
Flow type	Overall natural circulation

Due to the high thermal capacities of the graphite core structure, this accident is a quasi-steady phenomenon as far as the fluid physics is concerned. That is, fluid residence times in the core passages are much shorter that the characteristic thermal response times of the graphite blocks where these passages are located. The dominant convective heat transfer mechanism from the solid to the coolant can be treated, therefore, as instantaneously steady. During this accident the flow sequentially passes from the high-Reynolds-number turbulent regime, through the low-Reynolds-number turbulent and laminarizing regimens, to laminar flow driven by buoyancy forces. Design issues are the prediction of the buoyancy-driven coolant flow between hotter and cooler core channels and the evaluation of the thermal mixing of hot plumes in the core upper plenum before they reach metallic components. This task concentrates on identifying the computational techniques that are required to predict the heat transfer process for the complex geometry existing in the gas-cooled reactors under the low-Reynolds-number and laminarizing regimes. These are the conditions that are the most difficult and uncertain to analyze due also to the variation of gas properties with temperature (e.g., see work by Ezato et al. [1999], Satake et al. [2000] and Mikielewicz et al. [2002] as part of Tasks B and C).

During a LOFA accident there are two more cases of buoyancy-driven flow phenomena specific to gas-cooled reactor design that are of interest. The flow between the inner hotter and the outer cooler channels within the core and the flow between the reactor containment vessel outer surface and the cooling panels of the passive cooling system that encircle the vessel. In the core cooling channels the fluid is typically high-pressure helium and in the cavity cooling system it is air at atmospheric pressure or a mixture of air and helium. The design issue here is the need for an accurate prediction of the maximum fuel temperature of the reactor core during a LOFA. This temperature is directly correlated to a clear understanding of the buoyancy-driven heat transfer within the core and outside the reactor vessel.

During the extreme case of a LOCA followed by a LOFA the reactor loses the capability for forced cooling flow and the coolant reaches atmospheric conditions, so that there is no significant residual coolant in the core channels as opposed to the high pressure operating conditions. The main heat transfer mechanisms in this case become thermal conduction and thermal radiation. The important thermal questions become, therefore, an adequate evaluation of the thermal capacitances of the various materials in the reactor core and the thermal emissivities of the exposed surfaces involved, particularly the metals used in the reactor internals, the vessel and the cooling panels of the passive cavity cooling system.

At the beginning of this project GA provided GT-MHR performance parameters for normal and emergency operations to support the planning of related experiments and the development of computational techniques. These communications were followed by extended interactions between GA personnel and the analysts to assure that the results of this project would be applicable to gas-cooled reactor design with emphasis on improving safety. GA participation to this project also included a one-day visit by Dr. Baccaglini in May 2001 at the INEEL facilities in Idaho Falls for an informal review meeting and a one-day visit by Dr. Shenoy in August 2001 to review the status of this project and to discuss future contributions. The participation of General Atomics included review of the results from numerical simulation for laminarization of turbulent forced gas flow in GT-MHR core geometry [Satake et al., 2000; Nishimura et al., 2000; Mikielewicz et al., 2002] and of the data from the experiments done by Prof. Jackson and colleagues at the University of Manchester as Task F. Of particular interest was the computational work done using Large Eddy Simulation (LES) by Prof. Pletcher of Iowa State (Task D) and Direct Numerical Simulation (DNS) by Profs. Kunugi and Satake (Task C).

More specifically, there are **three areas** in the gas–cooled reactor core design **for** which GA was able to determine **applications of the results** generated by this project:

The ***first area*** is the "rejection of the heat by natural convection and thermal radiation at the vessel outer surface". This heat rejection involves buoyancy-driven flow within an irregular annular configuration. In this case some aspects of the experiments for vertical plate channels done by Wang, Li and Jackson [2001] in Task F and the LES code development done by Prof. Pletcher (Task D) for mixed convection can be applied in the range where natural convection is the dominant phenomenon. Nevertheless, before adopting a generalized LES analytical model, its boundary conditions must be modified to reflect the flow phenomena occurring in a closed space. Also data from the experiment with vertical annular passages done by W. S. Kim et al. [2001] may be applicable in the region where buoyancy effects are predominant.

The ***second area*** is a combination of "thermal mixing of hot jets in the reactor core lower plenum" and "thermal mixing of hot plumes in the reactor core upper plenum." Measurements of the mixing of passive scalars using a Particle Tracking Velocimetry system in the second experimental configuration of Task B could provide the most applicable information in this area, as proposed by INEEL and partners in their response to the FY-2002 NERI call.

The ***third area*** combines "coolant flow through the reactor core channels during normal operation" and "distribution of coolant flow between hotter/cooler reactor channels during a LOFA." As originally proposed, this area is the one most directly addressed by the present

project. The most directly applicable experimental results come from the measurements of Prof. Jackson. His experiments measured mixed convection in circular tubes (Task F) with the multi-sensor probes of Profs. Wallace and Vukoslavcevic (Task E). LES/DNS results from Tasks C and D should also apply. For examining potential overheating of control rods and possible future fuel rods as well as the Japanese HTTR and other proposed reactor geometries, the complex flow measurements in ribbed annuli by INEEL (Task B) and related LES/DNS developments are also pertinent.

The area of "prediction of heat transfer within the reactor core during depressurization" (LOCA) involves dominant thermal conduction and thermal radiation and, thereby, is outside the scope of the present project which concentrates on convection.

In general, the present code developments and experiments were aimed at providing results for assessing CFD codes which might be used by industry in reactor thermal design. However, some results would be useful in some of the scenarios ("areas") identified by General Atomics. The **following section** is a more detailed evaluation of the applicable experimental and analytical results for the three areas described above.

Rejection of heat by natural convection and thermal radiation at the vessel outer surface

There are two types of geometric configurations used in the calculations and experiments performed during this project that relate to a further understanding of the thermal hydraulic phenomenon of "rejection of the heat by natural convection and thermal radiation at the vessel outer surface": vertical plane channels and vertical annular configurations. ***As a consequence of the tasks in the original proposal, none of the present studies treated closed spaces*** (as in a reactor cavity). Thus, none is directly applicable to this scenario. However, some aspects of the mixed convection studies may be considered to be comparable. In particular, mixed convection results for high values of buoyancy parameters will show features like the pure natural convection of the application. It is also likely that the present annular LES code (Task D) could be extended to this application if further funding were available.

The vertical plane channel used in the experiment by Wang. Li and Jackson [2001] had openings above and below the channel (Task F). Their Figure 12 presents the measured Nusselt number ratio as a function of a buoyancy parameter. For a more appropriate physical modeling of the region between the reactor vessel and outer silo walls, the boundary conditions for this experiment need to be modified to reflect the closed space in which the reactor vessel rejects heat to the cooling panels. Future experiments should incorporate this recommendation and employ a more prototypical cross section (while considerable data for heat transfer in enclosures is available in the literature [Catton, 1978] it is unlikely the unique geometry of a reactor cavity has been treated well).

Lee and Pletcher [2001] studied the flow within vertical plate channels (Task D). Their LES results were provided as Nu/Nu_o vs. Gr/Re^2 in their Figure 2. The same closed space boundary conditions should also be applied here to model the enclosed space between the reactor vessel and the cooling panels better. More predictions than the existing three conditions should also be added in order to improve the correlation for buoyancy-dominated cases.

Kim et al. [2001] conducted measurements of flows within vertical annular passages (Task F) that could be used to simulate the flow between the core vessel and the panels of the passive cooling system. During a GT-MHR LOCA, buoyancy forces dominate the flow in this cavity. Therefore, the buoyancy parameters evaluated at a high value of Bo* could be used for an application of the data to this geometry. Their Figure 7 presents measurements of Nusselt number ratio (Nu/Nu_f) as a function of the Jackson buoyancy parameter (Bo*): A trendline could be fitted to these data to provide a useful heat transfer correlation. For mixed convection in water flow, the following correlation was presented by Wu et al. [2001] and Wu, Xu and Jackson [2001]:

$$Nu/Nu_f=[|1\pm1.25x10^5Bo^*(Nu/Nu_f)^{-2}|]^{0.46}$$

The non-dimensional variables may also make this correlation valid also for gas flow. (The difficulty in applying this result directly for estimates in the reactor cavity is lack of a basis to evaluate an equivalent value of Nu_f.)

Lee, Xu and Pletcher [2002] covered an LES approach for understanding heat transfer in a vertical annular passage (Task D). Results were not directly presented in terms of the Nusselt number for highly-heated cases where buoyancy forces dominate. Flow characteristics can be estimated from their Figure 12 (turbulent kinetic energy vs. radial distance from heated surface) and their Figure 10 (shear stress vs. radial distance from heated surface). However, only two conditions in these figures are applicable to significant buoyancy-driven flow.

Future studies on this thermal hydraulic phenomenon should account for realistic geometry configurations of the irregular GT-MHR annular region between the reactor vessel and outer silo walls. As mentioned before, the vertical plane channel geometries should be performed again with closed top and bottom boundary conditions. However, the results described in this section could at least be applied for insight concerning regions far away from top or bottom wall influences.

Mixing of hot jets in the reactor core lower plenum and hot plumes in the core upper plenum

Mixing of hot jets in the lower plenum of the reactor core. Some aspects of Task B are aimed at addressing the development of jets in the lower plenum of a typical GT-MHR reactor core. Studies were initiated but funding available was insufficient to examine the complete geometric transition from coolant channels into and across a lower plenum with core support columns.

A model design was developed and fabricated to investigate the flow phenomena occurring in the first stage of this transition: convergence into an intermediate plenum and then a perpendicular exit ("crossover") as in an GT-MHR by General Atomics. Figure B-1 shows the geometry involved. Measurements would provide data to assess CFD codes claiming the capability to treat configurations which involve flows converging, impinging as jets, mixing and exiting perpendicularly, all with an approximately constant cross section. Initial flow visualization results are presented in this report in the section on Task B.

The project we proposed to the 2002 NERI program would have addressed this topic for advanced gas-cooled reactors and gas-cooled fast-breeder reactors but it was not selected for funding.

Mixing of hot plumes in an upper plenum. A continuation of Task B is envisioned to develop benchmark data to assess CFD codes which treat thermal mixing of multiple hot plumes in the upper plenum of a typical gas-cooled reactor. In the existing model (Figure B-13) measurements of particle transport from one ninety-degree sector of the upstream annulus to another sector in the converging flow region would simulate the mixing of a passive scalar, such as some aspects of thermal mixing. The new INEEL Moving Particle Tracking velocimeter system would be employed to deduce the particle transport. Since the particles would be sufficiently small to follow the flow, their transport would simulate the mixing of a passive scalar. A CFD code proposed to treat the mixing of hot plumes in an upper plenum should be required to demonstrate reliable predictions for the mixing of passive scalars as a first step in the assessment before introducing the further complication of any buoyancy effects.

Our 2002 NERI project proposal also addressed this topic for advanced gas-cooled reactors and gas-cooled fast-breeder reactors but, as noted, it was not selected for funding.

Coolant flow through reactor core channels and distribution of coolant flow between hotter/cooler reactor core channels during LOFA

These studies are the ones upon which the original proposal aimed at concentrating its studies. The experimental and analytical data generated during this project were considered for **three** types of GT-MHR reactor core thermohydraulic **configurations**:

1. vertical annular flow between the core barrel and reactor vessel wall
2. vertical pipe flow through coolant channels
3. vertical annular flow through a control rod channel with control rod inserted

The latter configuration also corresponds to coolant flow along the fuel rods in the Japanese HTTR design.

Two of the geometries used in the experiments and calculations of this project apply to the ***first configuration***: vertical plane channels and vertical annular flow. Both of these geometries and their applicable heat transfer correlations for the GT-MHR have been mentioned in the section on "Rejection of heat by natural convection and thermal radiation at the vessel outer surface." Lee and Pletcher [2001] and Lee, Xu and Pletcher [2002] developed LES codes using a quasi-fully-developed approximation (Task D) and Wang, Li and Jackson [2001] and Kim et al. [2001] obtained measurements for these geometries with forced and mixed convection (Task F).

For the ***second configuration***, data from the experiments on vertical pipe airflow by Jackson and Li [2000] are applicable (Task F)**.** For near-uniform heat flux the suggested correlation is:

$$Nu/Nu_f=[|1-150000Bo(Nu/Nu_f)^{-2}|]^{0.46}$$

For uniform wall temperature it is:

$$Nu/Nu_f=[|1-2300Bo(Nu/Nu_f)^{-1.7}|]^{1.0}$$

These two correlations can be applied to helium flow in the GT-MHR through the coolant channels under normal operating conditions.

Vertical pipe airflow was also studied analytically and modeled with LES methods by Xu, Lee and Pletcher [2002] with a quasi-fully-developed approximation to account for the gas property variation. Gas properties were allowed to vary with temperature. Their results, however, were not directly presented in terms of Nusselt number as a function of a buoyancy term. Flow characteristics could be estimated from the distributions shown in their Figure 13 (turbulent kinetic energy vs. y^+) and their Figure 15 (shear stress vs. r/D). However, only three cases in their figures include buoyancy effects. Key parameters for each case (non-dimensional q_w, Gr/Re_b^2 and wall-to-bulk-temperature ratio) were as follows:

Case 1:	$q_w = 0$;	$Gr/Re_b^2 = 0$;	$T_w/T_b = 1.0$
Case 2:	$q_w = 1.8x10^{-3}$;	$Gr/Re_b^2 = 0.026$;	$T_w/T_b = 1.42$
Case 3:	$q_w = 3.5x10^{-3}$;	$Gr/Re_b^2 = 0.029$;	$T_w/T_b = 2.11$
Case 4:	$q_w = 0$;	$Gr/Re_b^2 = 0$;	$T_w/T_b = 1.0$
Case 5:	$q_w = 4.5x10^{-3}$;	$Gr/Re_b^2 = 0.01122$;	$T_w/T_b = 2.02$

Their results demonstrate that their circular LES code can be used for normal operation and other scenarios for the GT-HMR and comparable reactor cores.

The ***third*** reactor core ***configuration*** was studied by McCreery et al. [2002] for an annular geometry in their horizontal MIR facility at INEEL (Task B). Spacer ribs were included in the experiment, representing guide ribs for control rod insertion. Data were obtained for laminar and turbulent regimes. Local turbulence intensity was measured downstream of the spacer ribs and at other locations. (A more complete presentation of these experiments is presented under Task B of the present report.) These experiments should be valuable to assess CFD codes to be applied to complex geometries in the forced convection limit (negligible buoyancy effects and near constant properties) as for normal operating conditions. The data should be compared to turbulent predictions (e.g., k-ε, LES and DNS) to see whether local turbulence models can simulate regions affected by spacer ribs adequately.

Table A-1 below summarizes each of the references mentioned in this section, their applications and correlations/figures for the presented GT-MHR thermohydraulic issues. These references have been submitted as Topical Reports for the present project.

Summary

In the opinion of General Atomics, there are two key areas in which the results from this NERI project have direct commercial applications for gas-cooled reactors: a) turbulent gas flow through relative simple geometry but with large variations of the fluid properties and b) turbulent flows through complicated geometries at constant fluid properties. Both these types of flow are present inside a GT-MHR core under various operating conditions.

In the area of turbulent gas flow through a relative simple geometry but with large variations of the fluid properties, this project has provided correlations that can improve commercially available CFD codes. These codes generally do not provide an accurate simulation of the phenomena of flow "laminarization".

In the area of turbulent flows through complicated geometry at constant fluid properties, this project has provided a tool for selecting the most appropriate turbulence models when simulating these flows with the commercially available CFD codes. This selection will be done by comparing the experimental results from this task with the code predictions for the flow configurations of the experiments.

General Atomics started the process of selecting commercially available CFD codes capable of simulating flows through complicated geometry with constant and with large variations of the fluid properties. The selection of the codes was to be based on their capabilities to simulate turbulent flows through complicated geometry accurately under the condition of flow "laminarization" which can be present in a GT-MHR reactor core and on their flexibility to use the analytical and experimental results obtained from this project. Unfortunately, reductions of scope of this task for lack of funding did not allow the completion of this process. We recommend that the selection of CFD codes, their modification and verification with appropriate experimental data be considered as an extension to this project.

Moreover, further funding should be provided for the completion of Task B in their second experimental test facility. This Task models the GT-MHR plenum region extremely well and is essential for computer code advancement. It is also recommended that the vertical plane channel and annular studies be expanded to take into account closed top and bottom flow boundary conditions as for the natural circulation in a reactor cavity.

Table A-1. Highlights of Topical Technical Reports submitted during project.

Ref. #	Task #	Geometry	Thermohydraulic Issue(s)	Correlation(s)/Figure(s)
1, 2 and 3	C & D* (Ezato, Mikielewicz & Satake)	• Vertical circular tubes	• Heat transfer prediction from strongly heated flows from turbulent to laminarized conditions	Correlations between calculated and measured velocity and temperature distributions. Low-Reynolds number k-ε Launder and Sharma model Direct numerical simulation (DNS) properties with for constant properties
4	F* (D. Jackson, Manchester)	• Vertical plane channel • Uniformly heated and non-heated walls • Aiding and opposing air-flow • Thermal and flow development not complete	• Rejection of heat by natural convection and thermal radiation at the vessel outer surface • Distribution of coolant flow between hotter/cooler reactor core channels	For forced convection: $Nu = C_{therm} 0.0228 Re^{0.79} Pr^{0.4} (T_w/T_b)^{-0.34}$ where $C_{therm} = 1.0+[0.69+5520/Re(x/D_e)^{-0.7}](x/D_e)^{-0.29} \exp(-0.07x/D_e)$ For mixed convection, fit data in Figure 12 to define new Nusselt number correlation.
5	D* (R. Pletcher, Iowa State)	• LES • Vertical plane channel • Aiding air-flow • Uniformly heated and non-heated walls	• Rejection of heat by natural convection and thermal radiation at the vessel outer surface • Distribution of coolant flow between hotter/cooler reactor core channels	Fit predictions in Figure 2 to define new Nusselt number correlation. Note that there are only three conditions for both aiding and opposing flows.
6	F* (D. Jackson, Manchester)	• Vertical annular passage • Aiding and opposing air-flow • Uniformly heated core and insulated outer wall • D/d = 2.1	• Rejection of heat by natural convection and thermal radiation at the vessel outer surface • Distribution of coolant flow between hotter/cooler reactor core channels	Fit data in Figure 7 to define new Nusselt number correlation.

Ref. #	Task #	Geometry	Thermohydraulic Issue(s)	Correlation(s)/Figure(s)
7 and 8	F* (D. Jackson, Manchester)	• Vertical annular passage • Aiding and opposing water-flow • Uniformly heated core and insulated outer wall • D/d = 1.94	• Rejection of heat by natural convection and thermal radiation at the vessel outer surface • Distribution of coolant flow between hotter/cooler reactor core channels	For forced convection ($6{,}000 < Re < 20{,}000$): $Nu_f = 0.042Re^{0.74}Pr^{0.4}$ For forced convection ($4{,}000 < Re < 20{,}000$): $Nu_f = 0.024Re^{0.8}Pr^{0.4}$ For mixed convection: $Nu/Nu_f = [\lvert 1 \pm 1.25x10^5 Bo^* (Nu/Nu_f)^{-2} \rvert]^{0.46}$
9	D* (R. Pletcher, Iowa State)	• LES • Vertical annular passage • Uniformly heated core and insulated outer wall • Aiding air-flow • D/d = 0.3 and 0.5	• Rejection of heat by natural convection and thermal radiation at the vessel outer surface • Distribution of coolant flow between hotter/cooler reactor core channels	For moderately heated cases, fit predictions in Figure 4 to define new Nusselt number correlation. Note that there are only five conditions in the Figure. For highly heated cases, flow characteristics would be estimated from Figure 10 (sheer stress) and Figure 12 (turbulent kinetic energy) distributions. Note that only two buoyancy property values were used in the Figures
10	F* (D. Jackson, Manchester)	• Vertical heated cylinder • Uniform and non-uniform heating • Natural (buoyancy)-induced and pumped aided air-flow through cylinder • Fully-developed flow	• Coolant flow distribution through reactor core channels	For uniform heat flux: $Nu/Nu_f = [\lvert 1-150000Bo(Nu/Nu_f)^{-2} \rvert]^{0.46}$ For uniform wall temperature: $Nu/Nu_f = [\lvert 1-2300Bo(Nu/Nu_f)^{-1.7} \rvert]^{1.0}$
11	D* (R. Pletcher, Iowa State)	• LES • Vertical pipe channel • Pipe uniformly heated • Aiding air-flow	• Coolant flow distribution through reactor core channels	Flow characteristics would be estimated from Figure 13 (turbulent kinetic energy) and Figure 15 (sheer stress) distributions. Note that only three buoyancy property values were used in the Figures.
12	B* (D. McEligot, INEEL)	• Horizontal annular passage with spacer ribs • Fully-developed flow conditions	• Coolant flow distribution through reactor core channels	Suggested that more sophisticated computational models would be needed where laminar flow can determine bulk flow characteristics, and local turbulence models can determine regions affected by spacer ribs.

* See Annual Report

Reference numbers (see list of "References cited" for full citations)

1. Ezato, Shehata, Kunugi and McEligot [1999]
2. Mikielewicz, Shehata, Jackson and McEligot [2002]
3. Satake, Kunugi, Shehata and McEligot [2000]
4. Wang, Li and Jackson [2001]
5. Lee and Pletcher [2001]
6. Li, Talbot, Chung and Jackson [2001]
7. Wu, Xu, He and Jackson [2001]
8. Wu, Xu and Jackson [2001]
9. Lee, Xu and Pletcher [2002]
10. Jackson and Li [2000]
11. Xu, Lee and Pletcher [2002]
12. McCreery, Foust, McEligot, Condie and Pink [2002]

Task B. Measurements of velocity and turbulence fields for complex reactor geometries in MIR flow system -- D. M. McEligot, K. G. Condie, T. D. Foust, G. E. McCreery, R. J. Pink and D. E. Stacey, INEEL

The goals of the INEEL experimental portion of the study are to answer the scientific needs identified in the proposal and to guide code development and assess code capabilities for treating the generic forced convection problems in advanced reactors. Flow through idealized, complex reactor geometries has been examined without complicating thermal phenomena; laser Doppler anemometry and flow visualization were employed with INEEL's unique large Matched-Index-of-Refraction (MIR) flow facility to determine the velocity and turbulence fields and to provide visualization of the flow patterns. The innovation of the INEEL MIR system is its large size compared to comparable systems; it provides means for measurements for the portion of the study dwelling on forced convection in complex reactor geometries.

Experiments INEEL has conferred with General Atomics staff to identify generic features of complex advanced reactor geometries and to determine parameter ranges of interest. Required capabilities of predictive techniques and features of experiments to assess these capabilities were tabulated. Examples of typical geometries of flow channels in advanced gas reactor cores have been illustrated in Figure I-1. The typical characteristics of these geometries include:

- Hexagonal arrays
- "Unheated" inlets and exits (reflector)
- Coolant channels
  GA -- circular tubes
  HTTR -- annuli with 3 spacer ribs
- Control rod passages
  GA -- central circular hole and annular outer flow,
  4 spacer ribs, "cavities" between rods,
  gap > ribs giving possibility of eccentricity
- Reynolds number = zero to "high"

The geometries of the passages between the cooling channels and the exit plenum vary widely as shown for a few designs in Figure B-1. Examination reveals some generic features that would have to be treated by predictive techniques; some characteristics are:

- Hexagonal periodicity
- Geometric transition from coolant channels to jets
- Approximately fully-developed flow at "nozzle" entry

- Non-uniform temperature distribution at "nozzle" entry (from 2 or 3 different fuel columns)
- Convergence from larger region to smaller region
- Approximately constant cross sectional area to reduce contractions and expansions (pressure drop)
- "Short" geometric transitions
- Possible swirl flow due to asymmetric "manifold"
- Possible development section (constant shape)
- Confinement between core support posts (triangular pattern), characteristic lengths same order-of-magnitude
- Jets in negligible to strong crossflows
- Jet Reynolds number
- "Moderate" impingement distance

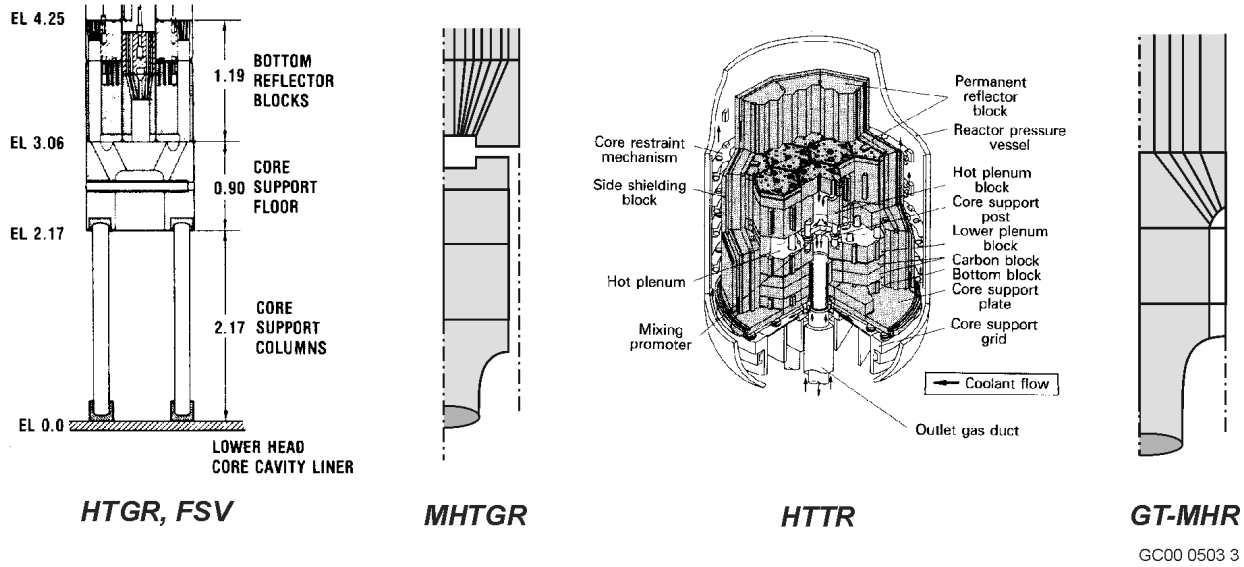

Fig. B-1. Examples of designs for the geometric transition from coolant channels to hot jet flow in the lower plenum of a gas reactor core.

Conceptual experimental models were developed for laser Doppler velocimeter measurements in the unique INEEL Matched-Index-of-Refraction flow system, consistent with the original proposal, to examine flow in complex core geometries (ribbed annular cooling channels and control rod configurations) and in the transition from cooling channels to formation

of jets issuing into a plenum. These experiments address two thermal/hydraulic phenomena selected by General Atomics: (1) normal operation at full or partial loads and (2) loss of forced reactor core cooling. Several exit geometries were considered.

The benefit of the **MIR technique** is that it permits optical measurements to determine flow characteristics in passages and around objects to be obtained without locating a disturbing transducer in the flow field and without distortion of the optical paths. With a transparent model of different refractive index than the working fluid, the optical rays can be refracted in such a manner that measurements are either impossible (e.g., cannot "see" the desired location) or require extensive, difficult calibrations. Thompson, Bouchery and Lowney [1995] demonstrated this situation when laser Doppler velocimetry is applied to a rod bundle; with refractive-index-matching the measurement and position determination are relatively straight forward while without matching the beams may not cross to form the measurement control volume at the desired focal length, if they cross at all. The MIR technique is not new itself; Corino and Brodkey [1969] employed it to measure turbulence structure in a circular tube earlier. Recent applications of the technique include, but are not limited to, those of Durst, Jovanovic and Sender [1993], Parker and Merati [1996], Cui and Adrian [1997] and Becker et al. [2002].

The **innovative advantage** of the INEEL system is its large size, leading to improved spatial and temporal resolution compared to others. To date most experiments with index matching have been small, with characteristic lengths of the order of five cm or less. In contrast, the INEEL MIR flow test section has a cross section of about 60 cm x 60 cm and is about two meters long, allowing the use of models of substantial size. The working fluid is a light mineral oil. With the fluid temperature controlled, the quartz components can barely be seen at wave lengths in the visible spectrum. The maximum flow rate should give Reynolds numbers up to about 10^5 based on the cross section. The refractive index of the oil is maintained at the desired value by a parallel temperature control system which maintains a constant temperature in the test section to within 0.1°C. In measurements for a boundary-layer-transition experiment, meaningful velocity and turbulence data were obtained as close to the surface as $y^+ \approx 0.1$ and less [Becker et al., 2002].

Budwig and his students measured the viscosity, density and refractive index of our mineral oil as a function of temperature in his laboratory at the University of Idaho [Orr, Thomson and Budwig, 1997]. The thermal conductivity of the preliminary sample of the oil was measured by Sparell [1995] at three temperatures using the test method of ASTM E1225, modified for liquids. Based on the specific gravity one may estimate the specific heat from handbook relations. From this information, one may estimate the Prandtl number ($Pr = \nu/\alpha$) to be about 250 at 24°C.

The main loop and temperature-control loop are equipped with several thermistor probes for temperature measurements. Differential pressure transducers and manometers can measure flow speed and static pressure using several pitot-static probes and various wall static pressure taps. Velocity and turbulence measurements are primarily obtained with a two-component, TSI fiberoptic-based laser Doppler velocimeter. Data acquisition is controlled via the FIND-W software for the LDV system. Desired traversing locations plus measuring parameters are specified by the operator and then the sequence is initiated. Data reduction to determine mean quantities and/or spectra is accomplished later, using other FIND-W subprograms. Ultimately,

the raw time series data are transferred to permanent magnetic or optical storage media such as compact discs (CDs).

While the backscattering LDV mode [Durst, Melling and Whitelaw, 1976] is more convenient in operation, the validated data rate is much lower than when using forward scattering for the same conditions. To obtain statistically meaningful results, longer measuring times are required with backscatter than forward scatter. Since its low velocities lead to inherently "slow" characteristic times for flow phenomena in the MIR system, it is desirable to employ forward scattering to avoid longer measuring times than needed. The traversing mechanism was designed to use the LDV in the forward scattering mode and to avoid relative motion between the test section and the optics. To accomplish the latter objective, it is mounted directly on the structure supporting the test section. For vertical motion, platforms on each side of the test section are moved simultaneously under precise computer control to maintain alignment of the transmitting and receiving optics.

During the Summer 2000, INEEL management decided to close the remote facility where our unique MIR flow system was located and to move our system into Idaho Falls. The move gives us a better system and more efficient data acquisition, but it was expected to be out of operation for about two months. Disassembly was started during the second week of October. The system was moved to the IEDF building in town and the Facilities staff did an excellent job of reassembly and installation of necessary new subsystems. It is a much better looking installation. Their tasks were completed in March with the installation of a laser cooling pump with an adequate flow rate. However, at the end of March, the variable frequency drive (vfd) for the main pump failed; after considerable effort to diagnose and repair the problem with the assistance of the manufacturer, a new vfd was purchased and installed in mid-May. At the end of May re-qualification experiments were conducted; a model for another waiting customer was installed in early June and results with it demonstrated that the MIR system still worked well. The first NERI model was installed in the MIR flow system and the initial experiments were conducted in early September 2001.

Two experimental models were employed. The first simulated flow in a control rod channel (GA) or a coolant channel, with annular passages interrupted by periodic spacer ribs. Figure B-2 depicts this model schematically. The second experiment addressed a ribbed annulus upstream of an idealized two-stage jet transition from generic coolant channels to a plenum (see Figure B-1b). It is envisioned as a combined experiment focusing on the first stage, a jet issuing from a converging flow into a collecting plenum (or impingement chamber).

Experiments with the **first model** were conducted with the MIR auxiliary flow system. It is a ribbed annulus forming an annular jet exhausting into the larger surrounding test section of the MIR flow system, as indicated in Figure B-2. Nominal dimensions are presented in Figure B-3. Three ribs are distributed equally around the circumference; these sets are spaced longitudinally with nominal pitch p/s of 25.3, approximately. The ribs have nominal widths W/s of about two and nominal lengths L/s of about eight. Outer diameter of the annulus is 85.2 ± 0.1 mm (3.3 in.) and the inner diameter is about 69.60 ± 0.03 mm, giving spacing $s \approx 7.80 \pm 0.05$ mm and a radius ratio of 0.82, approximately. Spacer width at the outer radius is 15.2 mm ± 0.1 mm and spacer length is 61.0 mm ± 0.1 mm giving a length-to-width ratio of 4.0 at the outer radius. Three ribs are distributed equally around the circumference, as shown in Figure B-3.

Axial distance between rows of spacers is 132 mm ± 2 mm. Experience shows streamwise periodic flow typically is reached after two to three repeating geometric cells [Berner, Durst and McEligot, 1984; Habib, Durst and McEligot, 1984]; likewise, one or two cells are needed at the end to avoid upstream influence from the exit. Therefore, a minimum of five spacer ribs are needed to establish a representative cell for measurements with its flow pattern corresponding to the periodic conditions of the application. Model length is about 1.22 meters (4 ft.) with six periodic cells formed by the spacer ribs. For this model the outer tube is quartz while the other transparent components are fabricated from acrylic plastic.

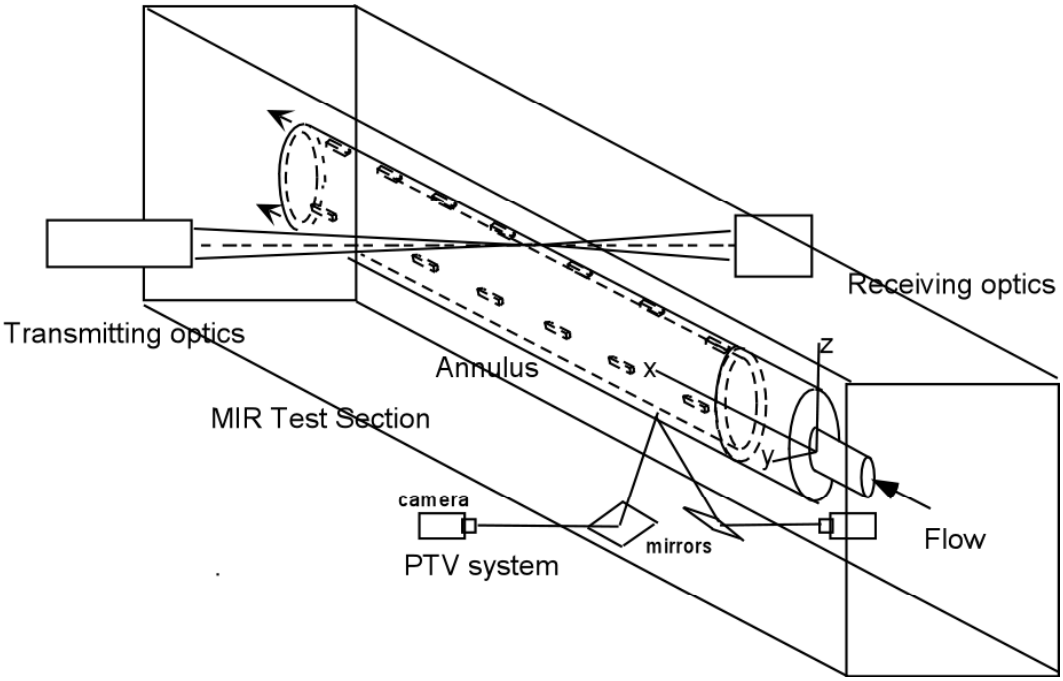

Fig. B-2. Schematic diagram of apparatus for experiments with the initial model using the laser Doppler velocimeter system (LDV). The potential application of a Particle Tracking Velocimeter system is also shown schematically.

The model is mounted longitudinally in the MIR test section with flow of the working fluid surrounding it to maintain the desired temperature; thus, optical access is via the plane side walls with the fluid and solid regions inside intended to be held at an equal, constant, uniform value of their refractive indices. Flow enters the model through a chamber containing a honeycomb structure to eliminate swirl; then an abrupt entrance to the annulus assists tripping the flow to turbulent, if not already in that state. Components outside the test section include the pump for the working fluid and a Coriolis flow meters.

With the existing loop auxiliary pump for circulating flow through the model, a maximum flow rate of about 100 kg/min has been demonstrated. This value corresponds to a maximum Reynolds number, based on nominal conditions, of about 1200.

Approximate coupled optical and thermal analyses were conducted to estimate the potential effects of room temperature variation on LDV accuracy in the new location for the MIR

flow system. Calculations show that the LDV focal shift due to external heating or cooling of the windows is not likely to be significant for any reasonable room temperatures.

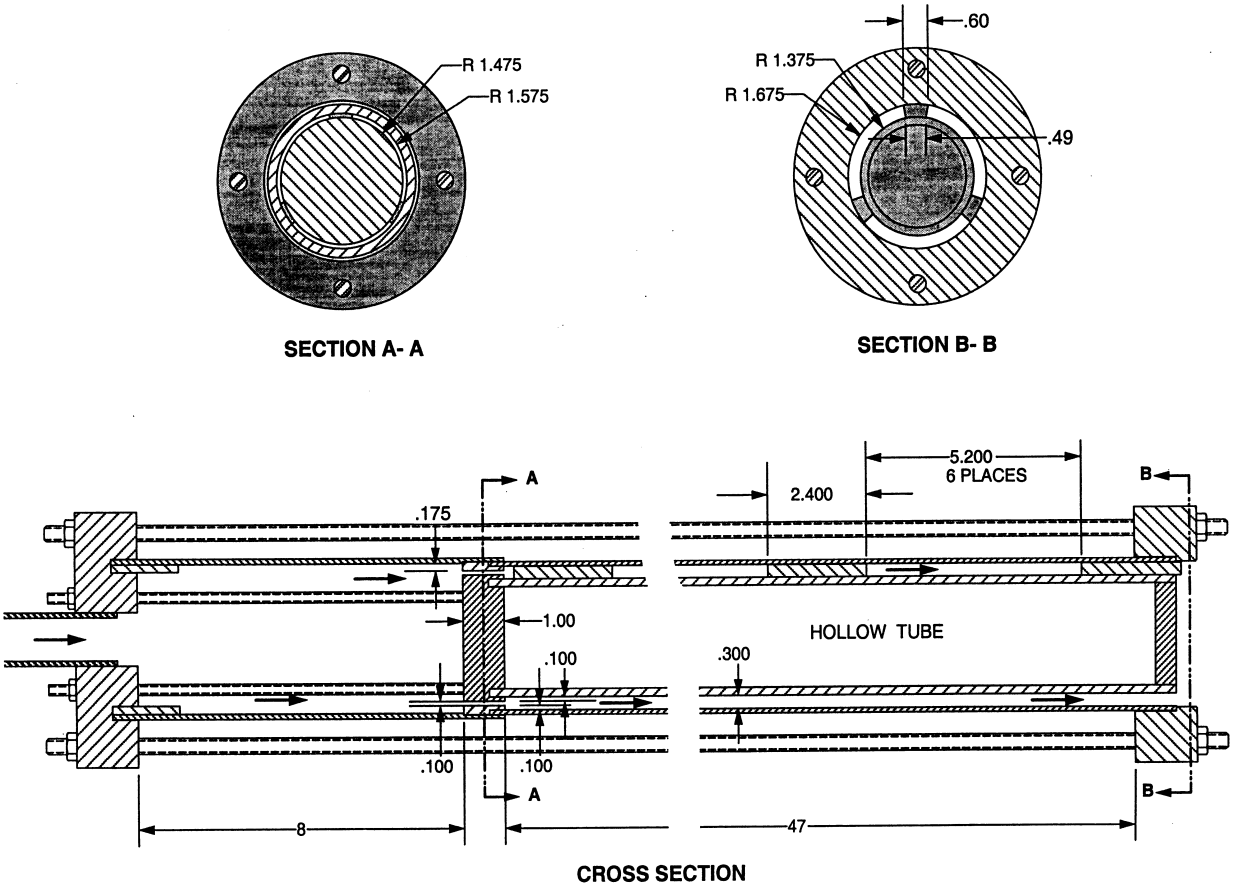

Fig. B-3. Design of initial model for experiments on fluid physics of complex geometries (= ribbed annulus), nominal dimensions given in inches.

Flow visualization experiments were conducted in the first model placed in a water flow loop. Recirculating regions were found behind the spacers, as expected, identifying regions of potentially high thermal resistances ("hot spots" in some applications). Sinuous unsteady flows were also seen at higher laminar flow Reynolds numbers between approximately 100 and 500, based on hydraulic diameter. The photographs presented in Figure B-4 show the development of sinuous unsteady flow between Re = 100 (top two photographs) and approximately 500 (bottom photograph) between the third and fourth spacers in one row of spacers. The amplitudes of the waves increase downstream with each spacer that the flow encounters. The dye, injected as a tracer, rapidly diffused for Reynolds numbers higher than 500. The combination of rapidly diffusing dye and lack of index-matching at the air-quartz and quartz-water interfaces made photography of the flow visualization difficult and impossible at high Reynolds numbers. Injection of small air bubbles in the oil flow has proven to be an effective flow visualization technique for use in the MIR flow loop (we used this technique effectively for internal flows and for external flows in other experiments in the MIR flow system) where dye injection would contaminate the oil.

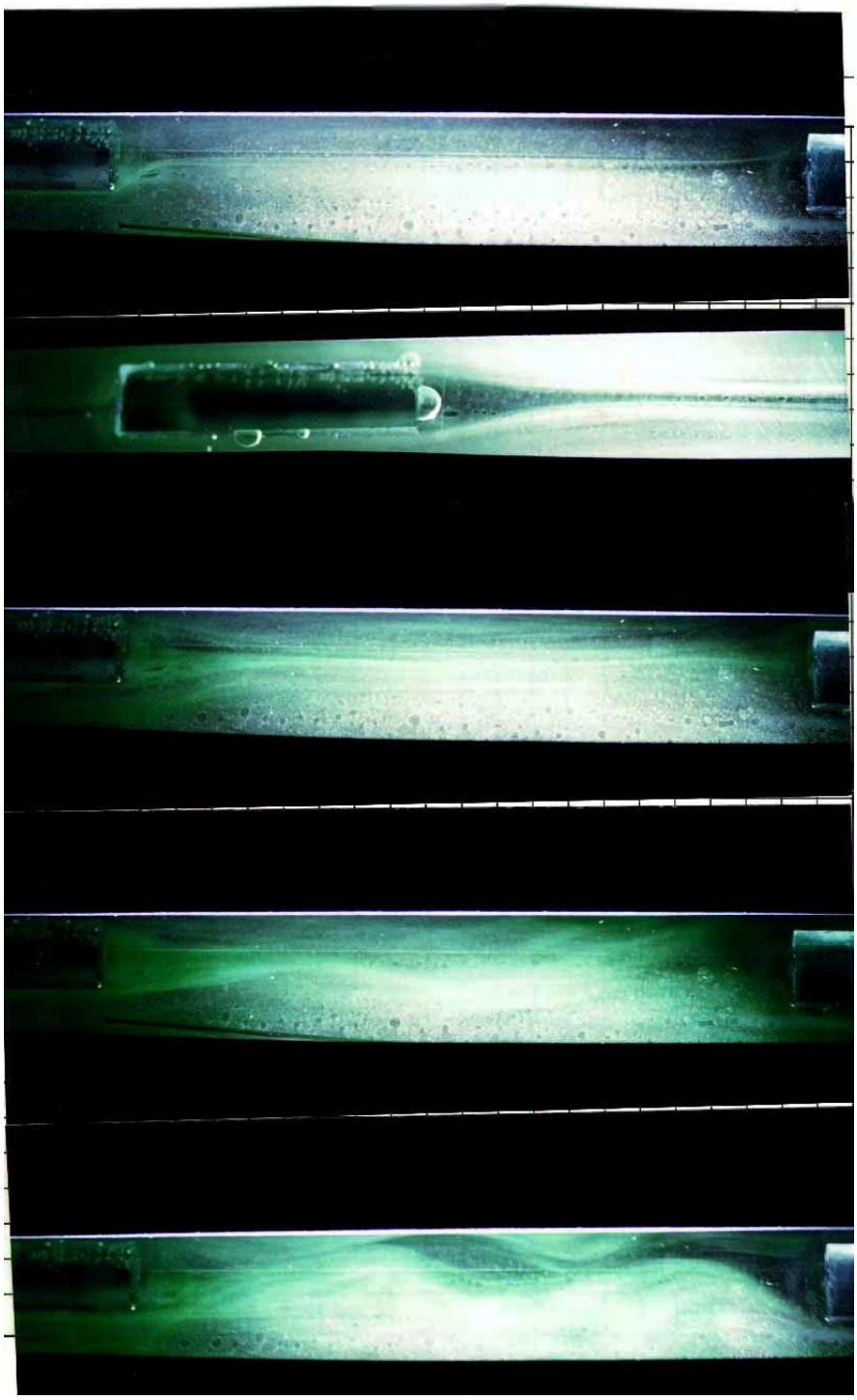

Fig. B-4. Water flow visualization in the first model of a ribbed annular geometry; flow is from left to right.

The **MIR experiments** with the **first model** were aimed at obtaining benchmark data to test the capabilities of CFD codes to handle ribbed annular geometries without the complications of turbulent transport (i.e., laminar flow requiring no turbulence modeling). LDV measurements were obtained with typically 20,000 samples per measurement location. The large number of

samples is necessary for determining higher order moments of turbulence statistics with good accuracy [Durst, Melling and Whitelaw, 1976]. For the velocity data, the Reynolds number (= 4 $\dot{m}$ /(Π (D_O+D_i)μ)) was 1120 ± 30. Three initial radial traverses were obtained to test the hypothesis that the flow is streamwise-periodic by the third representative cell between the ribs. The mean streamwise velocity profiles, shown in Figure B-5, were obtained for corresponding positions mid-way between spacers both axially and circumferentially in the cells between the third and fourth, the fourth and fifth, and the fifth and sixth sets of spacers. Measurements were obtained at approximately 25 radial positions for each traverse. The mean streamwise velocity profiles are similar to within ± 0.03 m/s at any radial position. This agreement supports the hypothesis that the flow is streamwise-periodic; consequently, measurements can be concentrated in a single representative cell such as between the third and fourth sets of spacers.

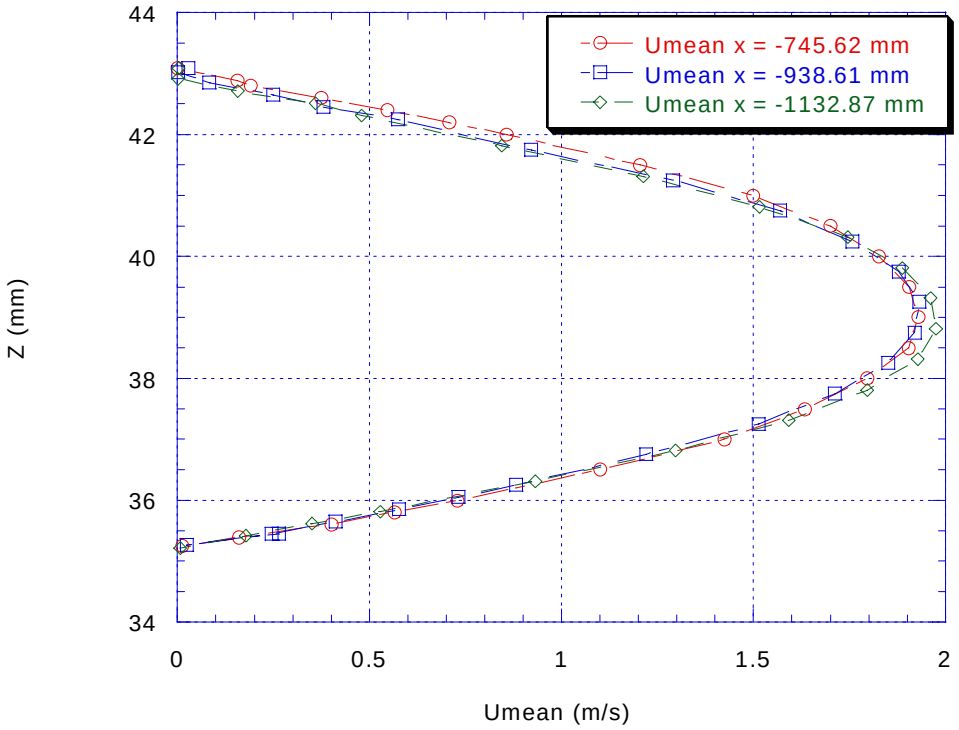

Fig. B-5. Radial profiles of mean streamwise velocities for three corresponding positions, circumferentially and axially midway between spacers.

In Figure B-6 the measured radial profile of the streamwise velocity component is compared to the analytical solution for laminar flow in an axisymmetric annulus (i.e., without ribs) presented by Kays [eqn. 8-22, 1966]. Normalization is by the nominal inside radius of the annulus and the bulk velocity one would have in a concentric annulus of the same nominal dimensions without ribs. With a radius ratio of about 0.82, the analytic solution is close to that of a parallel plate duct which would have u/V_b = 1.5 at the centerplane. Between ribs (circumferentially) the flow must accelerate due to the blockage of the ribs; although this profile was taken at the furthest location from the ribs, one sees the increased velocity perseveres. The shape of the measured profile agrees with the analytic prediction for a bulk velocity about twelve per cent higher than the value which applies, in a sense, in the space between the ribs axially.

The blockage of the ribs is one-sixth of the circumference or about seventeen per cent of the cross section. The radial mean velocity component was less than about one per cent of the streamwise maximum and the rms radial fluctuation was less than about 1-1/2 per cent of the streamwise maximum. The rms streamwise fluctuations were about five to ten per cent of the maximum, possibly corresponding to the fluctuating sinuous flow seen in the water visualizations.

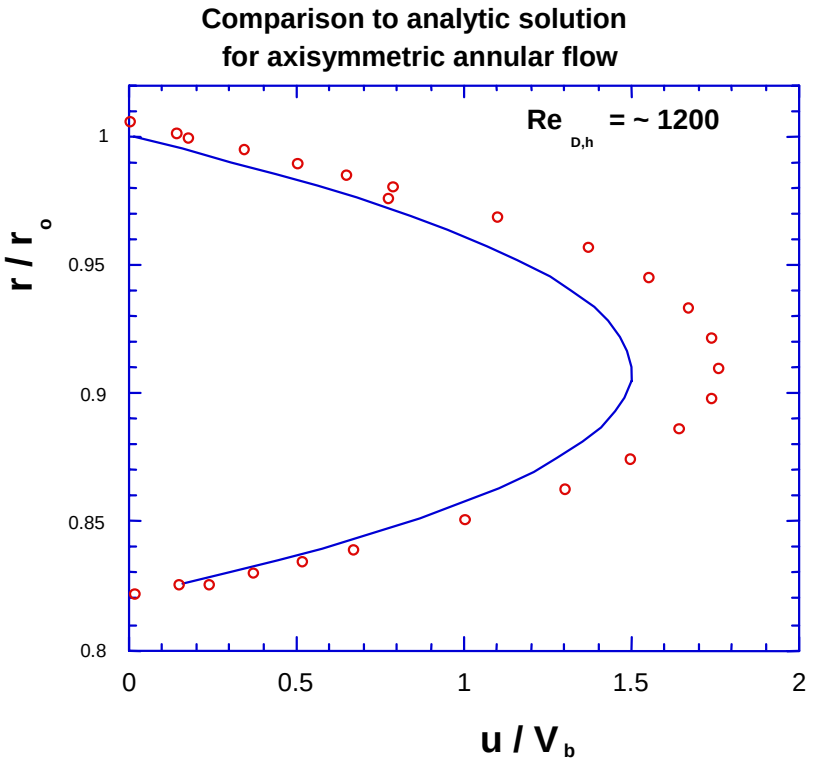

Fig. B-6. Comparison of measured profile in ribbed annulus to analytical prediction for laminar flow in an axisymmetric annulus at the same flow rate [Kays, 1966].

An axial traverse midway between the annulus surfaces and midway between the ribs (Figure B-7) demonstrates the acceleration and deceleration of the flow induced by the periodic spacers. In this figure flow is from right to left and the locations, indicated by the traversing mechanism, increase in the upstream direction. Approximate locations of the adjacent ribs are shown on the diagram. One sees that at the midpoint between spacers axially the mean velocity is near its minimum value. The maximum acceleration occurs at a location approximately in line circumferentially with the face of the downstream rib; it corresponds to an acceleration factor $K_v = (\nu/V^2)\, dV/dx$ of about 1.1×10^{-5}. This value normally would be expected to induce laminarization [Murphy, Chambers and McEligot, 1983; Chambers, Murphy and McEligot, 1983] but in this circumstance the favorable (non-dimensional) streamwise pressure gradient probably dominates the tendency towards laminarization. The deceleration is more gradual after passing between the ribs; the maximum value is about 6×10^{-6} and it occurs at about one-quarter of the axial distance between the ribs.

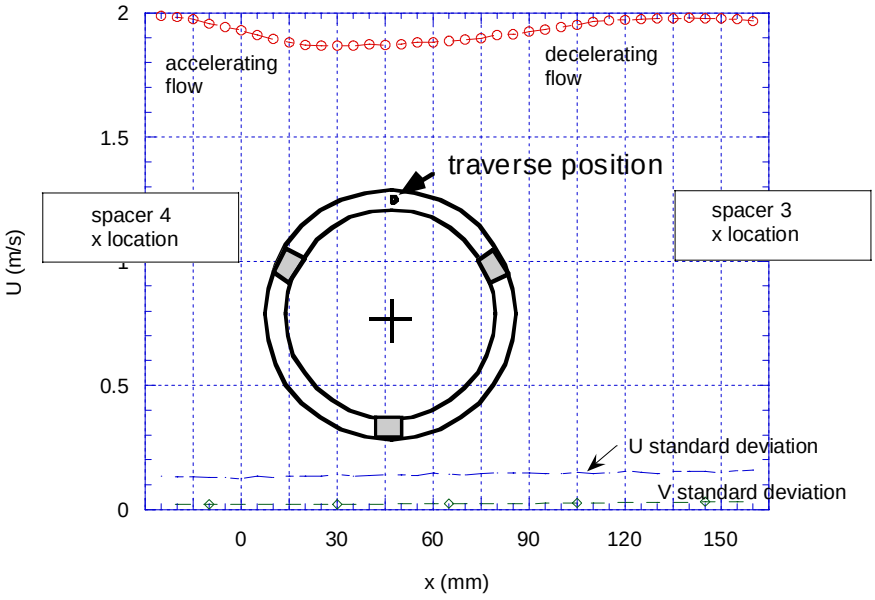

Fig. B-7. Axial streamwise velocity profile away from spacer ribs (flow is from right to left and the locations increase in the upstream direction from the fourth rib), Re ≈ 1120.

Since the flow visualization showed possible shedding of eddies behind a rib, power spectral densities of several LDV measurements were obtained to determine the vortex shedding frequency. The measurements were obtained at locations both downstream of a spacer and away from a spacer. Measurements consisted of 100,000 samples to insure sufficient data for statistical analysis. The duration of the measurements was several minutes, which insured that the measurements were obtained over a time duration of many times that of the slowest expected vortex shedding period. For (long) circular cylinders, eddy shedding at a non-dimensional frequency St ≈ 0.2 occurs for Re_D > about 50. For the present geometry, the predominant frequency at either location was measured to be 11 Hz ± 0.5 Hz, which corresponds to St = 0.135 ± 0.005, based on average spacer width and annulus bulk velocity. This result agrees well with CFD calculations by Zhang et al. [1997] who numerically modeled flow for inline and staggered parallel-plate fin heat exchangers. They calculated a Strouhal number based on width of St = 0.14 for Reynolds numbers varying from 381 to 1128. Their calculations are for a fin length divided by width ratio = 8.53 and Reynolds number based on hydraulic diameter of the channel. The length/width ratio of our spacers is about four. The results may imply that length/width ratio has only a small influence on eddy shedding frequency, at least for ratios much larger than unity, although further research would be necessary to confirm this hypothesis. For streamwise length/width ratios of much less than one (and large spans = height in the present orientation), St is expected to be approximately 0.2 at this Reynolds number, based on the work of Huang and Lin [2000] who report that St ≈ 0.2 for Re_d ranging from 1,000 to 1,500.

By rotating the model, it was possible to obtain profile measurements downstream from a rib conveniently. Data along the radial centerplane downstream of a spacer reveal some details of the recirculating eddy which forms behind a rib. Figure B-8 provides an axial traverse along the "centerline" downstream of a rib; again flow is from right to left and the locations, indicated

by the traversing mechanism, increase in the upstream direction from a reference of zero at the face of the downstream rib. Along this line the mean recirculating eddy appears to end at about x = 96 mm (U ---> 0) with negative streamwise velocities from there to the rear face of the upstream rib. The mean fluctuating components u′ and v′ are relatively constant downstream of the eddy with smaller values in the eddy and in the near vicinity of the downstream rib. The rms streamwise fluctuations for velocity profiles away from the spacer ribs were noted to be about five to ten per cent of the maximum. For these measurements in-line with the spacers, the rms streamwise fluctuations are larger than for measurements away from the spacer ribs. As shown in Figure B-8, the maximum rms fluctuation is approximately fifteen per cent of the maximum streamwise velocity. The magnitude of the fluctuating component of axial velocity exceeds the mean component near the boundary of the recirculation zone.

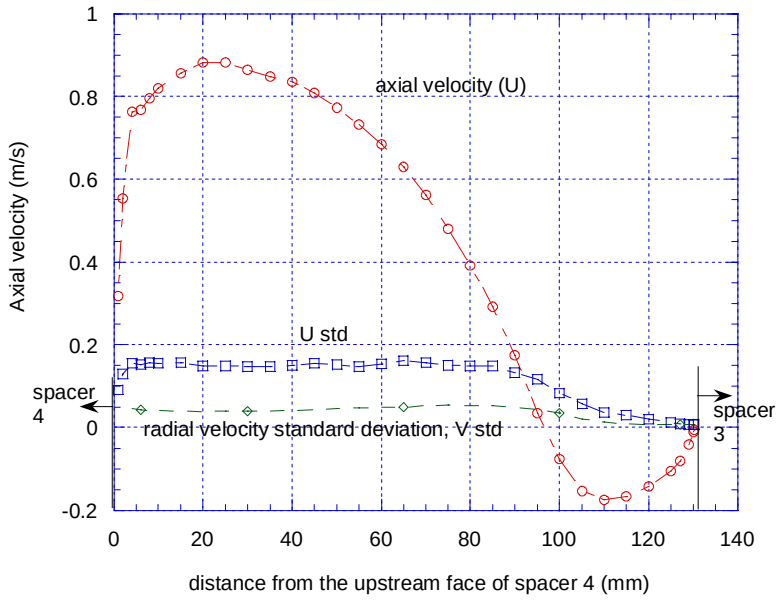

Fig. B-8. Axial profiles of mean velocity and fluctuations along "centerline" downstream of a rib (flow is from right to left and the locations increase in the upstream direction from the fourth rib).

Four radial traverses of mean streamwise velocity, taken along the centerplane downstream of rib 3, are provided in Figure B-9. They were located near the upstream rib (x = 120 mm), near the end of the mean eddy (x = 98 mm), midway (x = 65.5 mm) and approximately at the three-quarters point (x = 32 mm). With the exception of the one near the end of the eddy, all appear to be near parabolic, as expected for laminar flow between infinite parallel plates. Even the backflow behind the rib has this approximate appearance.

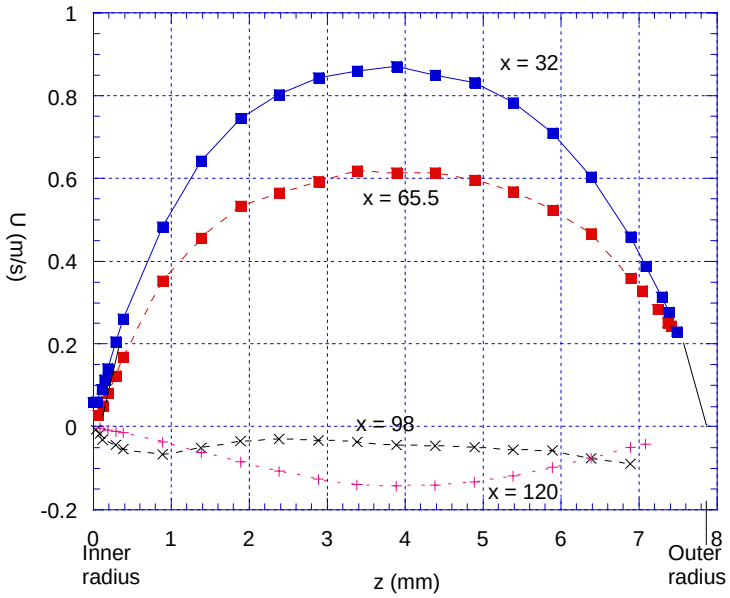

Fig. B-9. Radial profiles of mean streamwise velocity along centerplane downstream of a rib (locations increase in the upstream direction from the fourth rib where x is taken to be zero).

As expected, the LDV data showed that a slow recirculating region formed behind a rib. This region could be expected to produce a "hot spot" if the inner surface were heated as in fuel cooling channels of some gas-cooled reactors. However, as noted, frequency spectra for the flow in this region demonstrated an oscillating flow characteristic of eddy shedding from a circular cylinder. Increased levels of fluctuations u′and v′ were also observed. Consequently, at these flow conditions a "hot spot" would likely be ameliorated by the oscillating flow (and thermal conduction in the solid rod). Turbulence may also be indicated from profiles from radial traverses obtained at positions downstream of the spacers. For example, the profiles of streamwise mean velocity show steeper gradients near the wall than for the laminar flow further away from the ribs.

To examine the difficulties encountered in the application of commercial CFD codes to complex geometries calculations were conducted with the FLUENT code for the geometry of the first model. Calculations were performed for conditions identical to those for the experiments. A steady, laminar flow formulation was used to reflect the expected overall flow conditions. This numerical formulation effectively ignores turbulence which may occur downstream of the spacers. Since heat transfer and viscous heating are not concerns for these calculations, solution of the energy equation was not included in the simulation. Oil properties are assumed to be constant over the narrow temperature range of the experiment. The 3-D equations representing continuity and momentum using vector and indicial notation are as follows:

Continuity

$$\nabla \cdot \rho \boldsymbol{U} = 0 \qquad (1)$$

Momentum

$$\rho \boldsymbol{g} + \nabla \cdot \tau_{ij} - \nabla \boldsymbol{p} = \rho \frac{\boldsymbol{dU}}{\boldsymbol{dt}} \qquad (2)$$

where

$$\frac{\boldsymbol{dU}}{\boldsymbol{dt}} = \frac{\partial \boldsymbol{U}}{\partial \boldsymbol{t}} + (\boldsymbol{U} \cdot \nabla)\boldsymbol{U} \qquad \text{and} \qquad \tau_{ij} = \mu\left(\frac{\partial \boldsymbol{u_i}}{\partial \boldsymbol{x_j}} + \frac{\partial \boldsymbol{u_j}}{\partial \boldsymbol{x_i}}\right)$$

A structured meshing technique was utilized with hexahedral cells. The computational domain is an one-third circumferential slice of the domain to take full advantage of circumferential periodicity conditions to minimize computational expense. Periodic boundary conditions were employed.

A fine structured grid was constructed of hexahedral cells to minimize grid effects on the accuracy of the simulation. A "boundary layer" mesh was created for each surface of the annulus. The space between the two opposing boundary layers was treated with nine equi-spaced cells for a total of nineteen cells for the radial direction in the annulus. This approach resulted in a very large computational domain consisting of 281,560 computational cells.

The commercial FLUENT code was used for this analysis. A second-order upwind scheme was used for higher-order accuracy. A "PRESTO" (PREssure STaggering Option) scheme [Ferziger and Peric, 1997] was implemented to account for the tube wall curvature in the computational domain. This scheme uses a discrete continuity balance for a “staggered” control volume about the face to compute the “staggered” face pressure. This scheme minimizes errors that would be introduced at the tube wall by assuming the normal pressure gradient at the tube wall is zero. A "PISO" (Pressure-Implicit with Splitting of Operators) scheme for pressure-velocity coupling [Patankar, 1980] was utilized. It is part of the "SIMPLE" family of algorithms and is based on the higher degree of the approximate relation between the corrections for pressure and velocity.

All runs were made on an SGI Origin Shared Memory Workstation. The computational runs were performed in an eight parallel processing mode using physical domain decomposition for parallization purposes. This technique resulted in very reasonable run times with the various simulations requiring elapsed times of only a few hours to achieve convergence to 0.001 for residuals.

Code predictions of streamwise velocity distributions are compared with data for the radial center plane downstream of a rib in Figures B-10, B-11 and B-12. Figure B-10 presents a comparison of results of an axial traverse from the center point of an upstream face of a spacer to the center point of a downstream face of the next upstream spacer. The general trends are predicted but the magnitudes differ except in the immediate vicinities of the two ribs. The agreement would be closer if the length of the recirculation region were not underpredicted by approximately fifty percent.

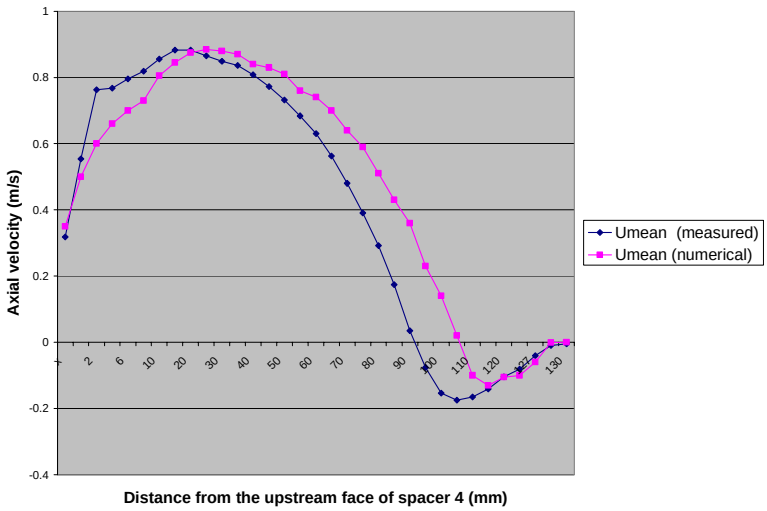

Fig. B-10. Comparison of results from commercial CFD code to measurements for streamwise velocity along the "centerline" downstream of a rib (flow is from right to left and the locations increase in the upstream direction from the fourth rib).

Figures B-11 and B-12 present comparisons of results for radial traverses along the radial centerplane downstream from a spacer. This region is affected by eddy shedding from the spacers and may exhibit localized turbulence. The measured profiles are lower than the predictions at these two locations, consistent with the differences between axial profiles presented in Figure B-10. While measurements show near-parabolic profiles that are nearly symmetric, the predictions are skewed towards the inner wall (i.e., maxima are closer to the inner wall) and the calculations near the surfaces show unexpected reverse curvatures. This latter observation may indicate problems with the treatments in the "boundary layer" sections of the numerical mesh.

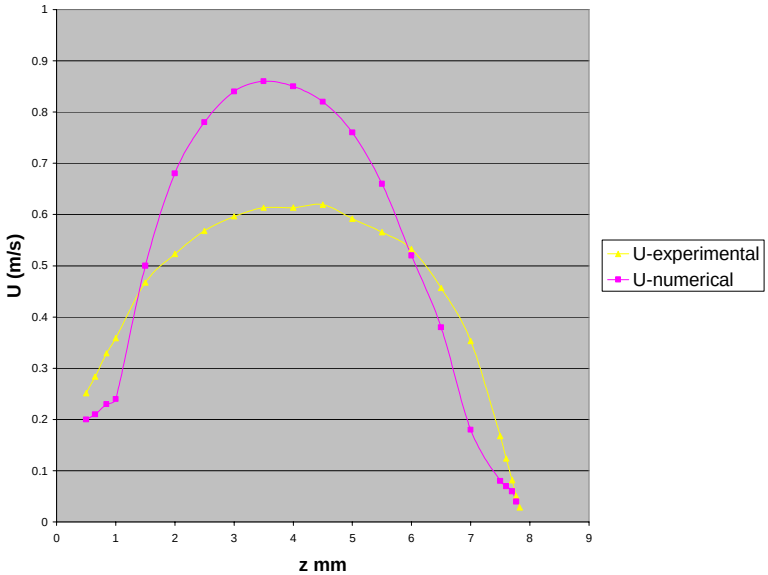

Fig. B-11. Comparison of radial profile predictions from commercial CFD code to measurements for streamwise velocity on the centerplane approximately midway between spacers (x = 65.5 mm upstream from rib 4).

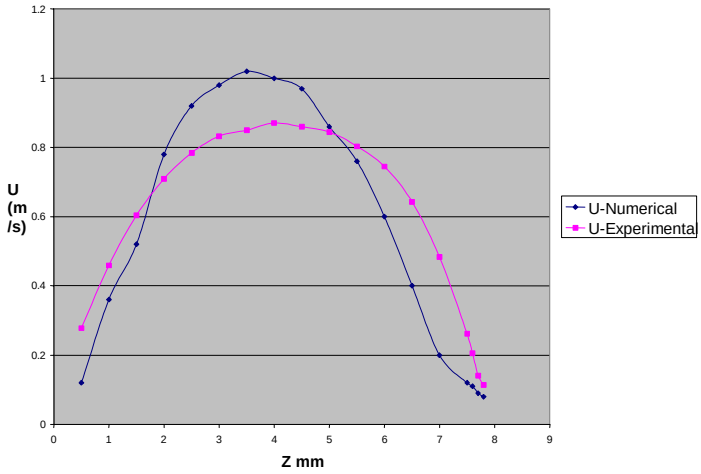

Fig. B-12. Comparison of radial profile predictions from commercial CFD code to measurements for streamwise velocity on the centerplane approximately three-quarters distance downstream from a spacer (x = 32.8 mm upstream from rib 4).

Although not shown, the calculations agree well with radial traverse data obtained away from the spacers [Foust, 2002]. The calculated profile has the same near-parabolic profile as the data and the analytical solution for an axisymmetric annulus. These comparisons therefore help validate the steady, laminar flow approach for simulation of mean flow characteristics away from the ribs.

Overall, it appears that use of a steady laminar treatment with this code is not an adequate approach for the detailed flow in this case involving periodic eddy shedding and possible turbulent transport in the free shear layers downstream from ribs. A laminar flow analysis may produce reasonably good results for mean flow characteristics away from the spacers but a more complicated approach would be necessary to simulate flow properties in the regions of the flow affected by the spacers, including possible turbulent free shear layers. Unfortunately, available funding did not permit attempting an unsteady laminar calculation or an unsteady RANS treatment. When turbulent transport does become significant, either at this Reynolds number or higher, this situation will provide a severe challenge to simple RANS codes. Either DNS or LES codes may be required to handle such a case fully. Some initial applications of Prof. Pletcher's LES treatments are discussed under Task D.

The **second model** adds the first stage of the idealized two-stage jet transition from generic coolant channels to a plenum (see Figure B-1b). It may be described as the geometric transition to a circular semi-confined jet with an upstream inlet of fully-developed annular flow modified by obstructions. For this experiment the desired features include:

- Symmetry and/or periodicity (to ease computations for comparisons)

- Flow sources from separate regions (simulating three fuel columns with flow to a common corner hole/jet)

- Approximately fully-developed flow at entry
- Convergence from larger region to smaller region
- Approximately constant cross sectional area to reduce contractions and expansions (pressure drop)
- "Short" transitions
- Possible development section (constant shape)
- Semi-confined or confined enclosure
- "Moderate" impingement distance
- Geometric ratios in generic idealization comparable to typical AGCR applications

Figure B-13 shows an overview of the experiment and Figure B-14 provides a cross section of the model; flow is from left to right. After the circular inlet plenum, the fluid passes over symmetric trips at the beginning of the ribbed annular section, passes along the annulus and through the constant-area convergence and then leaves via the circular mixing plenum and radial exit to the outlet plenum. With the exception of the periodic spacer ribs in the upstream annulus, the design is axisymmetric to ease the application of predictive calculations. One can see that the geometric ratios of the mixing plenum are comparable to those of Figure B-1b.

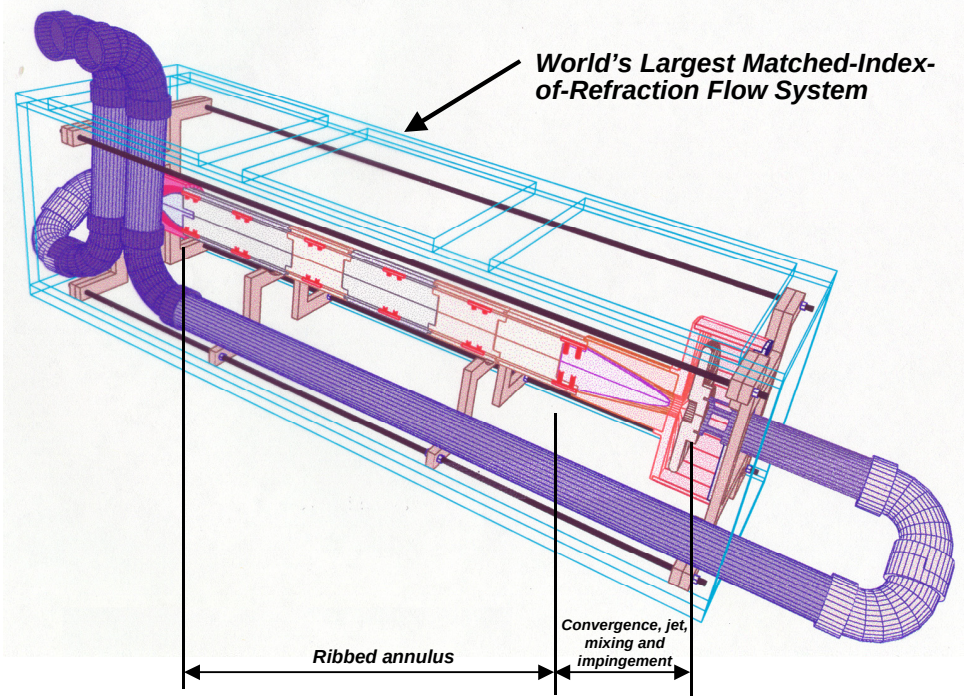

Fig. B-13. Overview of second experiment in MIR flow system.

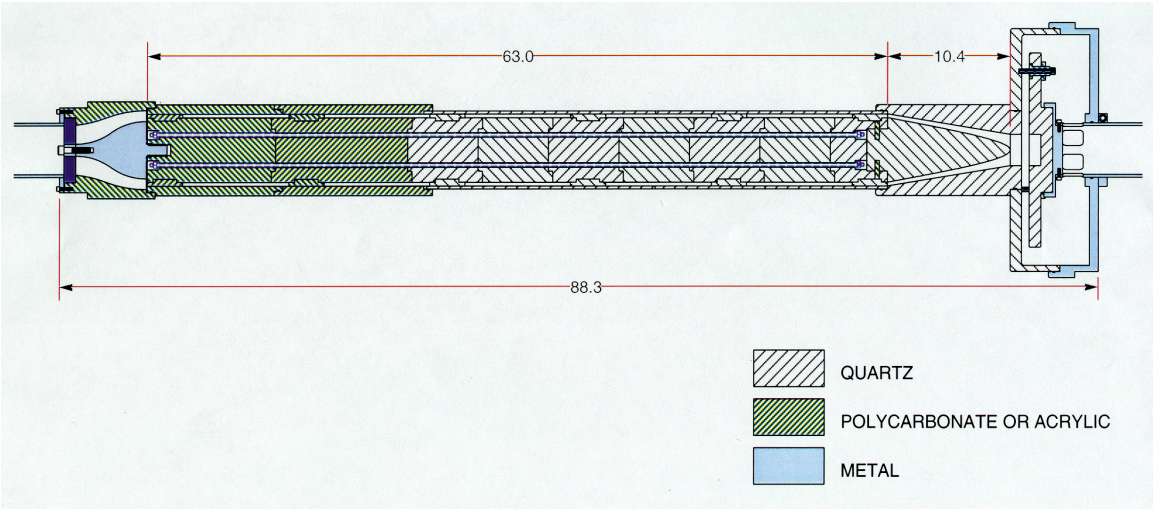

Fig. B-14. Design of second experiment, emphasizing annular flow and the first stage of an idealized two-stage jet transition from generic coolant channels to a plenum (dimensions in inches).

The circular annulus has a nominal outer diameter of about 150 mm (6 in.) and nominal inner diameter of about 135 mm (5.4 in.), a scaling of about three to four times the diameter of fuel rods in typical gas-cooled reactors. With a measuring control volume diameter of 60 μm, these dimensions give spatial resolution (s/d) of about 125 across the gap. Model length is about 1.5 meters with five periodic cells formed by the spacer ribs. Four ribs are distributed equally around the circumference; these sets are spaced longitudinally with pitch p/s of forty, approximately. The ribs have widths W/s of about two and lengths L/s of about ten for dimensions.

The diameter of the mixing plenum D and, therefore, the outlet of the convergence are 66 mm (2.62 in.), giving the same cross sectional area as the annulus. Depth is approximately equal to the diameter and the radial outlet, which simulates crossover tubes, has approximately the same flow area as the inlet to the mixing plenum. The centerplane of the outlet is at a distance x/D about 0.5 from the end of the plenum.

The model was mounted longitudinally in the MIR test section with flow of the working fluid surrounding it to maintain the desired temperature (Figure B-7); thus, optical access was via the plane side walls with the fluid and solid regions inside being held at equal, constant, uniform values of their refractive indices. Components outside the test section include the pump for the working fluid, an independent temperature control system, flow meters and insulation.

In order to approach the criterion of having equal flow areas through the annulus and the remainder of the model, the inside dimensions of the annulus outer tubes were measured when received and the sizes of the inner rod and the downstream components were adjusted accordingly. The component dimensions were measured and are within design tolerances. Fabrication of the acrylic, polycarbonate and aluminum components was completed at INEEL

shops. Before installation the model was assembled in a mockup of the MIR test section to check fitting of the individual components and to test procedures for installation.

In order to provide insight into the range of velocities and approximate flow patterns to be expected in the axisymmetric model for the MIR flow system, **preliminary flow visualization measurements** have been made with a two-dimensional planar model of the annular contraction and impingement chamber of the second experiment. The apparatus consists of a full-scale axial and radial representation of the axisymmetric MIR model. The length of the section representing the inlet conical annulus is shortened, as shown in Figure B-15. The thickness of the flow channel is 19 mm (0.75 in.). The rectangular cross-section was chosen for its greatly simplified construction in comparison with the axisymmetric geometry of the MIR model. Flow to this apparatus comes from a water flow loop developed for our EM Science project [McCreery et al., 1999]. Flow visualization and velocity determination were by streak line photography; a typical example is presented in Figure B-16. In the experiments the Reynolds number, based on inlet hydraulic diameter, was varied from about 500 to 2100.

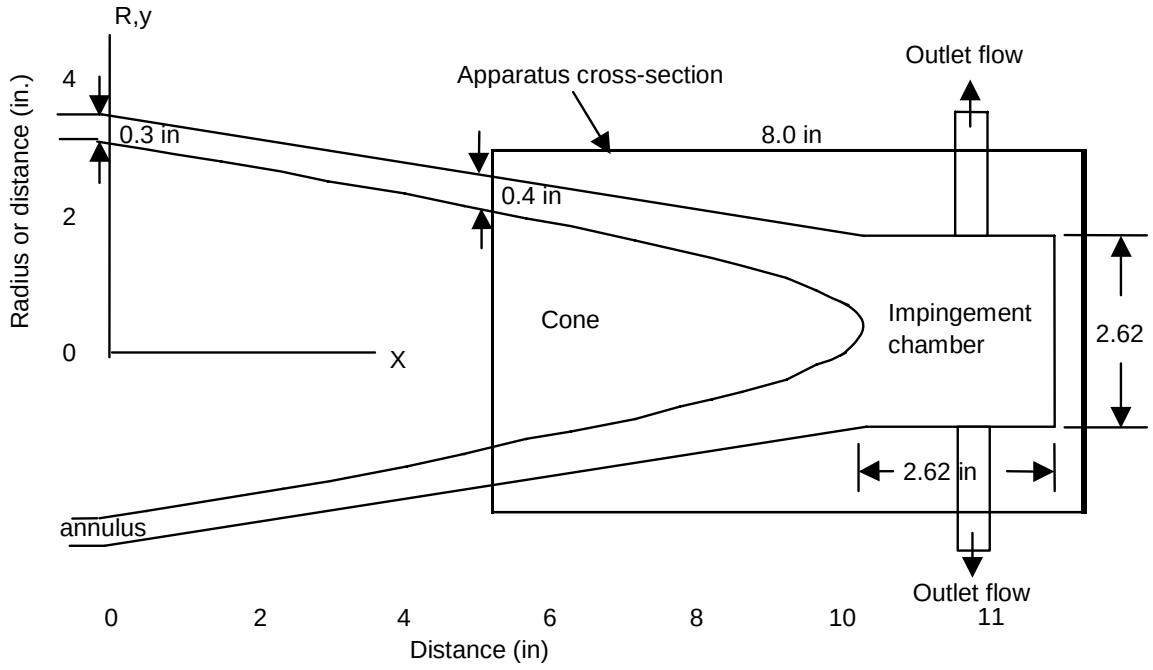

Fig. B-15. Cross-sectional view of preliminary flow visualization apparatus representing axisymmetric model for second experiment in MIR flow system.

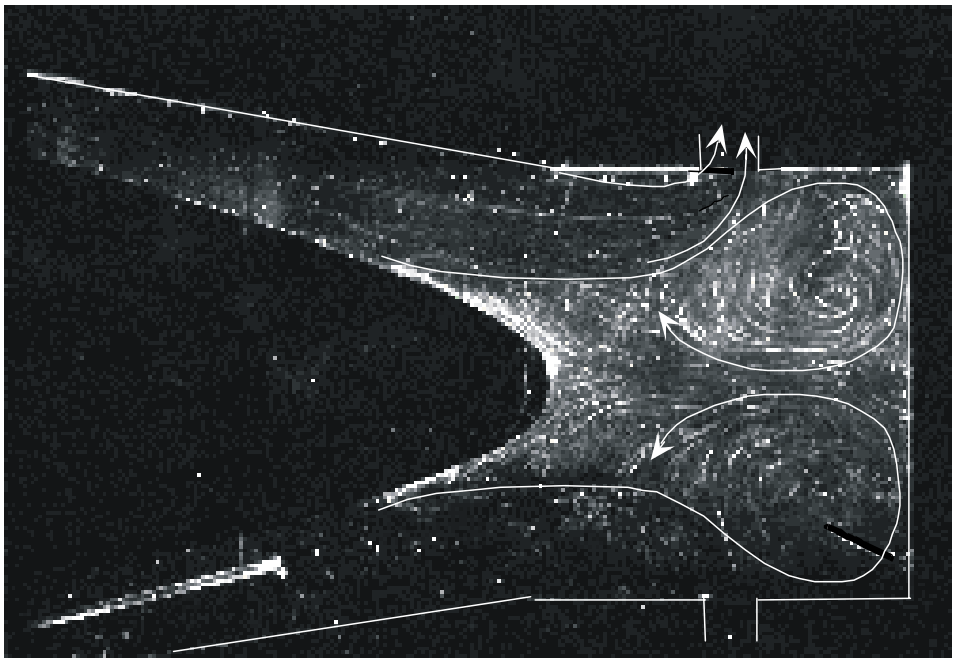

Fig. B-16. Streak-line photograph of flow in convergence and mixing plenum as simulated in two-dimensional planar model, $Re_{D,h} \approx 1000$.

The hydraulic diameter of the planar wall at either of the symmetric entrances is 13 mm (0.52 in.) and increases as the gap increases in the downstream direction. This dimension is comparable to the hydraulic diameter of the annulus in the MIR model of 15 mm (0.6 in). Thus, for equal entering velocities and viscosities, $Re_{D,h}$ in the MIR model would be about twelve per cent higher. However, the fluid velocity is reduced in the present apparatus as the fluid approaches the mixing plenum due to the expansion of the channel width; consequently, there is an adverse pressure gradient as with a diffuser. The fluid streamlines do not follow the curvature of the "cone," but separate at a distance from the tip of the cone; this separation distance increases with Reynolds number. In the MIR model this separation would be expected to be reduced or eliminated (with the exception of the tip of the cone with its sharp final curvature), as the constant cross sectional area will lead to a favorable pressure gradient and increasing Reynolds number with streamwise distance. With the exception of the separation, the flow patterns in the mixing plenum are expected to be comparable but sizes and positions will likely differ.

Figure B-17 presents an approximate interpretation of the flow patterns in the mixing plenum at an inlet Reynolds number of about 1000. Several eddies are evident; these eddies would be toroidal in the axi-symmetric geometry. The majority of the flow passes directly to the outlets. Within the rest of the mixing plenum, velocities are considerably lower. While one's intuition might expect this converging geometry to lead to jet impingement at the axis, the eddies in the mixing plenum indicate that in the axi-symmetric geometry there would be an annular impingement region at the end of the plenum with reversed flow along the axis. Flow near the wall impingement region is highly chaotic compared to the orderly impingement of a circular jet on a flat plate.

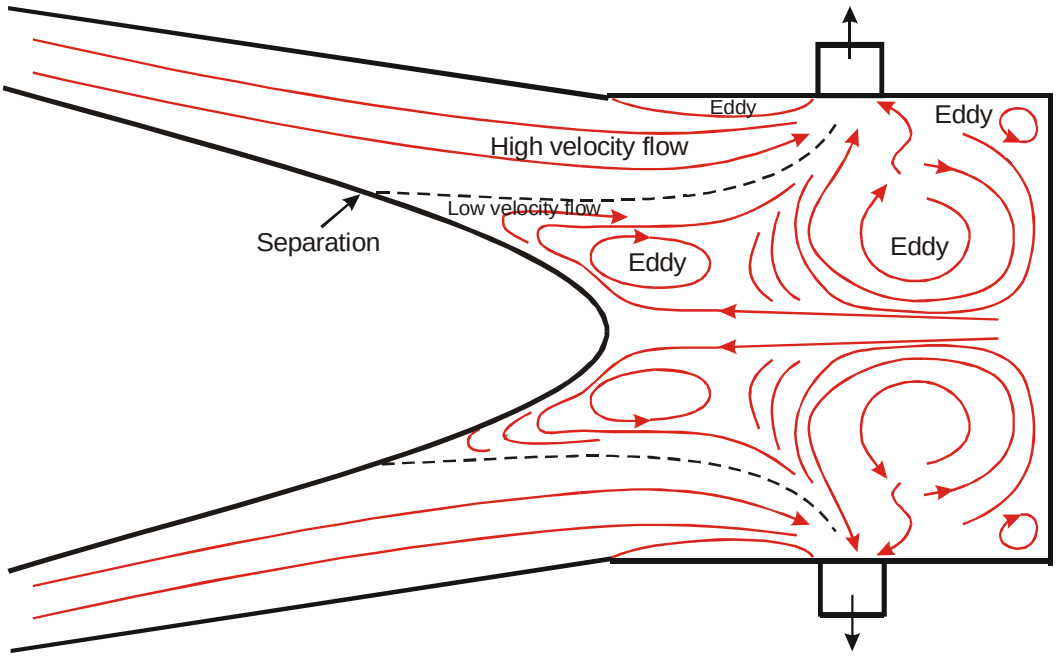

Fig. B-17. Deduced streamlines in convergence and mixing plenum as simulated in two-dimensional planar model, $Re_{D,h} \approx 1000$.

Flow patterns in the mixing plenum change with Reynolds number. At Reynolds numbers less than about 1000, two counter rotating vortices extend from the end of the plenum to the tip of the inlet "cone." At higher Reynolds numbers the vortices detach from the cone and a separate, highly chaotic vortex extends from the counter rotating vortices to the tip. The vortices are separated from the high velocity inlet flow by separation lines that extend from the cone to the exit tubes. The eddies oscillate in position, especially at low Reynolds numbers. It was observed that the position can oscillate from one side of the chamber to the other while exit flow rates appear to be reasonably steady in the two exit tubes. This observation may indicate the likelihood of circumferential oscillations at low Reynolds numbers in the axisymmetric model.

Flow visualization was also obtained in the MIR flow system with the large **axisymmetric model** installed. The Reynolds numbers in the upstream annulus (defined as $4\,\dot{m}/(\Pi\,(D_o+D_i)\mu)$) were about 3400 and 6300. Small air bubbles were injected upstream of the annulus and then flowed through the annulus into the converging section where they were photographed. The bubble path lines were recorded on film using side-scattered illumination from a plane sheet of white light. An example of the results is presented as Figure B-18 with interpreted mean streamlines sketched for the benefit of the reader. There was no significant difference between the observed patterns at the two Reynolds numbers.

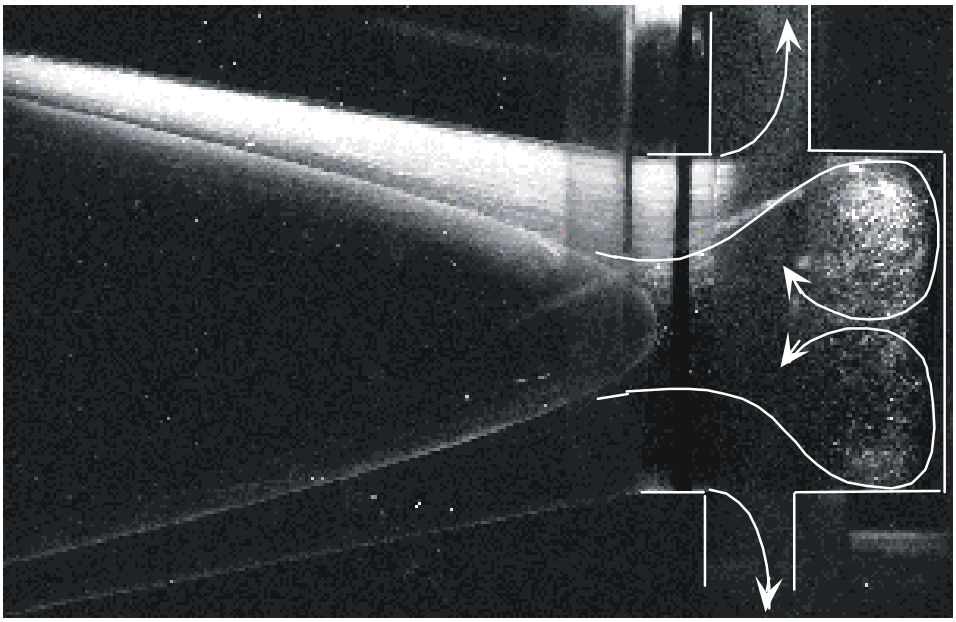

Fig. B-18. Visualization of flow pattern in axisymmetric convergence of second model in the MIR flow system and approximate interpretation of key streamlines, Re ≈ 3400.

The flow pattern in the axisymmetric model shows the same features as in the planar model (Figures B-16 and B-17). As expected, the separation from the central curved cone occurred nearer to the tip and this result modified the pattern in the mixing plenum slightly. Again the majority of the flow left the mixing plenum without impinging or recirculating near the end of that region. A possible reason for the close correspondence between the results in the two models is that the planar model has wall friction on its side walls that would be absent in a truly two-dimensional geometry. The additional favorable pressure drop due to this friction counters the unfavorable pressure gradient induced by the expansion in the planar model (to some extent). At the lower Reynolds number, the non-dimensional contribution of this wall friction would be increased.

The **key results with the second model** are the measured velocity and turbulence distributions in the ribbed annular section. Measurements were obtained by laser Doppler velocimetry (LDV). Instantaneous velocity components were obtained at fixed positions in the representative cell, as well as selected profiles upstream and downstream to verify periodicity. Mean velocities and mean turbulence statistics were determined from these time series. Typical results include time-resolved, pointwise distributions of the mean velocities, U, V, W, and turbulence. The time series are also available for spectral and wavelet analysis [leWalle, Ashpis and Sohn, 1997; Resnikoff and Wells, 1998].

For all three directions, LDV motion is accomplished with traversing mechanisms each consisting of a spindle and a stepper motor. The spindle advance is 40 threads/inch. The stepper motor gives 200 steps per revolution, corresponding to an advance of about 3 μm per step. The position is determined with an "Accu-Rite" indicator with manufacturer's specifications of an accuracy of +/- 0.0001 inch or about 2.5 μm; its meter reads in increments of 2 μm. Indicated

variation in position while the system is warming is about 5 μm. The positional accuracy becomes important in deducing the wall shear stress and the wall location from fitting the measurements for $y^+ < \sim 3$. Thus, the absolute uncertainty of a position is of the order of 5 μm but for positioning during a continuous traverse the relative positioning uncertainty is less.

After installation of the model, reference locations were established relative to the traversing mechanism. Traversing directions are labeled x (streamwise), y (spanwise) and z (vertical) relative to the test section. As a consequence of fabrication, x increases upstream against the flow and z increases in the downward direction.

The reference position (x,y,z = 0,0,0) was the horizontal (y) center-line position of the inner annulus wall at the axial, x, position of the upstream face of spacer set number 6 (the furthest downstream set of spacers), The x position (upstream face of spacer number 6) was obtained visually using one blue beam (vertical orientation). The y position was obtained from a spanwise traverse. Velocities were measured near the closest and furthest walls at mid-channel elevation. The centerline y position was then taken as the mid-position between walls. The centerline y position was determined at several axial positions and then correlated as a function of x. These correlated positions were used for the axial traverses. The zero z position, which corresponds to the upper inner radius at the axial position of the upstream face of spacer number 6, was first determined visually using one green beam, and then corrected using the results of a radial (z) traverse. The inner wall z positions were obtained at several axial (x) positions and the results correlated with the axial position. The mid-channel position was also determined from radial traverses and correlated with axial position. These correlated positions were used for axial traverses.

Since refractive index varies with wavelength as well as temperature, the refractive indices of two different color beams cannot be exactly matched at the same time. In most of our measurements with the two-component LDV, a compromise temperature was selected so that there was maximum overlap of the two measuring control volumes at some appropriate reference condition. Measurements with the LDV in coincidence mode showed this temperature to be about 23.7-23.8°C. However, in a region of sharp curvature of the interfaces, the two color beams will be deflected differently and the effective measuring control volume will be displaced relative to the indicated position of a traversing mechanism. As the angles change (e.g., in traversing across a tube), the difference in locations will vary.

For the LDV measurements with the second model, the model and test section temperatures were adjusted to about 24.4°C, the refractive-index-matching temperature for the green beams which provided the streamwise component. The LDV was operated in the random mode so that data came independently from the two separate measuring control volumes (rather than from an overlapping section which would vary with traversing). Consequently, the motion of the MCV of the streamwise component corresponded to the motion of the traversing system. (In some cases, data from the vertical or blue component are given but they are uncorrected for the continuous relative shift of MCV position and should be considered to be preliminary.) For ease of operation in the limited time available, data were collected using the LDV optics in the backscattering mode.

Some additional comments on estimated experimental uncertainties with our TSI LDV system are presented in a report on an earlier project [Condie, McCreery and McEligot, 2001] and in the paper by Becker et al. [2002].

Most data were obtained in the representative periodic cell between rib spacers 3 and 4. Outer diameter of the annulus was measured to be 150.94 ± 0.15 mm (5.943 in.) and the inner diameter was 135.53 ± 0.08 mm (5.336 in.), giving an average spacing of 7.70 ± 0.15 mm. Installed values of the geometric parameters were $r_i/r_o = 0.90$, $p/s \approx 39.6$, $w/s \approx 2.0$ at outer radius and $L_{rib}/s \approx 9.9$ for this cell. The spacer sets consisted of four ribs so their circumferential pitch was ninety degrees.

Compared to the experiments with the first model, a larger pump and a more sophisticated model temperature control system was installed. For the LDV data reported with the second model, the volumetric flow rate, measured with a calibrated turbine flowmeter, was held at 333 ± 2 gpm (75.6 m^3/sec). This flow rate corresponds to a Reynolds number ($= 4\ \dot{m}/(\Pi (D_o+D_i)\mu)$) of 6900 based on the dimensions and fluid viscosity. For this value, one would expect the flow conditions to be characterized as "low-Reynolds-number turbulent" in the comparable channel flow [Durst et al., 1998].

The experiment matrix covered approximately the same range as the first experiment. Radial profiles taken away from the ribs demonstrated that the condition of streamwise periodicity was essentially achieved. Measurements were concentrated in the representative cell between spacer locations 3 and 4. In the first orientation the vertical centerplane was located halfway between ribs in the circumferential direction. For the second orientation the model was rotated 45 degrees about its axis so a row of spacer ribs was centered on the vertical centerplane; data were obtained in the region between successive ribs.

Again an axial traverse midway between the annulus surfaces and in the first orientation (Figure B-19) was conduced to examine the flow acceleration and deceleration induced by the periodic spacers. In this figure flow is from right to left and the locations, as indicated by the traversing mechanism, increase in the upstream direction. The pattern is the same as before (Figure B-7) but the magnitudes differ. One sees that at the midpoint between spacers axially the mean velocity is near its minimum value. The maximum acceleration occurs at a location approximately in line circumferentially with the face of the downstream rib; it corresponds to an acceleration factor $K_v = (\nu/V^2)\ dV/dx$ of about 5.6×10^{-6}. The deceleration is more gradual after passing between the ribs; its maximum value is about 2.3×10^{-6} and it occurs at about one-quarter of the axial distance between the ribs. The streamwise rms fluctuation $u'\{x\}$ is seen to increase in the decelerating flow and to decrease as the flow accelerates between the ribs.

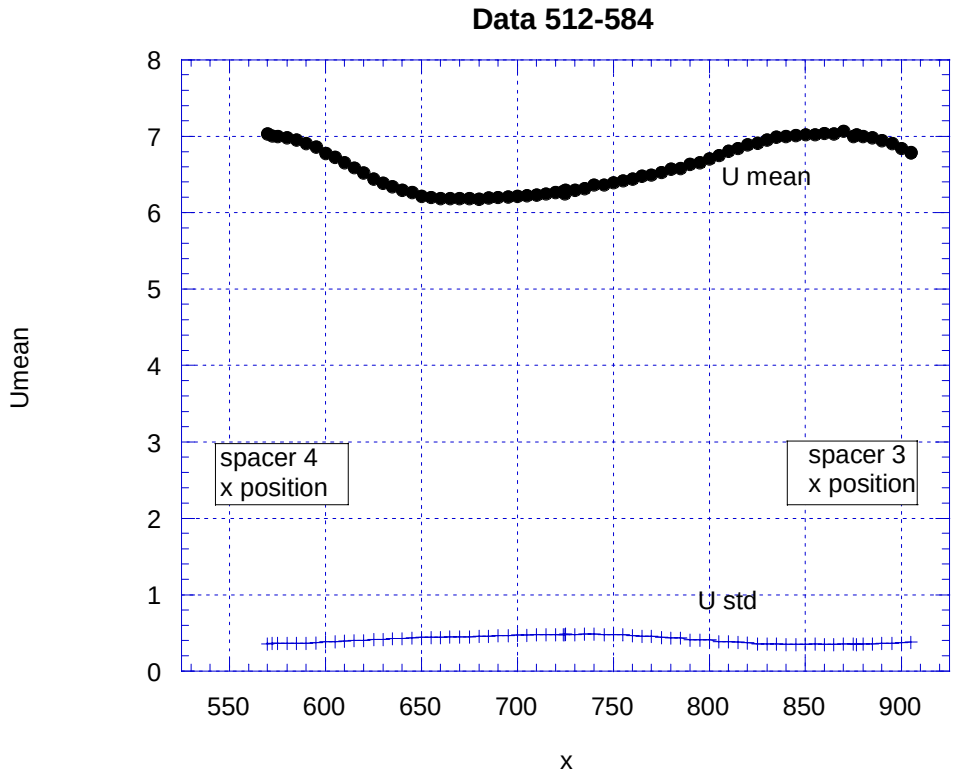

Fig. B-19. Axial streamwise velocity profile away from spacer ribs (flow is from right to left and the locations increase in the upstream direction from the fourth rib), Re ≈ 6900.

Four radial traverses of mean streamwise velocity U, taken along the centerplane of the first orientation, are provided in Figure B-20. They were located sequentially circumferentially between spacers (659, x = 904 mm), near the point of maximum deceleration (764, x = 800 mm), near midway axially (362, x = 724 mm) and near the point of maximum acceleration (703, x = 615 mm). All are near symmetric as expected for the high radius ratio and none are parabolic. Radial coordinates have not yet been readjusted to enforce the no-slip condition at r_i (= 0); the slight variation between the axis of the model and the traversing system provides some shifting in the vertical direction. Since the maxima are near the halfway point of the annulus radially, these maxima correspond in magnitude to the results presented in Figure B-19, e.g., the profile between ribs (659) shows the highest magnitude and the one furthest away (362) shows the lowest level.

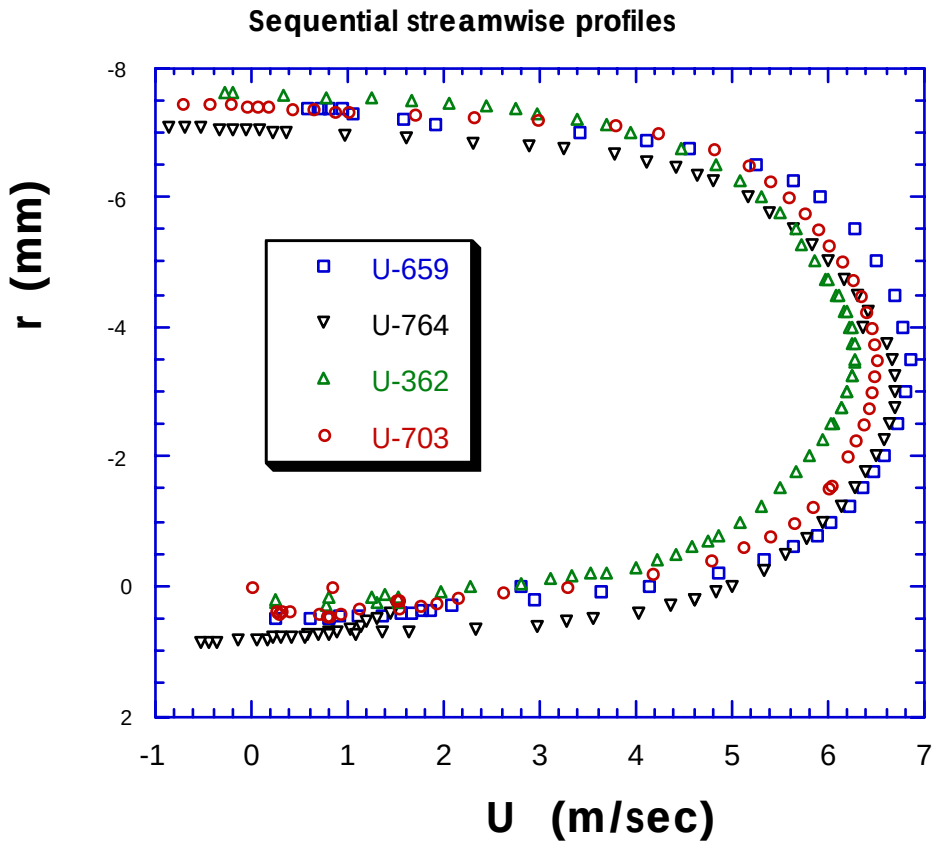

Fig. B-20. Radial profiles of mean streamwise velocity along centerplane circumferentially between ribs (locations increase in the upstream direction from the fourth rib where x is taken to be zero).

Corresponding profiles of streamwise velocity fluctuations u′ are shown in Figure B-21. The trends are as one might expect. Favorable streamwise pressure gradients (acceleration) are considered to be stabilizing and deceleration is considered to be destabilizing. The highest values of u′, both in the central region and near the wall, are seen at the midway position (362) near the end of the decelerating region. The lowest profile is the one circumferentially between spacers (659) near the end of the acceleration induced by the convergence into the opening between spacers. The other two profiles are consistent with these observations.

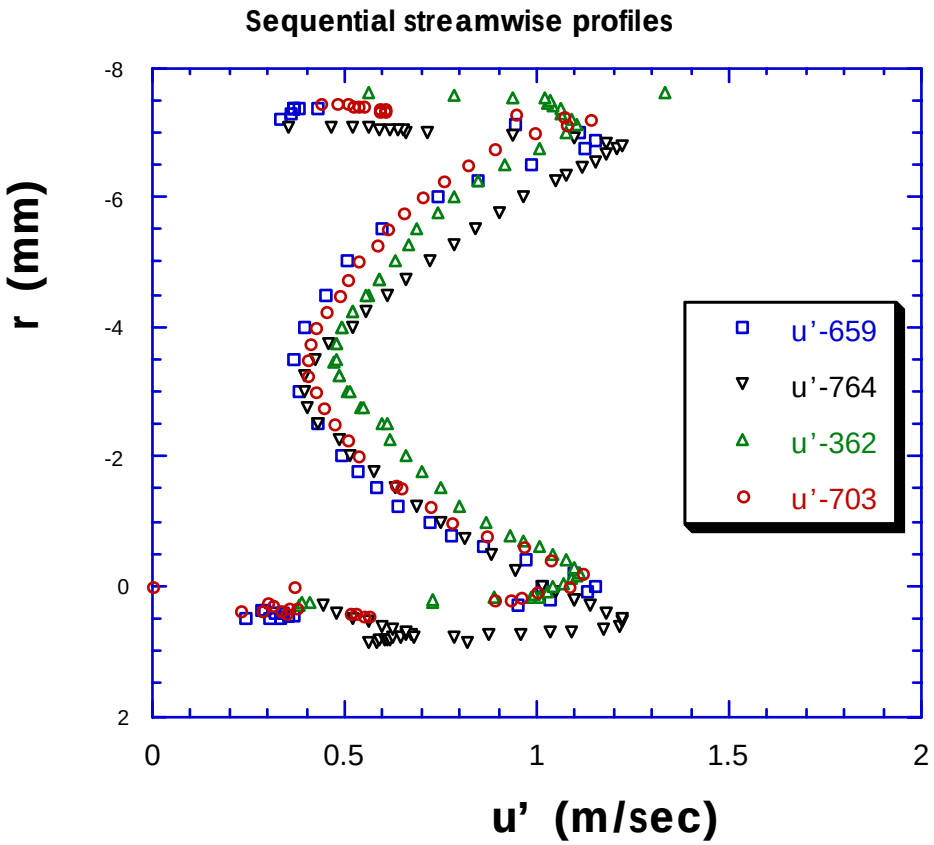

Fig. B-21. Radial profiles of mean streamwise velocity fluctuations along centerplane circumferentially between ribs (locations increase in the upstream direction from the fourth rib where x is taken to be zero).

Since the behavior of the viscous layer (typically $0 < y^+ < 30$ or so) can have a significant effect on convective thermal resistance [McEligot, 1986], it is of interest to examine these velocity measurements in terms of wall coordinates emphasizing the region. The near-wall region for the midway measurements (362) near the inner surface is shown in Figure B-22. The friction velocity u_τ in the definitions of u^+ and y^+ was determined by estimating the velocity gradient at the wall from the data within $y^+ < 4$. Classical asymptotes for flow in a circular tube or boundary layer are also shown for reference purposes. The measured mean velocity profile is seen to fall below the "universal velocity profile" for an asymptotic condition of a high Reynolds number, the so-called log "law." One might question whether this result is reasonable. Data by Rehme [1974] and large eddy simulations by Satake and Kawamura [1995] provide some information for flow in classical annuli at higher Reynolds numbers. In their results the level of the velocity profile falls below the asymptotic behavior as the radius ratio and the Reynolds number decrease. In the present case the radius ratio is higher than in their cases and the Reynolds number is lower. Another factor to consider is the effect of flow convergence and divergence around the ribs. McEligot and Eckelmann [1990, 2003] have shown that for laterally converging flows (acceleration) the mean velocity profile becomes higher than the accepted log "law" and the non-dimensional streamwise fluctuation $(u')^+$ is not affected significantly. The profiles shown in Figure B-22 are for a location at the end of the decelerating region or lateral

divergence so $u^+\{y^+\}$ might be expected to be lower than the log "law;" the non-dimensional fluctuation shows a peak value of about 2.5 near y^+ of 15 (approximately the same as in favorable and negligible streamwise pressure gradients).

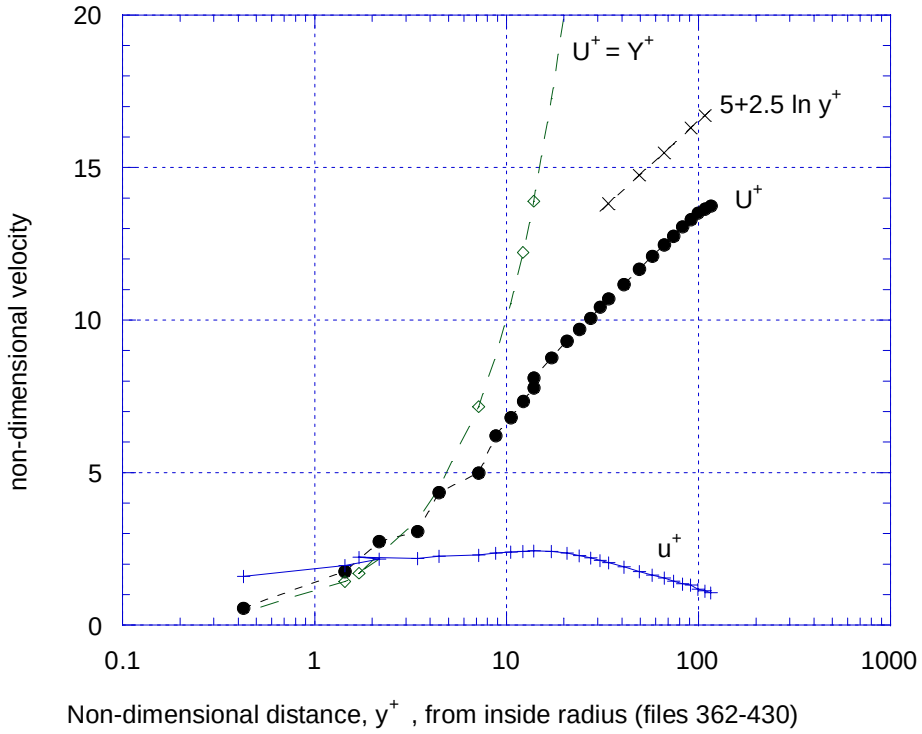

Fig. B-22. Inner wall behavior at midway location along radial centerplane between sets of spacers.

By rotating the model, it was possible to obtain profile measurements downstream from a rib conveniently. Data along the radial centerplane downstream of a spacer reveal some details of the recirculating eddy which forms behind a rib. Figure B-23 provides an axial traverse along the "centerline" downstream of a rib; again flow is from right to left and the locations, indicated by the traversing mechanism, increase in the upstream direction from the face of the downstream rib. Along this line the mean recirculating eddy appears to end at about x = 203 mm (U ---> 0) with negative streamwise velocities from there to the rear face of the upstream rib. The mean fluctuating component u′ is highest downstream of the end of the mean recirculating eddy; it decreases in magnitude within the eddy and, more gradually, in the downstream wake flow towards the next spacer.

Radial profiles of the streamwise velocities near the outer surface are presented in Figure B-24. The location was downstream of spacer 3 about halfway to the next spacer. It is seen that the mean velocities are low in the wake of the upstream spacer. The appearance is near-parabolic as in a laminar flow. If one were to calculate a Reynolds number based on this profile, it would be of the order of 3000 or so. For flow in a parallel plate duct, Durst et al. [1998] have shown a near laminar mean velocity profile for higher Reynolds numbers (their definition of a Reynolds number is based on plate spacing so the reported numerical values are half the normal duct Reynolds number based on hydraulic diameter). So the present observation is not surprising.

However, significant levels of the velocity fluctuations are seen in our experiment. Whether these fluctuations are primarily due to oscillations of the wake or are turbulent (or a combination) has not yet been determined. (Since the LDV was operated in the random mode, the Reynolds shear stress -- representing turbulent transport of momentum -- was not measured.) Again one would expect a CFD code using a RANS model to have difficulty properly predicting this flow situation. However, the Reynolds number is sufficiently low that DNS calculations should be feasible and Prof. Pletcher's LES code (Task D) should be applicable with a change in geometry from three to four ribs.

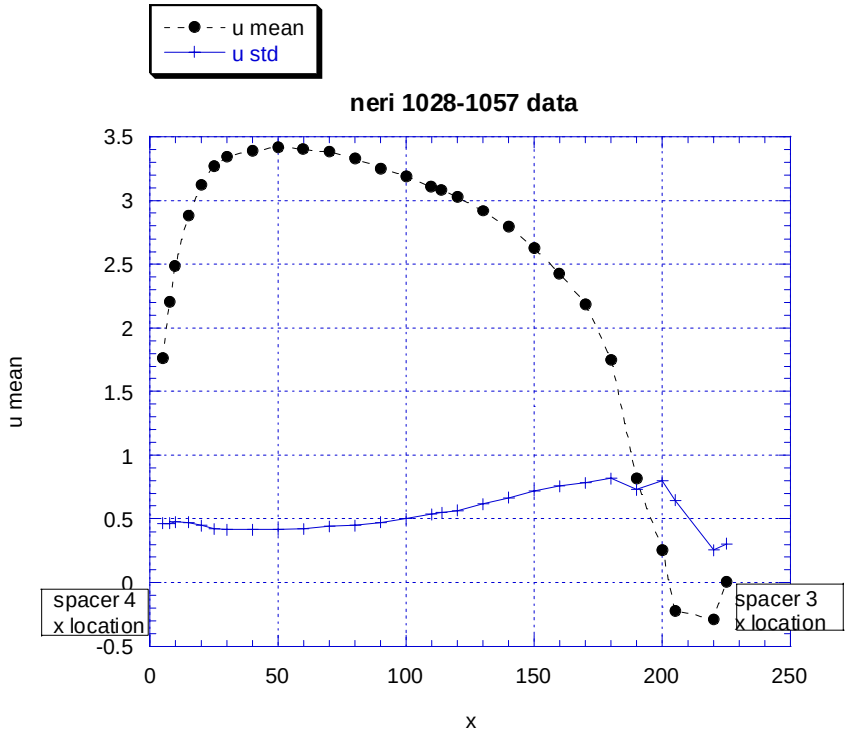

Fig. B-23. Axial profiles of mean velocity and fluctuations along "centerline" downstream of a rib (flow is from right to left and the locations increase in the upstream direction from the fourth rib).

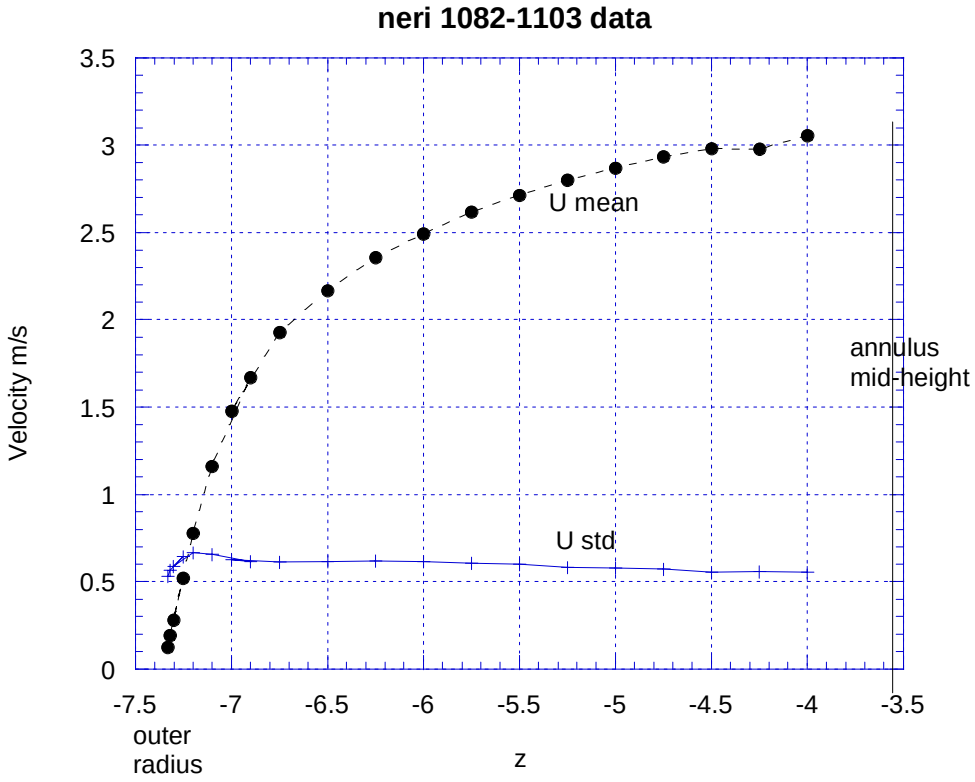

Fig. B-24. Radial profiles of mean streamwise velocity and velocity fluctuations midway along centerplane downstream of a rib.

Raw time series have been archived on compact discs (CDs) for potential later use by analysts. Tabulated mean measurements (in MS Excel or Claris Resolve spreadsheets) will be kept available to serve as benchmark data for the assessment of predictive capabilities of proposed CFD codes. For a number of reasons, one would not expect a standard k-ε turbulence model to be adequate. The low Reynolds number of this turbulent case should make DNS calculations feasible and the LES code of Prof. Pletcher (Task D) should be directly applicable.

Measurement of turbulence quantities in high temperature gas flow Turbulence modelers request measurements of the basic quantities (dependent variables) of their governing partial differential equations for assessment (and guidance), quantities such as turbulence kinetic energy and Reynolds stresses, $\overline{v^2}$, $\overline{uv}$, etc. These data have not been available for strongly-heated internal flows. In the original proposal the second main experimental task to be conducted at INEEL was aimed at providing these data for predominantly forced flow. This part of the study would concentrate on examining the effects of property variation without the complications of complex geometries; an axisymmetric two-dimensional geometry was chosen, i.e., a circular tube with axisymmetric boundary conditions. The results of this task could also provide useful insight for the potential hot spot problem of the lower plenum since the initial conditions of the non-uniform impinging jets are the exit conditions of the heated reactor channels. Unfortunately, the funding provided was not sufficient to conduct this task so it was removed from the contracted statement-of-work and deferred.

The general goal would be to obtain greater understanding of the structure of strongly-heated, internal, turbulent gas flows, with an emphasis on turbulence structure. Hence, objectives are to measure the fundamental turbulence structure and to obtain benchmark data to assess CTFD codes for high temperature gas flows that are predominantly in the forced convection region, for a range of conditions important in advanced reactors. Conceptually, DNS codes, as by Satake et al. [2000, 2002], could accomplish these aims and more; however, ***DNS calculations must also be compared to time-resolved experimental measurements to insure adequate spatial and temporal resolution, to uncover coding mistakes, to check for prediction of measurable quantities and consistent, useful definitions of those quantities, etc.***

The experiment would extend the existing methods of McEligot and Wallace and their colleagues. The probes developed by Profs. Wallace and Vukoslavcevic in Task E would be employed at INEEL to measure fluctuating velocity components and temperature in high temperature gas flow through a vertical circular tube for assessment of the predictions and to understand the fundamental effects of this heating on the physics of the flow.

While the initial ***experiments*** might be conducted using an open flow system incorporating a vertical, resistively-heated, circular test section exhausting directly to the atmosphere in the laboratory, the intent would be to develop a more versatile apparatus as shown in Figure B-25. The experiment would provide an approximately uniform wall heat flux boundary condition in a tube for ascending air, entering with a fully-developed turbulent velocity profile at a uniform temperature as in classical analyses. Controlled wall heat flux would be provided with a stable electrical power supply. The heated length would be relatively short to permit high heating rates with Inconel as the tube material while approaching quasi-developed conditions. The miniature multiple-sensor probes from Prof. Wallace and Vukoslavcevic would be inserted through the open exit to obtain pointwise temperature and velocity measurements. In general, the experimental methods would follow those of Shehata [Shehata and McEligot, 1995, 1998] except for the extension to the multi-sensor probes from Wallace and Vukoslavcevic and more modern data acquisition equipment.

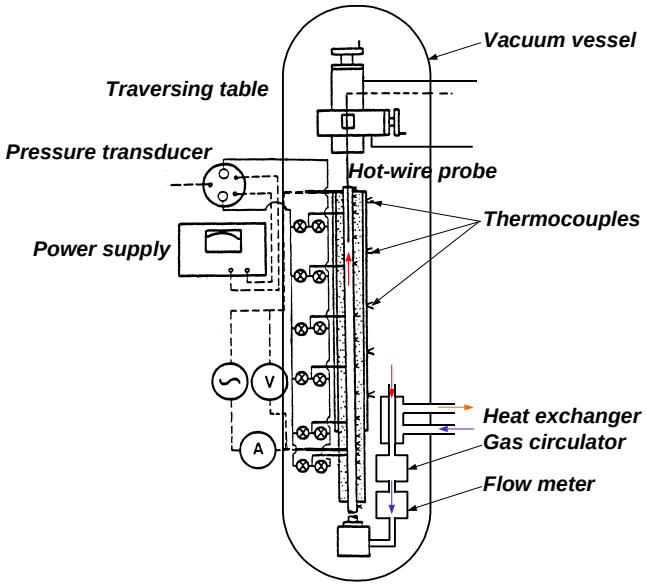

Fig. B-25. Conceptual design of experimental apparatus to measure distributions of fluctuating turbulent components and Reynolds stresses in dominant forced convection for strongly-heated gas flow.

The region controlling the transfer of heat and momentum in turbulent wall flows is primarily the ***viscous layer*** which occupies a small fraction of the cross section. This fraction grows as the Reynolds number is lowered. With strong heating, the large turbulent temperature fluctuations make simultaneous measurement of instantaneous temperature and velocity necessary; this situation is the reason for using the multi-sensor probes, but they would be larger than a miniature single-sensor probe. However, if one chooses a large tube and low Reynolds number (for thicker viscous layers) to improve spatial resolution, the problem quickly becomes one of dominant natural convection. The experimenter must compromise in order to obtain data which the theorist can extend to conditions where the experimenter cannot easily tread. In the present work, studies with significant buoyancy effects are being conducted by Professor Jackson and his colleagues at the University of Manchester (by using large tubes) as Task F; the test apparatus at INEEL would be developed to avoid significant buoyancy forces.

The inside diameter of the initial ***test section*** at the INEEL would be greater than three cm. (At the INEEL elevation of about 1400 meters, Grashof numbers are about thirty per cent less than they would be at sea level for comparable conditions, allowing slightly larger diameters when avoiding buoyancy effects.) The length of the test section would be chosen to permit measurements through and beyond the normal thermal entry region while attaining significant transport property variation, as exemplified by T_w/T_b and T_w/T_i, with common materials and gas. By employing Inconel 600 for the test section material, maximum surface temperatures of about 1000 C should be possible.

In addition to the usual difficulties of hot wire anemometry, the temperature range of this experiment would involve other problems. High temperature differences between the wall and prongs make thermal radiation to and from the walls an important consideration. The question arises: how to handle gas property variation in the convective heat transfer correlation which serves as the basis for calibration of the sensors? Thermal expansion affects positioning and its measurement. Solutions to these difficulties and others have been developed by Shehata [Shehata and McEligot, 1995] and by Profs. Wallace and Vukoslavcevic in Task E of the present work; they would be extended as necessary by these collaborators for use of the multi-sensor probes.

Target ***operating conditions*** would be an inlet Reynolds number range from about 2000 to 50,000 based on diameter. Inlet temperature would be 20 to 30°C. Thus, the maximum allowable temperature would permit a temperature ratio T_{wall}/T_{in} of about 4.3, giving a maximum viscosity ratio μ_w/μ_{in} of about 2.8 for common gases, i.e., significant property variation. The proposed multi-sensor probes would give meaningful measurements of turbulence structure in the viscous layer.

Development of a variable pressure, closed helium flow loop is the recommended approach to extend the range of meaningful data (e.g., larger diameter tube with lower Grashof numbers). For useful measurements in the viscous layer one needs good spatial resolution which may be achieved by having the sensor volume small compared to the viscous layer, say $D^+_{probe} << 30$. Thus the tube must be much larger than the size of the probe. Prof. Jackson has developed a criterion that a buoyancy number defined as $Bo = Gr^*/(Re^{3.425}Pr^{0.8})$ must be small

in order to have dominant forced convection (see Task F for example). The difficulty with using a large tube diameter is that the Grashof number,

$$Gr^* = g \rho^2 D^4 q''_{wall} / (\mu^2 k T)$$

is strongly dependent on the diameter. Comparing the properties of the desired gas - helium - to air, one finds the viscosities are about the same, k_{He} is about five times k_{air} and ρ_{He} is about $\rho_{air}/7$ at the same temperature and pressure. These differences help, but the diameter is still a strong factor. Since $\rho \approx p/RT$, a possible solution to reduce Gr* and, hence, Bo is to apply the approach of Zagarola and Smits [1998] in reverse. They used high pressures to obtain high densities and consequently achieved their desired high Reynolds numbers. Our idea is to reduce the pressure of helium sufficiently to compensate for an increase in the diameter of the tubular test section. Figure B-25 illustrates the concept of enclosing an experiment like that of Shehata and McEligot in a vacuum vessel with remote operation of the instrumentation and the traversing mechanism for the multi-sensor probe. The characteristics of a non-uniform, hot exit jet could also be determined; the top of the vacuum vessel could be used as a means of providing flow conditions comparable to the thermal fluid phenomena occurring with non-uniform impinging jets, as in the hot spot problem for the lower plenum of a gas-cooled reactor.

Typical ***results*** would include time-resolved, pointwise distributions of the mean velocities, U, V, and their Reynolds stress components as well as wall temperature and static pressure distributions for well-defined thermal boundary conditions. As with the annular experiment, the final test matrix would be developed interactively in collaboration with investigators who would be conducting the related numerical analyses. Throughout the experimental phase, the resulting data would be provided to these collaborators as soon as they become available. In addition to documentation of the experiment and the results of the measurements by technical papers, by presentations at technical meetings and by technical reports for more detail, the data would be stored in electronic form for ease of comparison by computational fluid dynamists using other codes.

Task C. Analyses and Direct Numerical Simulations -- Prof. S. I. Satake, Tokyo Univ. Science, and Prof. T. Kunugi, Kyoto U.

Profs. Satake and Kunugi **are developing DNS for use in high temperature gas (or superheated vapor) flows with transport property variation**. Their results will assist evaluation of sub-grid-scale models used in LES and of other CFD approaches and will also help in the interpretation of hot wire measurements in these conditions.

The current DNS code can numerically solve the continuity and momentum equations in cylindrical coordinates using the radial momentum flux formulation. A second-order finite volume discretization scheme is applied to the spatial derivatives on a staggered mesh system in order to avoid a singularity at the center axis of the pipe center. The Navier-Stokes and continuity equations are integrated in time by using the fractional-step method. The second-order Crank-Nicholson scheme is applied to the radial direction terms, which are treated implicitly, and a modified third-order Runge-Kutta scheme is used for other terms explicitly. In their previous study concerning a constant property turbulent pipe flow [Satake and Kunugi, 1998a], this DNS code has shown good agreement with the existing DNS results.

For the initial predictions for circular tubes with gas property variation, the computational domain has the same pipe length as the experiment of Shehata and McEligot [1998]. The experimental measurements are provided as a basis for the comparison with the computational results. For the first case, the inlet Reynolds number based on the bulk velocity, viscosity and the pipe diameter (D) is assumed to be 4300. This condition corresponds to ***Run 445*** of the experiments by Shehata and McEligot. Air is considered as the working fluid and the thermal properties are evaluated as power-law functions of the pointwise temperature and pressure with density estimated via the perfect gas approximation as by Perkins [1975].

Uniform mesh spacing is applied to the circumferential (ϕ) and the streamwise (z) directions. For the radial direction (r), non-uniform mesh spacing is employed, specified by a hyperbolic tangent function. The number of grid points is 768 x 64 x 128 in the z-, r- and ϕ -directions, respectively. The inlet boundary conditions are provided with an "inflow generator," that is, a fully turbulent pipe flow field with constant fluid properties is considered for the entry region as in the experiments. The number of computational nodes for the "inflow generator" is 128 x 64 x 128 points in the z-, r- and ϕ -directions, respectively.

A convective boundary condition [Lowery, Reynolds and Mansour, 1987] is imposed at the exit of the main computational domain. The temperature distribution along the pipe wall is interpolated from the data [Shehata and McEligot, 1998] and is used as the thermal boundary condition. Although the thermal boundary condition of the experiment was a slightly varying heat flux, it is difficult to impose a heat flux condition in a spatially developing problem with the current DNS except for periodic flow problems [Satake and Kunugi, 1998c]. Therefore, the initial purpose of this DNS is to investigate the turbulent heat and momentum transfer mechanism in a pipe with a known wall temperature distribution. The main computational domain and inflow generator are treated with a message-passing system with 8-nodes on the Fujitsu VPP500 vector-parallel super computer. This code is customized for vector-parallel machines [Watanabe, Satake and Kunugi, 1997].

Profs. Satake and Kunugi completed their technical paper [Satake et al., 2000] detailing the successful application of this DNS code to Run 445 of the experiments by Shehata and McEligot [IJHMT, 1998]. In that run the flow entered the heating section as a fully-developed turbulent one and, due to the strong heating (causing property variation and acceleration), was effectively laminarized within about twenty-five diameters.

This direct numerical simulation (DNS) of turbulent transport for a gas with variable properties has been conducted to grasp and understand the laminarization phenomena caused by strong heating. Turbulent quantities, such as the mean flow, temperature fluctuations, turbulent stresses and the turbulent statistics, were obtained. Predicted mean velocity and temperature distributions and integral parameters agreed well with the experiments.

The predicted spatial evolution of ***structures in the flow field*** with strong heating is visualized sequentially in Figures C-1 (a) for ***z/ D*** = 0-5, (b) 5-10, (c) 10-15, (d) 15-20 and (e) 20-25; it should be noted that the contour levels vary in these subfigures. The light and dark contour surfaces in the half view of the pipe represent the low-pressure and low-speed regions, corresponding to the vortical structures and wall-layer streaks, respectively. Within the first section (***z/D*** = 0-5), these structures become quite different from those of pipe flow without heating (Satake and Kunugi, 1998a). However, the low-pressure regions representing the vortical structures decay rapidly beyond ***z/D*** $\approx$ 3. The vortical structures disappear in this region and the low-speed streaks and their meandering become weak. One may recall that the meandering of streaks is interpreted as a dominant phase in the usual turbulence regeneration processes [Hamilton, Kim and Waleffe, 1995]. Thus, in the first section of the heated region (***z/D*** = 0-5), the turbulence is suppressed as a consequence of the strong heating and it is not regenerated in the downstream region. Whether this suppression fundamentally occurs due to the related property variations, acceleration, buoyancy or a combination thereof remains a question to be answered in future studies.

Some explanation for the appearance of "laminarization" in the mean velocity distributions is found in Figure C-2 (d), which shows the predicted distributions of ***Reynolds shear stress***. This quantity can be considered to be a measure of the turbulent contribution to momentum transport. It decreases along the streamwise direction. The cause of this reduction can be considered to be that the fluid behavior changes drastically in the near wall region due to strong heating which induces significant variations of the gas properties and, in turn, acceleration and buoyancy effects. In the visualization of the results, one sees that the vortical structures are primarily suppressed within the first section of the heated region (***z/D*** = 0 - 5) and are not regenerated further downstream. The Reynolds shear stress shows a reduction to negligible levels by z/D $\approx$ 14; as far as momentum transfer in concerned, it is predicted that the flow is effectively laminarized near the wall before this station. These results indicate that the transport is predominantly molecular. The DNS results are fairly in good agreement with the k-ε model of Ezato et al. [1999]. However, the RSM results of Nishimura et al. [2000] are relatively larger than the DNS and the k-ε model. Since these Reynolds-averaged models are sensitive to their differing low Reynolds number approximations, it is not surprising that they do not agree exactly.

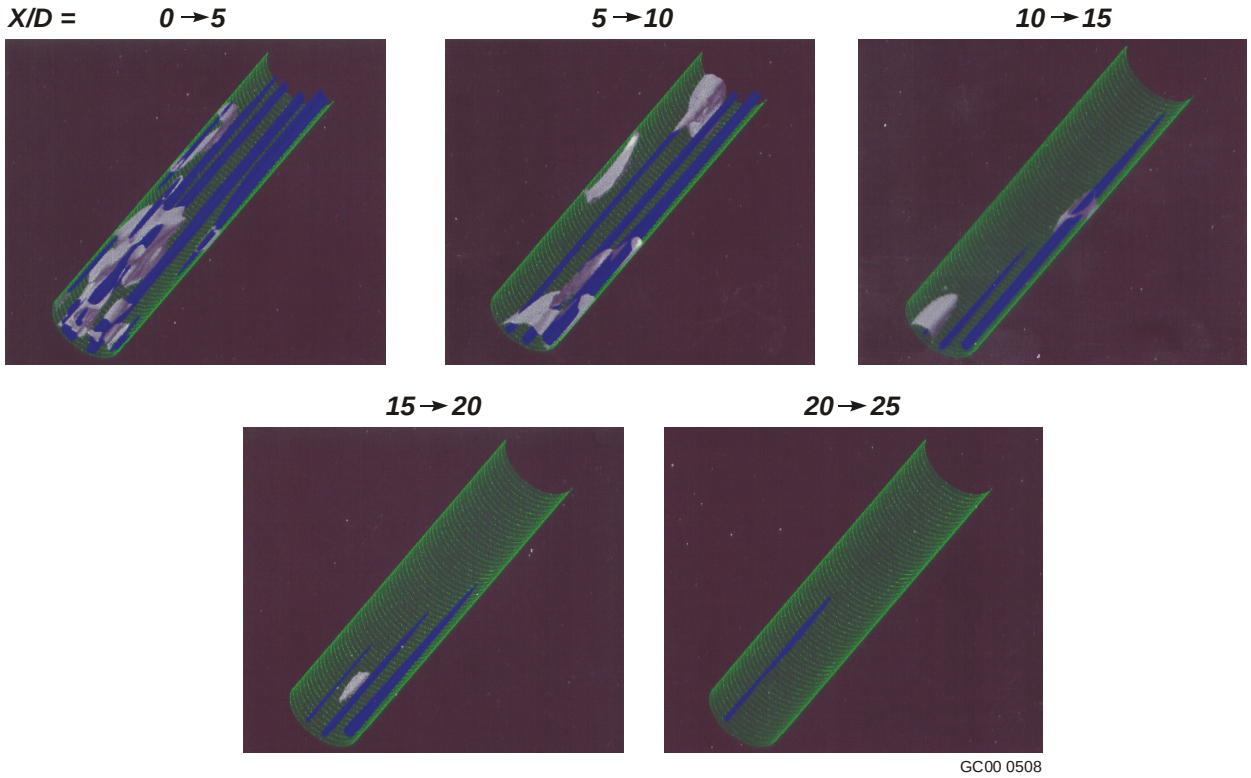

Fig. C-1. Predicted spatial evolution of structures in the flow field for the conditions of laminarizing run 445 by Shehata and McEligot [1998].

The ***Reynolds normal stresses*** as represented by the root-mean-square values of the velocity fluctuations in the streamwise, radial and circumferential directions are presented in Figures C-2 (a) through (c), respectively. All decrease significantly with axial distance. The streamwise component is small at the last station and the peak, that is usually near y^+ of 15 or so, is no longer clear. The first two components were compared to predictions from the RSM of Nishimura et al. and the trends were seen to be the same but the suppression of turbulent activity is slower with the RSM model. The ultimate effect of the significant property variation on the radial component is very strong; there appears to be an appreciable reduction within the first three diameters. Both the DNS and the RSM indicate that the reduction in Reynolds shear stress may be primarily a consequence of suppression of the radial component. For these conditions, the axial reduction in density due to heating leads to an acceleration parameter K_V of about 4×10^{-6}, approximately the magnitude where Kline et al. [1967] observed a reduction in turbulent bursting rate near the wall for external flows with favorable streamwise pressure gradients. The magnitudes of the radial and circumferential components are roughly the same. Some streamwise turbulent fluctuations are still observable at the last station and might be detected by a hot wire anemometer [Bankston, 1970] but they would not transport much momentum, as demonstrated by the Reynolds shear stress results (Figure C-2d).

DNS calculations were next initiated for ***Run 635***, at a higher Reynolds number and lower heating rate, conditions which other investigators have found difficult to predict adequately with so-called advanced turbulence models. In addition, calculations were initiated for ***Run 618***, at the same inlet Reynolds number as Run 635 but with a lower heating rate. Run

618 represents a turbulent flow that has reduced heat transfer parameters due to effects of property variation but no apparent laminarization; as such it is comparable to normal operating conditions for cooling channels in a GA advanced gas-cooled reactor. Runs 635 and 445 correspond to conditions expected to occur as the Reynolds number decreases during a transient LOFA.

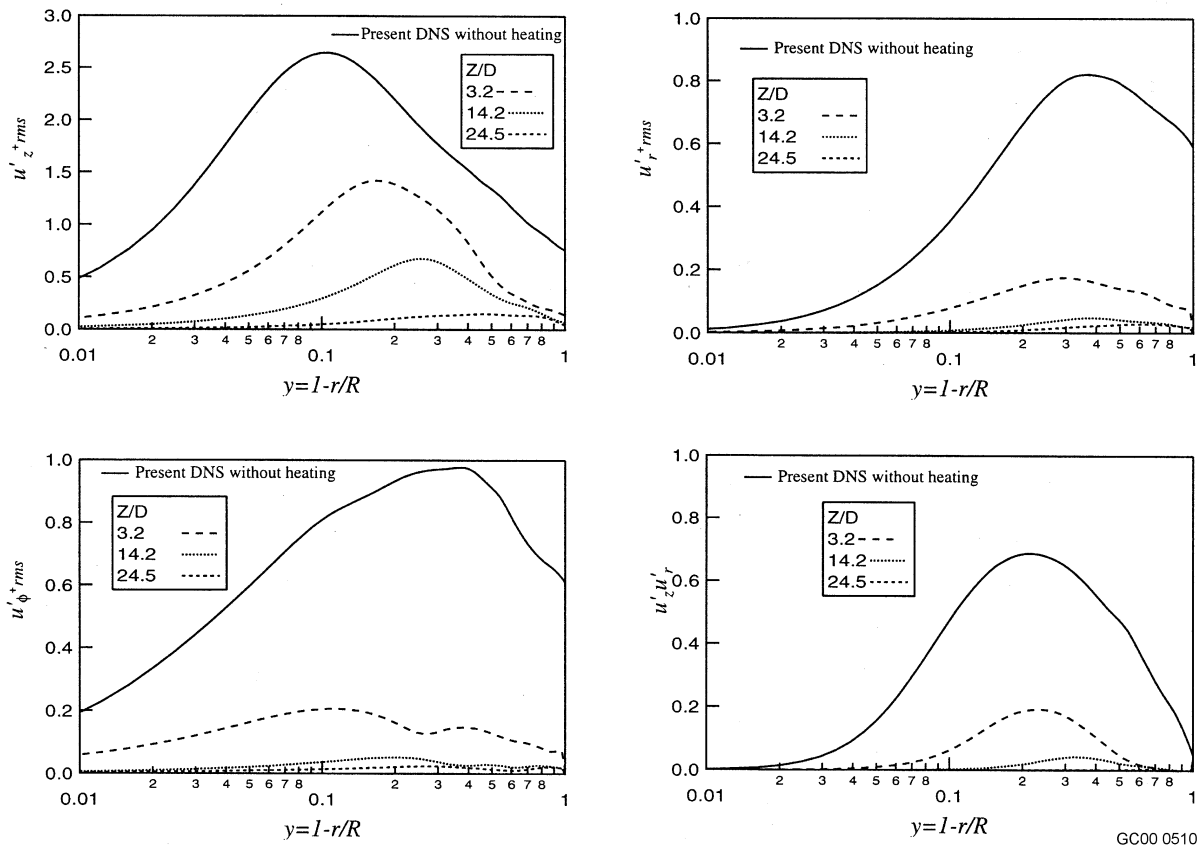

Fig. C-2. Predicted evolution of Reynolds stresses at the conditions of laminarizing run 445 by Shehata and McEligot [1998].

For these calculations, the same numerical grid was employed as for earlier Run 445 and the same approach was taken for boundary conditions. To start the temporal solutions, the initial conditions were taken from results for Run 445 so at first the velocity and temperature fields correspond to a lower Reynolds number than for Runs 618 and 635. As the solutions proceed, the fields respond to the entry flow at Re ≈ 6000.

Results for the mean velocity and temperature development are shown in Figure C-3 for Run 635 and Figure C-4 for Run 618. As seen later, it appears that the solution for Run 618 still needs more calculation time to converge. Predictions of the distribution of velocity components (u′, v′, w′) and the Reynolds shear stress are provided by Figures C-5 through C-8.

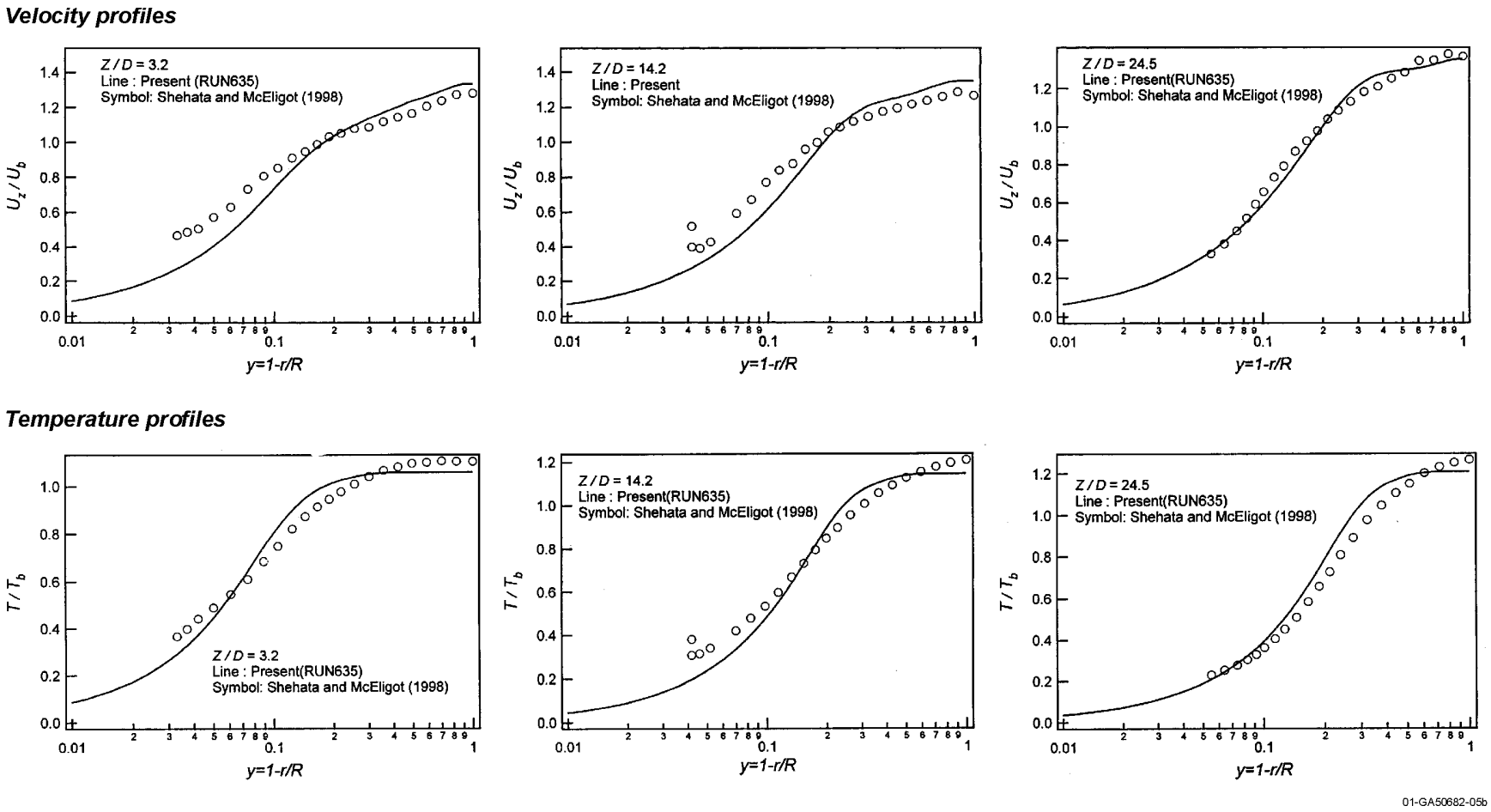

Fig. C-3. Predictions of mean velocity and temperature distributions for the conditions of "subturbulent" run 635 by Shehata and McEligot [1998].

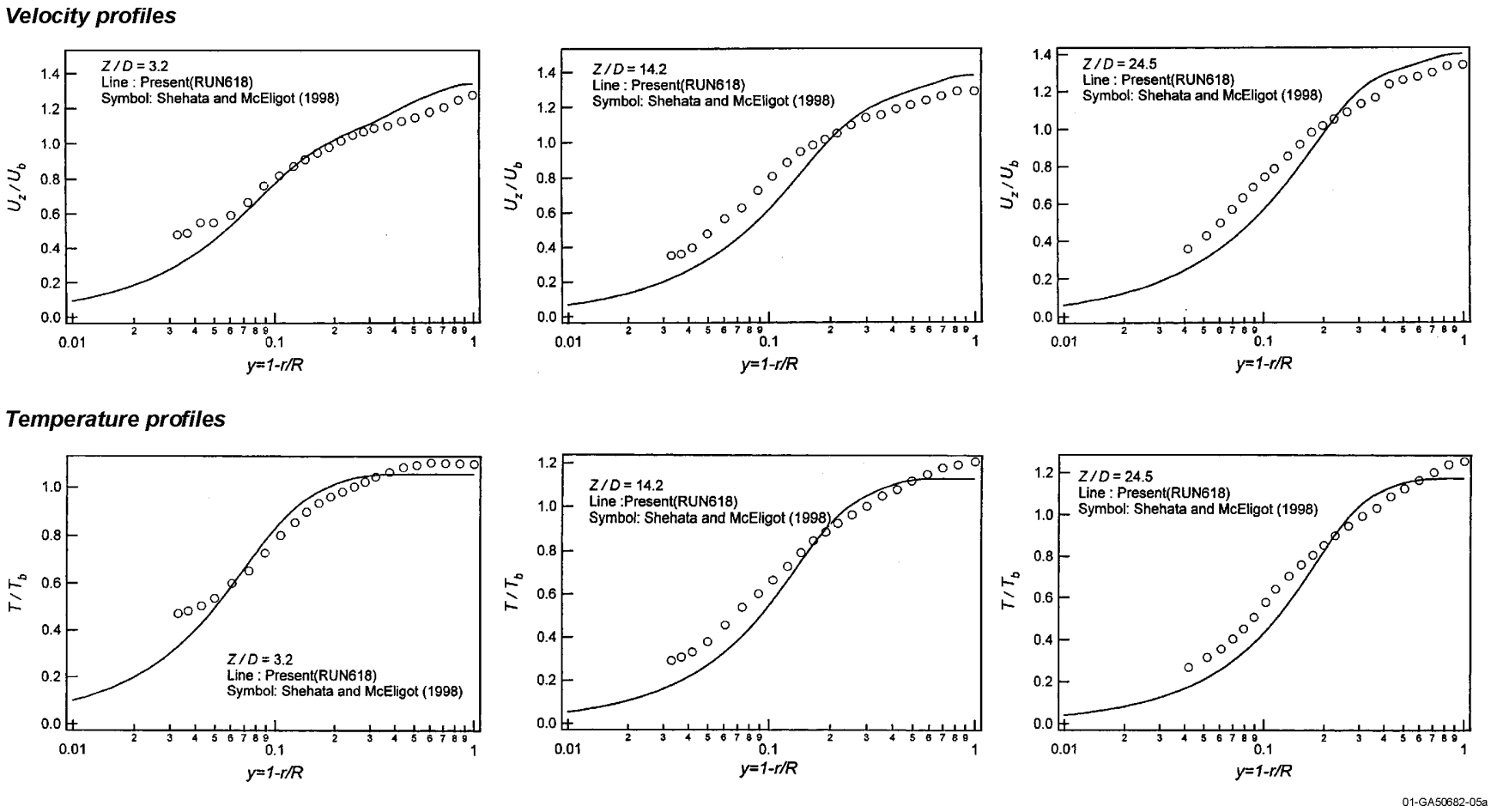

Fig. C-4. Predictions of mean velocity and temperature distributions for the conditions of "turbulent" run 618 by Shehata and McEligot [1998].

With these DNS calculations, it appears that the sub-turbulent state of Run 635 is easier to calculate than that of turbulent Run 618. In the case of Run 635, the turbulence initially decays in the streamwise direction and then continues decaying; Figure C-5 demonstrates this effect for the streamwise fluctuations. By $x/D \approx 24$ the turbulence has decreased substantially and the mean velocity and temperature distributions agree reasonably well with the measurements of Shehata and McEligot, probably since molecular transport may be dominant at that axial station. For Run 618 turbulence quantities are expected to decrease near the thermal entry and then recover or stabilize as seen in the reasonably successful predictions of Ezato et al. [1999] with a k-ε model. In the latter calculations, the Reynolds shear stress became approximately self-preserving by $x/D \approx 9$ in terms of wall coordinates; despite the oscillations in the DNS predictions away from the wall for this run, one sees that the same behavior may be occurring.

The DNS predictions of velocity fluctuations for Run 635 show the same general trends as for Run 445 and approach apparent laminarization. The radial fluctuation is affected more abruptly than the streamwise fluctuation. The calculations for Run 618 require more computer time to attain convergence (and to eliminate the oscillations in the fluctuation and Reynolds shear stress profiles away from the wall). However, it seems that all are approaching a condition of approximate self-preserving profiles downstream as predicted by some RANS calculations.

The spatial evolution of structures in these three flow fields is compared in Figure C-9 (comparable to Figure C-1). These results are consistent with the comments relative to the distributions of velocity fluctuations. The low-speed regions (relative to the pointwise mean velocities) disappear more slowly for Run 635 than for Run 445, indicating slower laminarization at the higher Reynolds number and lower non-dimensional heating rate. On the other hand, in Run 618 they retain their turbulent appearance throughout.

After the mini-meeting at TSFP-2 in Stockholm, Prof. Satake sent DNS predictions for pipe flows and some of his technical papers to Prof. Pletcher for checking his LES code (Task D below) and some DNS predictions of channel flows to Profs. Wallace and Vukoslavcevic (Task E below) so they may examine the spatial resolution of the miniaturized multi-sensor probes they are developing by using the DNS results to simulate probe response in four known flow fields. The direct numerical simulations of fully developed channel flow were performed to assist in calibrating multi-sensor probes. The computational domain is $5\pi\delta \times 2\delta \times 2\pi\delta$ in the streamwise, wall-normal and spanwise directions, respectively. This domain is 2356 x 300 x 942 in wall units and the numbers of nodes in the numerical mesh are 192 x 128 x 192. For the streamwise and spanwise directions, periodic boundary conditions are imposed with non-slip boundary conditions applied at both walls. The spatial data from DNS database is half the volume of a full channel region. Predictions of the instantaneous velocity fields at four different non-dimensional times are shown in Figure C-10 for $t^+ = 24, 48, 72, 96$. The Reynolds number, $Re_\tau = u_\tau\delta/\nu$, was 150. The objective of this simulation is to permit assessing the calibration of multi-sensor probes.

Initially, it had been intended to extend the circular tube calculations to annular flows and then annular ribbed geometries by modifying the boundary conditions. However, lack of funding and resources in Japan and high demand for the JAERI computer, reducing its availability, have led to deferring these sub-tasks.

During the summer 2001, Prof. Kunugi visited Prof. Jackson in Manchester and initiated joint collaboration on predictions and experiments on supercritical fluid flows, another case with strong fluid property variation. In future simulations, by using fictitious properties for idealized fluids, they will examine the effects of buoyancy, viscosity variation and acceleration independently to address basic questions about the fundamental flow physics involved.

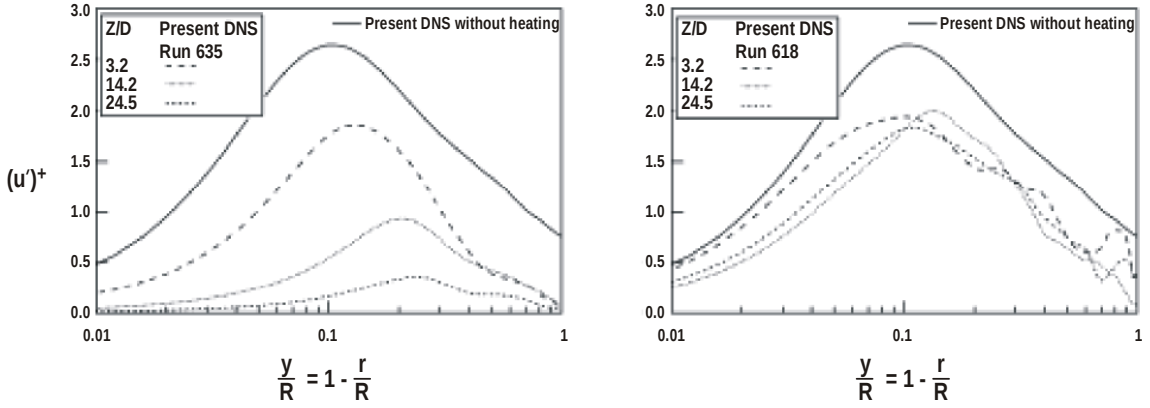

Fig. C-5. Predictions of evolution of streamwise velocity fluctuations for the conditions of "turbulent" run 618 and "subturbulent" run 635 by Shehata and McEligot [1998].

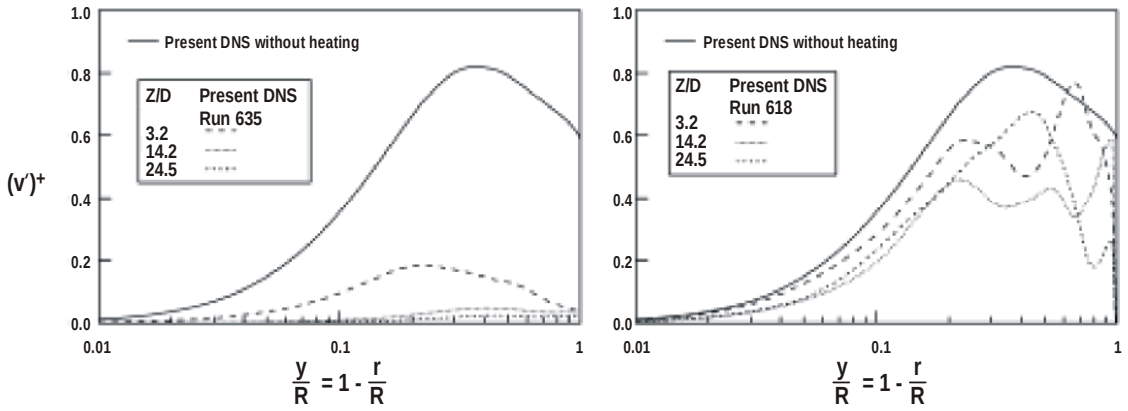

Fig. C-6. Predictions of evolution of radial velocity fluctuations for the conditions of "turbulent" run 618 and "subturbulent" run 635 by Shehata and McEligot [1998].

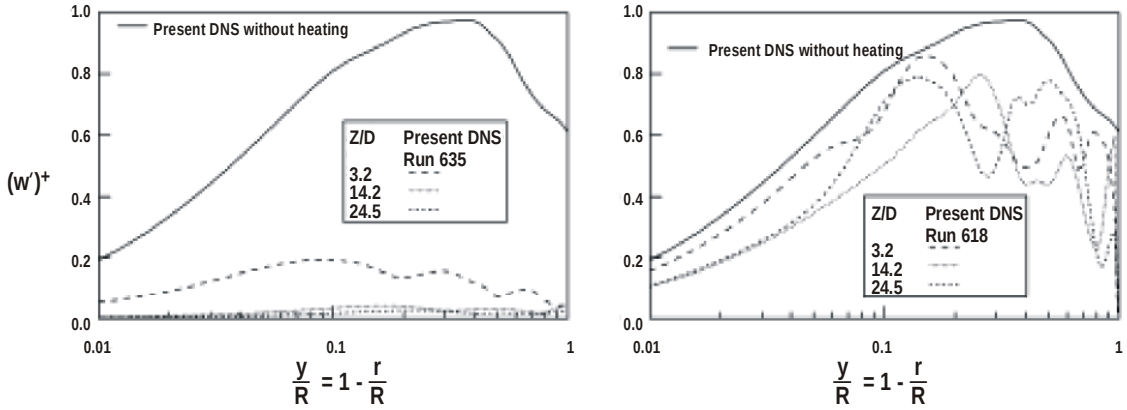

Fig. C-7. Predictions of evolution of circumferential velocity fluctuations for the conditions of "turbulent" run 618 and "subturbulent" run 635 by Shehata and McEligot [1998].

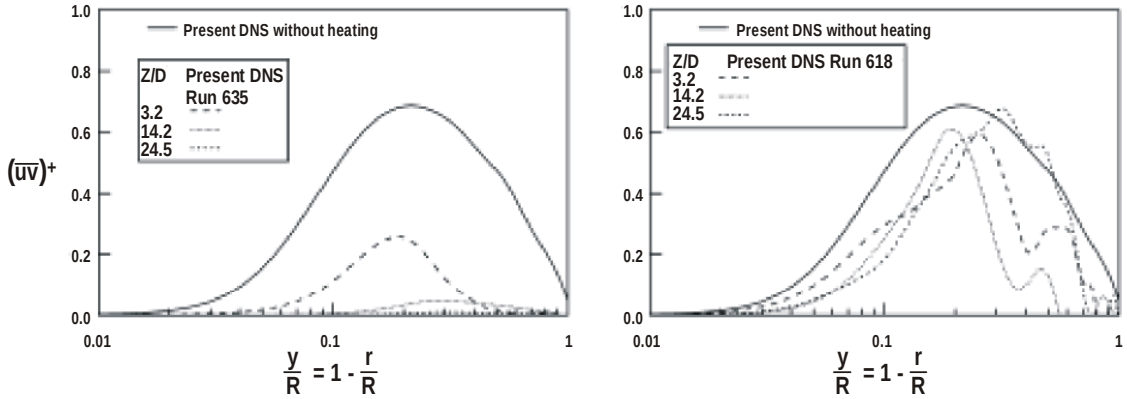

Fig. C-8. Predictions of evolution of Reynolds shear stress profiles for the conditions of "turbulent" run 618 and "subturbulent" run 635 by Shehata and McEligot [1998].

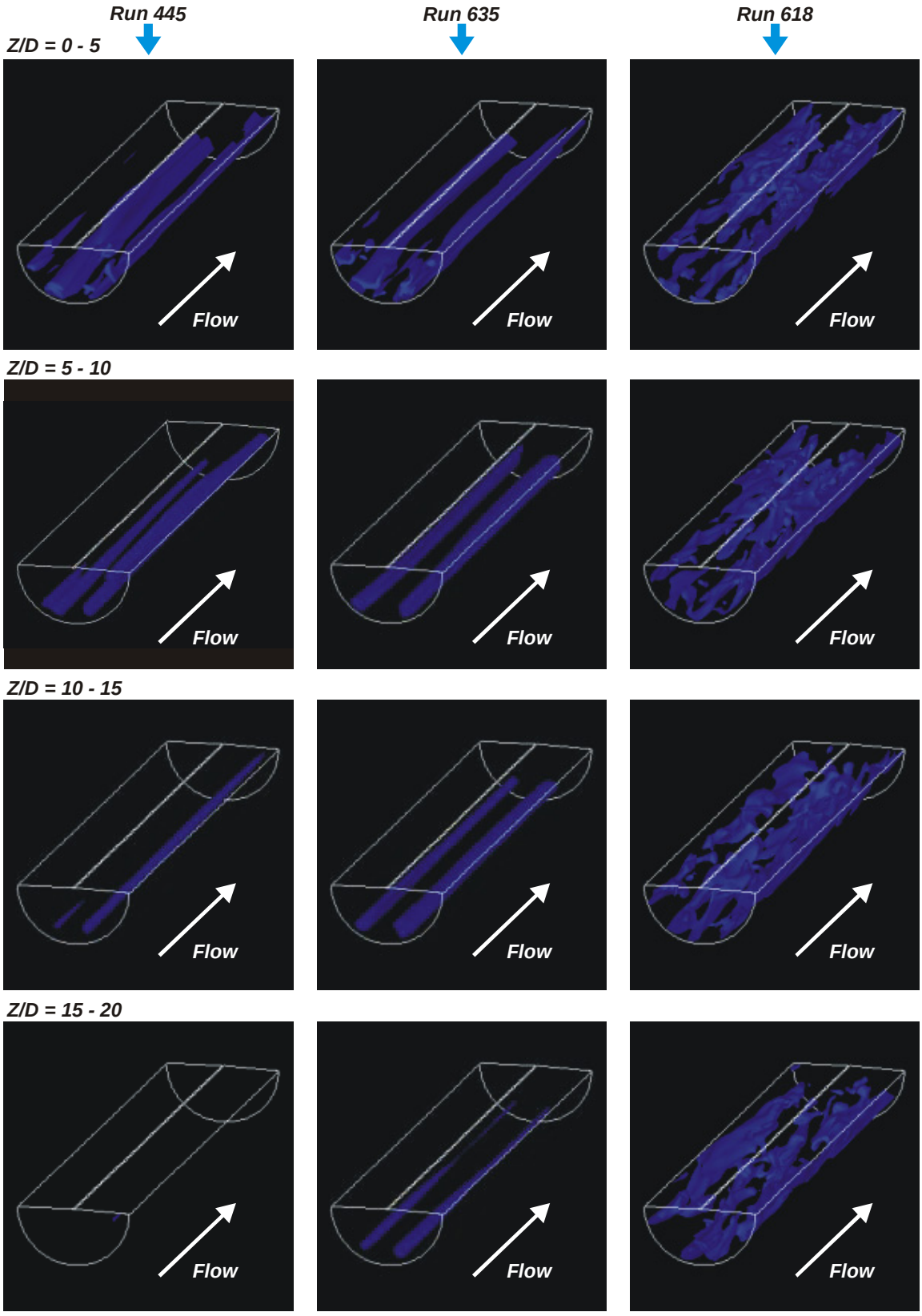

Fig. C-9. Contour surfaces of low-speed regions at various heating rates.

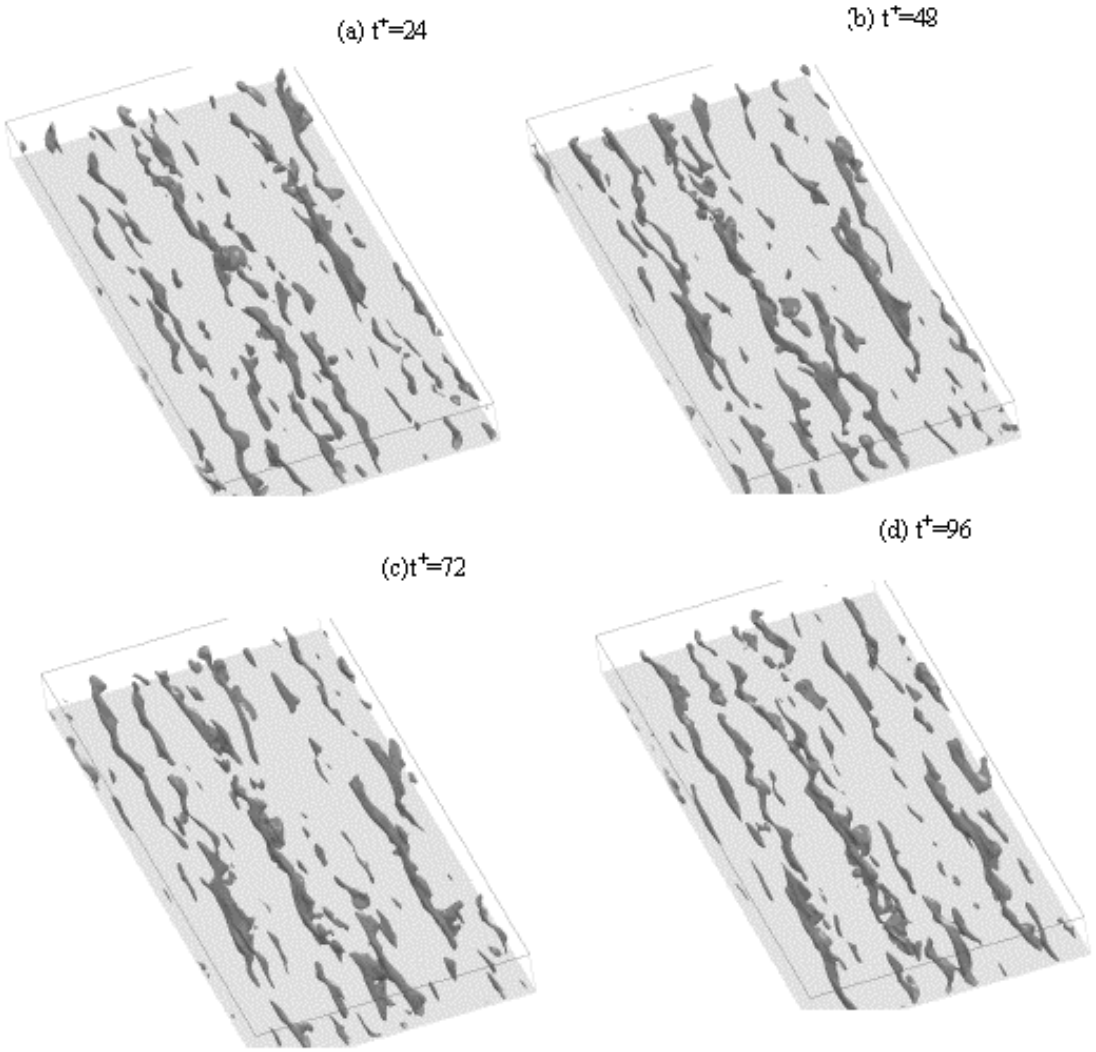

Fig. C-10. DNS predictions of instantaneous velocity fields for low speed streaks, $u^+ < 3$, in fully-developed channel flow to assist calibration of multi-sensor probes.

Task D. Analyses and Large Eddy Simulation -- Prof. R. H. Pletcher, Iowa State, Xiaofeng Xu and Joon Lee, Ph.D. students

Turbulence is one of the important unresolved problems in engineering and science. At the present time, no workable general theory is known by which the phenomena can be accurately predicted in configurations of practical interest. It is well established now that the three-dimensional Navier-Stokes equations along with appropriate forms of the continuity and energy equations govern turbulent flow, but limited computer resources prohibit the resolution of flows characteristic of most applications by direct numerical simulation. This situation is destined to change eventually. As computer hardware and algorithms improve, the frontier will be continuously pushed back, allowing flows of increasing practical interest to be computed by direct numerical simulations (DNS).

Large eddy simulation (LES), in which modeling is required only for the smallest scales, is another approach to simulating turbulence that will benefit increasingly with improvements in computer hardware. In fact, it is believed that the time is right for increased research in this area as more and more practical flow conditions come within reach of current and planned computers. Such an approach requires less computer power than DNS, but is still relatively computer intensive since -- even when a physical flow appears to be steady and two-dimensional in the mean -- LES requires a time-dependent, three-dimensional calculation in order to resolve scales larger than the filter scale. Modeling generally plays a fairly minor role in LES so that quite realistic results are expected. In all known comparisons in complex flows, LES results have been more accurate that those based on the Reynolds-averaged Navier-Stokes (RANS) equations that employ traditional turbulence models. Both DNS and LES approaches permit the calculation of features of the flow that are difficult or impossible to measure. Thus, DNS and LES studies can complement experimental studies of turbulent flow.

The **main thrust** of the research was to **extend LES methodology to** a broader class of flows with heat transfer, particularly **flows characteristic of those occurring in modern nuclear reactors**. The starting point for this research included computer codes for LES that have been validated by comparisons with experimental data for several flows in planar channels. The codes have also been used for flows with significant heat transfer [Wang and Pletcher, 1996; Dailey and Pletcher, 1998]. Good results have been observed using a dynamic subgrid-scale model. Such a model requires no arbitrary damping function or turbulent Prandtl number.

The **first research task** was to modify and validate the formulation for tube and annular flow geometries. Validation included comparisons with experimental data for cases in which the wall heat flux was specified. Part of this validation included establishing the merits and limitations of the quasi-developed flow model that was used successfully for LES by Dailey and Pletcher [1998]. The model makes three assumptions, namely that the temperature variations in the streamwise direction are step-periodic for the uniform heat flux case, that the mass flux is streamwise-periodic and that the mean pressure variations across the flow are negligible. This approach allows streamwise property variations to be taken into account. The temperature, density and streamwise velocity can all vary in the streamwise direction. The purpose of such a simulation is to determine the flow structure at locations somewhat removed from entry effects.

For the past few years our primary codes for large eddy simulation have been specialized to channel flows. Our first task in the present project was to modify our most efficient code to enable simulations in pipes and annuli. Simulations of laminar flow in a pipe checked out satisfactorily. The code was checked by comparisons of its simulations to experiments and to DNS results for isothermal flow.

The LES computer codes that were used for several years for channel flows have been modified to compute circular tube and annular geometries. As an initial step in the validation for the ***tube geometry***, comparisons have been made with the DNS results reported by Eggels et al. [1994] and the experimental data of Westerweel et al. [1996]. The Reynolds number of the constant property flow was 5300 (based on tube diameter and bulk velocity) and LES results have been obtained for two grid sizes, $40 \times 80 \times 64$ and $40 \times 100 \times 64$ in the radial, azimuthal, and streamwise directions, respectively. A dynamic subgrid-scale model was used in the simulations.

Figure D-1 compares the velocity profiles in wall coordinates obtained by LES with the measurements and DNS results. The symbols represent the measurements reported by Westerweel et al. [1996]. Good agreement is noted. The root-mean-square fluctuations are compared in Figure D-2 and again reasonably good agreement is observed. The total and resolved turbulent stresses are shown in Figure D-3. To validate the heat transfer formulation, a comparison has been made with the DNS results of Satake and Kunugi [1999] that were based on treating temperature as a passive scalar (i.e., effects of property variations were neglected). Figure D-4 compares LES results for the non-dimensional temperature distribution in wall coordinates with the DNS results for a Reynolds number of 5286 based on the bulk velocity.

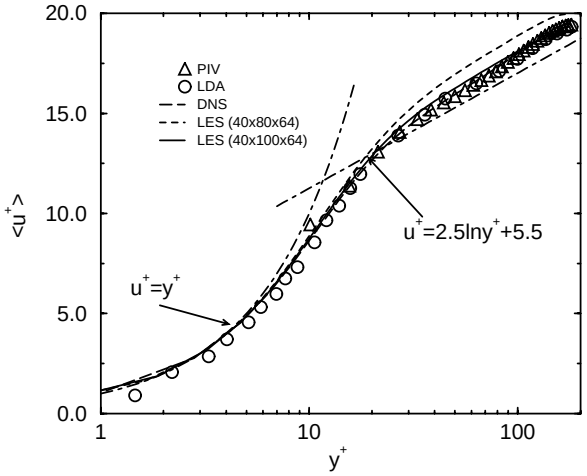

Fig. D-1. Tube flow velocity profile comparisons in wall coordinates.

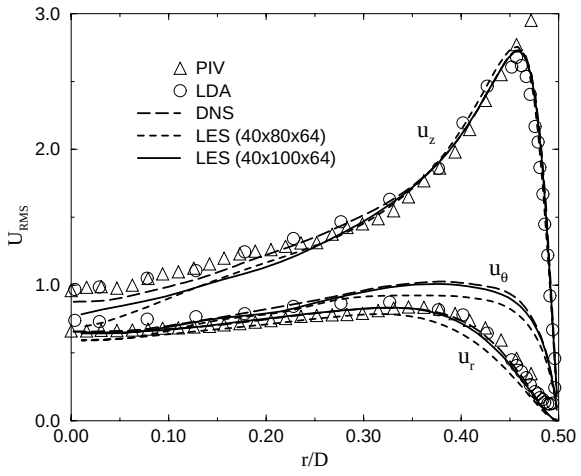

Fig. D-2. Tube flow rms velocity comparisons.

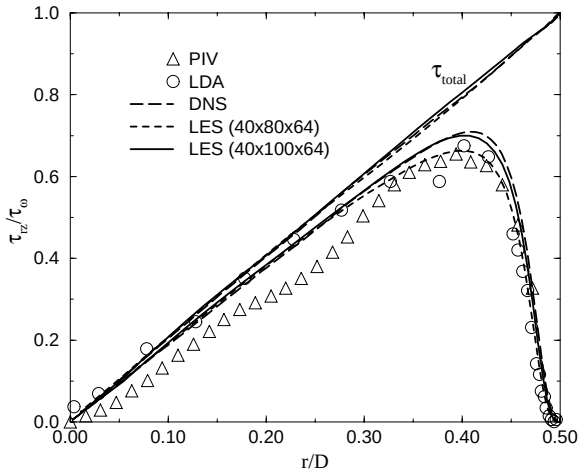

Fig. D-3. Comparison of total and resolved turbulent stresses.

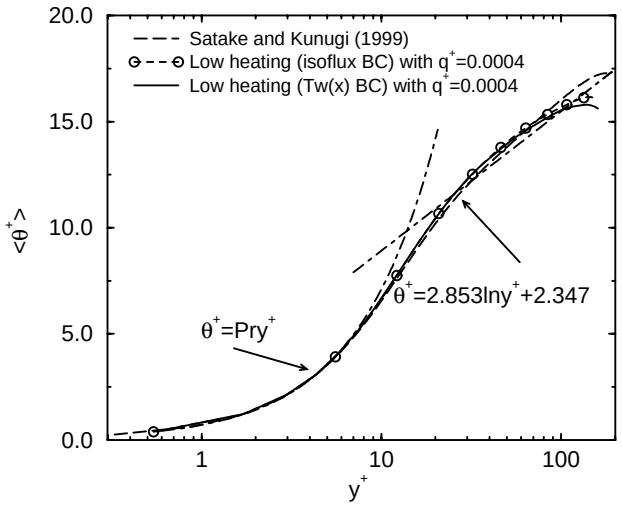

Fig. D-4. Tube flow temperature profile comparisons in wall coordinates.

The first step taken to validate the formulation for the ***annular geometry*** was to compare the results obtained in a channel of large radius ratio (0.95) with benchmark channel flow data. The Reynolds number was 11,200 based on the hydraulic diameter and bulk velocity. Figure D-5 compares the present LES results with the DNS predictions of Kim et al. [1987] and the data of Niederschulte et al. [1990]. Root mean square fluctuations are shown in Figure D-6. Agreement was considered satisfactory and work moved to annular flows with heat transfer.

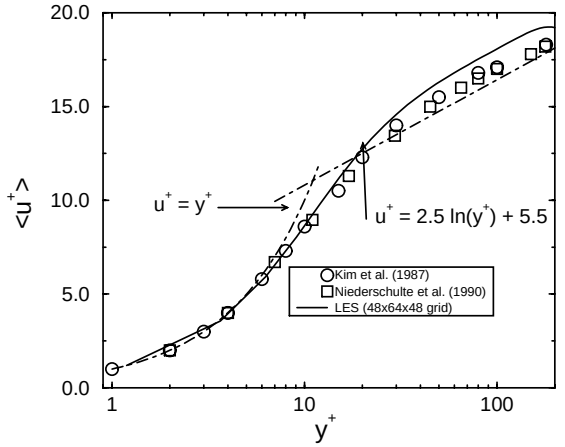

Fig. D-5. Velocity profile in wall coordinates, annular flow, $r_i/r_o = 0.95$.

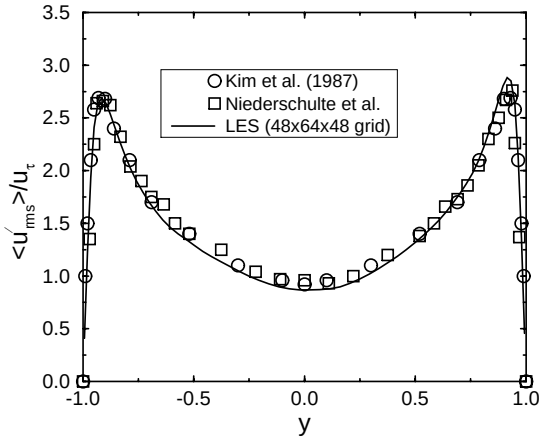

Fig. D-6. Streamwise rms velocity distribution, annular flow, $r_i/r_o = 0.95$.

Two ***annular*** heat transfer cases without buoyancy effects have been simulated for a radius ratio of 0.5 and a Reynolds number based on the hydraulic diameter of 12,000. Uniform heat flux heating was applied to the inner wall and the outer wall was taken as adiabatic as in an idealization of fuel cooling channels in some gas-cooled reactors. A low heat flux case (nearly

constant properties) has been included to enable comparisons with isothermal predictions. The other heat transfer case employed a larger heat flux that created a wall-to-bulk temperature ratio of 1.5, approximately. Figure D-7 shows the mean temperature distribution for the high heat flux case. To date it has not been possible to compare the high heat flux results with experiments or DNS results that take into account property variations. However, some comparisons have been made with the constant property DNS results of Chung et al. [2001]. The mean streamwise velocity distribution is compared with the DNS predictions of Chung et al. [2001] in Figure D-8. The results for a low heating rate agree reasonably well with the DNS calculations. The effects of property variations can be seen in the high heat flux results. Root-mean-squared velocity results are compared in Figure D-9. The agreement between the present LES results and the DNS predictions of Chung et al. [2001] is reasonably good. The LES results show a larger peak near the inner wall than near the outer. Other results in the literature [Zarate et al., 2001] tend to support that trend. The Nusselt numbers from the present simulations are within three to four per cent of the constant property results given by Kays and Crawford [1993].

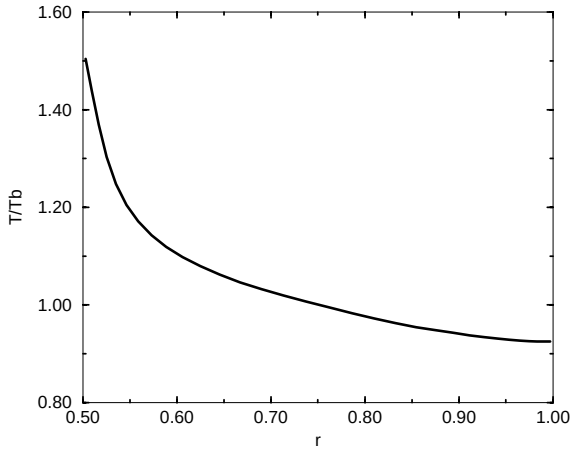

Fig. D-7. Temperature distribution, annular flow, inner wall heated, outer wall adiabatic, $r_i/r_o = 0.5$.

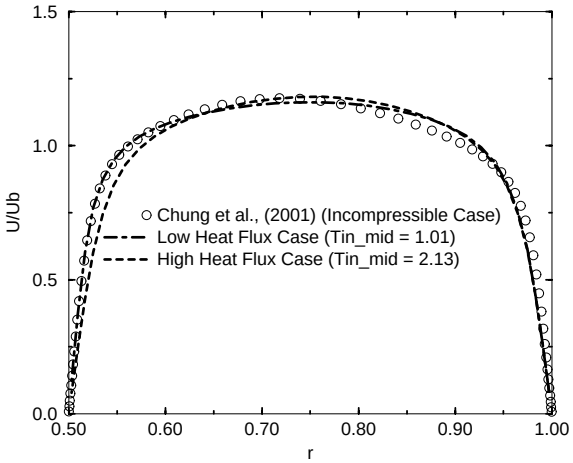

Fig. D-8. Streamwise velocity distribution, annular flow, inner wall heated, outer wall adiabatic, $r_i/r_o = 0.5$.

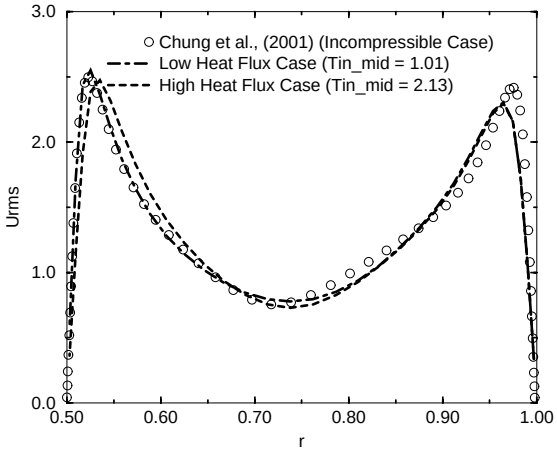

Fig. D-9. Streamwise rms velocity distribution, annular flow, inner wall heated, outer wall adiabatic, $r_i/r_o = 0.5$.

The **second phase** of the study focused on understanding the effects of buoyancy and high levels of heating on the flow. Studies in the literature suggest that the dynamic subgrid-scale model needs no modification in order to deal with buoyancy. Flow conditions were varied in order to study the cause of laminarization. The dynamic subgrid-scale model appeared to accommodate the effects of laminarization correctly .

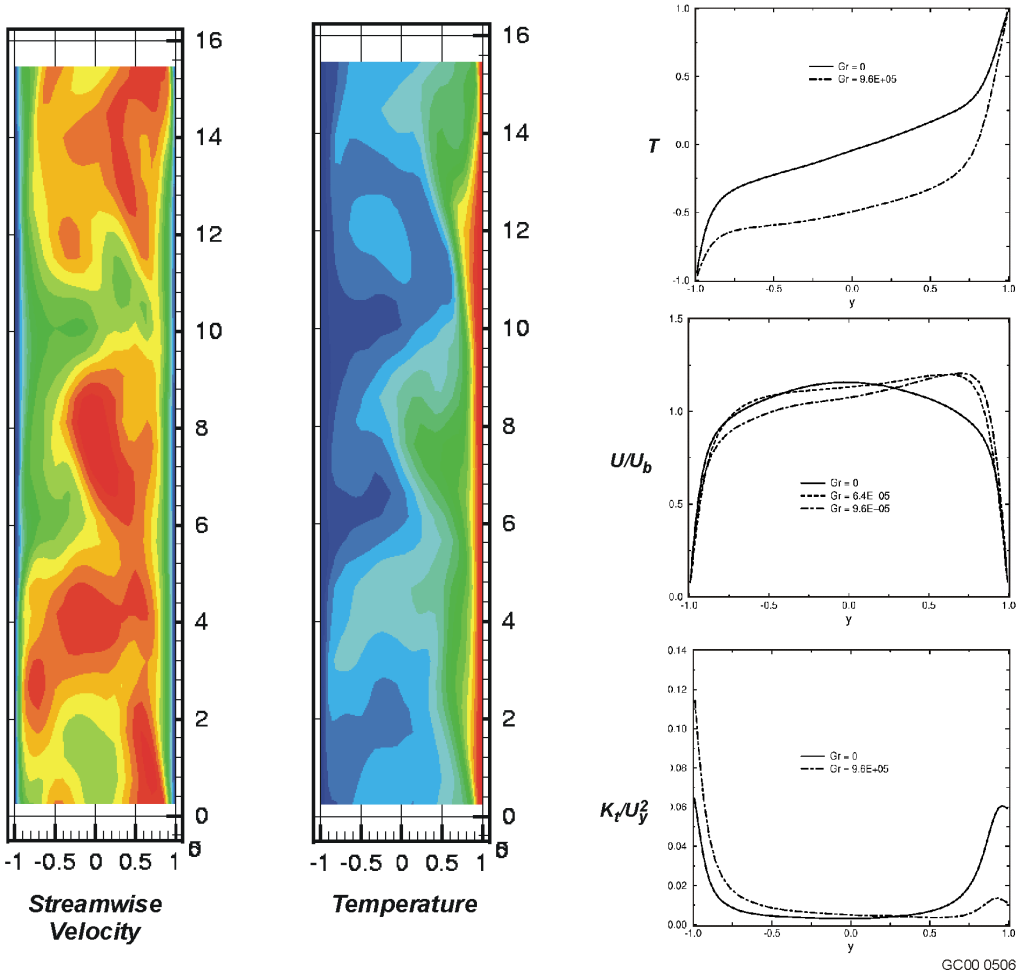

Fig. D-10. LES simulations of flow in a vertical heated channel (left wall cooled).

It has been possible to make some progress toward tasks involving the effects of high heating and buoyancy. In particular, some large eddy simulation results have been obtained for vertical upward flow of air in a ***channel*** heated on one side and cooled on the other where the effects of buoyancy were included. Such a channel flow corresponds closely to flow in an annular passage of large radius ratio, e.g., the vertical annular flow between the core barrel and the reactor vessel wall and fuel coolant passages of the Japanese HTTR. Variations in fluid properties were taken into account in these simulations. Our earlier simulations for horizontal flow with buoyancy effects have indicated that property variations make a considerable difference in the calculated results. A dynamic subgrid-scale model was used. Simulations were obtained for two different grids, 32 x 32 x 24 and 48 x 48 x 48, and two values of Grashof

number. All cases have employed a Prandtl number of 0.71 and a Reynolds number of 12,800 based on hydraulic diameter, bulk velocity and bulk properties. One case employed a wall temperature ratio of three resulting in a Grashof number of 960,000 where the Grashof number is defined as $Gr = g\beta\,(T_{w,in} - T_b)(D_o-D_i)^3 / (\nu_b^2)$. The value of Jackson's Bo parameter (Task F), defined as $Bo^* = Gr / (Re_b^{3.425}\, Pr^{0.8})$, was 1.08×10^{-8}. A second case employed a wall temperature ratio of two. The effects of the heating and cooling on the resolved shear stress can be seen in Fig. D-11. The left side is cooled and the right side heated. The case labeled 3 employed a temperature ratio of 2, whereas the case labeled 4 employed at temperature ratio of 3. The effects of property variations and buoyancy on the rms fluctuations can be seen in Fig. D-12. The buoyancy effect is most dramatic on the heated side where a significant suppression of the streamwise fluctuations can be noted. A similar trend can be seen in the distribution of kinetic energy (Figure D-13). Interestingly, Figure D-14 indicates that the rms temperature fluctuations (scaled by the mean friction temperature) are enhanced rather than suppressed near the heated wall. This result is thought to be due to the fact that the temperature gradient is steeper near the heated wall, more than compensating for the decrease in velocity fluctuations.

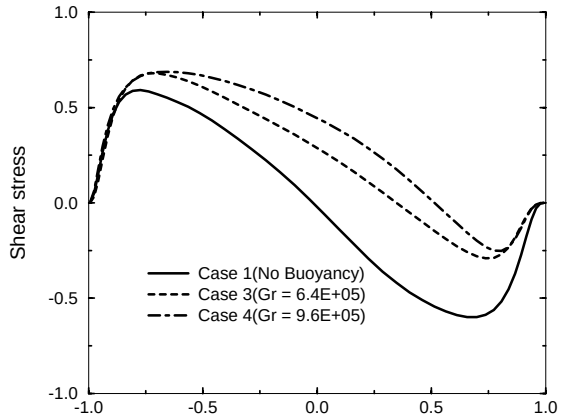

Fig. D-11. Effect of buoyancy on distribution of resolved turbulent shear stress, vertical channel.

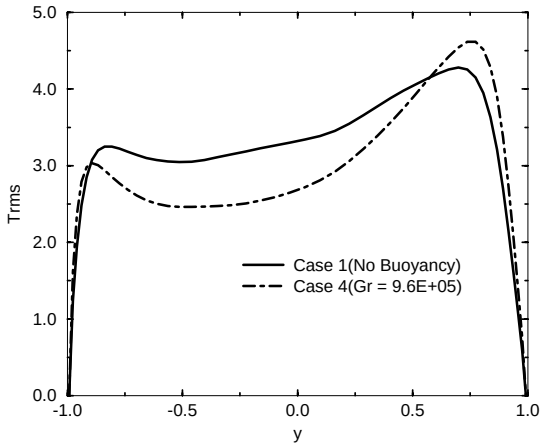

Fig. D-12. Effect of buoyancy on distribution of turbulent kinetic energy, vertical channel.

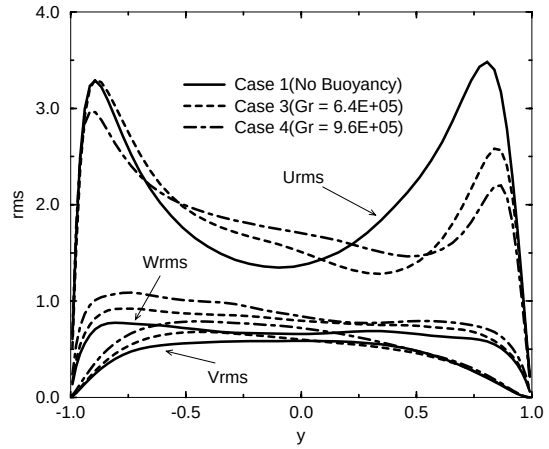

Fig. D-13. Effect of buoyancy on distribution of rms velocities, vertical channel.

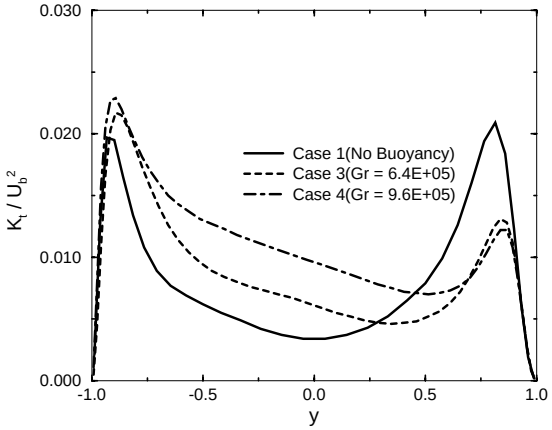

Fig. 14 Effect of buoyancy on distribution of rms temperature fluctuations, vertical channel.

In contrast with predictions for horizontal flow, the location of the maximum velocity shifts toward the hot wall. On the other hand, the temperature distribution tends to flatten out in the central region resulting in a more symmetric distribution of the mass flux. Because the bulk fluid temperature is closer to the cold wall value, the Nusselt number is about nine per cent greater on the cold side. The skin friction coefficient is larger on the hot side. A quick look at statistics suggests that turbulence is suppressed more on the hot side. The rms fluctuations are smaller there. The resolved Reynolds shear stresses indicate a reduction compared to non-buoyant flow, more so on the hot side. At this point a laminarizing effect seems evident. The results are quite interesting since this represents the first known LES study of a vertical flow accounting for buoyancy and variations in fluid properties. More results are given by Lee and Pletcher [2001].

More recently, simulations have been initiated for a vertical channel with the goal to make comparisons with the experimental data reported by Moro, Saez and Hopfinger [1998] for the COPPEC facility of CEA Grenoble. To date, only comparisons for isothermal flow at a Reynolds number of 6775 based on the mean velocity and channel half-width have been completed Figure D-15(a) shows a comparison for the mean streamwise velocity and Fig. D-15(b) for the streamwise rms velocity.

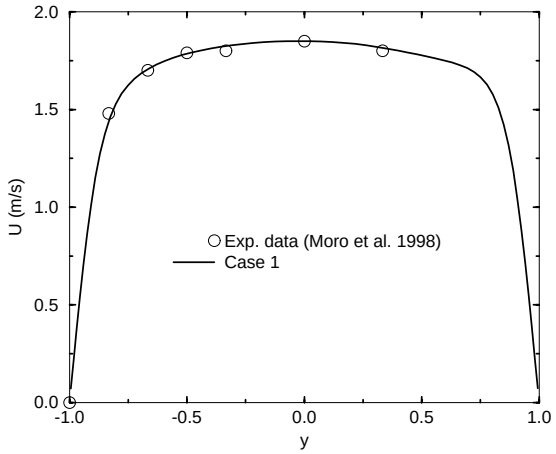

Fig. D-15(a). Comparison of velocity distribution with experimental results; vertical channel.

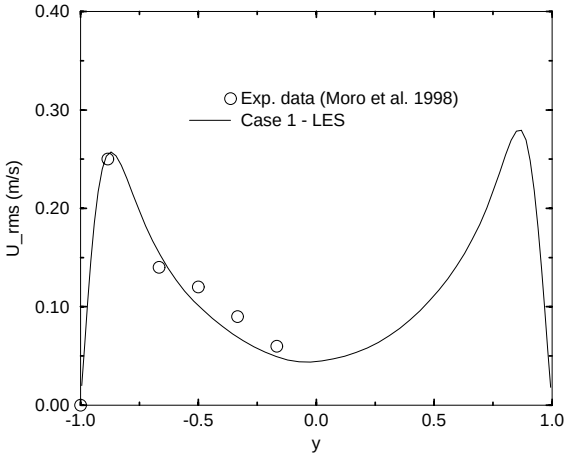

Fig. D-15(b). Comparison of streamwise rms velocity distribution with experimental results; vertical channel.

Several simulations were completed for upflow in a ***vertical annulus*** with a uniform heat flux applied on the inner surface and adiabatic conditions imposed on the outer surface. The fluid was air with a Prandtl number of 0.71 and property variations were considered. The results showed that strong heating caused distortions in the flow structure resulting in reduction of turbulent intensities, shear stress, and heat flux, particularly near the inner wall. Complete laminarization was not observed. The conditions for the cases simulated are tabulated below:

Table D-1. Nondimensional Parameters for Annular Cases Computed

Case	q_w	Gr	Bo^*	$T_b/T_{w,in}$	Re_{in}	r_1/r_2
1. aiding	2×10^{-4}	23,031	2.4×10^{-8}	0.97444	6200	0.5
2. aiding	2×10^{-4}	35,382	2.4×10^{-8}	0.97388	7100	0.5
3. aiding	2×10^{-4}	98,320	2.23×10^{-8}	0.97160	9700	0.5
4. aiding	5×10^{-3}	1,938,787	1.3×10^{-6}	0.40638	7100	0.3
5. aiding	5×10^{-3}	5,540,896	1.29×10^{-6}	0.37879	9700	0.3
6. no buoy.	2×10^{-3}	0	0	0.68276	8000	0.3
7. aiding	2×10^{-3}	1,100273	4.96×10^{-7}	0.63147	8000	0.3
8. no buoy.	2×10^{-3}	0	0	0.63189	8000	0.5
9. aiding	2×10^{-3}	1,234,223	5.56×10^{-7}	0.60365	8000	0.5

The nondimensional heat flux was determined by dividing the heat flux by the energy flux at the inlet of the computational domain (using specific heat at constant pressure) per unit cross sectional area. The Reynolds number in the table above is based on the hydraulic diameter and the bulk velocity and viscosity. The Grashof number was evaluated as specified above and the parameter Bo* is defined as $Bo^* = \dfrac{gD_h^4 q_w''}{\nu_b^2 k_b T_b Re_b^{3.425} Pr^{0.8}}$ where q_w'' is the dimensional heat flux.

The flow was assumed to be fully-developed and periodic or step-wise periodic in the streamwise direction over a distance of 4.5 hydraulic diameters. The grid employed was $48 \times 48 \times 80$. Results were compared to DNS predictions and empirical correlations. An example of the effect of buoyancy on turbulence can be seen in Fig. D-16 where the turbulent kinetic energy is plotted for cases 6 and 7. Flow conditions were the same for both conditions except there was no buoyancy force for case 6. More results can be found in the technical paper by Lee, Xu and Pletcher [2002].

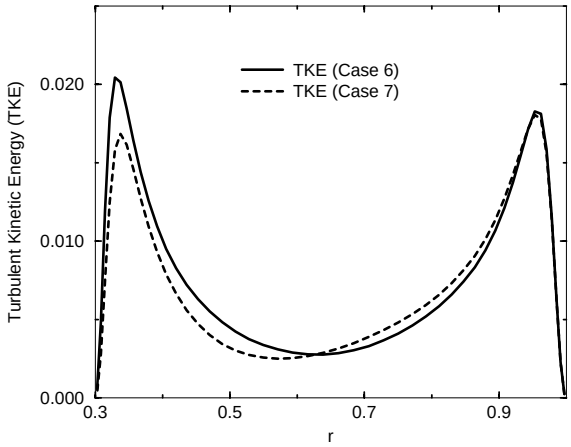

Fig. D-16. Effect of buoyancy and temperature on turbulent kinetic energy, annular flow.

Using streamwise step-periodicity, several vertical ***pipe flow*** cases were simulated and compared with the experiments of Shehata and McEligot [1998]. As the amount of heating

increases with accompanying flow acceleration, the streamwise step-periodicity approximation used in the simulations becomes more approximate. Nevertheless, it appears possible to determine global parameters such as Nusselt number with fairly good accuracy in a number of cases. To do so requires information as to the local Reynolds number and wall temperature. Table D-2 gives the conditions used in the simulations and compares the resulting Nusselt numbers with the experimental values. Table D-3 gives the buoyancy related parameters, Gr* and Bo*, for these comparisons. In this table Gr^* was computed using the heat flux as $Gr^* = \frac{gD_h^4 q''_w}{\nu_b^2 k_b T_b}$. Case numbers (first three digits) refer to the experiments by Shehata and McEligot [1998] and the numbers in parentheses refer to the case numbers for the simulations reported by Xu [2003]. The Reynolds number in the table is based on the tube diameter, bulk velocity and bulk viscosity. The Nusselt number is based on the diameter and the bulk thermal conductivity. It was not possible in the simulations to match the experimental temperature ratios and Reynolds numbers exactly. More details on the simulations and comparisons can be found in the thesis of Xu [2003]. The higher heating rate used in case 445 results in a reduction of approximately fifty per cent in the Nusselt number; the simulations capture that trend reasonably well.

Table D-2. Parameters for LES of Vertical Pipe Flow

Case	x/D	T_w/T_b	q_{in}	Re_b	Nu_b	Nu_{expt}
618(1)	14.195	1.40	1.8×10^{-3}	5728	15.55	15.57
618(4)	24.54	1.44	1.8×10^{-3}	5402	13.70	13.60
635(2)	19.87	1.91	3.5×10^{-3}	5131	11.04	11.4
635(5)	24.54	1.84	3.5×10^{-3}	4821	9.49	10.21
445(3)	14.195	2.02	4.5×10^{-3}	3683	8.86	9.5
445(6)	24.54	2.09	4.5×10^{-3}	3271	7.32	7.45

Table D-3. Buoyancy Parameters for LES of Vertical Pipe Flow

Case	x/D	Gr^*/Re_b^2	$Gr^*/Re_b^2)_{expt}$	Bo^*	Bo^*_{expt}
618(1)	14.195	0.116	0.11	3.52×10^{-7}	3.40×10^{-7}
618(4)	24.54	0.04	0.09	1.32×10^{-7}	1.72×10^{-7}
635(2)	19.87	0.15	0.13	5.37×10^{-7}	4.78×10^{-7}
635(5)	24.54	0.073	0.12	2.87×10^{-7}	4.61×10^{-7}
445(3)	14.195	0.202	0.30	1.18×10^{-6}	1.83×10^{-6}
445(6)	24.54	0.246	0.19	1.73×10^{-6}	1.33×10^{-6}

Figures D-17 and D-18 compare the velocity profiles at two axial locations for case 618 (a moderate heating rate) with the data of Sheheta and McEligot [1998]. Non-dimensional temperature profiles are compared in Figs. D-19 and D-20. Similar comparisons are shown in Figs. D-21 to D-24 for the case with the highest heating rate, 445. From these comparisons it is

clear that the heating rate and the associated flow acceleration significantly influence the velocity and temperature distributions. The simulations indicate that as the heating rate increases turbulence is suppressed, particularly near the wall and the flow shows many characteristics of laminar flow. Turbulent kinetic energy is increasingly reduced as the heating rate increases and the velocity profile moves toward a laminar like profile. Several examples of this behavior can be found in the thesis by Xu [2003]. Some indication of this observation can be seen by comparing the instantaneous velocity contours for the most fully turbulent case, 618 (x/D = 24.54), shown in Fig. D-25, with the contours for case 445 (x/D = 24.54) shown in Fig. D-26. The surface in the circumferential direction is at r/R = 0.96. In Fig. D-25 the contours appear quite smooth as they would be for a laminar flow.

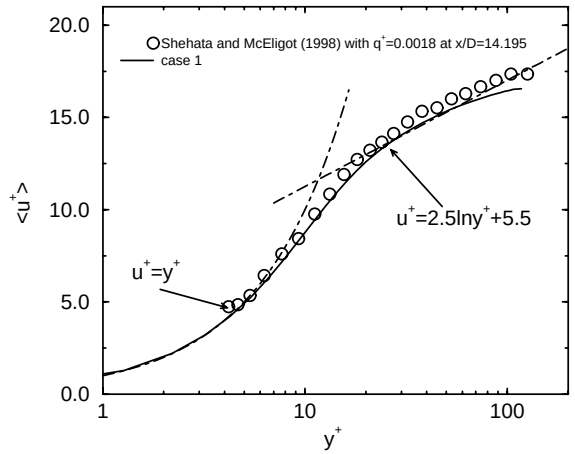

Fig. D-17. Comparison of computed mean velocity in wall coordinates with experimental results, case 618, x/D = 14.195.

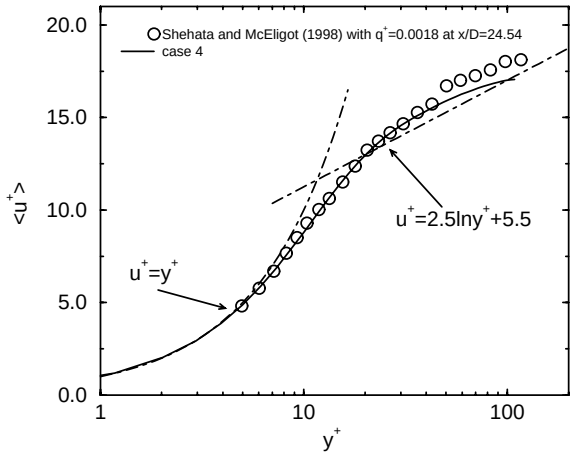

Fig. D-18. Comparison of computed mean velocity in wall coordinates with experimental results, case 618, x/D = 24.54.

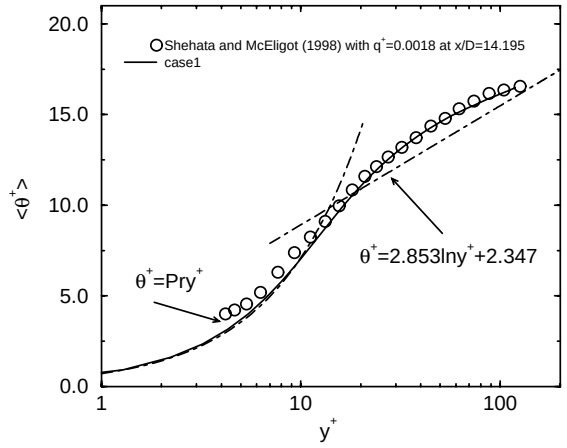

Fig. D-19. Comparison of computed mean temperature in wall coordinates with experimental results, case 618, x/D = 14.195.

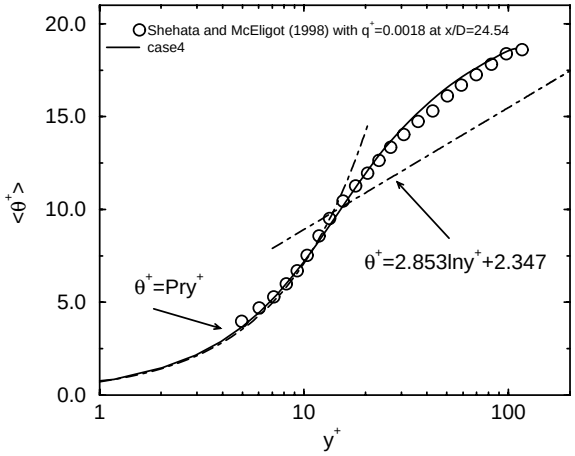

Fig. D-20. Comparison of computed mean temperature in wall coordinates with experimental results, case 618, x/D = 24.54.

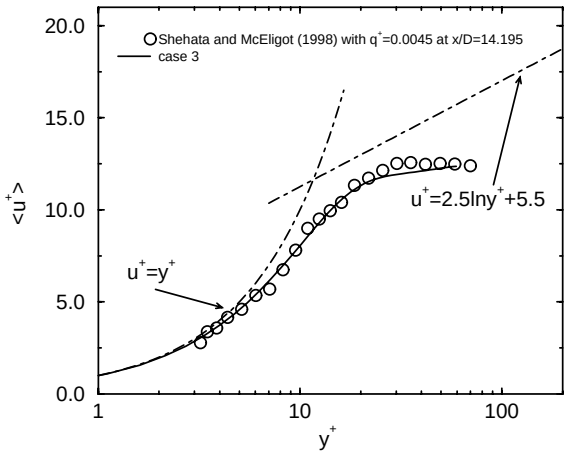

Fig. D-21. Comparison of computed mean velocity in wall coordinates with experimental results, case 445, x/D = 14.195.

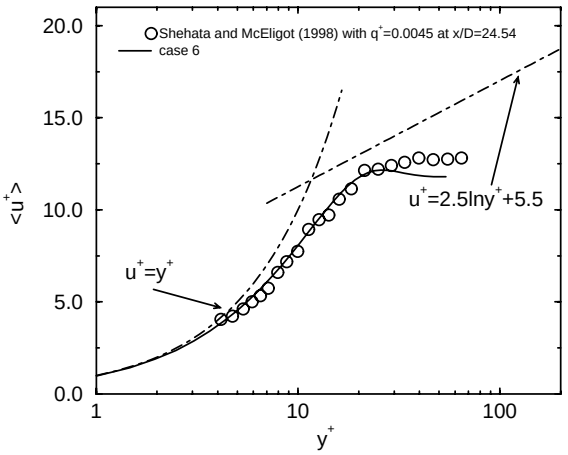

Fig. D-22. Comparison of computed mean velocity in wall coordinates with experimental results, case 445, x/D = 24.54.

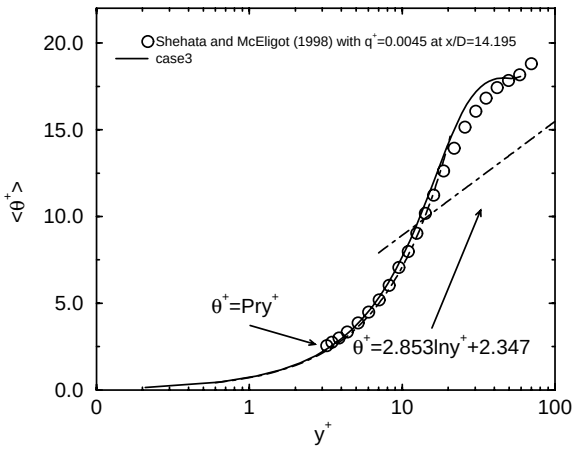

Fig. D-23. Comparison of computed mean temperature in wall coordinates with experimental results, case 445, x/D = 14.195.

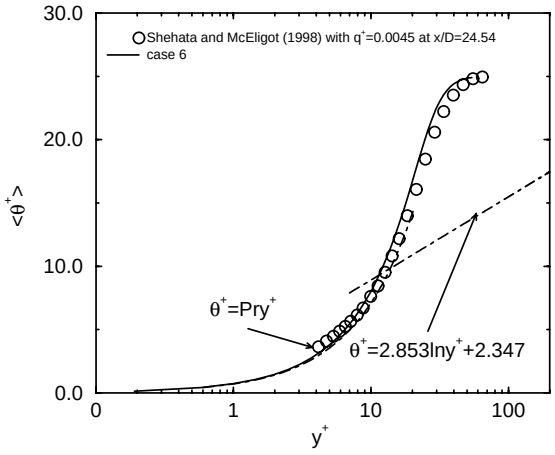

Fig. D-24. Comparison of computed mean temperature in wall coordinates with experimental results, case 445, x/D = 24.54.

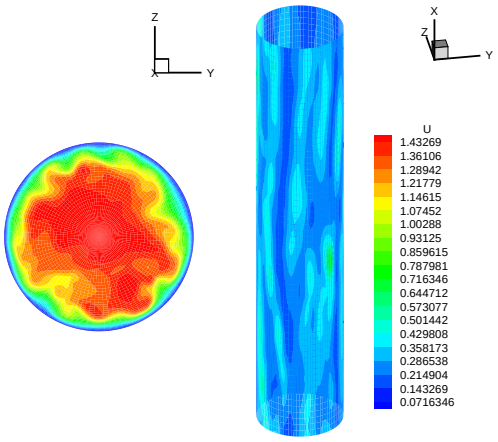

Fig. D-25. Instantaneous streamwise velocity, case 618, x/D = 24.54.

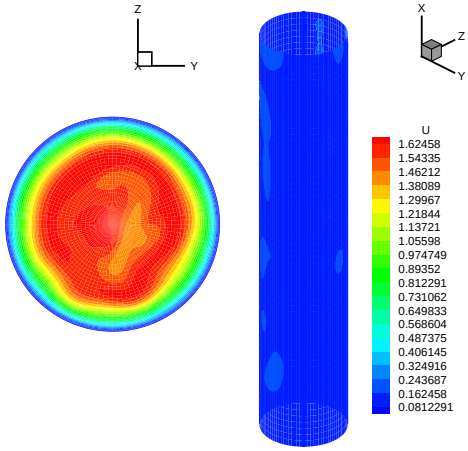

Fig. D-26. Instantaneous streamwise velocity, case 445, x/D = 24.54.

The **third task** concerned extending the LES capability to simulate ***entrance region*** flows and **annular flows with spacer ribs** in place. Both DNS and LES rely heavily on the use of spatially-periodic flow conditions to achieve economy in the simulations. Proposed here was the development of a strategy to utilize more general inflow conditions in order to treat developing flow in an ***entrance region***. This treatment can be achieved but requires more computational effort in order to provide realistic detailed time-dependent inflow conditions, particularly for the turbulent fluctuations. This approach is technically feasible and has been done in some related studies [Avancha and Pletcher, 2001] and the DNS calculations of Satake et al. [2000, 2002] in Task C. This task was modified in the final work statement made after the budget was reduced as a task to be achieved "as time permits." Time did not permit completion of this task but the relatively good success achieved at matching experimental data for the high heating pipe cases indicates that the spatially step-periodic approach has a fairly wide range of applicability.

In the case where a series of fairly short (in terms of hydraulic diameters) ***ribbed spacers*** are used in an annulus, as in the experiments of Task B and the coolant channels for GA control rods and HTTR fuel elements, it should be possible to embed a set of ribs within a quasi-developed spatially-periodic computational region. This approach should enable the simulation of the complete flow field around the ribbed region and should provide valuable detailed information about the flow including information that would be difficult to achieve experimentally. Such a procedure was implemented. Figure D-27 illustrates the configuration studied. Simulations were made for Reynolds numbers of 500 and 1200 based on the bulk velocity and hydraulic diameter both evaluated for the unobstructed portion of the annulus. The mid-annulus streamwise velocity directly behind the spacer (section A-A in Fig. D-27) is plotted against axial distance in Fig. D-28 for Re = 1200. A similar plot for section B-B is shown in Fig. D-29. Measured and computed profiles of mean streamwise velocity midway (axially and circumferentially) between the spacers are shown in Fig. D-30 and quite good agreement can be noted. The general flow pattern around the spacers can be seen in the contours of mean streamwise centerline velocity shown in Fig. D-31 for Re = 500 and in Fig. D-32 for Re = 1200. Rough plots of streamlines (on a surface midway between the walls) for the two flows are shown in Figs. D-33 and D-34.

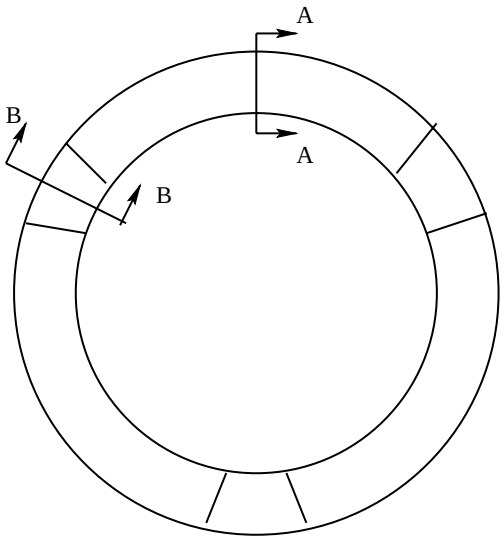

Fig. D-27. Configuration studied for annulus with ribbed spacers.

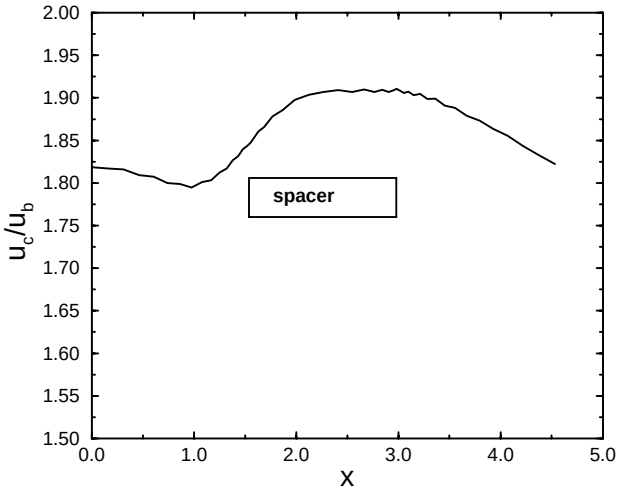

Fig. D-28. Mid-annulus streamwise velocity, section A-A

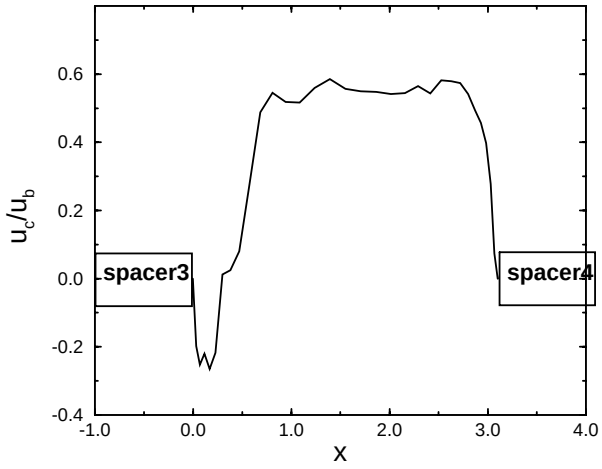

Fig. D-29. Mid-annulus streamwise velocity, section B-B.

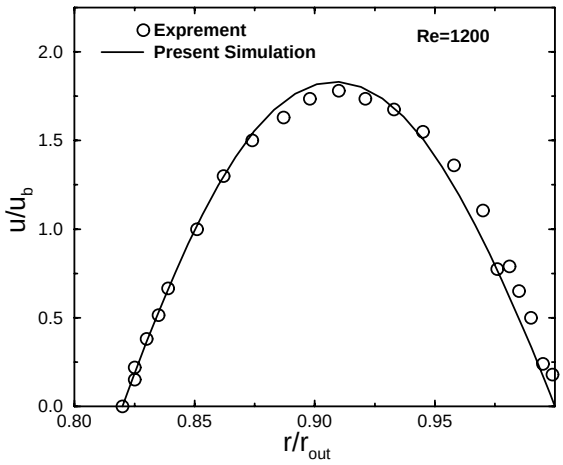

Fig. D-30. Comparison of computed streamwise velocity with experimental results.

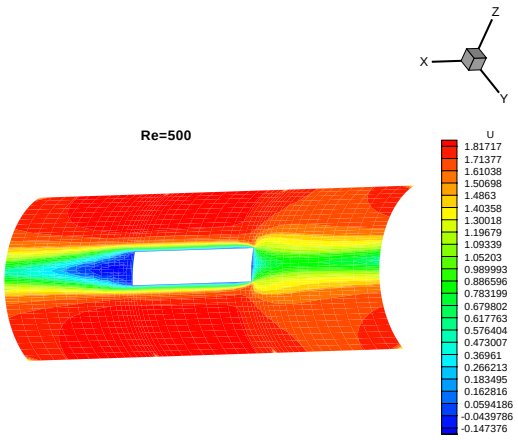

Fig. D-31. Contours of mean streamwise velocity midway between walls, ribbed annulus, Re = 500.

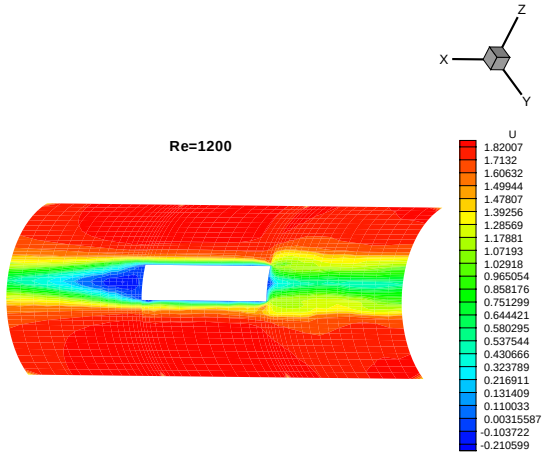

Fig. D-32. Contours of mean streamwise velocity midway between walls, ribbed annulus, Re = 1200.

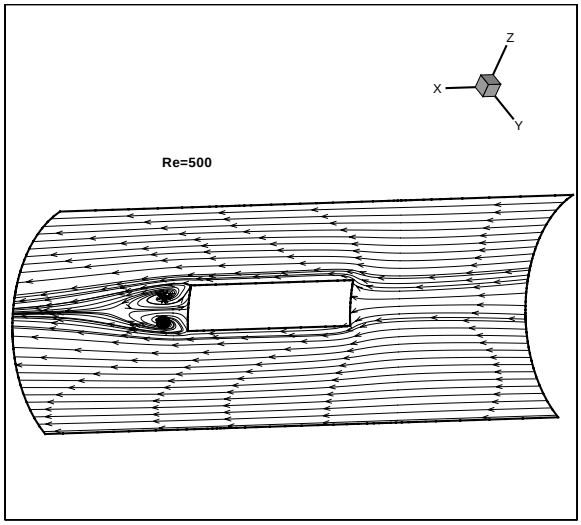

Fig. D-33. Streamlines on a surface midway between wall, ribbed annulus, Re = 500.

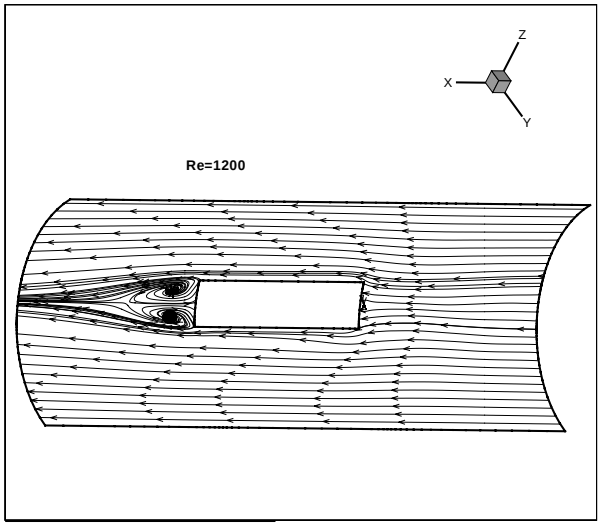

Fig. D-34. Streamlines on a surface midway between wall, ribbed annulus, Re = 1200.

Task E. Miniaturized multi-sensor probes for high temperatures -- Prof. J. M. Wallace, U. Maryland, and Visiting Prof. P. Vukoslavcevic, University of Montenegro (Montenegro)

Prof. Wallace and Visiting Prof. Vukoslavcevic developed miniaturized multi-sensor probes to measure instantaneous turbulence components in high temperature flows. These probes are for employment at U. Manchester and later at INEEL to measure fluctuating velocity components and temperature in high temperature gas flow through a vertical circular tube for assessment of the predictions and to understand the fundamental effects of this heating on the physics of the flow.

The University of Maryland group subtasks (objectives) are:

1. Design, develop, fabricate and test miniature hot-wire probes to measure simultaneously the streamwise and wall normal velocity components and the temperature in a high temperature gas flow in a vertical circular tube.

2. Design and fabricate a calibration and test flow facility that will enable the probes to be calibrated and tested under the same conditions as for proposed experiments at U. Manchester (Task F) and INEEL.

3. Create and test accurate and efficient data reduction algorithms in order to convert digital outputs of the hot-wire anemometry voltages into velocity and temperature components.

4. Create and test data analysis algorithms that will take the reduced data from the U. Manchester experiments and produce the experimental benchmark information required to assess the DNS and LES codes that are a major part of this integrated research project.

E-1. Probe Design

The probes should be designed to measure two velocity components of the turbulent velocity field simultaneously with the turbulent temperature fluctuations of a hot air flow with the best spatial resolution possible. The velocity range the probe must cover is from 0.5 to 15 m/s and the temperature range is from ambient room temperature up to 700 °C. Such probes are not commercially available. They can only be commercially purchased at a very high price, especially if they are miniaturized. The main characteristics of the probes described below are: the number of their sensors and their geometrical arrangements, the spatial resolution of the probes and their operational temperature and speed ranges.

- To meet the measurement requirements, the probe should have at least three sensors: two for the two velocity components and one for temperature. The most compact arrangement is an X-array of the two velocity sensors, operated in the constant temperature (CTA) mode, and a cold sensor for the temperature measurements, operated in the constant current (CCA) mode.

- The probe should be small enough to be able to resolve the smallest spatial scales of the turbulent flow. These are of the same order as the Kolmogorov microscale. As is well

known, for boundary layer flows it is practically impossible to construct a multisensor probe that can resolve these smallest scales. However, it has been determined that a probe with a spatial resolution of 5 – 10 Kolmogorov lengths measures almost all the dissipation-rate energy, which is the essential requirement. Obviously the probe dimension should be made as small as practically possible. Sensor supporting prongs and anemometer characteristics limit the smallest dimensions of the probe. A minimum length to diameter ratio l/d has to be satisfied to avoid substantial conduction to the prongs so that a convenient cooling law can be used. To avoid low frequency attenuation of the temperature sensor a minimum l/d ratio also must be chosen. Therefore, the choice of wire diameter with an appropriate l/d ratio determines the best spatial resolution that can be achieved. This choice is limited by the minimum wire diameter that is robust enough to survive in the flow.

- The temperature range is important in two respects. The first is that sensors, prongs and the other probe parts (stem, holder, junctions, etc.) must be made of materials that can sustain the highest expected temperatures. The second is the influence of temperature on the fluid properties. For the broad temperature range from ambient to 700°C to which this probe will be exposed, the temperature has to be measured to account for its influence on the fluid properties. It is also well known that the velocity sensors are sensitive to the parasitic influence of temperature variations as well as the temperature sensor to the parasitic influence of velocity variations. To correct these influences, therefore, the instantaneous temperature as well as the velocity must be known.

In order to determine the best probe geometrical arrangement and sensor separation, several probe designs, shown in Figure E-1, have been constructed and tested.

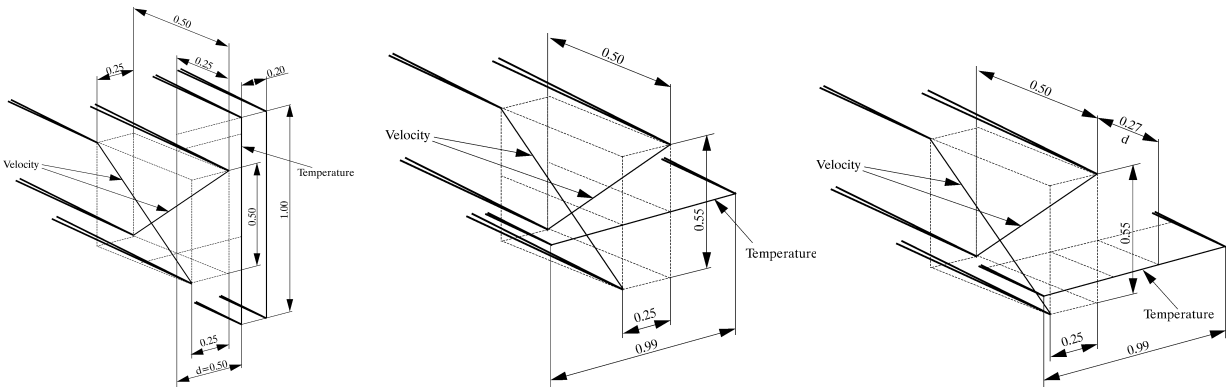

VTS **VTF** **VTFD**

Fig. E-1. Test probe versions: VTS, VTF and VTFD models

The first of these is designated as the VTS model. It has two temperature sensors side by side with the velocity sensors. The second is the VTF model with a single temperature sensor in front of the velocity sensors in a plane passing through the tips of velocity sensor prongs. The third is

the VTFD model with the temperature sensor placed in front of the plane passing through the tips of the prongs of the velocity sensors.

A 2.5 micron Platinum + 10% Rhodium wire is used for the X-array velocity sensors. This alloy can stand temperatures over 700°C. Assuming an l/d = 280, which is reasonable to have a convenient cooling law, the prong separation is 0.5 mm. A smaller wire of 1-micron diameter or even less also is commercially available. Assuming a 1-micron wire diameter and the same overheat ratio, the probe spatial resolution could be reduced 2.5 times. Unfortunately, the sensor becomes much more fragile, which can be a serious problem for the measurement conditions planned for these probes whereby the probe must be positioned deep within a pipe at locations not accessible to view. The prongs are made of stainless steel. They are 0.25 mm diameter at the base and are tapered to 0.05 mm at the tips. These dimensions are chosen to avoid prong vibration that can damage the sensors and to reduce the blockage of the flow. The sensor supporting prongs are placed in ceramic tubes of 1.7 mm, which are sealed by ceramic epoxy in a stainless steal tube. The velocity sensor separation has been initially chosen at 0.25 mm, but this dimension is varied.

To achieve the best frequency response of the temperature sensor, the smallest diameter wire possible should be used, but this increases the probe fragility. On the other hand, a larger wire diameter can be used and the frequency response can be compensated if the velocity field is known, as is the case for these probes. Our estimate is that one micron wire should be the best compromise. This choice meets the low frequency attenuation criterion that l/d be at least 1000 for a 1 micron wire. The separations of the temperature and velocity sensors have to be optimized. If they are too close together the hotter velocity sensors can influence the temperature sensors and, if they are too far apart, the probe spatial resolution is degraded. Different distances and positions are examined.

It is quite obvious that for small air speeds the cold sensor can be affected by the hot ones due to conduction as well as to natural convection heat transfer. Increasing the air speed, the hot air around the velocity sensors will be swept downstream reducing the heating of the cold sensor. From that point of view, the most convenient position of cold sensor should be in front of the hot one, as is the case for the VTF and VTFD models shown in Figure E-1. The test results of these models are presented in Figure E-2.

For a sufficiently small current through the sensor, its voltage output should not depend on speed, if the speed is high enough to sweep downstream the hot air around the velocity sensors. This voltage is defined as E_∞. Decreasing the air speed around the sensors, the temperature sensor will be heated by the velocity sensors, which will change the cold sensor output, E. The difference $E- E_\infty$ is the measure of this effect. It can be seen from Figure E-5(a) that, in the case of the VTF model and overheat ratio OHR=1.6 (velocity sensor temperature about 400°C), this effect becomes significant for speeds under 1.8 m/s, which we denote as the critical speed for this model and OHR. Reducing the OHR and, therefore, the velocity sensor temperature by about 100°C, does not change significantly the critical speed, Figure E-5(b), although the influence at very low speeds is much smaller.

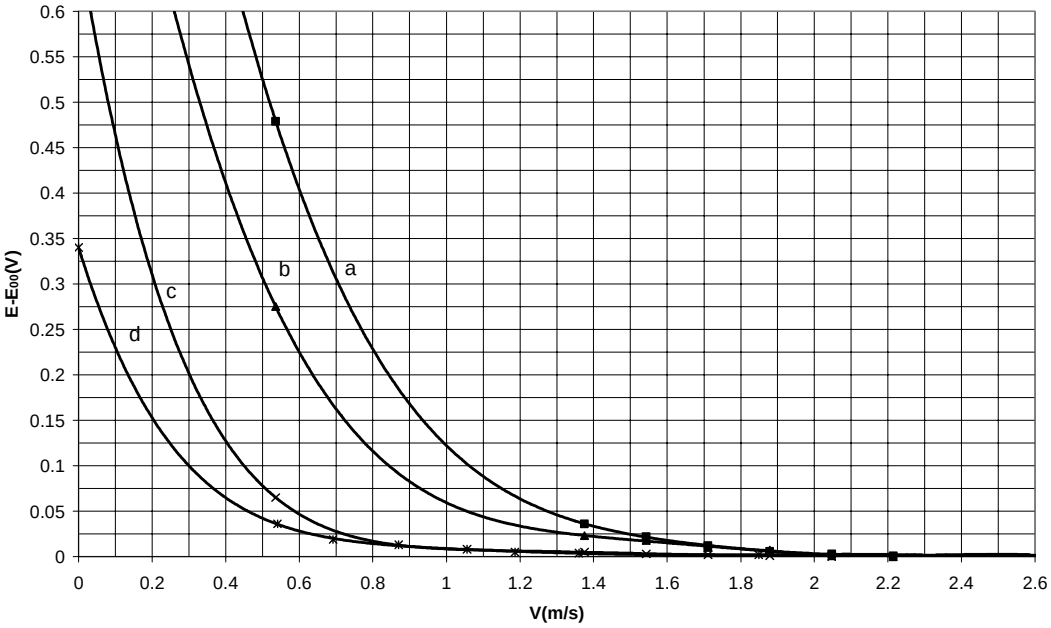

Fig. E-2. Cold sensor voltage output as a function of air speed: (a) VTF model with OHR=1.60, (b) VTF model with OHR=1.42, (c) VTFD model with OHR=1.42, (d) VTS model with OHR=1.42.

Further decreasing of the velocity sensor temperature (under 300°C) will strongly decrease its sensitivity to velocity at the higher air temperatures expected for the experimental conditions at the University of Manchester (up to 200°C). Therefore, the only way to further decrease the critical speed was to increase the hot and cold sensor separation. Doubling the distance from the intersection point of the velocity sensors, as was done with model VTFD, the critical speed was reduced to about 0.9 m/s, Figure E-5(c). The bottom line (d) in Figure E-5 represents the cold sensor output in the case when the cold sensor is placed side by side with the hot sensors, as is the case for the first temperature sensor of model VTS, Figure E-1. The critical speed is slightly lower than in the previous case.

Increasing the distance between the velocity and temperature sensors of model does not change the critical speed significantly. This can be seen from Figure E-3 where simultaneous outputs of the first and second temperature sensors of VTS model are presented. The critical speeds of both sensors are practically the same. The sensors response differently in the range of very low speed where both of them are affected by velocity sensors.

In order to examine the influence of free convection, model VTS was placed in three positions with the first temperature sensor under, side by side and above the velocity sensors. The voltage outputs for these three cases are presented in Figure E-4. The results are practically the same in all three cases, showing that the influence of free convection is negligible. Otherwise, the cold sensor would be much more affected in the position above the hot one. This means that the heat transfer from the velocity to the temperature sensor is mainly due to conduction. Therefore, the sensor separation as well as the OHR are the main parameters affecting mutual sensor influence.

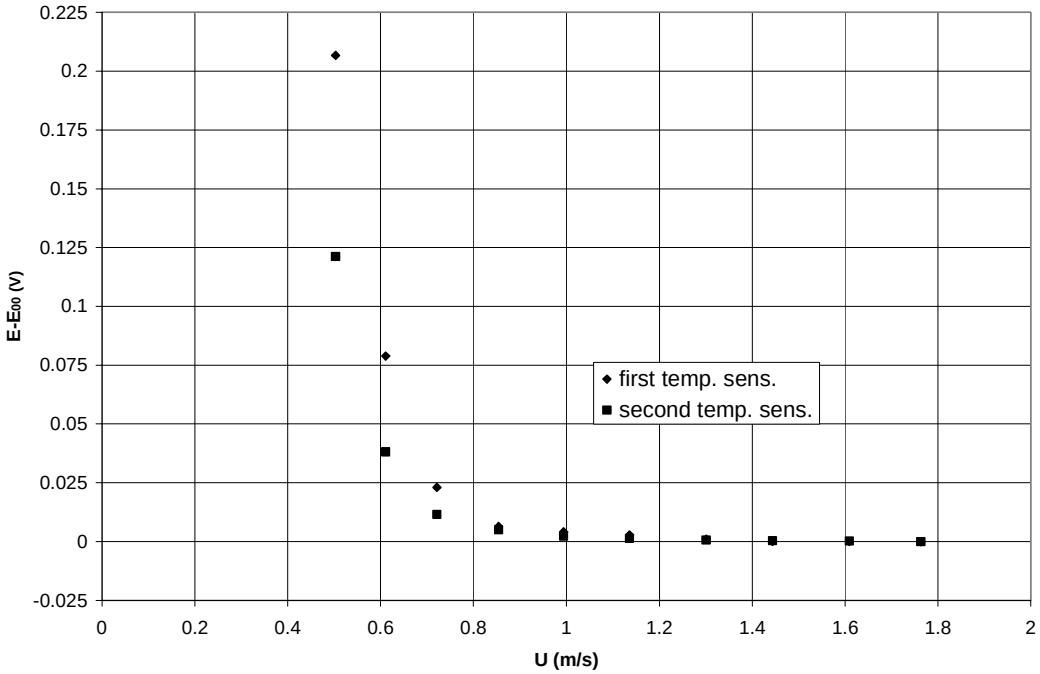

Fig. E-3. First and second cold sensor voltage outputs of the VTS test model probe

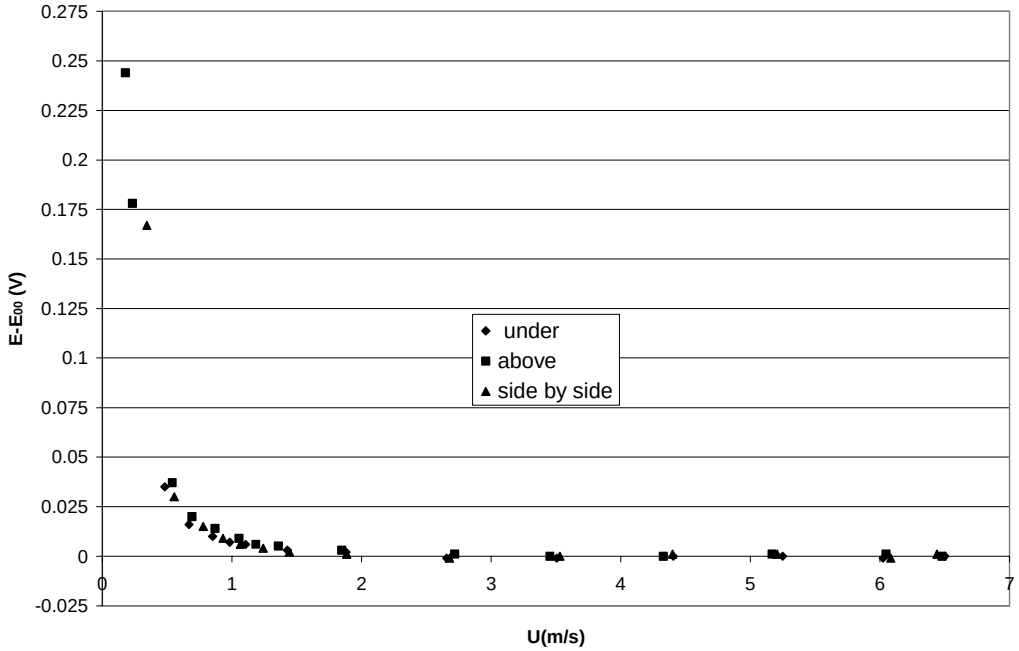

Fig. E-4. Cold sensor output for different position of hot sensors; under, side by side and above.

Based on this analysis, it follows that model VTS, with the first temperature sensor, and model VTFD have the best geometrical arrangements. The advantages of the VTS model are the smaller mean velocity and temperature gradients between the hot and cold sensors for the case of application in a bounded flow (University of Manchester and INEEL). The advantage of the

VTFD model is the constant mean temperature along the temperature sensor in a bounded flow application. This is why the VTS and VTFD models were chosen for the final probe versions shown in Figure E-5.

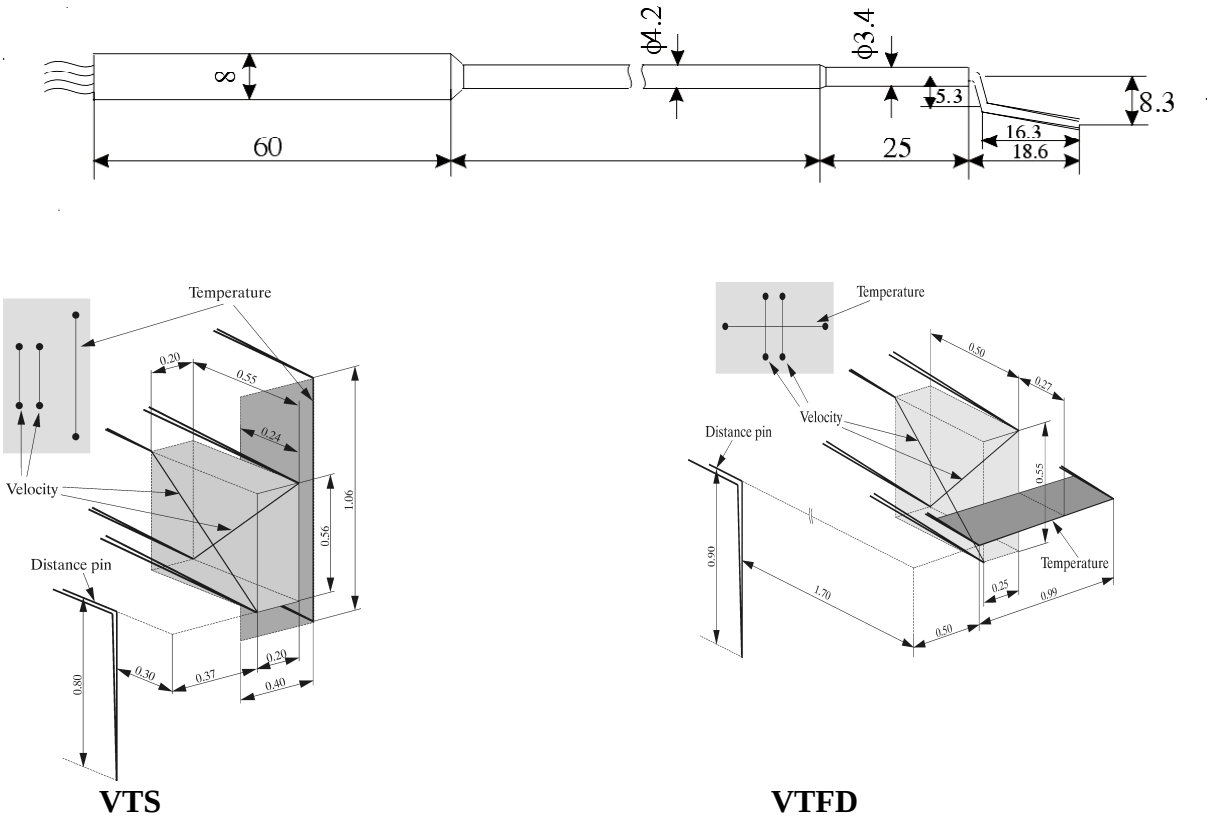

Fig. E-5. Boundary layer type probes

The final versions are similar to the test versions. The main difference is that they are boundary layer type probes in order to be able to get as close as possible to the wall. They also have an additional prong, designed to be used as a spatial distancer. By connecting this prong to a light or sound source, the distance of the probe from a conducted wall can be determined with an accuracy of 0.02 mm. This is important for measurements in a pipe with a metal (non-transparent) wall such as that at the University of Manchester.

E-2. Calibration and Testing Facility

A facility was designed and built to emulate the flow conditions of the proposed experiments at the Univ. of Manchester and at INEEL. This facility is a very low turbulence jet that can be heated over the range of experimental temperatures desired. The flow at the exit of a short extension to the nozzle can be used to calibrate the probes. The probes can be systematically subjected to a matrix of pitch and yaw angles at different speeds and temperatures. It can provide a variable and uniform velocity flow field in the range of 0.5 to 15 m/s and a temperature range from ambient room temperature to 700°C. In order to achieve these requirements the facility consists of a:

- jet

- heater with variable power input
- blower with variable airflow rate
- pitching and/or yawing assembly.

A sketch of this heated jet is shown in Figure E-6, and a photograph of the jet assembly together is shown in Figure E-7. Insulation is subsequently wrapped around the complete assembly and it is enclosed in an aluminum alloy cylinder.

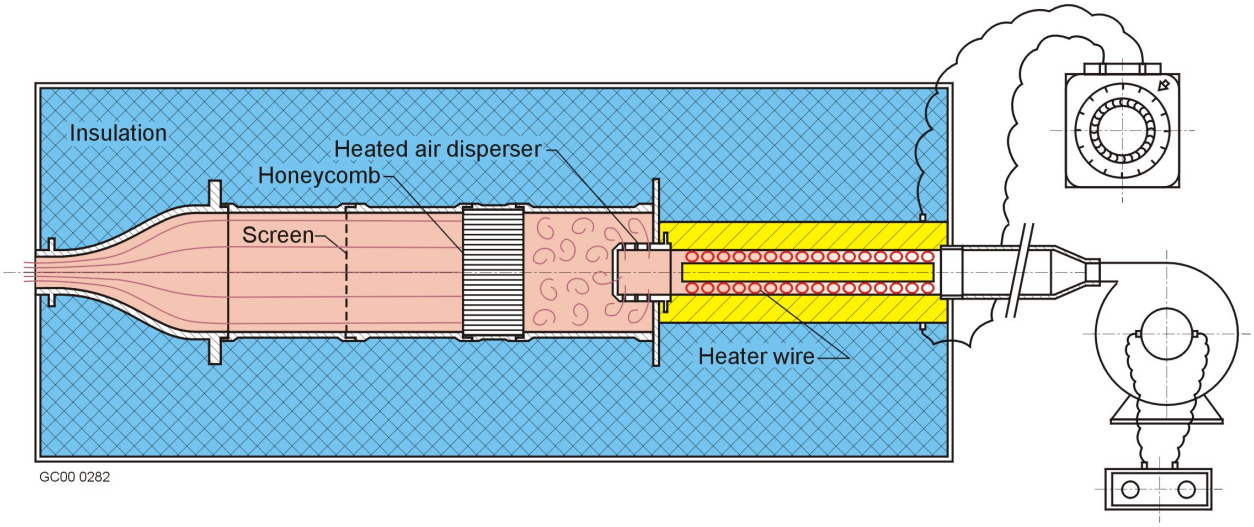

Fig. E-6. Sketch of heated jet assembly.

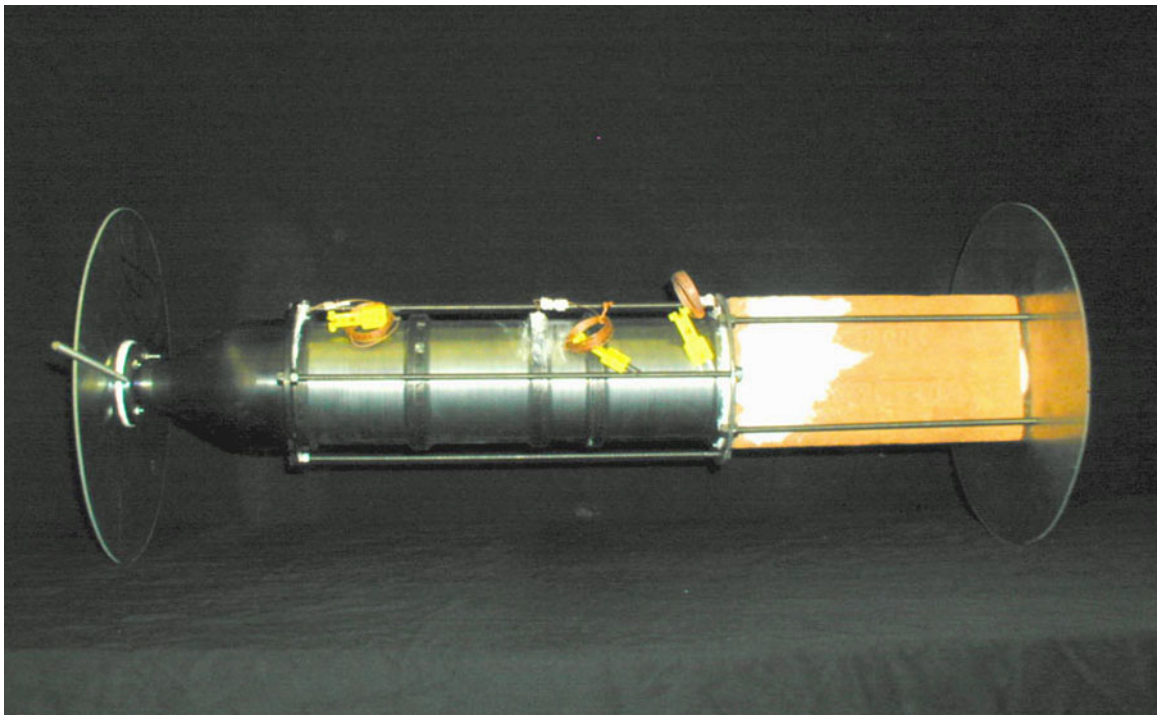

Fig. E-7. Photograph of jet.

The dimensions, materials and other characteristics of each part of the facility have been chosen to make it as compact as possible, in order to minimize the power consumption and also to minimize the heat loss to the surroundings. The jet dimensions are practically defined by the nozzle exit diameter. The smaller the nozzle diameter, the smaller the flow rate will be and, as a consequence, the smaller the power consumption for the same flow speed and temperature. On the other hand, the nozzle area has to be large enough to place the probe, thermocouple and a pitot tube simultaneously in the calibration flow without significantly altering it. We estimated that a nozzle of 30 mm exit diameter should be an optimal to meet these requirements. A cubic profile was chosen for the nozzle shape. It has been shown that the exit mean velocity and turbulent intensity distribution given by this nozzle produces the smallest adverse pressure gradient compared to that of other shapes. A nozzle of this shape has a minimum length, which is important in order to minimize the thermal inertia of the system. A contraction ratio of eleven has been chosen which means that the inlet nozzle diameter is 99.5 mm. A screen has been placed in the middle of the 200 mm long settling chamber, 100 mm downstream of a honeycomb. The honeycomb cell size is 3.175 mm and its length is 50 mm, as shown in the sketch in Figure E-6. Upstream of the honeycomb, in a mixing chamber 105 mm long, a heat disperser, shown in the sketch in Fig. 6, has been placed to increase the mixing of the hot air. This is needed in order to achieve a uniform temperature at the nozzle exit. All parts are sealed with ceramic epoxy. Thermocouple sensors have been placed at different positions in order to monitor the jet temperature. The jet and heater are insulated by a 100 mm thick insulation layer to reduce the heat loses and outside shell temperature. The insulation has been chosen to give an outside temperature slightly over 100°C and a heat loss of 230 W in the worse case. The nozzle, jet honeycomb and disperser are made of stainless steal.

A simple calculation shows that, for an exit air temperature of 500°C and an air speed of 15 m/s, the heat power should be about 2.5 kW. For an exit temperature of 700°C and the same air speed this power should be about 2.7 kW. Adding an expected heat loss of 230 W, the maximum thermal power required should be about 3 kW. Heaters with this power and with an exchangeable core are commercially available. Unfortunately, the pressure drop through these commercial heaters for the maximum required flow rate is of the order of 1.5 psi, requiring the use of a relatively high-pressure blower. The flow rate of such blowers is not easy to regulate. This difficulty was the reason to design a heater with the highest possible Nusselt number and as small a pressure drop as possible. To this end, an annulus made of two ceramic tubes filled with a spiral Kanthal wire is used, as illustrated in Figure E-6. The annulus dimensions, as well as the wire spiral dimensions are chosen to give a large contact surface between the Kanthal resistance wire and the airflow. Tests showed that the heater can heat an air stream of 15 m/s to at least 500°C. A transformer with variable voltage output of 0-240V is used to deliver 0 – 3.6 kW to the heater.

A variable flow blower with a speed controller and a DC power supply has been chosen to drive the air through the heater and jet. The blower characteristics are: (1) a static pressure variation of 0.05 - 0.4 psi and (2) a 2 - 35 SCFM flow rate. For example, for a pressure drop of 0.25 psi, the flow rate is 23 SCFM giving an exit air speed of 15 m/s at standard conditions. Heating the air does not change the static pressure drop significantly, but the air speed can be increased to over 20 m/s by its density change.

The blower gives a linear jet speed characteristic, as a function of E_k input DC power supply voltage, as shown in Figure E-8. The velocity can vary from zero to over 15 m/s at room temperature. Heating the air, the velocity can be increased by an additional fifty percent because of the decreased density. A typical temperature curve, for the cold air speed of 5.9 m/s (Ek=0.9), is shown in Figure E- 9.

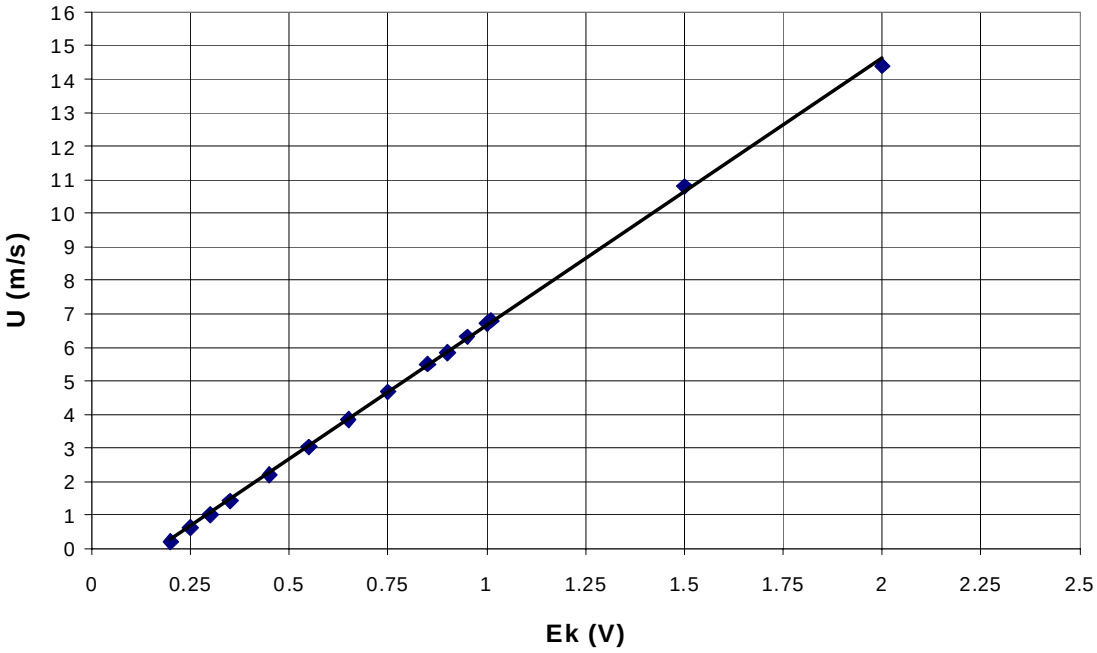

Fig. E-8 Jet speed characteristics.

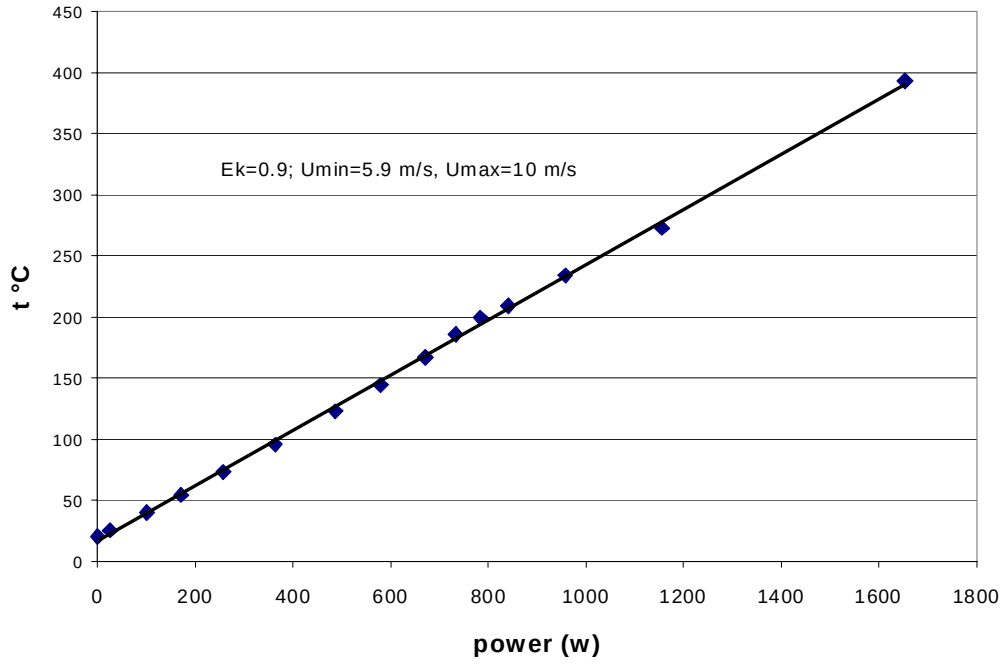

Fig. E-9. Jet temperature variation with heater input power at constant blower input DC voltage.

The jet air temperature can be increased from an ambient temperature of 20°C to about 400°C, by changing the heater power from zero to 1.6kW. This is less than a half of the available heater input power. The temperature characteristics are linear, so it is quite obvious that a temperature over 700°C can be achieved with the full available power of 3.6 kW for this airflow. Due to the decreased density, the air speed increased from 5.9 m/s, at room temperature, to 10 m/s at 400°C. Starting from different speeds of cold air and changing the heater power, a set of the temperature characteristics, similar to the one shown in Figure E-9, can be obtained.

The speed and temperature profiles are uniform over most of the nozzle exit area for different speeds and the temperature range. Typical temperature characteristics are shown in Figure E-10, from nearly –8 mm to + 8 mm on either side of the jet axis. The variation is less then 1% in this region in which the probe, temperature and velocity sensors has been tested and calibrated.

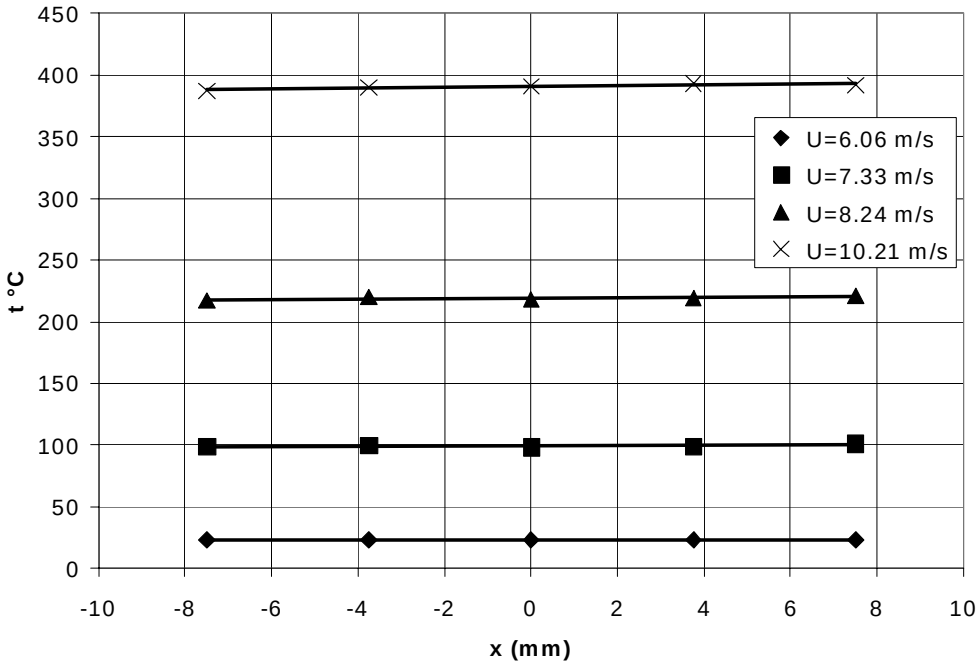

Fig. E-10. Temperature variation across jet at different speeds.

To determine the calibration constants, simultaneous changes of velocity and temperature can be performed in the range expected for the measurement conditions. A desired speed can be set up by choosing the appropriate blower RPM number or DC voltage controller input E_k. The temperature change, over a given range, can be induced by the variable heater power input. This will also affect the air speed intensity due to the density variation caused by different temperatures, as can be seen in Figure E-9. To achieve a broad speed change the procedure should be repeated for different E_k.

The directional sensitivity can be determined by pitching the probe at different speeds and temperatures. Two pitch and/or yaw devices were designed. One, which is computer

controlled, is capable of inducing a V/U or W/U ratio up to 0.7. The other, which is manually controlled and is attached to the nozzle exit, has the same angle range and can be used in case the computer-controlled device does not perform well under the high temperature conditions.

3. Data Reduction Algorithm – Testing Probe Accuracy

Starting with the energy equation

$$\frac{dU}{dt} = P - F\,, \tag{3.1}$$

and using the well known expression for the internal energy, U, of the sensor, the heat, P, generated in the sensor by Joule's effect and the energy, F, transferred to the surroundings mainly by convective heat flux [Blackwelder (1981)], the following expression can be derived for both velocity and temperature sensors:

$$\frac{E_w^2}{R_w} = \lambda\pi L_w (A + BR_e^n)(T_w - T_f) + \rho_w \frac{D_w^2\pi}{4} L_w c_w \frac{dT_w}{dt}\,. \tag{3.2}$$

Here, c_w, T_w, R_w, D_w, ρ_w and L_w are the specific heat, temperature, resistance, diameter, density and length of the sensor wire. The fluid characteristics are the thermal conductivity λ and temperature T_f. The Reynolds number is based on the effective cooling velocity, U_e, and sensor diameter, D_w. It is related to the Nusselt number by parameters A and B, which are, in principle, functions of Prandtl number, P_r, and overheat ratio, a_T, i.e.

$$N_u = A(P_r, a_T) + B(P_r, a_T) R_e^n\,, \tag{3.3}$$

Velocity Sensors The velocity sensors are operated in the constant temperature mode (CTA) with sensor temperature, T_w, and, therefore, the sensor resistance is held constant. It follows from (3.2) that a sensor's voltage, E_w, will depend on the effective velocity, U_e, cooling the sensor, and thus on R_e, and fluid temperature, T_f, so that

$$E_w^2 = \lambda\pi L_w R_w (A + BR_e^n)(T_w - T_f)\,. \tag{3.4}$$

For the case of constant fluid temperature, equation (3.4) reduces to the well known cooling law [King, 1914]

$$E_w^2 = M + NU_e^n\,, \tag{3.5}$$

where n ~ 0.5. When the fluid temperature, T_f, is variable, all fluid properties are dependent on temperature. The temperature dependence of λ, μ and ρ can be expressed [Brunn, 1995] as

$$\frac{\lambda}{\lambda_r} = \left(\frac{T}{T_r}\right)^a, \frac{\mu}{\mu_r} = \left(\frac{T}{T_r}\right)^b, \frac{\rho}{\rho_r} = \frac{T}{T_r}\,, \tag{3.6}$$

where T_r is some reference temperature and a = 0.8 - 0.86 and b = 0.76 - 0.9. Evaluating the fluid properties at the so-called "film" temperature, defined as $(T_w+T_f)/2$, and assuming T_0 as the reference temperature, the voltage, $E_{w,}$ can be expressed as

$$E_w^2 = \left[X\left(\frac{T_w + T_f}{T_w + T_0}\right)^a + Y\left(\frac{T_w + T_f}{T_w + T_0}\right)^{a-n-nb} U_e^n \right](T_w - T_f), \tag{3.7}$$

with $X = R_w A \pi L_w \lambda_0$ and $Y = R_w B \pi L_w D_w^n \lambda_0 \left(\frac{\rho_0}{\mu_0}\right)^n$.

Knowing that the sum a – n - nb is close to zero, a more general form of equation (3.7) is

$$E_w^2 = [Z(T) + YU_e^n](T_w - T_f). \tag{3.8}$$

In place of expressions (3.5) and (3.8), different polynomial fits have been used by many authors. In fact, in the case of constant fluid temperature, the effective cooling velocity from equation (3.5) can be expressed as

$$U_e = \left(\frac{E_w^2 - M}{N}\right)^{\frac{1}{n}}, \tag{3.9}$$

which is approximated well by different types of polynomial fits,

$$U_e = \sum_{i=0}^{p} A_i E_w^i \text{ or } U_e^2 = \sum_{i=0}^{k} A_i \left(E_w^2\right)^i, \tag{3.10}$$

because M, N and n are weak functions of U.

Rewriting equation (3.8) in the form

$$\left(\frac{E_w}{\sqrt{T_w - T_f}}\right)^2 = Z_{(T)} + YU_e^n, \quad \text{or } U_e = \left[\frac{(E_w/\sqrt{T_w - T_f})^2 - Z(T)}{Y}\right]^{\frac{1}{n}}, \tag{3.11}$$

it follows in the case of variable temperature, that an analog polynomial fit to relate wire voltage, E_w, effective velocity, $U_{e,}$ and fluid temperature, T_f, should be

$$U_e^2 = \sum_{i=0}^{4} D_i \left[\left(\frac{E_w}{\sqrt{T - T_{fw}}}\right)^2\right]^i, \tag{3.12}$$

because Y, Z and n are weak functions of U and T for T < 200°C. In the case of higher temperatures an analogous expression can be derived using the temperature dependence Z(T), given in equation (3.7) or using different fits for each temperature subrange.

One of the possibilities to express the effective velocity cooling a sensor is based on Jorgensen's [1971] definition

$$\boldsymbol{U_e^2 = U_n^2 + k_t U_t^2 + k_b U_b^2}. \tag{3.13}$$

Relating the normal U_n, tangential U_t and binormal U_b velocity components to the Cartesian coordinate velocity components U, V and W, a final form of the cooling law is obtained as,

$$\begin{aligned} &\boldsymbol{B_{0_{1,2}} + B_{1_{1,2}}\left(\frac{E_w}{\sqrt{T_w - T_f}}\right)^2 + B_{2_{1,2}}\left(\frac{E_w}{\sqrt{T_w - T_f}}\right)^4 + B_{3_{1,2}}\left(\frac{E_w}{\sqrt{T_w - T_f}}\right)^6 + B_{4_{1,2}}\left(\frac{E_w}{\sqrt{T_w - T_f}}\right)^8} \\ &\quad = \boldsymbol{U^2 + A_{1_{1,2}} V^2 + A_{2_{1,2}} UV} \end{aligned} \tag{3.14}$$

These two nonlinear algebraic equations (3.14), for the velocity sensors 1 and 2, are functions of the two unknown velocity components and the unknown fluid temperature. Each of them has seven constants to be determined by calibration.

A variety of different expressions relating the velocity and temperature fields to the voltage outputs of the sensors for different temperature ranges have been put forward by, among others, Blair and Bennett [1987], Fabris [1978], Chevray and Tutu [1972], Hishida and Nagano [1978] and Benjamin and Roberts [2001].

The common characteristics of all of these approaches are that the sensitivities to flow speed and direction and to temperature are determined in separate calibration procedures. The parameter Z in equation (3.8) is assumed to be a linear or exponential function of temperature, and Y is assumed to be a linear function or a constant. Values of Z and Y first are determined by varying the speed at a constant reference temperature, using an assumed value for the exponent n or optimizing it in the calibration procedure. Then, by varying the temperature, the Z(T) and Y(T) dependencies are determined. For the case of X-wire probes, the flow angle sensitivity is assumed to follow the cosine law or the k^2 law of Champagne, Sleicher and Wehrmann [1967], depending on the l/d sensor ratio and speed intensity. The parameter k^2 is determined by pitching or yawing the probe at different speeds. Another approach, proposed by Benjamin and Roberts [2001], is to calibrate the probe at room temperature, assuming King's [1914] cooling law, and then to correct the measured values of voltage at elevated temperature. They analyzed and proposed different correction methods.

The proposed calibration method does not require an assumption of a specified dependence of the calibration constants on temperature. Furthermore, the calibration should be faster than the methods cited above, because the sensitivities to flow speed and direction as well as to temperature are determined simultaneously.

Temperature sensor The temperature sensor is operated in the constant current (CCA) mode, behaving as a resistance thermometer. The wire voltage E_w is sensitive to any variation of parameters relevant to heat exchange between the sensor wire and its environment. Taking into account that the wire resistance R_w varies linearly with temperature over a temperature range that is not too great, i.e.,

$$\boldsymbol{R_w = R_0\left[1+\alpha(T_w - T_0)\right]} \tag{3.15}$$

equation (3.2) can be rewritten as

$$\boldsymbol{M\frac{dR_w}{dt} + R_w = \varphi(t)}, \tag{3.16}$$

where

$$\boldsymbol{M = \frac{\rho_w D_w^2 L_w c_w}{4\lambda L_w(A+BR_e^n) - R_0\alpha I^2}}, \quad \boldsymbol{\varphi(t) = \frac{\lambda\pi L_w(A+BR_e^n}{\lambda\pi L_w(A+BR_e^n) - R_0\alpha I^2}R_f}. \tag{3.17}$$

It is obvious that M is the time constant of the sensor's response (with resistance R_w) to the forcing function φ(t). For a small current I, the term $\boldsymbol{R_0\alpha I^2}$ can be neglected giving

$$\boldsymbol{M = \frac{\rho_w c_w D_w^2}{4\lambda(A+BR_e^n)}}, \ \boldsymbol{\varphi(t) = R_f}. \tag{3.18}$$

For a sufficiently small time constant M, which can be achieved using a sensor with small diameter D_w and low current, equation (3.16) reduces to the simpler form $\boldsymbol{R_w = R_f}$ or $\boldsymbol{T_w = T_f}$, which is equivalent to a linear function between anemometer output voltage, $E_{w,}$ and fluid temperature, $T_{f,}$

$$\boldsymbol{E_w = k_0 + k_1 T_f}. \tag{3.19}$$

For higher temperature ranges, the second order terms in the relation $R_w = F(T_w)$ could be significant, resulting in a relation $E_w = F(T_f)$ of second order with an additional calibration constant**.** The constants k_0 and k_1, which should not depend on speed and temperature, can be determined experimentally by a calibration procedure. If the time constant M is not small enough, i.e., the temperature fluctuation frequency is at or above a critical value defined by fc = $1/2\pi$M, an iterative approach should be applied in order to determine the dependence of M on speed and temperature. The temperature can be determined in the first approximation from equation (3.19), then the speed from equation (3.14), and finally the time constant M. The second and higher temperature iterations follow from (3.16), which can be rewritten in the following form

$$\boldsymbol{M\frac{dE_w}{dt} + E_w = k_0 + k_1 T_f}. \tag{3.20}$$

Sensitivities of sensors Both the velocity and temperature sensors are sensitive to both velocity and temperature changes. Assuming that the fluid properties will not change significantly due to small temperature variations, the sensitivities of the velocity sensor to velocity, S_U^{CT}, and temperature, S_T^{CT}, can be obtained as partial derivatives from equation (3.2):

$$S_U^{CT} = \frac{n\lambda\pi L_w B R_e^n}{2}\sqrt{\frac{R_w(T_w - T_f)}{\lambda\pi L_w(A + BR_e^n)}} \text{ and } S_T^{CT} = -\frac{1}{2}\sqrt{\frac{R_w\lambda\pi L_w(A + BR_e^n)}{T_w - T_f}}. \qquad (3.21)$$

The sensitivities of the cold (temperature) sensor can be obtained similarly as partial derivatives from equation (3.16) by analyzing small variations of velocity and temperature for the stationary conditions, $dR_w/dt = 0$ and $E_w = R_w I$. This yields

$$S_U^{CC} = -\frac{\alpha n R_0 R_f \lambda\pi L_w B R_e^n I^3}{U_e\left[\lambda\pi L_w(A + BR_e^n) - R_0\alpha I^2\right]^2} \text{ and } S_T^{CC} = \frac{\alpha R_0\lambda\pi L_w(A + BR_e^n)}{\lambda\pi L_w(A + BR_e^n) - R_0\alpha I^2}. \qquad (3.22)$$

For a sufficiently small current, the temperature sensor will be sensitive only to temperature:

$$S_U^{CC} = 0, \quad S_T^{CC} = R_0\alpha I. \qquad (3.23)$$

The sensitivities of the velocity and temperature sensors also have been discussed by many other investigators (see Brunn [1995]). The expressions (3.21), (3.22) and (3.23) represent an ideal case. In practice, calibration of both velocity and temperature sensors is necessary.

The measurement accuracy The coefficients that have to be defined in the calibration procedure are $B_{k_{1,2}}$ (k = 0 - 5) and $A_{j_{1,2}}$ (j = 1,2) from equation (3.14), as well as the constants k_0 and k_1, that appear in equation (3.19) and relate the temperature and corresponding voltage output of the temperature sensor. By placing the probe in a nominally irrotational calibration jet flow at different speeds and temperatures and pitching or yawing it, an optimal number of different flow realizations U_n, V_n, and T_{fn} can be induced. These known flow realizations and measured voltages yield a corresponding number of linear equations for each sensor with the $B_{k_{1,2}}$, $A_{j_{1,2}}$, as well as k_0 and k_1, coefficients unknown. The number of equations must, of course, be equal or greater than the number of unknown calibration coefficients (seven for the velocity sensors and two for the temperature sensor). These equations can be solved using the least squares fit method.

The calibration coefficients should be determined in flow conditions that are as close as possible to those expected for the turbulent flow to be investigated. The first flow that this probe was used in was a turbulent air flow in a vertical pipe with the wall heated to 200°C, a centreline mean speed to 2.5 m/s and a variation in the mean speed of 0.5 - 3 m/s.

In order to test the probe's angular sensitivity, it was pitched in the range $-20° < \varphi < 20°$, in steps of 5°, at different speeds (1, 1.5, 2 and 2.5 m/s) and at room temperature. To test the simultaneous speed and temperature influence, the blower was set to give approximately 1 m/s at room temperature, and then the heater was turned on. The speed, temperature and voltage outputs

of the speed and temperature sensors were recorded for each temperature increment of 5°C. After each temperature change of about 30°C, the probe was pitched through the range of angles in order to account for speed, temperature and directional sensitivity simultaneously. The procedure was repeated starting from different initial speeds at room temperature. In this way the ranges of flow conditions of 0.9 - 3 m/s and 27 - 200°C, with a maximum wall normal velocity component $V = \pm 0.34U$ were treated. A great number of different U_n, V_n and T_{fn} combinations were induced, giving an adequate number of linear equations. Using the least squares fit method, these equations were solved for the seven unknown calibration coeficients for each velocity sensor and the two coefficients for the temperature sensor, giving a set of sixteen calibration coefficients.

A comparison of the induced and measured U component values for zero pitch (V = 0) at different temperatures, for the VTS probe configuration, is given in Figure E-11. The measured values match the induced ones with a difference of the order of less than one per cent of the induced values, using the same set of calibration coefficients over a wide temperature range. A set of measured and induced U and V components during the pitch variation at different temperatures is shown in Figures. E-12 and E-13. The difference between the induced and measured values are of the same order as they are in the case of zero pitch variation.

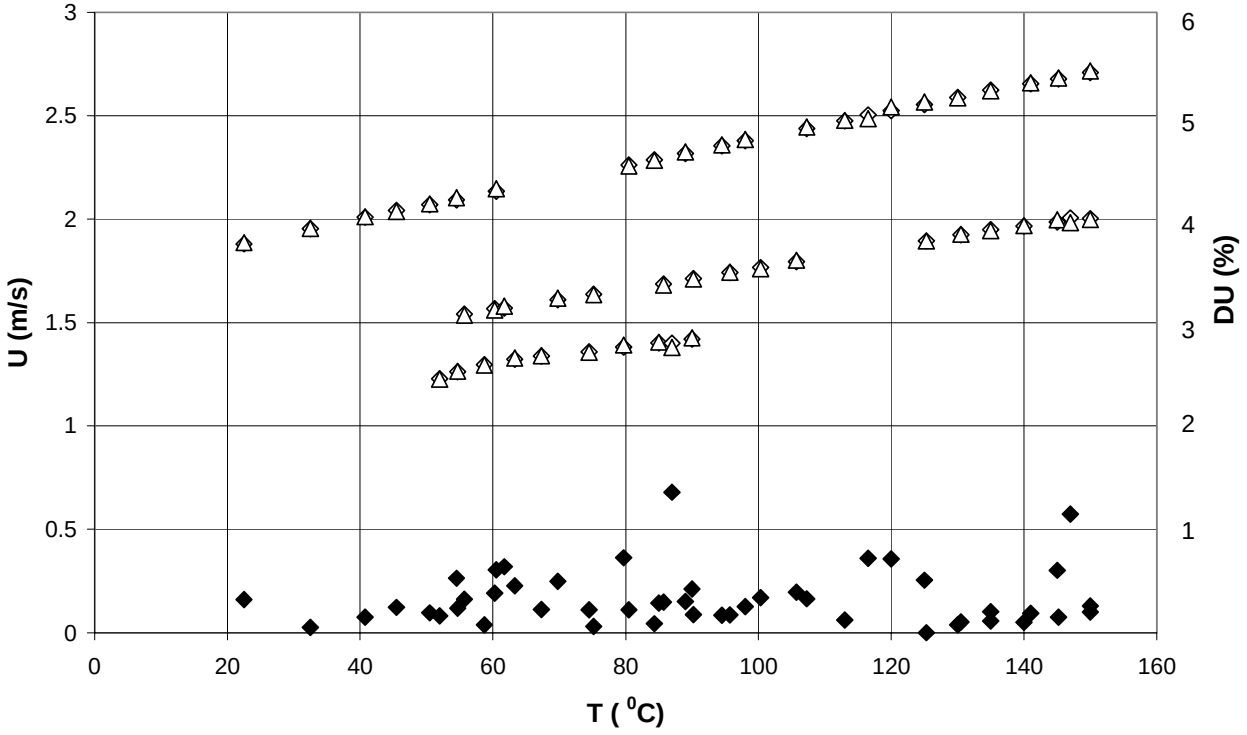

Fig. E-11. Induced and measured U component values and the percentage difference of their values, DU, with respect to the induced values, for zero pitch and at different temperatures: Δ, U induced; ◊, U measured; ♦, DU.

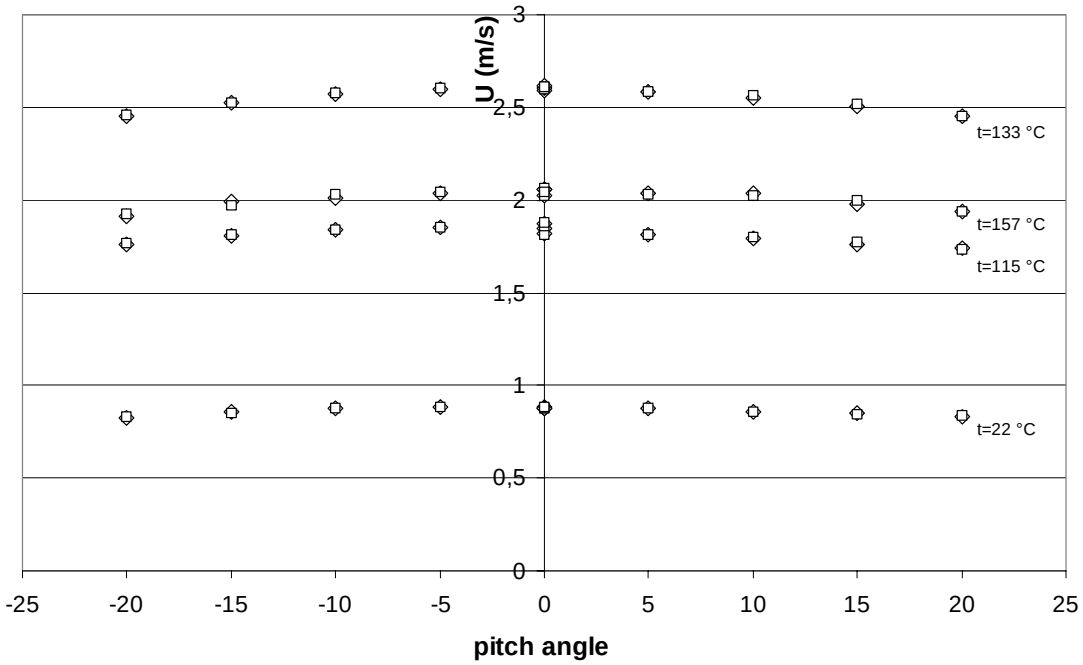

Fig. E-12. Induced and measured U component at different temperatures and pitch variation: □, U induced; ◊, U measured.

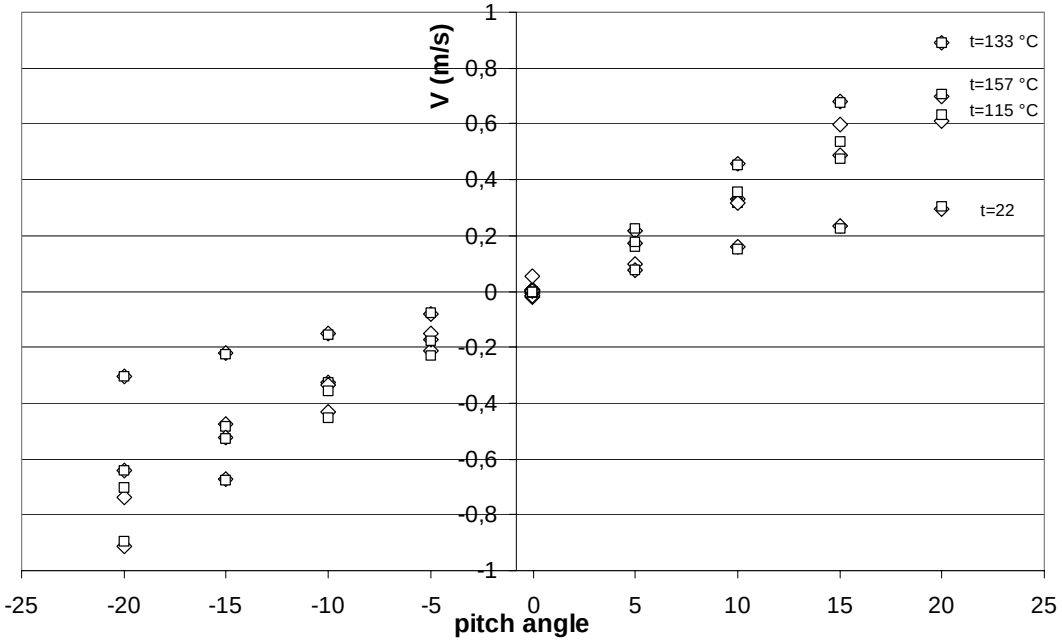

Fig. E-13. Induced and measured V component at different temperatures; □, V induced; ◊, V measured.

The responses of the temperature sensors of two diameters (1 and 2.5 microns) were tested at constant and variable speed. The results are given in Figure E-14. The response is linear at constant as well as at variable speed. This means that the current through the sensor (0.3 mA at the top of the bridge) is sufficiently small to neglect I^2 in accordance with equation (3.22). In this case, the influence of speed on the forcing function φ cancels out, as seen in equation (3.17), and the temperature sensor's output should not depend on speed. The same conclusion holds for turbulent fluctuation measurements if the time constant M is small enough. On the other hand, the influence of speed on M has to be taken into account in accordance with equation (3.18). Even for such small currents the sensitivity to temperature is high enough, i.e., about 18 mV/°C for 2.5 μm diameter temperature sensors. In the case of the 1 μm diameter sensor, according to equation (3.22) the sensitivity will be much higher for the wire of the same same length, because of the higher value of R_0. In this case it is about 25 mV/°C, which enables the measurement of small temperature fluctuations of the order of 0.1°C or less.

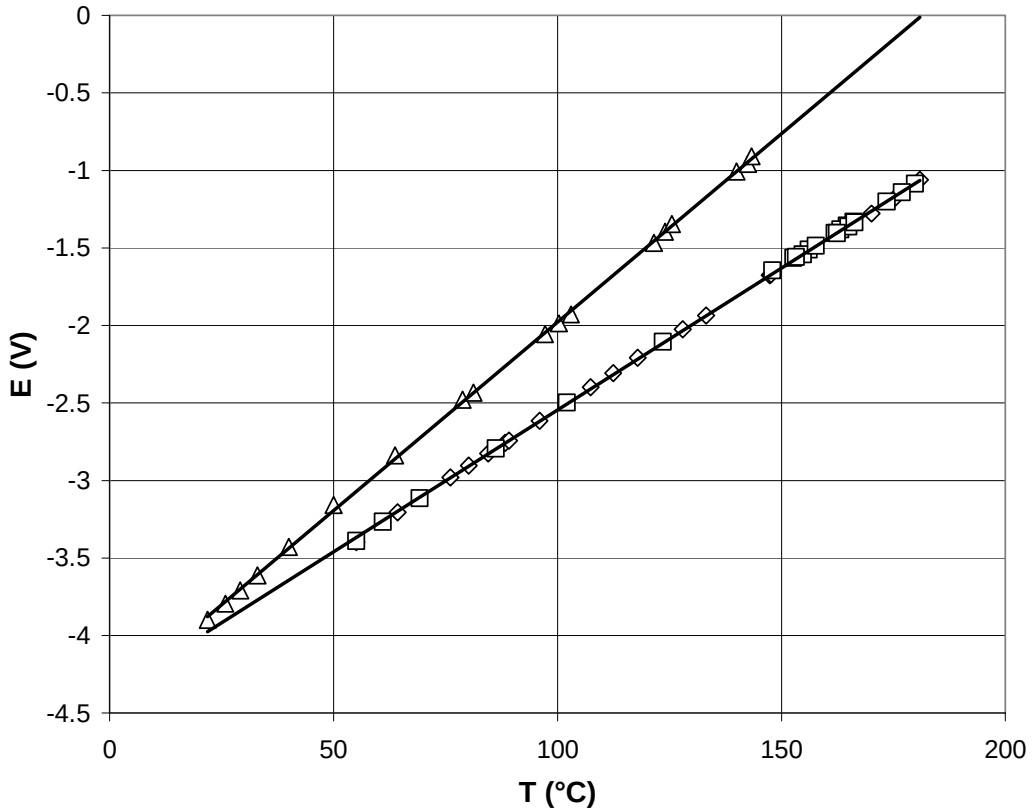

Fig. E-14. The temperature sensor response to temperature and speed variation: ◊, U = 1 m/s, D_w = 2.5 μm; □, U = 0.9 – 4 m/s, D_w=2.5 μm; Δ, U = 0.9 - 4 m/s, D_w = 1 μm

The agreement between induced and measured temperature values is very good, as can be seen from Figure E-15, where the induced and measured values, as well as their differences, DT, are shown for different speed variations. The most critical condition is the low velocity range. The mutual sensor influence could be a source of measurement error in that range. However, the agreement of induced and measured temperatures for velocities of about 1 m/s is also within one percent.

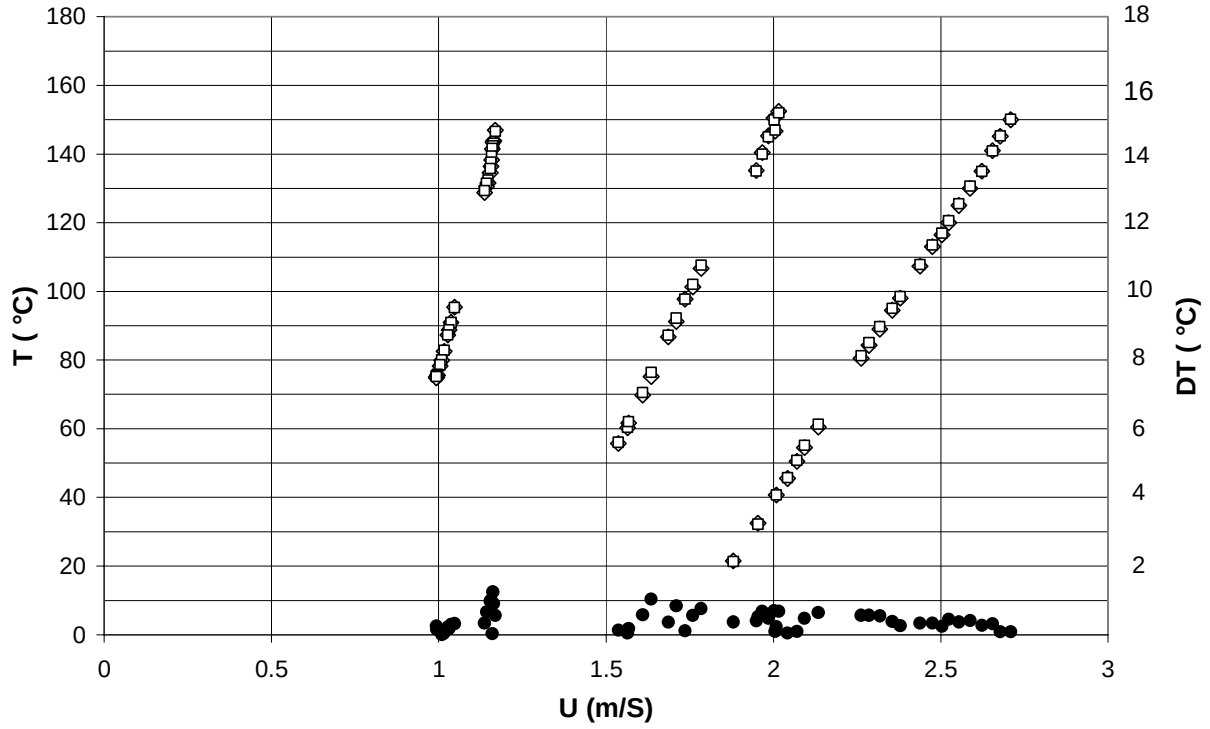

Fig. E-15 Induced and measured temperatures for different speed ranges. □, T induced; ◊, T measured; ●, the difference, DT, between the induced and measured temperature.

It follows from the analysis given here that the probe is capable of simultaneous measurement of turbulent velocity fluctuations for flows with means speeds as low as 1 m/s and with moderate temperature fluctuations, with a difference between the induced and measured values of about one percent. This high accuracy is notable given the difficulties of mutual sensors interference and the deviation of the cooling law at low speeds. Similar calibration results were also obtained with the VTFD probe.

4. Data Analysis Algorithm

The two boundary layer VTS and VTFD model probes, shown in Figure E-5, were designed and tested for the ***University of Manchester experiment (Task F)***. Details about the experiment facility in which they were used are given in the original proposal for this project and in Task F. The facility consists of a vertical pipe with controlled heating and variable air speed and temperature. A traversing mechanism was designed to position the probe at different distances from the wall along the pipe axis. The probe was tested for the expected speed and temperature variation in a calibration rig designed for this purpose and was positioned near the experimental facilities. In this way, the probe could be positioned in the pipe, after calibration was performed, without disconnecting or switching off the electronics equipment. The probe was successfully calibrated using the data reduction algorithm and process described in section E-3. The same data reduction algorithm and process can be used to produce the experimental benchmark information.

Examples of time series data for the streamwise and wall normal velocity components in the vertical pipe at a location halfway between the wall and centerline, with wall temperature of 150°C, is given in Figures E-16 and E-17 while the temperature series is shown in Figure E-18. The mean values of velocity and temperature are in good agreement with the data obtained b a pitot tube and thermocouple at the same location , confirming good performance of the probe in these conditions.

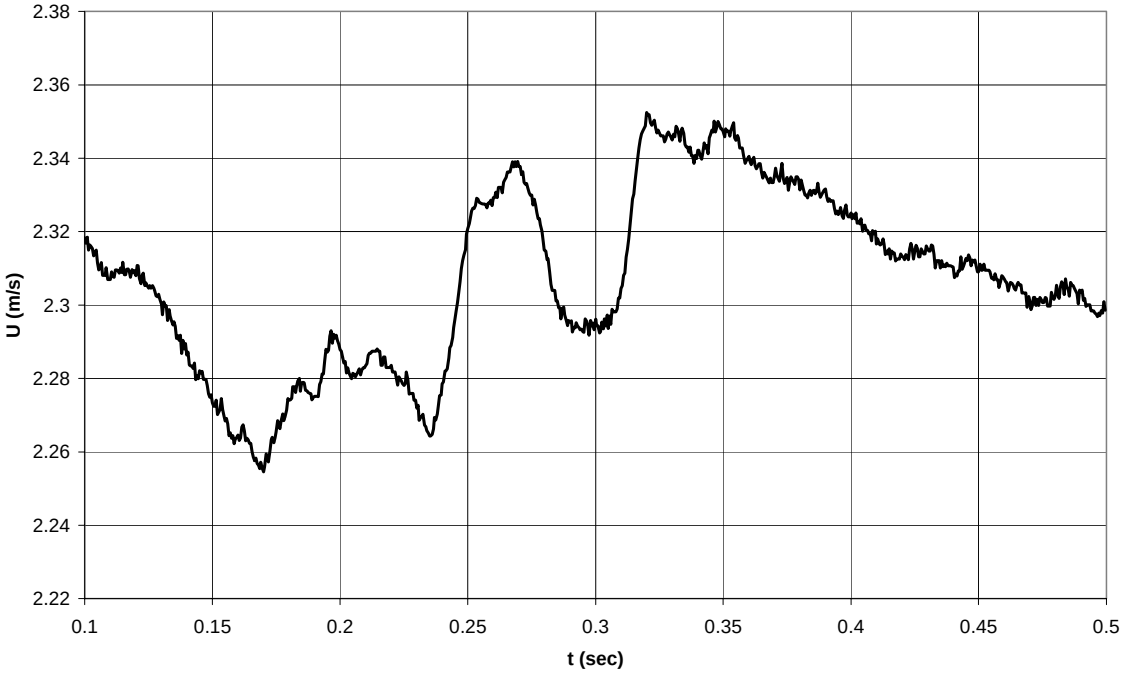

Fig. E-16. Instantaneous time-series of the U(t) velocity component.

It can be seen from the Figure E-18 that the higher temperature fluctuation frequencies are less than 100 Hz. Thus, a sensor of 2.5 micron diameter has acceptable frequency response. This is very important, because handling of the probe with 1 or 0.65 micron temperature sensor diameters will be practically impossible in these conditions.

The data are taken deep in the pipe at different locations from the wall. The pin designed to position the probe with respect to the wall performed well, enabling the positioning with an accuracy of ±0.01 mm. It would be desirable to improve the probe's traversing mechanism and repeat the measurements at different locations along the probe axis and at different wall and air temperatures in order to form a reliable benchmark dataset to test the CFD codes.

The so-called COPPEC (COnvection Parois Paralleles ECartees) facility at CEA-Grenoble is designed to simulate mixed or free convection (Task F) in the heat exchange at the wall of the nuclear waste container. It is characterized by very low air speeds, below 1 m/s, and moderate temperatures up to 100°C. A modified version of the VTFD probe model, shown in Figure E-5, was designed for that application. The critical speed had to be reduced below 1 m/s in order to meet the conditions of ***COPPEC experiments***. The only way to achieve that while still maintaining adequate spatial resolution, was to use 1 micron wire for velocity as well as for temperature sensors and to increase the velocity sensor separation slightly. As a result of these

modifications, the critical speed was reduced to about 0.6 m/s. That is, the difference between the cold sensor and air temperature will reach a critical 1°C at a speed around 0.6 m/s, as is shown in Figure E-19.

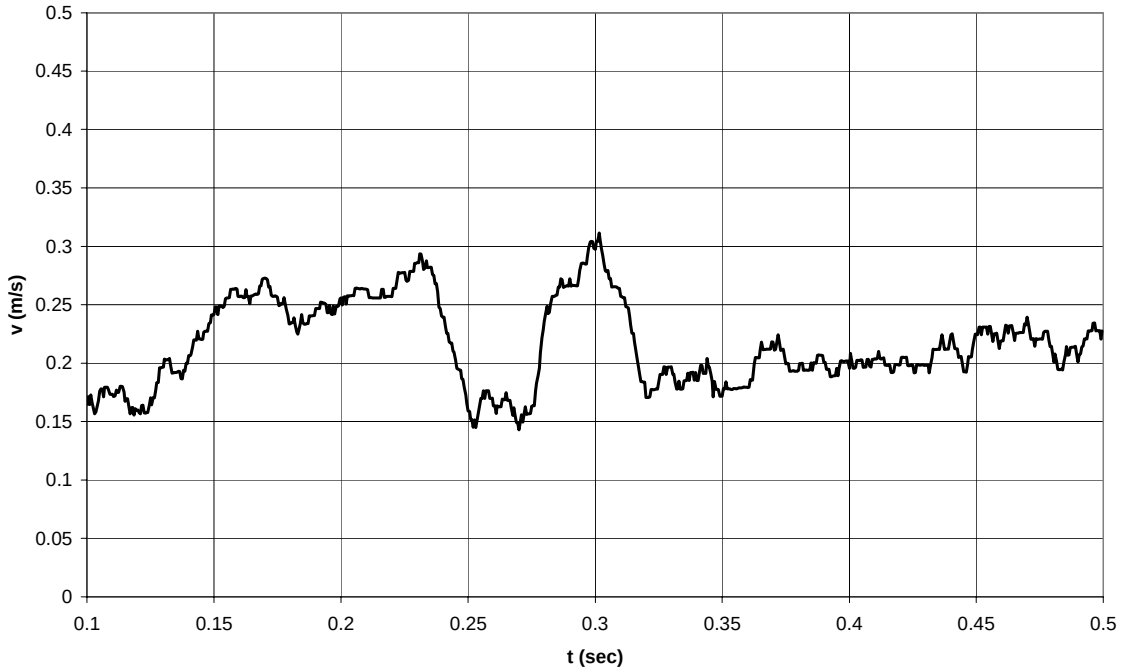

Fig. E-17. Instantaneous time series of the V(t) velocity component

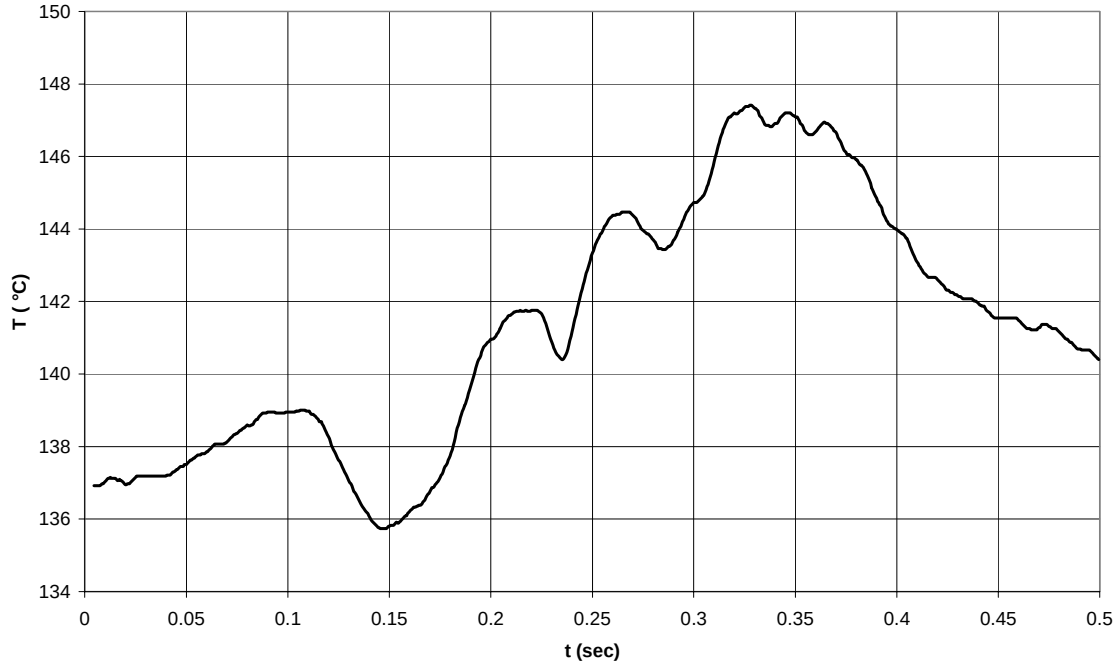

Fig. E-18. Instantaneous time series of the temperature T(t).

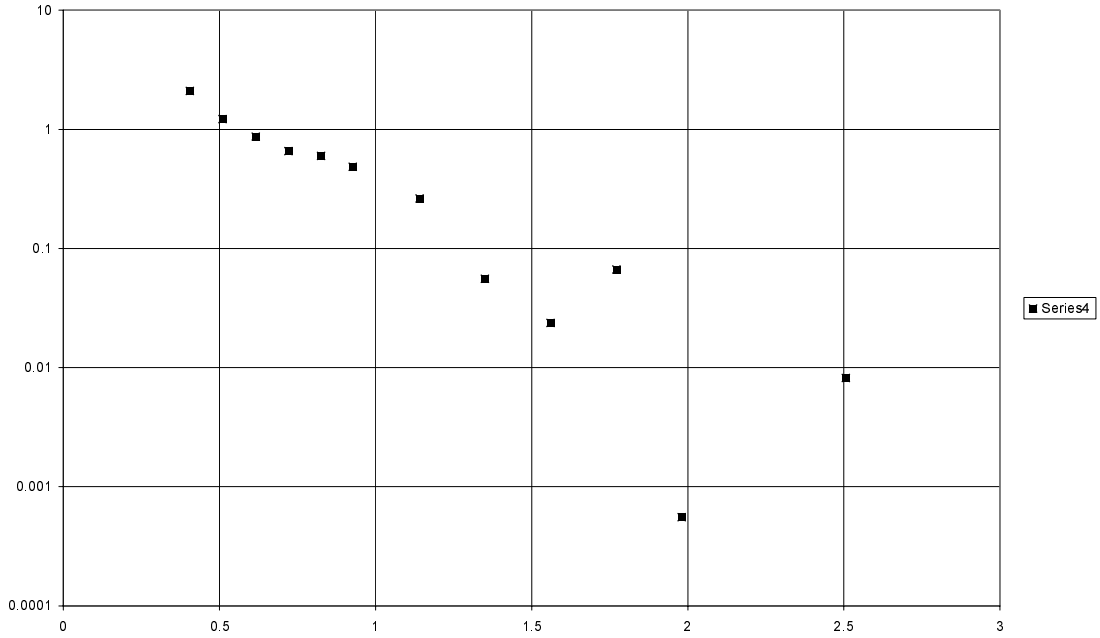

Fig. E-19. The diffference between cold sensor and air temperature as a function of the air speed.

The other problem to be solved was the data reduction algorithm for such low speeds. Due to the mutual velocity and temperature sensors influence the accuracy of the data reduction algorithm, described in section E-3, is considerably reduced for speeds under 1 m/s, giving high errors for speeds below 0.5 m/s. To avoid this problem with that data reduction method, it would be necessary to generate a new set of calibration coefficients for each value of mean speed below 1 m/s. The alternative was to develop a different calibration approach.

A careful analysis of the cooling law in this low speed range has been performed at constant and variable temperature. Expressing the effective cooling velocity, $U_{e,}$ as a function of velocity magnitude, $U_{0,}$ and its angle, $\theta_{y,}$ with respect to the normal to the sensor axis, equation (3.5) can be rewritten in general form as

$$\boldsymbol{E}_{\boldsymbol{w}}^{2} = \boldsymbol{M} + \boldsymbol{P}(\theta_{\boldsymbol{y}})\boldsymbol{U}_{0}^{\boldsymbol{n}}. \qquad (4.1)$$

The parameter M should be constant for a given fluid temperature, T_a, and parameter P is a function of the yaw angle, θ_y, a widely accepted assumption for the higher speed ranges. In the lower speed ranges, specially under 1 m/s, both parameters depend on angle, $\theta_{y.}$ Thus, the general form of expresion (4.1), in the low speed range, should be

$$\boldsymbol{E}_{\boldsymbol{w}}^{2} = \boldsymbol{M}(\theta_{\boldsymbol{y}}) + \boldsymbol{P}(\theta_{\boldsymbol{y}})\boldsymbol{U}_{0}^{\boldsymbol{n}} \qquad (4.2)$$

This means that, no matter what form of cooling law is choosen, a measurement error will appear as a consequence of assuming the parameter M to be constant.

The dependence of parameters M and P on θ_y can be defined very accurately using a second order fit in the form

$$\boldsymbol{M}(\theta_y) = \boldsymbol{M}_0 + \boldsymbol{M}_1\theta_y + \boldsymbol{M}_2\theta_y^2,\ \boldsymbol{P}(\theta_y) = \boldsymbol{P}_0 + \boldsymbol{P}_1\theta_y + \boldsymbol{P}_2\theta_y^2, \tag{4.3}$$

with a corelation factor R > 0.99. This result leads us to propose and test the following cooling law hypothesis

$$\boldsymbol{E}_{w_{1,2}}^2 = \boldsymbol{M}_{0_{1,2}} + \boldsymbol{M}_{1_{1,2}}\theta_y + \boldsymbol{M}_{2_{1,2}}\theta_y^2 + (\boldsymbol{P}_{0_{1,2}} + \boldsymbol{P}_{1_{1,2}}\theta_y + \boldsymbol{P}_{2_{1,2}}\theta_y^2)\boldsymbol{U}_0^n \tag{4.4}$$

for the two wires of an X-wire probe. A simple algorithm can be derived to solve the two equations (4.4) for θ_y and U_0 in order to determine the two velocity components $U = U_0\cos(\theta_y)$ and $V = U_0\sin(\theta_y)$. In the case of variable fluid temperature the cooling law should be

$$\boldsymbol{E}_w^2 = \boldsymbol{M}(\boldsymbol{T},\theta_y) + \boldsymbol{P}(\boldsymbol{T},\theta_y)\boldsymbol{U}_0^n \tag{4.5}$$

It is quite obvious from equation (3.8) that the parameter M(T) could be a second or higher order function of temperature, T_a, while P(T) is a linear function of temperature T_a. Assuming the same dependence (4.3) on angle θ_y, as in the case of constant fluid temperature (a second order polynomial fit of parameter M and linear fit of parameter P on temperature), the cooling law (4.5) can be expressed as

$$\boldsymbol{E}_{w_{1,2}}^2 = \boldsymbol{M}(\boldsymbol{T})_{0_{1,2}} + \boldsymbol{M}(\boldsymbol{T})_{1_{1,2}}\theta_y + \boldsymbol{M}(\boldsymbol{T})_{2_{1,2}}\theta_y^2 + (\boldsymbol{P}(\boldsymbol{T})_{0_{1,2}} + \boldsymbol{P}(\boldsymbol{T})_{1_{1,2}}\theta_y + \boldsymbol{P}(\boldsymbol{T})_{2_{1,2}}\theta_y^2)\boldsymbol{U}_0^n \tag{4.6}$$

where

$$\boldsymbol{M}(\boldsymbol{T})_{i_{1,2}} = \boldsymbol{M}_{i1_{1,2}} + \boldsymbol{M}_{i2_{1,2}}\Delta\boldsymbol{T} + \boldsymbol{M}_{i3_{1,2}}\Delta\boldsymbol{T}^2, \qquad \boldsymbol{P}(\boldsymbol{T})_{1_{1,2}} = \boldsymbol{P}_{i1_{1,2}} + \boldsymbol{P}_{i2_{1,2}}\Delta\boldsymbol{T}, \quad \boldsymbol{i} = 0,1,2 \tag{4.7}$$

with $\Delta T = T_a - T_0$.

If a cold wire of sufficiently small diameter is used, then the temperature field can be determined independently from the velocity field. With known temperature, equations (4.6) reduce to the form of equation (4.4) describing the case of the constant fluid temperature. This means that the same numerical algorithm can be used to determine the velocity components U and V.

The probe was first tested at constant (room) temperature. The speed was varied from 0.4 to 3 m/s. The probe was pitched at about 0.5, 1, 1.5 and 2 m/s in the range ± 20°, with a step of 5°. This way 53 realizations of U and V or U_0 and θ_y could be induced in order to find the six calibration coefficients for each sensor in expression (4.4). The results, similar for both probes, are shown in Table E-1. A very good convergence of the polynomial fits (4.3) is evident. Using these calibration coefficients, the speed can be calculated for each value of U_0 and θ_y within the calibration range. The induced and calculated values, using the same calibration coefficients over the whole range of speed magnitude and angular variation, are shown in Figures E-20 and E-21. The agreement of induced and measured values is very good, with an error of about one percent

of induced U. The standard deviations of U and V are 1.3 cm/s and 1.5 cm/s respectively. The maximum deviation is about 2.5 cm/s for both velocity components.

Table E-1. Calibration Coefficients, $M_{i,}$ and P_i, for the case of constant fluid temperature.

	M_0	M_1	M_2	P_0	P_1	P_2
Senz 1	0.870699	-0.003862	0.000115	0.769486	0.005889	-0.000104
Senz 2	0.837445	0.003821	0.000088	0.650272	-0.005503	-0.000075

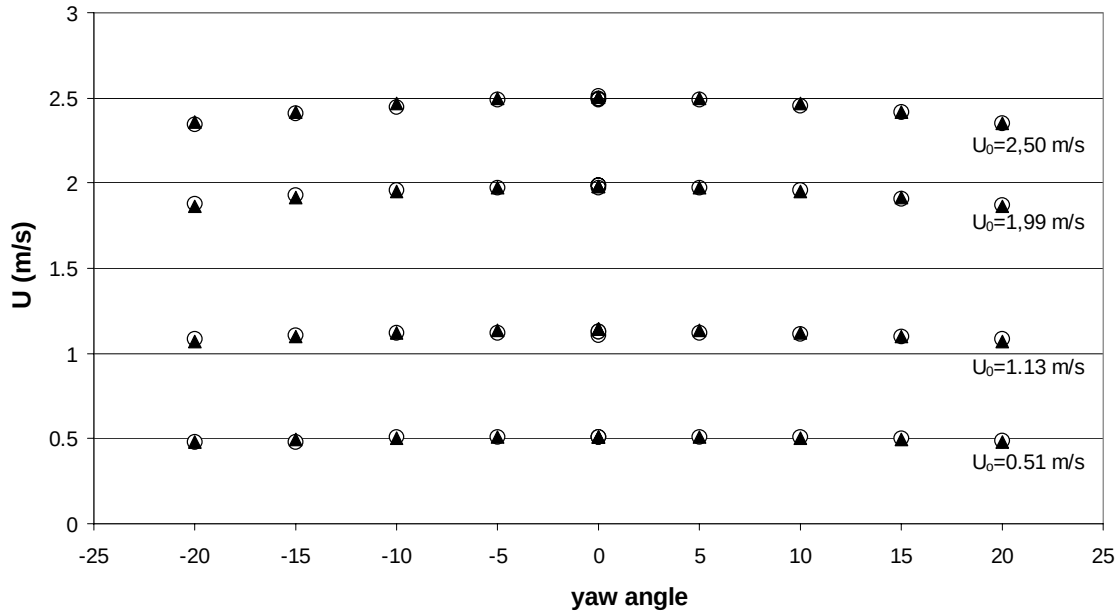

Fig. E-20. The comparison of induced (O) and measured (▲) values of U at constant temperature.

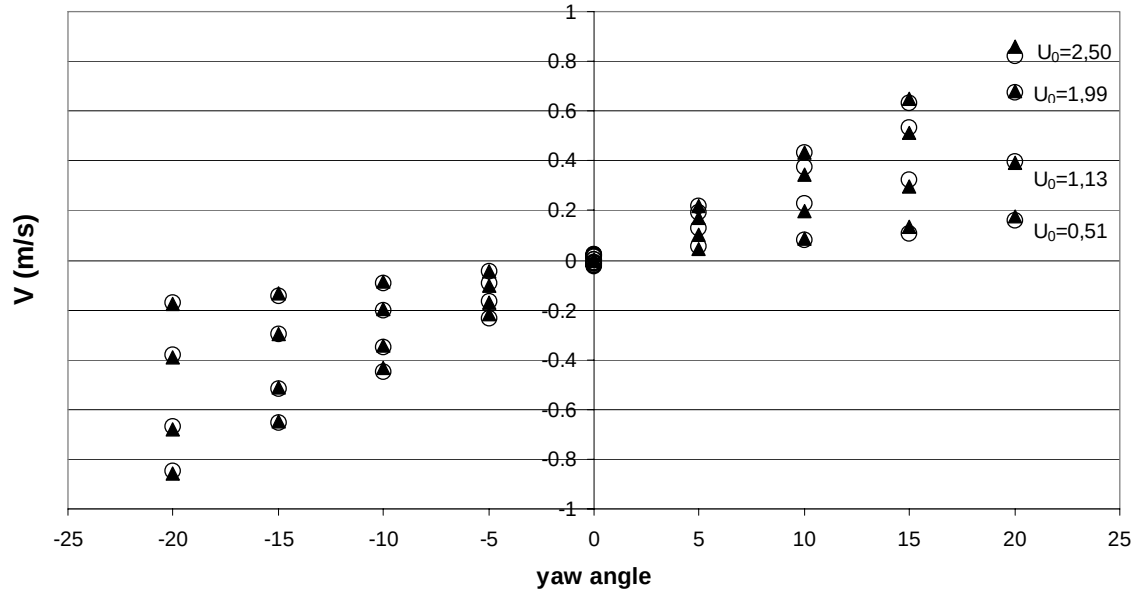

Fig. E-21. The comparison of induced (O) and measured (▲) values of V at constant temperature.

If the previous approach described in section E-3 is used, separate sets of calibration coefficients are necessary for the low speed ranges below 1 m/s. Otherwise, the standard deviation of U and V will be much higher, about three times for the mean speed of 0.5 m/s. In order to test the cooling law (4.6), in the case of variable fluid temperature, the temperature was varied in the range from room to 120 °C with the same flow as in the case of constant fluid temperature. Using a set of calibration coefficients covering the velocity range from 0.4 - 2.5 m/s, with a pitch variation of ±20° and temperature range from 28-120°C, the polynomial fits (4.7) for sensor 1 are

$$\boldsymbol{M}(\boldsymbol{T})_{0_1} = 0.85364423 + 0.03679005\Delta\boldsymbol{T} + 0.00001848\Delta\boldsymbol{T}^2$$
$$\boldsymbol{M}(\boldsymbol{T})_{1_1} = -0.00406032 + 0.00031787\Delta\boldsymbol{T} + 0.00000031\Delta\boldsymbol{T}^2$$
$$\boldsymbol{M}(\boldsymbol{T})_{2_1} = 0.00012136 - 0.00001627\Delta\boldsymbol{T} - 0.00000001\Delta\boldsymbol{T}^2$$
$$\boldsymbol{P}(\boldsymbol{T})_{0_1} = 0.78505740 - 0.03513864\Delta\boldsymbol{T}$$
$$\boldsymbol{P}(\boldsymbol{T})_{1_1} = 0.00603643 - 0.00027112\Delta\boldsymbol{T}$$
$$\boldsymbol{P}(\boldsymbol{T})_{2_1} = -0.00010746 + 0.00001338\Delta\boldsymbol{T}$$

A very good convergence on temperature, as well as on yaw angle θ_y is evident. Similar results were obtained for the second sensor. The standard deviations of U and V are slightly higher than in the case of constant temperature. As an example, the induced and measured values for two different speeds and temperatures (the smallest speed and higher temperature) are shown in Figures E-22 and E-23.

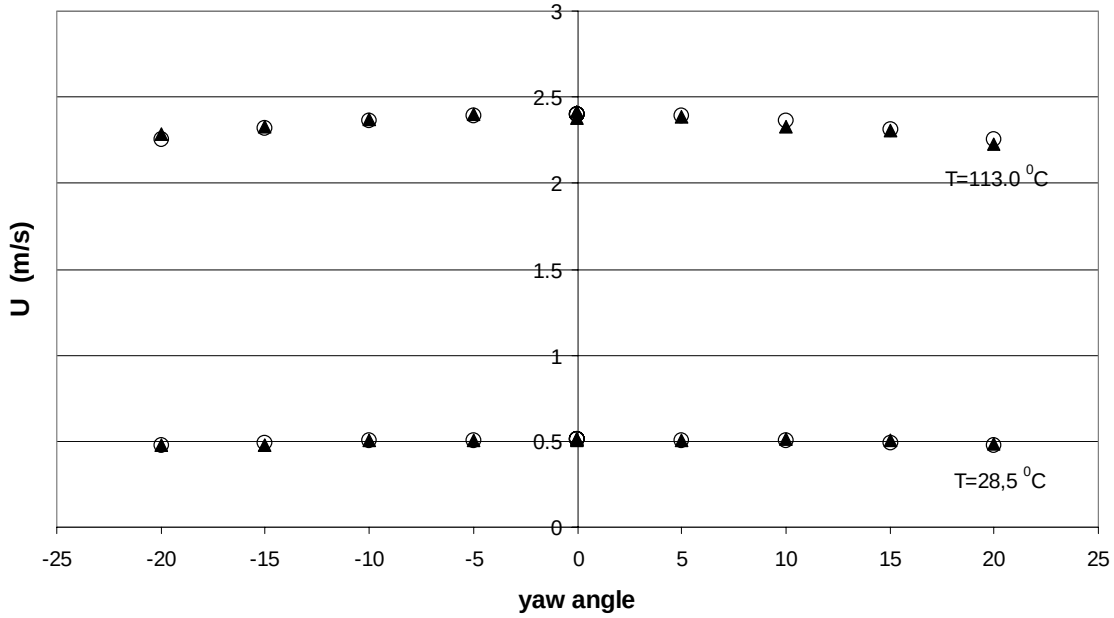

Fig. E-22. The comparison of induced (O) and measured (▲) values of U at variable temperatures

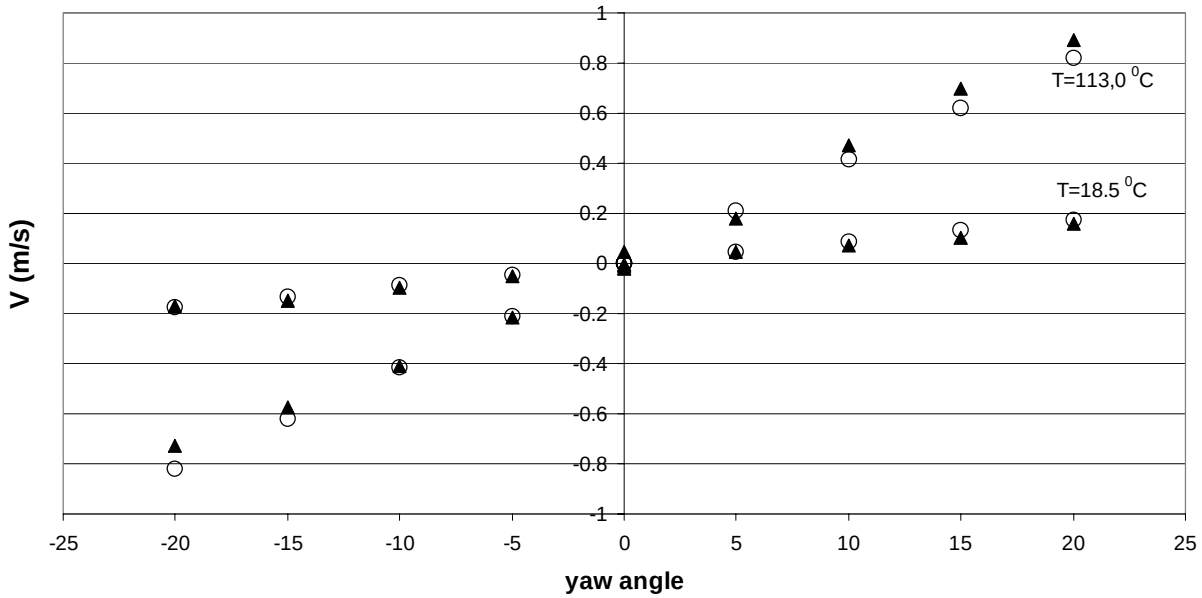

Fig. E-23. The comparison of induced (O) and measured (▲) values of V at variable temperatures

It follows from the analysis presented that the proposed calibration technique, based on polynomial fits, is very accurate and simple to use at constant and elevated fluid temperatures. It can cover the very low and moderate speed ranges (0.3 - 3 m/s) with the same set of calibration coefficients over a temperature range from room to 120°C. It should also perform well at higher temperatures.

A nice feature of the proposed calibration technique is that the temperature does not have to be constant while varying the velocity, or vice versa. A random set of calibration points can be sampled covering the range of expected velocity and temperatures in order to define the calibration constants.

Task F. Measurements of the effects of buoyancy forces on flow in circular tubes and annuli -- Prof. J. D. Jackson, U. Manchester (UK)

Prof. Jackson and colleagues at Manchester conducted several experiments emphasizing buoyancy effects. The first obtained data on velocity in strongly heated air flow through a heated pipe under conditions of mixed convection to determine the effects of buoyancy forces combined with property variation on local mean velocity and turbulent fluctuations. A second experiment measured the influence of the temperature dependence of fluid properties and buoyancy on heat transfer for the case of air flowing in a passage of annular cross section with a heated core. In the third experiment they measured local mean velocities and turbulent fluctuations using laser Doppler velocimetry (LDV) in an annular flow of water with a heated core under conditions of mixed convection.

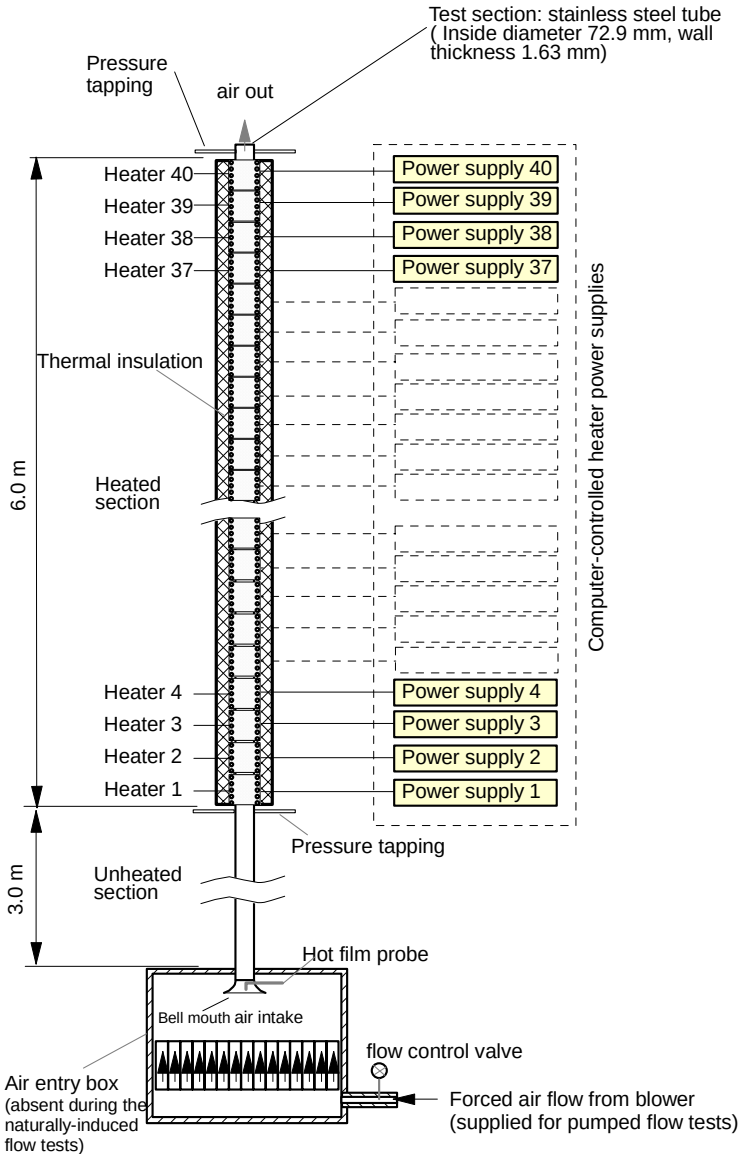

Fig. F-1. Schematic diagram of facility to examine the influence of fluid property variation and buoyancy on heat transfer to air.

Vertical flow in a circular tube In the **first study** Prof. Jackson has measured local heat transfer coefficients and also **mean fields and turbulence in the case of airflow through a vertical tube** with prescribed distributions of wall temperature or heat flux under conditions where there are significant variations of temperature dependent fluid properties and also buoyancy influences. Earlier work on this topic has mainly involved the measurement of integral parameters only on test sections which were uniformly heated.

The experimental facility used in the present study is shown in Figure F-1. The test section, which was made from stainless steel tube of inside diameter 72.9 mm and wall thickness 1.63 mm, is suspended vertically in a space of height 15 m. It can be used for experiments with either naturally-induced flow or pumped flow.

In the case of naturally induced flow, the entry box is absent and air passes from the laboratory into the bellmouth intake and upwards through an unheated flow development section of length 3 m and a heated section above it of length 6 m before discharging at the top. Motion occurs simply as a result of heat being applied to the test section. The velocity at inlet is measured using a calibrated hot film probe mounted in the center of the bellmouth intake.

In the case of pumped flow, air is supplied to the entry box at the bottom of the test section by a blower and then flows upwards through the test section. The mass flow rate can be measured using a metering nozzle installed at the exit. The hot film probe was calibrated against this flow metering nozzle. Wall static pressure tappings are provided at the top and bottom of the heated section. The pressure difference is measured using a high precision electronic micro-manometer. Reynolds number may be varied between 2500 and 40,000. This combination of flow range and diameter allows measurements that are either buoyancy-affected or predominantly buoyancy-free.

Numerous thermocouples attached to the outside of the heated length of the test section enable the wall temperature distribution to be measured in detail. The heated length is well lagged on the outside with pre-formed thermal insulation of low thermal conductivity to minimize heat transfer to the surroundings. The small losses which do occur can be accurately accounted for using data from calibration experiments which were performed at the commissioning stage. Heat can be applied to the test section either uniformly or non-uniformly by means of forty separate, individually-controlled heaters distributed along its length. These were made using proprietary heater cable which was wound tightly around the outside of the stainless steel tube. Electrical power is supplied to the heaters from the mains via variable auto-transformers through the specially designed computer-based power control and measurement system. This system supplies power to each heater at a rate needed to maintain the tube at a specified temperature at that location and also enables the power to be measured. The power is controlled by allowing a proportion of the half cycles of the incoming AC supply to pass to the heater. For each of the forty heaters there is a control signal generator and a zero-crossing solid state relay. The former generates a control signal which enables the latter to pass a programmable number of half cycles from the supply to the heater during a specified time interval of 0.16 s. The signal generators are connected to a computer via a PC interface. The computer can write a number to each of the forty signal generators under the action of software. The power to each heater is controlled by these numbers. Knowing this number, the voltage of the incoming supply and the electrical resistance of the heater, the power generated can be calculated. In operation, the computer reads temperatures using the Intercole data acquisition system. It then compares each

wall temperature with a pre-set value, calculates a new number using the PID technique and sends it to the corresponding signal generator. The power supply system can also be operated in such a manner that a specified distribution of heat input is applied to the test section. A Pentium PC connected to a 208 channel data acquisition system is used for signal collection and processing. The software package which is used to drive the data logger and the power control and measurement system was developed and tested 'in house' using Visual Basic under the Windows 95 environment.

Initially, commissioning tests were performed on the test facility using the pumped flow arrangement to demonstrate that everything was operating satisfactorily. Friction factors determined from pressure drop measurements made under conditions of isothermal flow through the test section were compared with values calculated using the well-established correlation equation of Blasius for fully developed turbulent flow in a smooth tube. The maximum discrepancy was less than six per cent.

Local values of Nusselt number were determined at various locations along the tube from experiments performed under conditions of dominant forced convection with uniform heating. The results were compared with the distribution of Nusselt number calculated using the established empirical correlation equation of Petukhov, Kurganov and Gladuntsov [1972]. The agreement was very satisfactory.

The purpose of the present work is to contribute to the understanding of buoyancy-influenced gas flows in vertical passages by performing basic experiments backed up by computational simulations. The problem addressed is buoyancy-aided flow of gas in a vertical passage. Contrary to expectations the effectiveness of heat transfer can be impaired under such conditions as a result of the turbulent structure in the boundary layer being modified. It then exhibits the characteristics of flow at a lower value of Reynolds number.

Air was supplied to the bottom of the test section by the blower. Local values of heat transfer coefficient could be determined accurately over the entire heated section. Distributions of Nusselt number were produced for a range of values of Reynolds and Grashof number. The local Nusselt number data for mixed convection show very clear evidence of the importance of the thermal boundary condition on mixed convection heat transfer and that severe impairment of heat transfer can occur in a variety of ways. Figure F-2 shows such a distribution for a condition of impaired mixed convection. As can be seen, it lies well below the corresponding one for forced convection from the empirical equation of Petukhov, Kurganov and Gladuntsov [1972]. Also shown is a computational simulation made using a buoyancy-influenced, variable property, developing wall shear flow formulation incorporating the turbulence model of Launder and Sharma [1974]. As can be seen, observed behavior is reproduced quite well.

Measurements of mean velocity and temperature profiles in the radial direction have been obtained near the exit for the upward flow case under buoyancy-influenced conditions at Reynolds numbers from 6,000 to 20,000. A traversing arrangement installed at the top of the test facility enabled the radial distributions of velocity and temperature to be measured within the flow near the end of the heated section using a Pitot tube/thermocouple probe. Figure F-3 shows measurements of velocity and temperature for the conditions of the heat transfer experiment referred to earlier. Also shown are the profiles from the computational simulation. Flow in the wall region is accelerated by buoyancy to the extent that velocity reaches a peak value there and the profile becomes inverted in

the core region. However, it is apparent that the thermal layer extends over about forty per cent of the radius. This observation indicates that the viscous sub-layer is very considerably thicker than for normal fully developed pipe flow which is consistent with the strongly impaired effectiveness of heat transfer. The measured velocity profile is reproduced extremely well by the simulation. Agreement is less satisfactory in the case of temperature. Nevertheless, the model does predict a greatly increased thermal layer thickness.

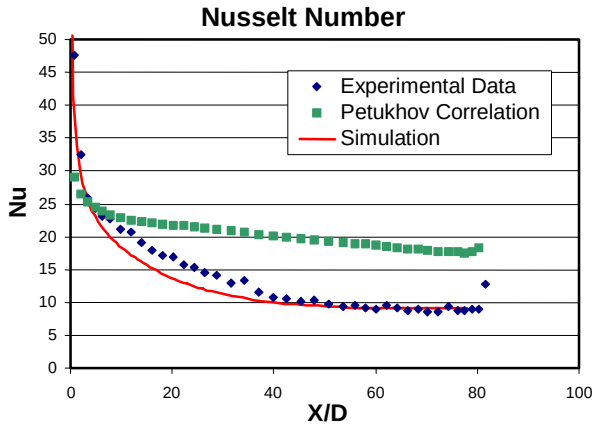

Fig. F-2. Local convective heat transfer with upward flow in a uniformly-heated tube under buoyancy-influenced conditions, Re = 6200, Gr* = 5.1 x 10^7

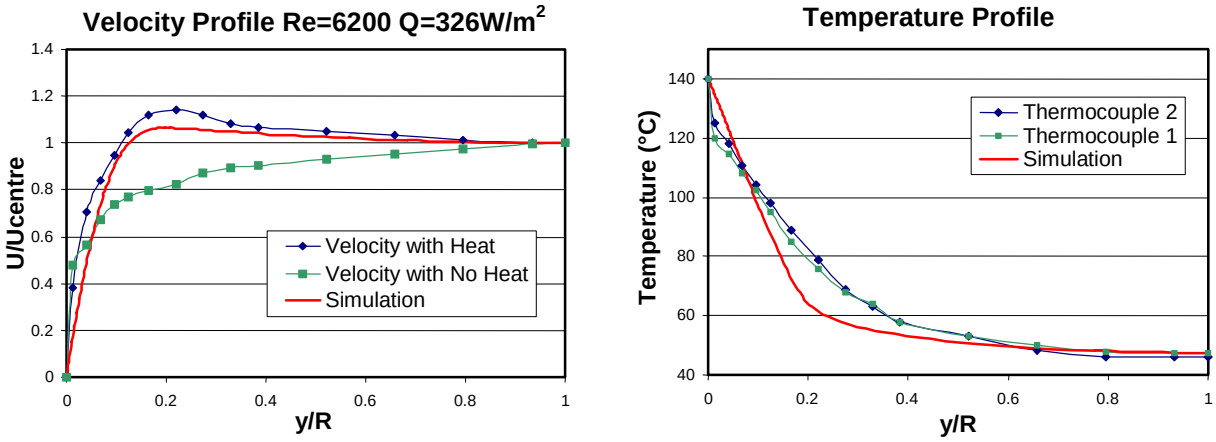

Fig. 3. Velocity and temperature distributions near exit with upward flow in a uniformly-heated tube under buoyancy-influenced conditions, Re = 6200, Gr* = 5.1 x 10^7.

A free jet calibration facility for use with the miniaturized multi-sensor velocity / temperature probe provided by the University of Maryland was designed, manufactured and installed by the side of the circular tube test facility. Associated equipment for attaching wires to the probe was developed. A mechanical arrangement for transferring the probe from the calibration jet into the test section and traversing it radially was also designed, manufactured and installed on the test facility. This equipment was successfully brought into service in the course of a visit to the

University of Manchester by Professor Petar Vukoslavcevic. It has subsequently been used in a series of proving tests which have demonstrated the feasibility of making measurements of velocity, turbulence and temperature using the probe in the airflow near the top of the circular tube.

Preliminary results for both isothermal and buoyancy-influenced conditions are presented in Figures F-4 and F-5, respectively.

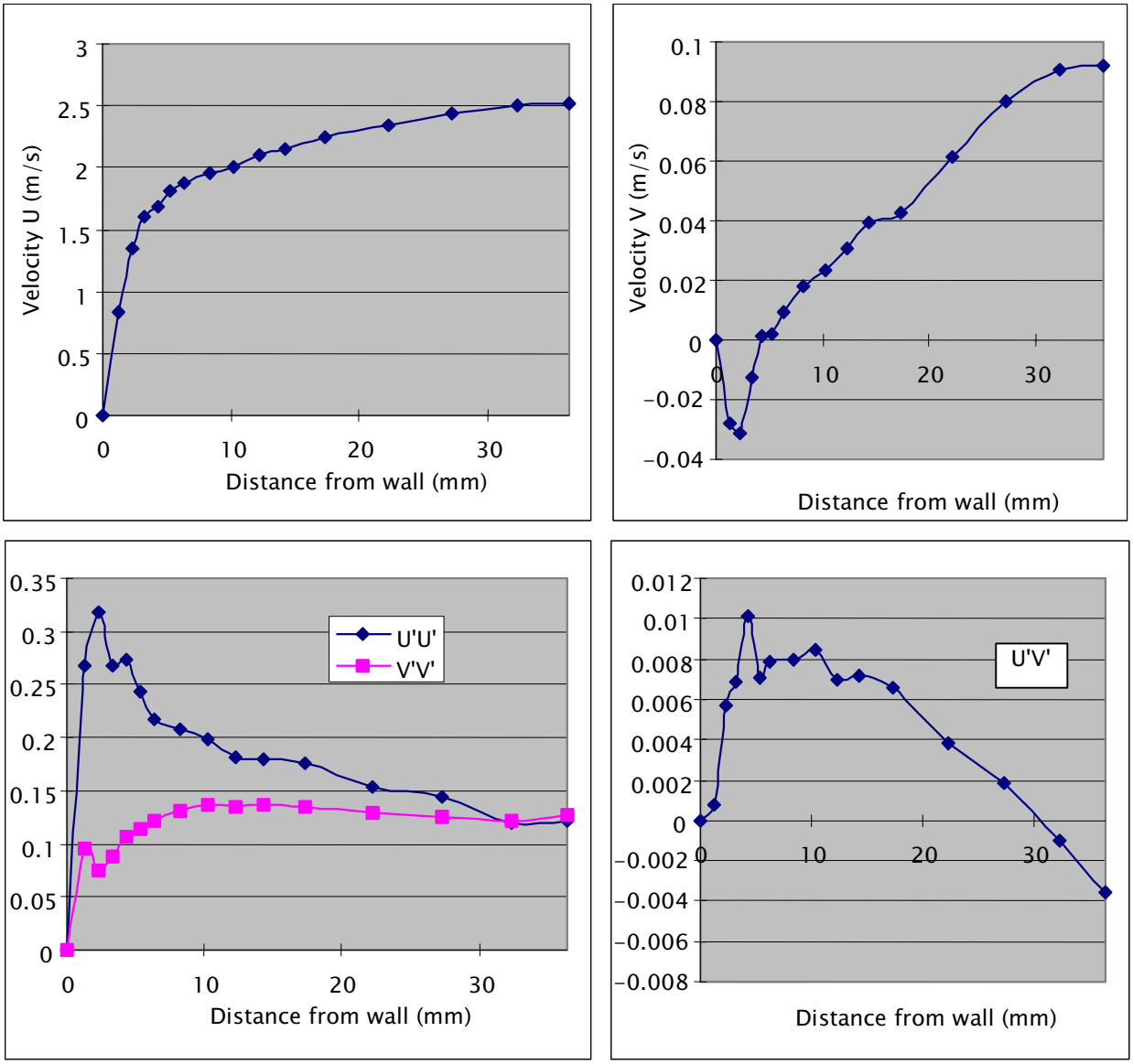

Fig. F-4. Preliminary measurements of velocity and turbulence profiles for conditions of isothermal flow (mass flowrate ≈ 0.00935 kg/s).

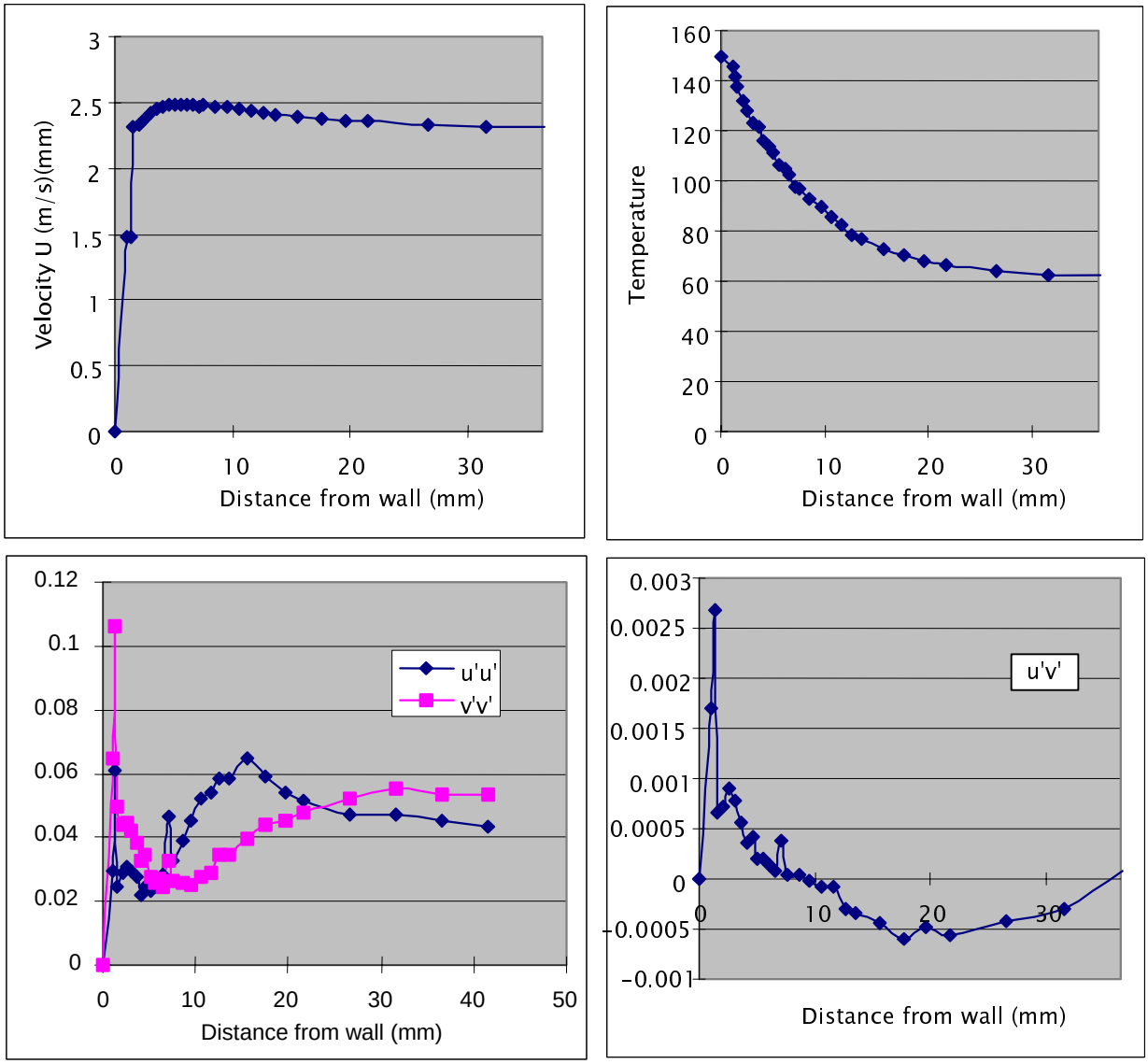

Fig. F-5. Preliminary measurements of velocity, turbulence and temperature profiles for buoyancy-aided heated flow (mass flow rate ≈ 0.0944 kg/s, wall temperature = 150 C).

Measurements of local heat transfer to air flowing in an annulus under variable property, buoyancy-influenced conditions The experimental facility used in this study is shown in Figure F-6. The test section was a passage of annular cross section made from stainless steel of length 10.5 m with an inner diameter of 76.2 mm and an outer diameter of 163 mm. The casing was thermally insulated on the outside and the core was heated uniformly over the middle 4.5 m of its length. The unheated sections of the core at the top and bottom were each of length 3.0 m. A centrifugal air blower was used to draw air through the test section either upwards or downwards. Thus, the arrangement was vertically symmetrical and the flow was fully developed at the start of heating in each case. A thermally developed condition was achieved near the end of the heated section.

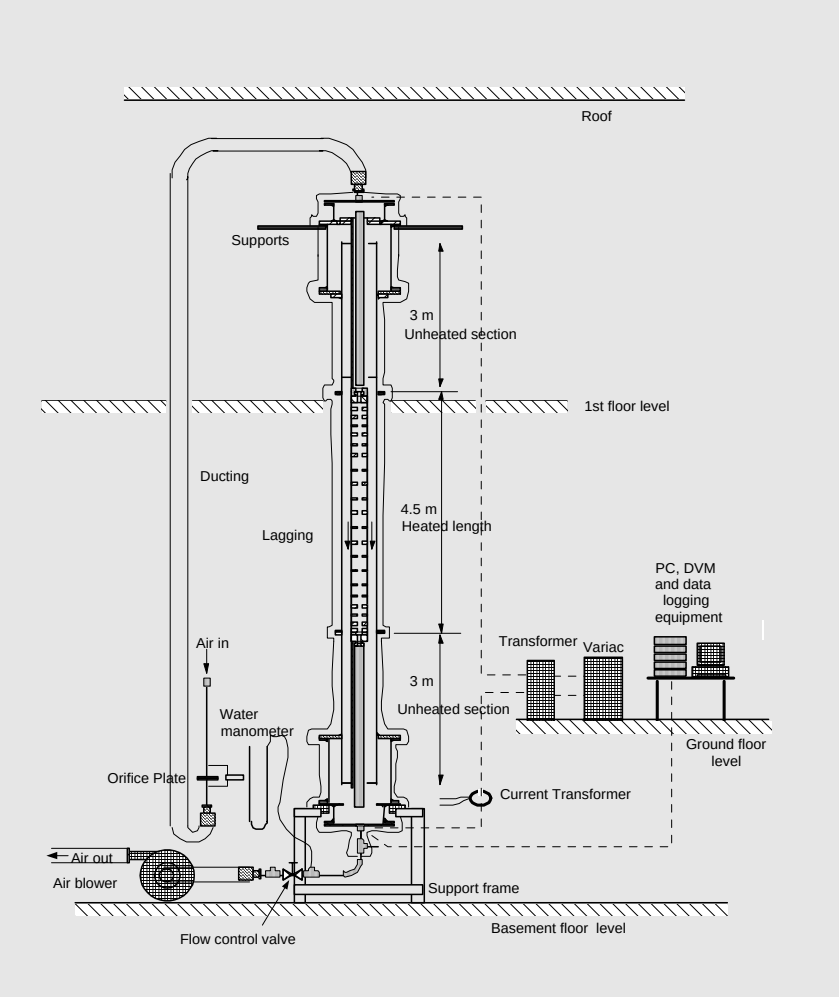

Fig. F-6. Test facility for measurements of local heat transfer to air flowing in an annulus under variable property, buoyancy-influenced conditions.

The flow rate of air was measured using an orifice plate flowmeter situated upstream of the test section. Sixty chromel alumel thermocouples with junctions in contact with the inside surface of the core were used to measure its temperature distribution. The thermocouple emfs were measured using a high precision digital voltmeter built into a computer-controlled data acquisition system. The temperature of the outer casing was measured at a number of axial locations by chromel-alumel thermocouples attached to its outside surface. This approach enabled the radiant heat transfer between the core and casing to be determined. The outer casing was heavily lagged with low conductivity, pre-formed fibre glass insulation of known thermal conductivity. The heat losses to the surroundings could be determined knowing the casing temperature distribution and the thermal conductivity of the thermal insulation. A low voltage, high current power supply system were used to heat the core resistively. This system consisted of a variable auto-transformer and a step down transformer. The current flowing through the core and the voltage applied across it were both measured by precision instruments and were used to determine the power input to heat it.

Knowing the temperature of the air at inlet, the mass flow rate of air, the electrical power supplied to heat the core and the temperature of the core at various axial positions, local values of heat transfer coefficient could be determined after making suitable corrections to account for radiant heat transfer and heat losses to the surroundings.

A comprehensive program of experiments to study the effects of property variations and buoyancy on local heat transfer with upward and downward flow has been completed using this experimental facility. Typical axial distributions of Nusselt number for variable property, thermally developing heat transfer under conditions of predominant forced convection at a Reynolds number of about 30,000 are presented in Figure F-7 for upward and downward flow at very similar values of Reynolds and Grashof number.

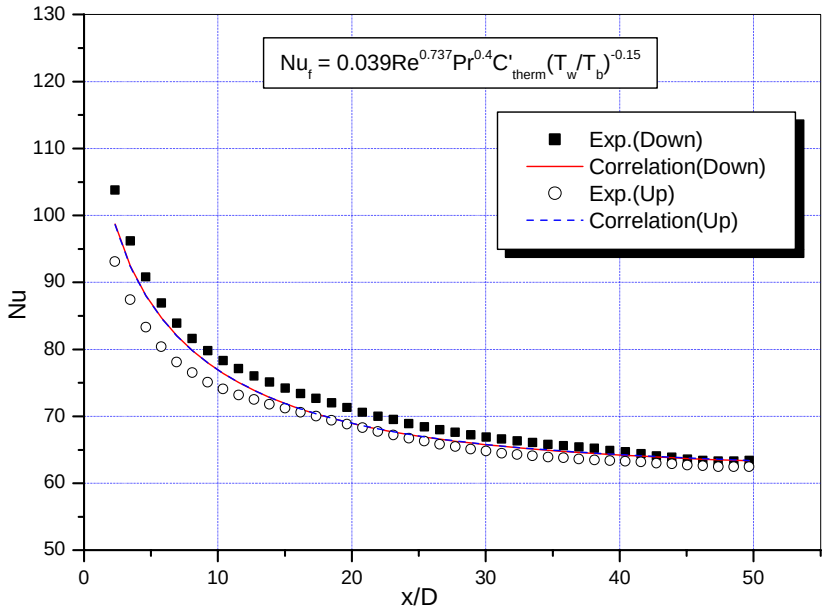

Fig. F-7. Comparison between typical forced convection results for upward and downward flow and the forced convection correlation equation, Re_{in} ~ 30,000.

Also shown is the distribution of Nusselt number given by the following forced convection correlation which has been fitted to data where very similar results were obtained in experiments with upward and downward flow (which indicated that buoyancy effects were negligible)

$$Nu_f = 0.039\, C'_{therm}\, Re^{0.74}\, Pr^{0.4} \left(\frac{T_w}{T_b}\right)^{-0.15}$$

in which C'_{therm} is a thermal entry development function given by

$$C'_{therm} = 1.0 + \exp\left(-0.08\frac{x}{D_e}\right)\left(\frac{x}{D_e}\right)^{-0.25}\left[0.65 + \frac{2925}{Re}\left(\frac{x}{D_e}\right)^{-0.3}\right].$$

As can be seen from this equation, the effects of variable properties have been accounted for in the experiments using a wall-to-bulk temperature-ratio correction factor $(T_w/T_b)^{-0.15}$. The index ***–0.15*** should be contrasted with the value of about ***–0.40*** which is needed to account for such effects in the case of a circular tube. It is apparent from this difference that variable property effects are weaker with a passage of annular cross section having a heated inner surface and an adiabatic outer one than with a circular tube. This result is not unexpected because only the inner boundary layer experiences increased damping of turbulence due the kinematic viscosity being increased.

The next figure shows examples from the present study of axial distributions of Nusselt number for variable property, thermally-developing, buoyancy-influenced heat transfer with upward and also downward flow at a Reynolds number of about 11,000 (Figure F-8). The corresponding correlations of Nusselt number for forced convection are also shown. It can be seen that under the conditions of these buoyancy-influenced experiments, heat transfer is slightly impaired with upward flow and is significantly enhanced with downward flow.

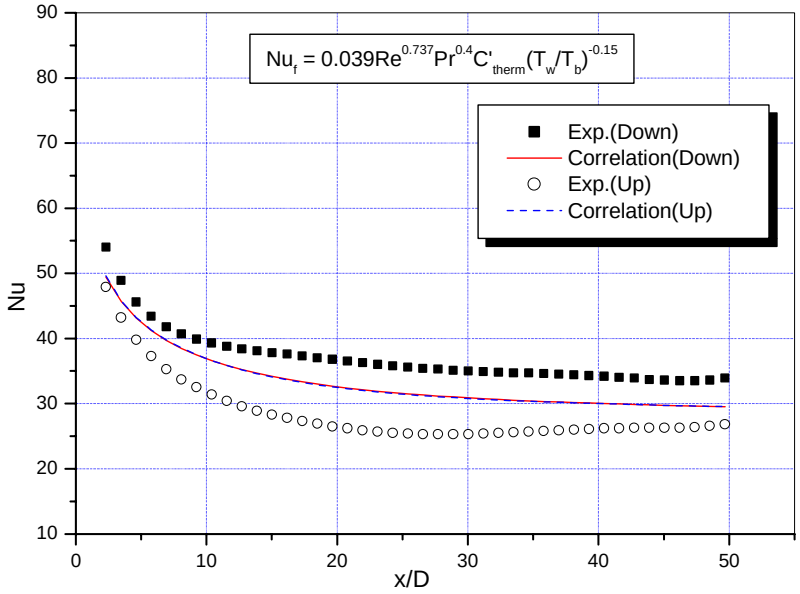

Fig. F-8. Comparison between typical impaired and enhanced mixed convection results for upward and downward flow, Re_{in} ~ 11,000.

Further results are presented in Figure F-9 for conditions with even stronger buoyancy influence as a result of operating at a very low flow rate (Reynolds number about 4000). Here, heat transfer is enhanced with both upward and downward flow. However, the behavior is very different in the two cases. With downward flow, enhancement of heat transfer evolves rapidly in the thermal entry region just downstream of the start of heating. A fully-developed condition is achieved after only about ten equivalent diameters, with the effectiveness of heat transfer then being uniformly higher than for forced convection by a factor of about two. In contrast, the Nusselt number for upward flow varies in a non-monotonic manner.

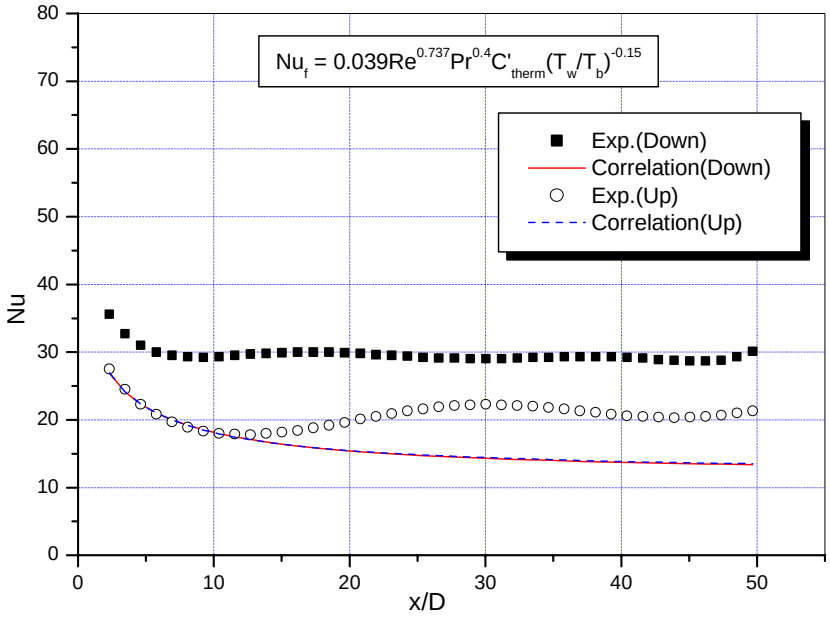

Fig. F-9. Comparison between typical enhanced mixed convection results for upward and downward flow, $Re_{in} \sim 4000$.

The next figure shows data for the downstream location $x/D_e =$ 46 plotted in the form suggested by the semi-empirical model of Jackson and Hall for mixed convection in circular tubes (Figure F-10). From this figure it can be seen that, as in the case of circular tubes, the downward flow data exhibit systematic enhancement of heat transfer with increase of buoyancy influence in relation to forced convection under corresponding conditions. For upward flow some impairment of heat transfer develops with the onset of buoyancy influences but this impairment is followed by enhancement of heat transfer. The impairment is only slight in comparison with that found with circular tubes and it develops more gradually and at somewhat higher values of the buoyancy parameter.

As can be seen from Figure F-10, the downward flow behavior is satisfactorily described by the following equation using the plus sign.

$$\frac{Nu}{Nu_f} = \left(\left| 1 \pm 1.5 \times 10^5 \, Bo^* \left(\frac{Nu}{Nu_f} \right)^{-2} \right| \right)^{0.46} .$$

This equation is of the same form as that which fits data for fully-developed mixed convection in circular tubes, but the constant 2.5×10^5 has been replaced by 1.5×10^5. It is apparent, therefore, that buoyancy effects are weaker in the case of the present experiments with an annulus than with a circular tube. This result is to be expected in view of the fact that only one surface is heated and only one boundary layer experiences a buoyancy influence.

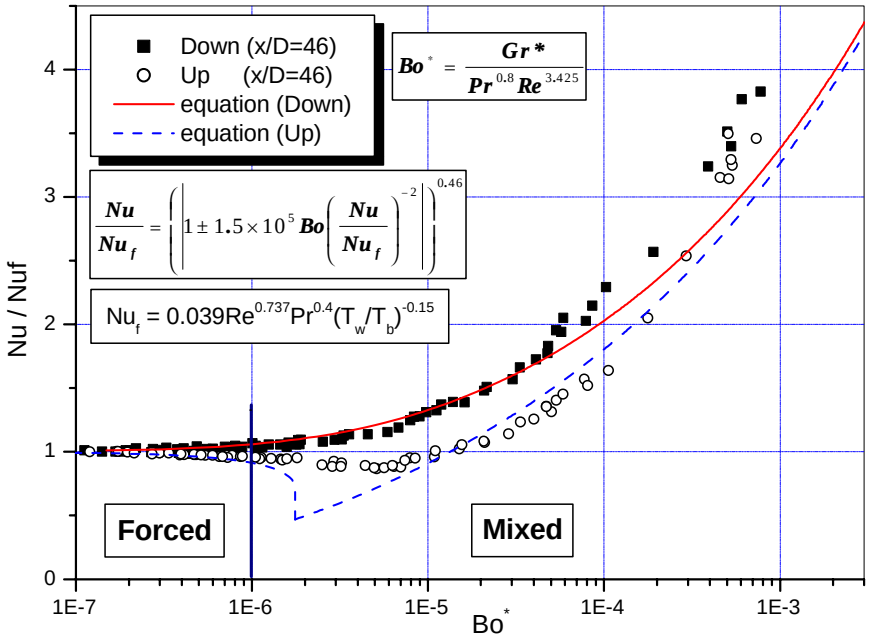

Fig. F-10. Results for fully-developed upward and downward air flow in a heated annulus compared with the predictions of semi-empirical equation

Also shown on Figure F-10 is the curve for upward flow given by the above equation using the minus sign rather than the plus. As can been seen, this equation describes the upward flow data satisfactorily in the enhanced heat transfer region ($Bo^* > 2\text{x}10^{-5}$) but it fails to do so in the impaired heat transfer region $2\text{x}10^{-6} < Bo^* < 2\text{x}10^{-5}$. Again the reason is that only the boundary layer on the heated surface is influenced by buoyancy. The turbulence in the boundary layer on the outer surface (which is about four times the area of the inner one) is not directly affected.

Measurements of local heat transfer to water flowing in an annulus and profiles of velocity, turbulence and temperature Prof. Jackson and his colleagues at Manchester have been contributing to this NERI project by performing experiments to study the effects of property variation and buoyancy in the case of flows in vertical passages. In the third experiment, they studied the influence of buoyancy on local heat transfer and profiles of velocity and turbulence quantities in the case of water flowing through a test section of annular cross section. The justification for doing experiments with water as part of a study aimed at understanding the fundamental thermal physics of strongly-heated gas flows is as follows. Having performed variable-property mixed-convection experiments with air in a passage of annular cross section and having developed a heat transfer correlation which separately accounts for influences of property variation and buoyancy, they have next been able to perform buoyancy-influenced experiments with water under conditions where variable property effects were negligible and to establish a correlation which accounts for the buoyancy effects. By demonstrating that the buoyancy effects in this case are similar to those in the earlier experiments with air they have been able to establish with confidence that the effects of property variation and buoyancy have been separated satisfactorily in that case.

A further justification for doing experiments with water as well as air is that they wish to be able to validate commonly used turbulence models and CFD codes in terms of their ability to handle variable property, buoyancy-influenced flows in vertical passages. Clearly it will be helpful to have data for flows in which the effects of property variation and buoyancy are both present and also for flows which are only affected by buoyancy for evaluating such models and codes.

Another reason for doing some experiments with water is that because the fluid is at atmospheric pressure the outer casing can be made of transparent plexiglass. Thus, LDA measurements of velocity and turbulence can be conveniently made with the laser beams passing through the outer casing. In the case of the air experiment, because it is designed for operation at high pressure, the outer casing has to be made of steel so that it can act as the pressure containment. This situation makes it much more difficult to arrange for optical access to the flow for the purpose of measuring velocity and turbulence. A particularly valuable outcome of the water experiments is a set of data which should lead to a better understanding of the influence of buoyancy on turbulence in the case of flows in vertical passages. A useful by-product of the water experiments is that they are providing useful data on the thermal physics of flows in advanced water-cooled reactors as well.

The experimental facility available for this study is shown in Figure F-11. The flow circuit arrangement shown is for the downward flow case. Water from the header tank flows to the top of the test section and then downwards through it. On leaving the test section it is returned by a centrifugal pump to the header tank via a flow control valve, an orifice plate flowmeter and a shell and tube heat exchanger. The circuit is designed so that it can be readily modified to give upward rather than downward flow through the annulus.

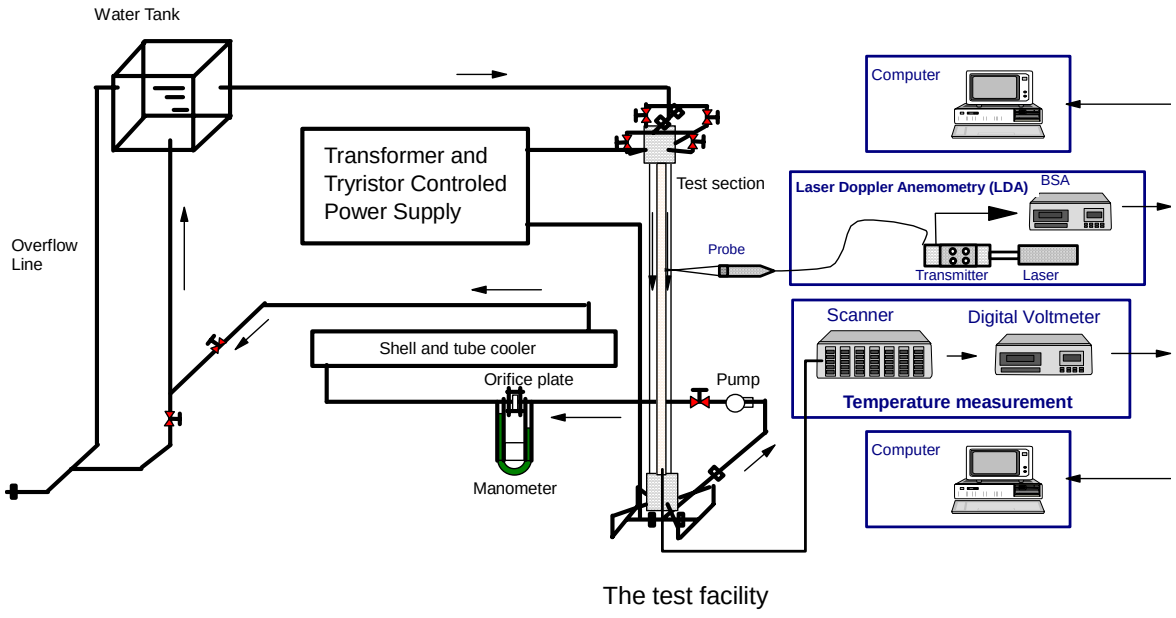

Fig. F-11. Test facility for measurements of velocity, turbulence and temperature distributions in an annulus.

The test section is shown in Figure F-12. In order to achieve a symmetrical flow at entry, the water is supplied to it through a manifold arrangement. Four tubes 90° apart feed into a cylindrical entry section. The diameter ratio of the annulus is 1.94 (or $r_i/r_o \approx 0.52$, comparable to some calculations in Task D). The core is made from stainless steel tube of external diameter 76 mm and wall thickness 1.6 mm. It is uniformly heated by resistive means over a length of 3.0 m. Above and below the heated section are unheated lengths. About 90 chromel-alumel thermocouples are used on the heated section of the core to measure its temperature distribution. The outer casing is made from perspex and has an internal diameter of 140 mm. Heat losses to the surroundings from this casing are very small indeed and, therefore, the thermal boundary condition is effectively an adiabatic one.

Two sheathed, mineral insulated, chromel-alumel thermocouples situated in the flow at the inlet and outlet of the test section are used to measure the water temperature at those locations. The electrical power to heat the test section is supplied by a low voltage, high current, thysistor-controlled system. Integrated mean values of current and voltage are used to determine the heat input. The signals from the instrumentation are all recorded automatically by a computer-based data acquisition system, incorporating a precision, microprocessor – controlled digital voltmeter, and then processed on line.

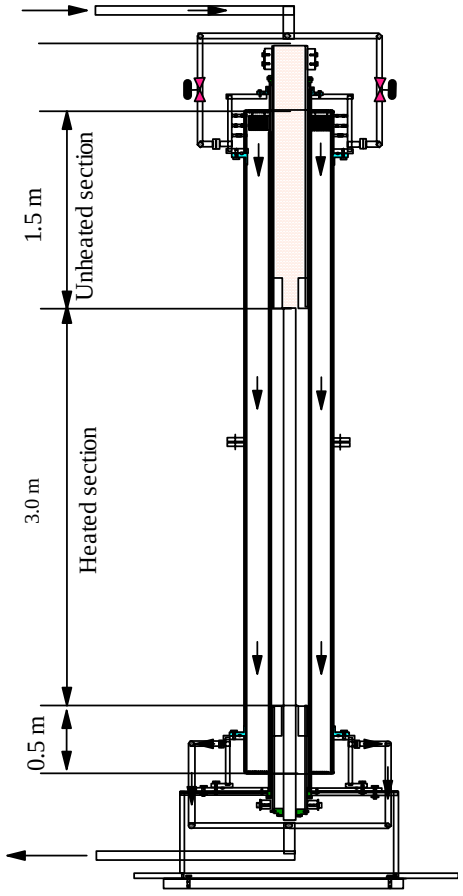

Fig. F-12. Test section for measurements of velocity, turbulence and temperature distributions in an annulus.

The test facility just described is provided with a laser Doppler anemometer system which enables radial profiles of velocity and turbulence to be measured within the flow. Temperature profiles can be measured using a traversable thermocouple. Measurements of local heat transfer coefficient and the profiles of velocity, turbulence quantities and temperature were made for upward flow under conditions ranging from forced convection to buoyancy-dominated mixed convection.

The test section has a uniformly heated inner surface and an adiabatic outer surface. Local heat transfer coefficients have been determined under conditions of turbulent, ascending and also descending flow with buoyancy influences. These were readily produced by increasing the heating and reducing the flow rate. The mode of heat transfer was varied from forced convection with negligible influence of buoyancy to mixed convection with very strong influences of buoyancy.

As in the case of the related study with air flowing through an annulus, reported earlier, the results obtained with water demonstrate that the effects of buoyancy on heat transfer in such a

passage generally follow a similar pattern to those found with uniformly heated tubes. Axial distributions of Nusselt number were produced for a range of values of Grashof number and Reynolds number. It was observed that, with downward flow, heat transfer was systematically enhanced as a result of increased buoyancy influence and a fully-developed thermal condition was achieved more and more readily. With upward flow, heat transfer was either impaired or enhanced depending on the strength of the buoyancy influence. In general, the thermal development is then non-monotonic and a fully-developed thermal condition is not readily achieved. The contrasting behaviour for the upward and downward flow has been emphasized by plotting the ratio of Nusselt number for mixed convection to that for forced convection against a parameter which combines Reynolds number, Grashof number and Prandtl number in a manner which characterises the strength of buoyancy influence.

Just as in the earlier related study using air, there are some clear differences between the present results and those obtained in similar experiments with circular tubes. The onset of buoyancy-induced enhancement and impairment of heat transfer is delayed, the former occurs more gradually and the maximum impairment of heat transfer is reduced. Such trends are not unexpected. In a uniformly heated circular tube, modification of the flow and turbulence occurs as a result of influences of buoyancy which are present over the entire surface. However, in an annulus with a heated core and an adiabatic outer casing only the inner boundary layer is directly affected.

Measurements of velocity and turbulence were obtained using laser Doppler anemometry under both buoyancy-free and buoyancy-influenced conditions. A comprehensive programme of experiments has been completed with both upward and downward flow which has produced detailed information for conditions ranging from forced convection to buoyancy-dominated mixed convection [Xu, 2002]. The Reynolds number was varied from 20,000 down to 1500 and the Grashof number, Gr*, from 2×10^8 to 1.5×10^9. Measurements of velocity and turbulence were also made under isothermal conditions (i.e., without any heat transfer).

Radial profiles of time mean velocity U and turbulence quantities $\sqrt{\overline{u'^2}}$, $\sqrt{\overline{v'^2}}$ and $\overline{uv}$ (in which u′ and v′ are the axial and radial components of turbulent velocity fluctuation, respectively) have been produced for a series of experiments with increasingly strong influences of buoyancy. In each case results were obtained for both buoyancy-aided and buoyancy-opposed flow along with the corresponding ones for unheated (isothermal) flow. The increase of velocity in the flow near the surface of the heated core due to buoyancy influence in the case of upward flow and the corresponding decrease with downward flow are both clearly apparent. The distortion of the velocity profiles increased systematically with increase of buoyancy influence. The effects of buoyancy on the root mean square values of the radial and axial components of turbulent velocity fluctuation are also clearly apparent, particularly in the case of upward flow, where it can be seen that the turbulence was significantly reduced in the shear layer near the heated surface but increased further out. In the case of downward flow the observed effects are in the opposite sense and of reduced magnitude. The most striking effects of buoyancy on turbulence are exhibited by the profiles of turbulent shear stress. With upward flow $\overline{uv}$ is greatly reduced in the shear layer near the heated surface. It is clear that the production of turbulence in that region is reduced. Thus, turbulent diffusion of heat is less effective as a result of the influence of buoyancy. This effect is why it is found that heat transfer is impaired. With downward flow the observed effects are in the opposite sense and consistent with the observed

enhancement of heat transfer. The measurements of turbulence in buoyancy-influenced flow made in the present study provide valuable direct confirmation of the mechanism by which buoyancy influences heat transfer in vertical passages.

Some results have been obtained for Reynolds numbers below the so-called "lower critical value" of about 2000. Without any heating applied the flow is laminar. The measured velocity profile is parabolic in shape and in good agreement with that predicted by theory for fully-developed laminar flow in an annulus. However, when heating is applied the situation is very different as a result of the influence of buoyancy. The mean flow is actually reversed near the heated surface in the case of downward flow and is very turbulent. This latter result is also so in the case of upward flow. The velocity fluctuations are greater than those found for isothermal (unheated) flow at a Reynolds number of 8500. The turbulent shear stress is very high. Its maximum value also is greater than that for isothermal flow at a Reynolds number of 8500.

A snapshot of the results is shown in Figure F-13. Results of computational simulations of the experiments -- using a developing flow formulation which takes account of variable properties and buoyancy influence and incorporates the low Reynolds number k-ε turbulence model of Launder and Sharma -- were also accomplished and were compared directly with measurements of velocity, turbulence and heat transfer.

Further details are provided in a recent thesis by Xu [2002].

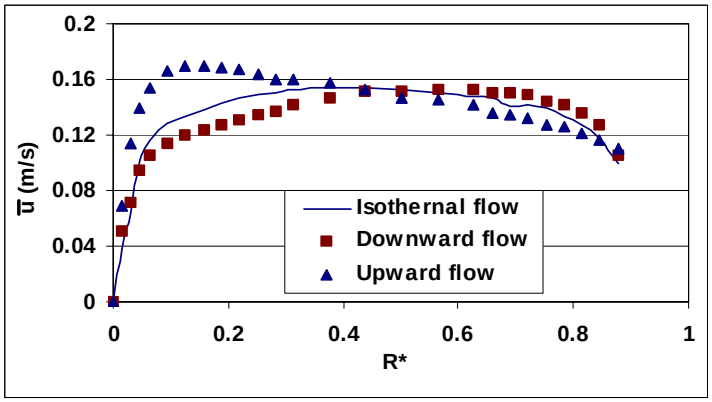

(a) Mean velocity

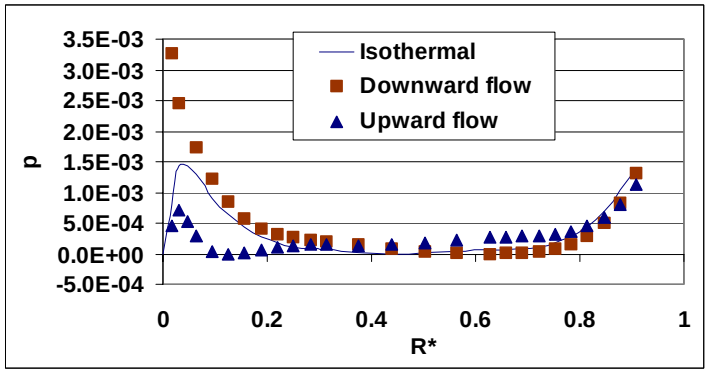

(b) Turbulence production

Fig. F-13. Examples of radial profiles of streamwise mean velocity and turbulence measured using laser Doppler velocimetry under buoyancy-influenced flow conditions in an annular vertical passage.

Accomplishments

The overall accomplishments during the project may be summarized as follows:

- o GA identified areas of concern and provided support in planning required computational techniques and experiments
- o DNS of laminarizing and "subturbulent" gas flow completed, turbulent initiated, for circular tubes
- o First LES conducted for vertical mixed convection with property variation; channel code extended to circular tubes, annuli and ribbed annuli
- o MIR experiment for flow in complex reactor geometry (ribbed annuli) designed, fabricated, tested and employed for LDV measurements
- o Three- and four-sensor miniature probes developed, tested, calibrated and operated
- o Obtained data for mixed convection with property variation and arbitrary thermal boundary conditions in tubes, channels and annuli
- o Prof. S.-i. Satake selected as Outstanding Young Engineering Scientist by JSME
- o Prof. J. M. Wallace elected for succession to Chairman of the APS Fluid Dynamics Division
- o Prof. D. M. McEligot selected as 2002 Distinguished Scientist by Idaho Academy of Science
- o 22 technical publications, 49 presentations and 20 invited talks related to project
- o Brought fluid mechanics authorities and students into nuclear science community

Concluding remarks

An overview of the project includes:

- o Assembled productive international team of recognized engineering scientists in fluid mechanics and heat transfer
- o New basic experiments and analyses accomplished to address operation of advanced gas-cooled reactors at full or partial loads and loss of forced reactor core cooling
- o New students and faculty brought into nuclear science and engineering community
- o Team and resulting accomplishments have benefited from contributions of experienced scientists from Japan, UK, France and Montenegro – has supplemented DoE investment
- o New fundamental results obtained in Large Eddy Simulation, Direct Numerical Simulation and measurements for complex flow geometries and mixed convection with property variation
- o Technical papers, presentations and reports completed and other recognition received

References cited

Abe, K., T. Kondoh and Y. Nagano, 1994. A new turbulence model for predicting fluid flow and heat transfer in separating and reattaching flows -- I. Flow field calculations. *Int. J. Heat Mass Transfer*, 37, pp. 139-151.

Avancha, R. V. R., and R. H. Pletcher, 2002. Large eddy simulation of the turbulent flow past a backward-facing step with heat transfer and property variations. *International J. Heat Fluid Flow*, 23, pp. 601-614.

Balint, J.-L., J. M. Wallace and P. Vukoslavcevic, 1991. The velocity and vorticity vector fields of a turbulent boundary layer. Part II. Statistical Properties. *J. Fluid Mech.* 228, pp. 53-86.

Bankston, C. A., 1970. The transition from turbulent to laminar gas flow in a heated pipe. *J. Heat Transfer*, 92, pp. 569-579.

Bankston, C. A., and D. M. McEligot, 1970. Turbulent and laminar heat transfer to gases with varying properties in the entry region of circular ducts. *Int. J. Heat Mass Transfer*, 13, pp. 319-344.

Bates, J. A., R. A. Schmall, G. A. Hasen and D. M. McEligot, 1974. Effects of buoyant body forces on forced convection in heated laminarizing flows. *Heat Transfer 1974* (Proc., 5th Intl. Heat Transfer Conf., Tokyo), vol. II, pp. 141-145.

Becker, S., C. M. Stoots, K. G. Condie, F. Durst and D. M. McEligot, 2002. LDA-measurements of transitional flows induced by a square rib. *J. Fluids Engr.*, 124, pp. 108-117.

Benjamin, S. F., and C. A. Roberts, 2001. Measuring flow velocity at elevated temperatures with hot wire anemometer calibrated in cold flow. *Int. J. Heat Mass Transfer*, 45, pp. 703-706.

Berner, C., F. Durst and D. M. McEligot, 1984. Flow over baffles. *J. Heat Transfer*, 106, pp. 743-749.

Blackwelder, R. F., 1981. Hot-wire and hot-film anemometers. *Methods of Experimental Physics: Fluid Dynamics* (R. J. Emerich, Ed.), New York: Academic Press.

Blair, M. F., and J. C. Bennett, 1987. Hot wire measurements of velocity and temperature fluctuations in a heated turbulent boundary layer. *J. Phys. (Sci. Instr.)*, 20, pp. 209-216.

Brunn, H. H., 1995. *Hot-wire anemometry*. Oxford: Oxford University Press.

Catton, I., 1978. Natural convection in enclosures. Proc., 6th Int. Heat Transfer Conf., Toronto, Vol. 6, pp. 13-31.

Chambers, F. W., H. D. Murphy and D. M. McEligot, 1983. Laterally converging flow. II: Temporal wall shear stress. *J. Fluid Mech.*, 127, pp. 403-428.

Champagne, F. H., C. A. Sleicher and O. H. Wehrmann, 1967. Turbulence measurements with inclined hot-wires. Part I - Heat transfer experiments with inclined hot-wires, Part II - Hot wire response equations. *J. Fluid Mech.*, 28, pp. 153-182.

Chevray, R., and N. K. Tutu, 1972. Simultaneous measurements of temperature and velocity in heated flow. *Rev. Sci. Inst.*, 43, pp. 1417-1421.

Chung, S. Y., G. H. Rhee and H. J. Sung, 2001. Direct numerical simulation of turbulent concentric annular pipe flow. Proc., Second Int. Symp. Turbulence and Shear Flow Phenomena, Vol. 1, pp. 377-382.

Condie, K. G., G. E. McCreery and D. M. McEligot, 2001. Measurements of fundamental fluid physics of SNF storage cannisters. Tech. rpt. INEEL/EXT-2001-1269.

Cooper, D., D. C. Jackson, B. E. Launder and G. X. Liao, 1993. Impinging jet studies for turbulence model assessment - I. Flow-field experiments. *Int. J. Heat Mass Transfer*, 36, pp. 2675-2684.

Corino, E. R., and R. S. Brodkey, 1969. A visual observation of the wall region in turbulent flow. *J. Fluid Mech.*, 37, pp. 1-30.

Cotton, M. A., and P. J. Kerwin, 1995. A variant of the low-Reynolds-number two-equation turbulence model applied to variable property mixed convection flows. *Int. J. Heat Fluid Flow*, 16, pp. 486-492.

Cui, M. M., and R. J. Adrian, 1997. Refractive index matching and marking methods for highly concentrated solid-liquid flows. *Exp. Fluids*, 22, pp. 261-264.

Dailey, L. D., and R. H. Pletcher, 1998. Large eddy simulations of constant heat flux turbulent channel flow with property variations. AIAA paper 98-0791.

Downs, H. T., and E. H. James, 1987. Jet impingement heat transfer - A literature survey. ASME paper 87-HT-35.

Durst, F., M. Fischer, J. Jovanovic and H. Kikura, 1998. Methods to set up and investigate low Reynolds number, fully developed turbulent plane channel flows. *J. Fluids Engr.*, 120, pp. 496-503.

Durst, F., J. Jovanovic and J. Sender, 1993. Detailed measurements of the near wall region of turbulent pipe flows. Proc., 9th Symp. Turb. Shear Flows, Kyoto, paper 2-2.

Durst, F., A. Melling and J. H. Whitelaw, 1976. *Principles and practise of laser-Doppler anemometry.* London: Academic Press.

Eggels, J. G. M., F. Unger and M. W. Weiss, 1994. Fully developed turbulent pipe flow: a comparison between direct numerical simulation and experiment. *J. Fluid Mech.*, 268, pp. 175-209.

Ezato, K., A. M. Shehata, T. Kunugi and D. M. McEligot, 1999. Numerical predictions of transitional features of turbulent forced gas flows in circular tubes with strong heating. *J. Heat Transfer*, 121, pp. 546-555.

Fabris, G., 1978. Probe and method for simultaneous measurements of "true" instantenous temperature and three velocity components in turbulent flow. *Rev. Sci. Inst.*, 49, pp. 654-664.

Ferziger, J.H., and M. Pelic, 1997. *Computational methods for fluid dynamics.* Berlin: Springer, Chapter 7, pp. 164-170.

Fisher, Jovanovic and Durst, 1998. See Durst et al. [1998].

Folz, A., 1996. An experimental study of the near-surface turbulence in the atmospheric boundary layer. Ph.D. Diss., University of Maryland.

Foust, T. D., 2002. Personal communication, Idaho National Engineering and Environmental Laboratory.

Fujii, S., N. Akino, M. Hishida, H. Kawamura and K. Sanokawa, 1991. Experimental and theoretical investigations on heat transfer of strongly heated turbulent gas flow in an annular duct. *JSME International J., Ser II*, 34, No. 3, pp. 348-354.

Gardon, R., and J. C. Akfirat, 1965. The role of turbulence in determining the heat transfer characteristics of impinging jets. *Int. J. Heat Mass Transfer*, 8, pp. 1261-1272.

Goldstein, R. J., and A. L. Behbahani, 1982. Impingement of a circular jet with and without cross flow. *Int. J. Heat Mass Transfer*, 25, pp. 1377-1382.

Habib, M. A., F. Durst and D. M. McEligot, 1984. Streamwise-periodic flow around baffles. Proc., 2nd Int. Symp. Appl. Laser Anemometry to Fluid Mechanics, Lisbon, July.

Hamilton, J., J. Kim and F. Waleffe, 1995. Regeneration mechanisms of near-wall turbulence structures. *J. Fluid Mech.*, 287, pp. 317-348.

Hishida, M., and Y. Nagano, 1978. Simultaneous measurements of velocity and temperature in nonisothermal flows. *J. Heat Transfer*, 100, pp. 340-345.

Hrycak, P., 1981. Heat transfer from impinging jets - A literature review. Tech. rpt. AFWAL-TR-81-3504.

Hrycak, P., 1983. Heat transfer from round impinging jets to a flat plate. *Int. J. Heat Mass Transfer*, 26, pp. 1857-1865.

Huang, R. F., and C. L. Lin, 2000. Velocity field of a bluff body wake. *J. Wind Eng. Ind. Aero.*, 85, pp. 31-45.

Iacovides, H., and B. E. Launder, 1995. Computational fluid dynamics applied to internal gas-turbine blade cooling: a review. *Int. J. Heat Fluid Flow*, 16, pp. 454-470.

Jackson, J. D., M. A. Cotton and B. P. Axcell, 1989. Studies of mixed convection in vertical tubes. *Int. J. Heat Fluid Flow*, 10, pp. 2-15.

Jackson, J. D., and W. B. Hall, 1979. Influences of buoyancy on heat transfer to fluids flowing in vertical tubes under turbulent conditions. *Turbulent forced convection in channels and bundles* (Ed.: S. Kakac and D. B. Spalding), Washington: Hemisphere, vol. 2, pp. 613-640.

Jackson, J. D., and J. Li, 2000. Influences of buoyancy and thermal boundary conditions on heat transfer with naturally-induced flow. Technical Committee Meeting on Natural Circulation Data and Methods for Innovative Nuclear Power Plant Design, Vienna, Austria, July

Jorgensen, F., 1971. Directional sensitivity of wire and fibre film probes. *DISA Information*, No.11, pp. 31-37.

Kasagi, N., and A. Matsunaga, 1995. Three-dimensional particle-tracking velocimetry measurement of turbulence statistics and energy budget in a backwards-facing step flow. *Int. J. Heat Fluid Flow*, 16, pp. 477-485.

Kawamura, H., 1979. Analysis of laminarization of heated turbulent gas using a two-equation model of turbulence. Proc., 2nd Intl. Symp. Turb. Shear Flow, London, pp. 18.16-18.21.

Kawamura, H., S. Nakamura, S. Satake and T. Kunugi, 1994. Large eddy simulation of turbulent heat transfer in a concentric annulus. *Thermal Science & Engineering*, pp. 16-25 (in Japanese).

Kays, W. M., 1966. *Convective heat and mass transfer.* New York: McGraw-Hill.

Kays, W. M., and M. E. Crawford, 1993. *Convective heat and mass transfer, 3rd ed.* New York: McGraw-Hill.

Kim, J., P. Moin and R. Moser, 1987. Turbulence statistics in fully developed channel flow at low Reynolds numbers. *J. Fluid Mech.* 177, pp. 133-166.

Kim, W. S., C. Talbot, B. J. Chung and J. D. Jackson, 2002. Mixed convection heat transfer with variable properties to air flowing through a vertical passage of annular cross section. *Trans., Institution of Chemical Engineers Part A, Chemical Engineering Research and Design,* 80, Part A, pp. 239-245.

King, L. W., 1914. On the convection of heat from small cylinders in a stream of fluid. *Philos. Trans. Royal Soc., Ser. A,* 214, pp. 272-432.

Kline, S. J., W. C. Reynolds, F. A. Schraub and P. W. Rundstadler, 1967. The structure of turbulent boundary layers. *J. Fluid Mech.*, 30, pp 741-773.

Kugeler, K., 1996. Nuclear safety and the expectation to HTGRs deployment. Proc., 3rd JAERI Symp. HTGR Technologies, Oarai, Japan, pp. 22-35.

Launder, B. E., and B. I. Sharma, 1974. Application of the energy-dissipation model of turbulence to the calculation of flow near a spinning disc. *Lett. Heat Transfer*, 1, pp. 131-138.

Lee, J. S., and R. H. Pletcher, 2001. Large eddy simulation of a turbulent channel flow with buoyancy effects. AIAA paper 2001-0431, 39th AIAA Aerospace Sciences Meeting.

Lee, J. S., and R. H. Pletcher, 2001. Large eddy simulation of variable property turbulent flow in a vertical channel with buoyancy effects and heat transfer. ASME paper NHTC01-1556, Proc., 35th National Heat Transfer Conference, June.

Lee, J. S., X. Xu and R. H. Pletcher, 2002. Large eddy simulation of mixed convection in a vertical turbulent annular pipe flow. ASME paper IMECE2002-HT-32746, 2002 ASME International Mechanical Engineering Congress, .

leWalle, J., D. E. Ashpis and K.-H. Sohn, 1997. Demonstration of wavelet techniques in the spectral analysis of bypass transition data. NASA TP-3555.

Li, J., C. Talbot, W.S. Kim, J. D. Jackson and B.J. Chung, 2001. On the mechanism of impairment of heat transfer in buoyancy-aided turbulent pipeflow. Turbulent Heat Transfer III, Anchorage, Alaska, USA, March.

Liu, X., and J. H. Lienhard V, 1993. Extremely high heat fluxes beneath impinging liquid jets. *J. Heat Transfer*, 115, pp. 472-476.

Loucks, R., 1998. An experimental examination of the velocity and vorticity fields in a plane mixing layer. Ph.D. Diss., University of Maryland.

Ma, C. F., Q. Zheng, S. C. Lee and T. Gomi, 1997. Impingement heat transfer and recovery effect with submerged jets of large Prandtl number liquid - I. Unconfined circular jets. *Int. J. Heat Mass Transfer*, 40, pp. 1481-1490.

Ma, C. F., Q. Zheng, H. Sun, K. Wu, T. Gomi and B. W. Webb, 1997. Local characteristics of impingement heat transfer with oblique round free-surface jets of large Prandtl number fluid. *Int. J. Heat Mass Transfer*, 40, pp. 2249-2259.

Marasli, B., P. Nguyen and J. M. Wallace, 1996. A calibration technique for multiple-sensor hot-wire probes and its application to vorticity measurements in the wake of a circular cylinder. *Exp. Fluids* 15, pp. 209-218.

Martin, H., 1977. Heat and mass transfer between impinging gas jets and solid surfaces. *Adv. Heat Transfer*, 13, pp. 1-60.

McCreery, G. E., K. G. Condie, R. L. Clarksean and D. M. McEligot, 2002. Convective processes in spent nuclear fuel canisters. *Heat Transfer 2002* (Proc., 12th Int. Heat Transfer Conf., Grenoble), pp. 663-668.

McCreery, G. E., K. G. Condie, D. M. McEligot, J. C. Crepeau, R. Clarksean, Y. G. Guzennec and R. S. Brodkey, 1999. Flow visualization and velocity measurements in a model fuel storage canister. Global '99 - International Conference on Future Energy Systems, Jackson, Wyo., August .

McCreery, G. E., T. D. Foust, D. M. McEligot, K. G. Condie and R. J. Pink, 2002. Measurements and code comparisons for advanced gas reactor coolant channels containing spacer ribs. Paper IMECE2002-33597, ASME International Mechanical Engineering Congress, New Orleans, November.

McEligot, D. M., 1986. Convective heat transfer in internal gas flows with temperature-dependent properties. *Adv. Transport Processes*, 4, pp 113-200.

McEligot, D. M., and C. A. Bankston, 1969. Turbulent predictions for circular tube laminarization by heating. ASME paper 69-HT-52.

McEligot, D. M., and H. Eckelmann, 1990. Effects of streamwise pressure gradients on turbulence structure in the viscous layer. Tech. rpt. WNSD/HYDRO-90-03, Westinghouse Naval Sys. Div. Also DTIC AD No. A225 048.

McEligot, D. M., and H. Eckelmann, 2003. Effects of laterally converging flows on mean turbulence structure in the viscous layer. Tech. rpt. INEEL/EXT-2002-697.

McEligot, D. M., A. M. Shehata and T. Kunugi, 1998. Prediction of strongly-heated internal gas flows. Proc., Eng. Foundation 2nd Int. Conf. Turbulent Heat Transfer, Manchester, UK, vol. I, pp. 1-33 to 1-47.

Mikielewicz, D. P., 1994. Comparative studies of turbulence models under conditions of mixed convection with variable properties in heated vertical tubes. Ph.D. thesis, Univ. Manchester.

Mikielewicz, D. P., A. M. Shehata, J. D. Jackson and D. M. McEligot, 2002. Temperature, velocity and mean turbulence structure in strongly-heated internal gas flows. Comparison of numerical predictions with data. *Int. J. Heat Mass Transfer*, 45, pp. 4333-4352.

Moro, J.-P., M. Saez and E. Hopfinger, 1998. An experimental study of mixed convection. Proc., Eng. Foundation 2nd Int. Conf. Turbulent Heat Transfer, Manchester, U. K., June, pp. P-39 to P-45.

Murphy, H. D., F. W. Chambers and D.M. McEligot, 1983. Laterally converging flow. I: Mean flow. *J. Fluid Mech.*, 127, pp. 379-401.

Nagano, Y., and M. Shimada, 1995. Computational modeling and simulation of turbulent flows. *Computational Fluid Dynamics Review 1995* (Ed.: M. Hafez and K. Oshima), Chichester: John Wiley & Sons, pp. 695-714.

Nguyen, P., 1993. Simultaneous measurements of the velocity and vorticity vector fields in the turbulent near wake of a circular cylinder. Ph.D. diss., University of Maryland.

Niederschulte, M. A., R. J. Adrian and T. J. Hanratty, 1990. Measurements of turbulent flow in a channel at low Reynolds numbers. *Exp. Fluids*, 9, pp. 222-230.

Nishimura, M., S. Fujii, A. M. Shehata, T. Kunugi and D. M. McEligot, 2000. Prediction of forced gas flows in circular tubes at high heat fluxes accompanied by laminarization. *J. Nuc. Science and Technology*, 37, pp. 581-594.

Nishio, K., M. Samada, K. Kasuya and K. Torii, 1996. Turbulence statistics in the stagnation region of an axisymmetric impinging jet flow. *Int. J. Heat Fluid Flow*, 17, pp. 193-201.

Ogawa, M., 1998. Personal communication, Japan Atomic Energy Research Institute, Tokai.

Ogawa, M., and H. Kawamura, 1986. Experimental and analytical studies on friction factor of heated gas flow in circular tube. *J. At. Energy Soc., Japan*, 28, No. 10, pp. 957-965 (in Japanese).

Ogawa, M., H. Kawamura, T. Takizuka and N. Akino, 1982. Experiment on laminarization of strongly heated gas flow in a circular tube. *J. At. Energy Soc., Japan*, 24, No. 1, pp. 60-67 (in Japanese).

Orr, B., E. Thomson and R. S. Budwig, 1997. Drakeol 5 thermophysical property measurements. Technical report, Mech. Engr. Dept., U. Idaho.

Park, S. R., and J. M. Wallace, 1993. The influence of instantaneous velocity gradients on turbulence properties measured with multi-sensor hot-wire probes. *Exp. Fluids* 16, pp. 17-26.

Parker, J., and P. Merati, 1996. An investigation of turbulent Taylor-Couette flow using laser Doppler velocimetry in a refractive index matched facility. *J. Fluids Engr.*, 118, pp. 810-818.

Patankar, S. V., 1980. *Numerical heat transfer and fluid flow.* Washington: Hemisphere, Chapter 6, pp. 126-135.

Perkins, K. R., 1975. Turbulence structure in gas flows laminarizing by heating. Ph.D. thesis, Univ. Arizona.

Perkins, K. R., and D. M. McEligot, 1975. Mean temperature profiles in heated laminarizing air flows. *J. Heat Transfer*, 97, pp. 589-593.

Petukhov, B. S., V. A. Kurganov and A. I. Gladuntsov, 1972. Turbulent heat transfer in tubes to gases with variable physical properties. *Heat and Mass Transfer*, Izd. ITMO AN BSSR, Minsk, Vol. 1, pp.117-127.

Pletcher, R. H., and K.-H. Chen, 1993. On solving the compressible Navier-Stokes equations for unsteady flows at very low Mach numbers. AIAA Paper No. 93-3368-CP, 11th Computational Fluid Dynamics Conf.

Rehme, K., 1974. Turbulent flow in smooth concentric annuli with small radius ratios. *J. Fluid Mech.*, 64, pp. 263-287.

Resnikoff, H. L., and R. O. Wells, 1998. *Wavelet analysis.* Berlin: Springer.

Satake , S., and N. Kasagi , 1996. Turbulence control with a wall adjacent thin layer damping spanwise velocity fluctuations. *Int. J. Heat Fluid Flow*, 17, pp. 343 - 352.

Satake, S., and H. Kawamura, 1995. Large eddy simulation of turbulent flow in concentric annuli with a thin inner rod. *Turbulent Shear Flows 9* (Ed.: F. Durst, N. Kasagi, B. E. Launder, F. W. Schmidt, K. Suzuki and J. H. Whitelaw), Berlin: Springer, pp. 259-281.

Satake, S., and T. Kunugi, 1998a. Direct numerical simulation of turbulent pipe flow. *Bulletin, JSME*, 64, pp. 65--70 (in Japanese).

Satake, S., and T. Kunugi, 1998b. Direct numerical simulation of an impinging jet into parallel disks. *Int. J. Num. Methods Heat Fluid Flow*, 8, pp. 768-780.

Satake, S., and T. Kunugi, 1998c. Direct numerical simulation of turbulent pipe flow with nonuniform surface heat flux. *Thermal Sci. Eng.*, 6, No. 2, pp. 1-7 (in Japanese).

Satake, S., and T. Kunugi, 1999. Direct numerical simulation of turbulent pipe flow with uniform surface heat flux. *Trans. JSME*, 65-631B, pp. 192-197 (in Japanese).

Satake, S.-i., T. Kunugi, A. M. Shehata and D. M. McEligot, 2000. Direct numerical simulation on laminarization of turbulent forced gas flows in circular tubes with strong heating. *Int. J. Heat Fluid Flow*, 21, pp. 526-534.

Satake, S.-i., T. Kunugi, A. M. Shehata and D. M. McEligot, 2002. DNS of forced gas flows in circular tubes at various heating rates. Presentation OFS 12, Twelfth Int. Heat Transfer Conf., Grenoble, August.

Schumann, U., 1975. Sub-grid scale model for finite difference simulation of turbulent channel flows in plane channels and annuli. *J. Comput. Phys.*, 18, pp. 376-404.

Shehata, A. M., 1984. Mean turbulence structure in strongly heated air flows. Ph.D. thesis, Univ. Arizona.

Shehata, A. M., and D. M. McEligot, 1995. Turbulence structure in the viscous layer of strongly heated gas flows. Tech. report INEL-95/0223, Idaho National Engineering Laboratory.

Shehata, A. M., and D. M. McEligot, 1998. Mean turbulence structure in the viscous layer of strongly-heated internal gas flows. Measurements. *Int. J. Heat Mass Transfer*, 41, pp. 4297-4313.

Sparrell, J. K., 1995. Letter, Sparrell Engineering Research Corporation, P. O. Box 130, Damariscotta, Maine 04543 USA, 14 March.

Takase, K., 1996. Experimental results of heat transfer coefficients and friction factors in a 2D/3D rib-roughened annulus. *Exp. Therm. Fluid Science*, 13 (2), p. 142-151.

Takase, K., 1996. Numerical prediction of augmented turbulent heat transfer in an annular fuel channel with repeated two-dimensional square ribs. *Nuc. Eng. Design*, 165, pp. 225-237.

Takase, K., 1997. Three-dimensional numerical simulations of heat transfer in an annular fuel channel with periodic spacer ribs under a fully developed turbulent flow. *Nuclear Tech.*, 118, pp. 175-185.

Thompson, B. E., O. Bouchery and K. D. Lowney, 1995. Refractive-index-matching laser velocimetry for complex nozzle entrance flow. *Laser Anemometry - 1995*, ASME FED-Vol. 229, pp. 365-370.

Torii, S., A. Shimizu, S. Hasegawa and M. Higasa, 1993. Numerical analysis of laminarizing circular tube flows by means of a Reynolds stress turbulence model. *Heat Transfer - Japanese Research*, 22, pp. 154-170.

Torii, S., A. Shimizu, S. Hasegawa and N. Kusama, 1991. Laminarization of strongly heated annular gas flows. *JSME International J., Ser II*, 34, No. 2, pp. 157-168.

Torii, S., and W.-J. Yang, 1997. Laminarization of turbulent gas flow inside a strongly heated tube. *Int. J. Heat Mass Transfer*, 40, pp. 3105-3117.

Vukoslavcevic, P., and J.M. Wallace, 1981. Influence of velocity gradients on measurements of velocity and streamwise vorticity with hot-wire X-array probes. *Rev. Sci. Instrum.* 52(6), pp. 869-879.

Vukoslavcevic, P., and J. M. Wallace, 1996. A 12-sensor hot-wire probe to measure the velocity and vorticity vectors in turbulent flow. *Meas. Sci. Technol.* 7, pp. 1451-1461.

Vukoslavcevic, P., J. M. Wallace and J.-L. Balint, 1991. The velocity and vorticity vector fields of a turbulent boundary layer. Part 1. Simultaneous measurement by hot-wire anemometry. *J. Fluid Mech.* 228, pp. 25-54.

Wallace, J.M., 1986. Methods of measuring vorticity in turbulent flows. *Exp. Fluids* 4, pp. 61-71.

Wallace, J.M., and J. F. Foss, 1995. The measurement of vorticity in turbulent flows. *Ann. Rev. Fluid Mech.* 27, pp. 469-514.

Wang, J., J. Li and J. D. Jackson, 2002. Mixed convection heat transfer to air flowing upwards through a vertical plane passage. *Trans., Institution of Chemical Engineers Part A, Chemical Engineering Research and Design*, 80, Part A, pp. 252-260.

Wang, W.-P., and R. H. Pletcher, 1996. On the large eddy simulation of a turbulent channel flow with significant heat transfer. *Phys. Fluids* 8 (12), pp. 3354-3366.

Watanabe, H., S. Satake and T. Kunugi, 1997. Parallelization of cylindrical direct numerical simulation code on VPP 500. Proc., 11th Computational Fluid Dynamics Conf., Tokyo, pp. 129-130.

Webb, B. W., and C.-F. Ma, 1995. Single phase liquid jet impingement heat transfer. *Adv. Heat Transfer*, 26, pp. 105-217.

Westerweel, J., A. A. Draad, J. G. Th. Van der Hoeven and J. van Oord, 1996. Measurement of fully-developed turbulent pipe flow with digital particle image velocimetry. *Exp. Fluids*, 20, pp. 165-177.

Wu, T.-H., Z. Xu, S. He and J. D. Jackson, 2001. Influence of buoyancy on mean flow and turbulence under conditions of mixed convection in an annulus. 2nd Int. Symp. Turbulence and Shear Flow Phenomena, Stockholm, Sweden, June.

Wu, T.-H., Z. Xu and J. D. Jackson, 2002. Mixed convection heat transfer to water flowing through a vertical passage of annular cross section. *Trans., Institution of Chemical Engineers Part A, Chemical Engineering Research and Design*, 80, Part A, pp. 246-251.

Xu, X., 2003. Large eddy simulation of turbulent pipe flow with property variations. Ph.D. dissertation, Iowa State Univ.

Xu, X., J. S. Lee and R. H. Pletcher, 2002. Cartesian-based finite volume formulation for LES of mixed convection in a vertical turbulent pipe flow. Paper IMECE2002-HT-32748, ASME International Mechanical Engineering Congress, New Orleans, November.

Xu, Z., 2002. Studies of influences of buoyancy on turbulent flow and heat transfer in a vertical passage of annular cross section. Ph. D. thesis, Univ. Manchester, December.

Zagarola, M. V., and A. J. Smits, 1998. Mean-flow scaling of turbulent pipe flow. *J. Fluid Mech.*, 373, pp. 33-79.

Zarate, J. A., R. P. Roy and A. Laporta, 2001. Isothermal and heated turbulent upflow in a vertical annular channel - Part II. *Int. J. Heat Mass Transfer*, 44, pp. 1185-1199.

Zhang, L.W., D. K. Balachandar, D.K. Tafti and F. M. Najjar, 1997. Heat transfer enhancement mechanisms in inline and staggered parallel-plate fin heat exchangers. *Int. J. Heat Mass Transfer*, 40, pp. 2307-2325.